Acceleration Feedback in Dynamic Positioning

PhD Dissertation

Karl-Petter W. Lindegaard

Report 2003:4-W
Department of Engineering Cybernetics
Norwegian University of Science and Technology
NO-7491 Trondheim, NORWAY
September 2003

Abstract

This dissertation contains new results on the design of dynamic positioning (DP) systems for marine surface vessels.

A positioned ship is continuously exposed to environmental disturbances, and the objective of the DP system is to maintain the desired position and heading by applying adequate propeller thrust. The disturbances can be categorized into three classes. First, there are stationary forces mainly due to wind, ocean currents, and static wave drift. Secondly, there are slowly-varying forces mainly due to wave drift, a phenomenon experienced in irregular seas. Finally there are rapid, zero mean linear wave loads causing oscillatory motion with the same frequency as the incoming wave train.

The main contribution of this dissertation is a method for better compensation of the second type of disturbances, slowly-varying forces, by introducing feedback from measured acceleration. It is shown theoretically and through model experiments that positioning performance can be improved without compromising on thruster usage. The specific contributions are:

- *Observer design:* Two observers with wave filtering capabilities was developed, analyzed, and tested experimentally. Both of them incorporate position and, if available, velocity and acceleration measurements. Filtering out the rapid, zero mean motion induced by linear wave loads is particularly important whenever measured acceleration is to be used by the DP controller, because in an acceleration signal, the high frequency contributions from the linear wave loads dominate.
- *Controller design:* A low speed tracking controller has been developed. The proposed control law can be regarded as an extension of any conventional PID-like design, and stability was guaranteed for bounded yaw rate. A method for numerically calculating this upper bound was proposed, and for most ships the resulting bound will be higher than the physical limitation. For completeness, the missing nonlinear term that, if included in the controller, would ensure global exponential stability was identified.

The second contribution of this dissertation is a new method for mapping controller action into thruster forces. A low speed control allocation method for overactuated ships equipped with propellers and rudders was derived. Active use of rudders, together with propeller action, is advantageous in a DP operation, because the overall fuel consumption can be reduced.

A new model ship, Cybership II, together with a low-cost position reference system was developed with the aim of testing the proposed concepts. The acceleration experiments were carried out at the recently developed Marine Cybernetics Laboratory, while the control allocation experiment was carried out at the Guidance, Navigation and Control Laboratory.

The main results of this dissertation have been published or are still under review for publication in international journals and at international conferences.

Acknowledgements

This dissertation is submitted in partial fulfillment of the requirements for the PhD degree at the Norwegian University of Science and Technology (NTNU). The research has been carried out at the Department of Engineering Cybernetics, during the period February 1999 to March 2002.

First of all I would like to thank my advisor Professor Thor I. Fossen and my co-advisor Professor Asgeir J. Sørensen. Their capabilities as motivators and inventors cannot be underestimated.

I would also like to express my gratitude to friends and colleagues at NTNU, especially Bjørnar Vik for his algorithms and experiences with the IMU. Stefano Bertelli and the technical staff are particularly recognized for their contributions developing Cybership II. I am also grateful to Ole Morten Aamo, Roger Skjetne, Jan Tommy Gravdahl, Professor Anton Shiriaev, Jon-Morten Godhavn, Lars Imsland, Vegar Johansen, Marit Ronæss, Enric Hospital, Amund Skavhaug, and Professor Olav Egeland.

Without the help and support from Torgeir Wahl and Knut Arne Hegstad at the Department of Marine Hydrodynamics it would be impossible to conduct experiments with Cybership II at the Marine Cybernetics Laboratory.

I have benefitted greatly from continuous discussions with present and former colleagues at ABB and Kongsberg Maritime. When I look back, I am thankful for having been a teammate of Jann Peter Strand, Trygve Lauvdal, Einar Ole Hansen, Marius Aarset, Einar Berglund, Åslaug Grøvlen, Kjetil Røe, Torgeir Enkerud, Geir Martin Holtan, Børre Gundersen, Jens Petter Thomassen, Paul Fredrik Gjerpe, Jostein Ekre, and Audun Bruås. Their humor, engineering skill, dedication, and practical experience will forever be highly appreciated.

The thesis was mainly supported by the Norwegian Research through the Strategic University Program (SUP) on Marine Cybernetics. Additional financial and travelling support was provided by ABB AS from January 2000 to February 2002. Kongsberg Maritime supported the completion of the thesis.

Last but not least I am grateful to my whole family whose support and efforts made this dissertation possible. To my wife Tone and our two children Marius and Åsne, you are my most precious and I will always love you.

Karl-Petter Winderen Lindegaard

Oslo, August 2003

Contents

Chapter 1

Introduction

1.1 Positioning Control Overview

Automatic control of ships has been studied for almost a century. In 1911 *Elmer Sperry* constructed the first automatic ship steering mechanism called *"Metal Mike"*. Today, the range of marine vessels covers a huge diversity of vehicles such as remotely operated vehicles (ROVs) and semi-submersible rigs. Automatic control systems for heading and depth control, way-point tracking control, fin and rudder-roll damping, dynamic positioning (DP), thruster assisted position mooring (PM) etc. are commercial products.

The main purpose of a positioning control system is to make sure that a vessel maintains a specified position and compass heading unaffected by the disturbances acting upon it. The positioning control problem is thus one of attenuating these disturbances by applying proper counteracting forces. There are two categories of such control systems; DP and PM. A dynamically positioned vessel maintains its position exclusively by means of active thrusters whilst for a moored vessel thrusters are complementary to the anchor system. In the latter configuration the majority of the environmental disturbances are compensated by the anchor lines and the dimensioning requirements to the thruster system are generally significantly lower than for a DP operated vessel.

The safety requirements upon a positioning system are high due to the high risk for crew and equipment especially in severe weather. Rules and regulations are enforced by international certification societies such as Lloyd's Register of Shipping, The American Bureau of Shipping (ABS) and Det Norske Veritas (DNV). Sea trials are to be carried out under the supervision of representatives from the classification issuer before a new installation can be put into service.

Dynamic positioning systems have been commercially available since the 1960s, and today a DP system is a natural component in the delivery of many new vessels. A modern DP system is not only capable of maintaining a single vessel in a fixed position, and depending on the supported functionality we may crudely

divide DP market into two segments. First, there is a high-end market demanding tailor-made solutions and high operational safety. Typically, the high-end market demands:

- *Operational safety*: The system has to be redundant, which in essence means that no single-point failure is allowed to trigger a total system failure; the operation is not to be aborted. This requires, from a DP manufacturer's side, a redundant sensor configuration, control computer system, control network, operator panels etc. and a watchdog supervising the hardware. Figure 1.1 presents a schematic overview of a dual-class DP system. Furthermore, the actions taken by the DP software should not cause failures elsewhere. As an example, the DP system has to monitor available thruster power and restrict, if necessary, the commanded propeller thrust so as to prevent power blackouts.

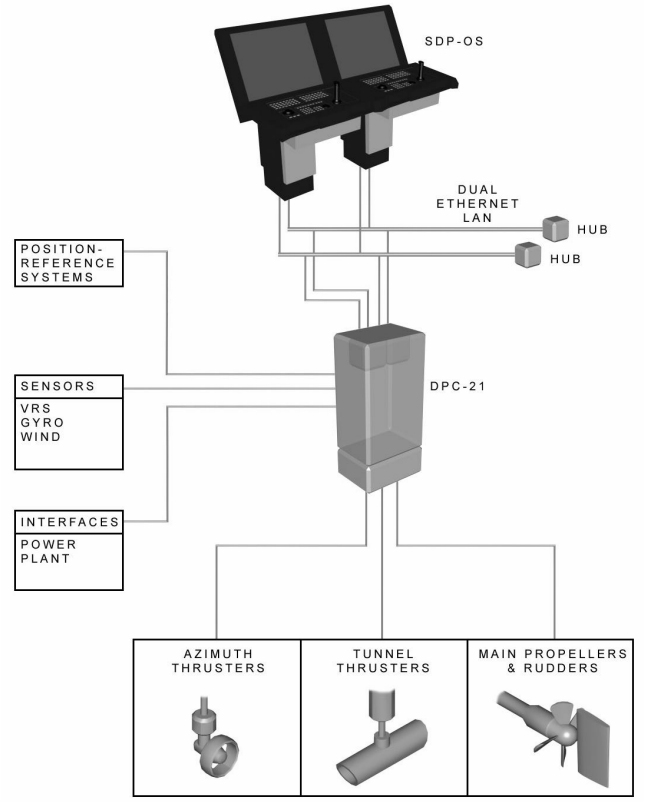

Figure 1.1: The Kongsberg Maritime SDP-21 dual-redundant DP control system. (Courtesy Kongsberg Maritime, Norway)

- *Performance*: Any operation must be performed as accurately as possible. For instance, the positioning performance, the vessel's ability to track or to

stay in its desired position, should be high. The DP system is also expected to apply thrust intelligently in order to keep the energy consumption down.

- *Versatility*: The DP system has to support a large range of operational modes. Examples of such are manual joystick control, station keeping, mixed manual and automatic control, change position and/or heading, low speed tracking, and follow target. Among the more sophisticated operational modes are weather optimal heading and position control. These basic operational modes together form the basis for performing advanced applications.
- *Advisory systems*: On-line advisory systems analyse the current status of the vessel in order to identify possibly hazardous scenarios in case of a failure. The operator can thus take a priori actions to increase safety margins during ongoing operations. By using off-line tools such as simulators, the operator is given the opportunity to plan and train future operations in a safe environment.

Approximately 200 high-end DP systems were sold world-wide in 2002. The costs of such high-end systems depend heavily on the configuration and the number of delivered sensors and position reference systems.

In the lower end of the spectrum, there are lightweight systems offering a selection of the functionality available in the high-end brands. These systems typically offer simple station keeping functionality, course-keeping autopilots, and manual joystick control.

1.1.1 Control System Description

A positioning control system for marine vehicles can be separated into a set of dedicated modules with designated tasks. The most significant modules, see Figure 1.2, are:

- **Guidance system**: The guidance system is used in planning the ship's path from one location to the destination. Advanced guidance systems usually offer way-point tracking functionality and the possibility to interface with external map systems. In a DP operation, the guidance module provides a smooth reference trajectory from one position and heading to the next.
- **Signal processing**: The signal processing unit monitors the measured signals and performs quality tests identifying high variance, wild points, frozen signals, and signal drift. Erroneous signals is to be rejected and not used further in the sequence of operations. The signal processor should perform signal voting and weighing based on the individual sensor tests when redundant measurement are available. Roll and pitch compensation of position measurements is also performed in this module. A typical DP vessel is equipped with two or three gyro compasses and an equal amount of position reference systems (POSREF). The individual POSREFs' measurements are transformed to a common point, e.g. the vessel's centre of gravity. This

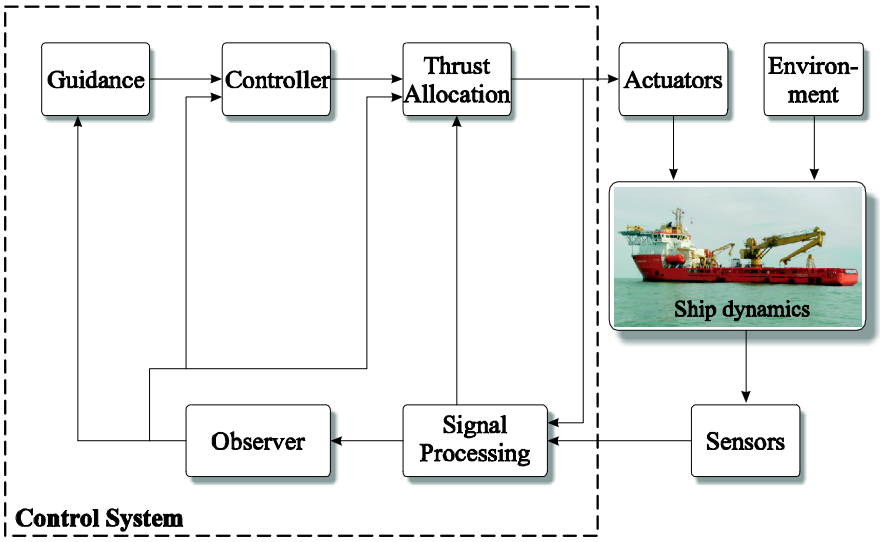

Figure 1.2: Schematic overview of a ship control system and its major components.

requires knowledge of the vertical motion of the ship, because rolling and pitching influence the measured positions greatly. Therefore, a vertical reference unit (VRU), which is an inertial sensor package measuring the heaving, rolling, and pitching motions, will be needed.

- **Observer**: The main objective of the observer is to provide low-frequency estimates of the vessel's positions, heading, and velocities. The rapid, purely oscillatory motion induced by linear wave loads has to be filtered out. Wave frequency components in the applied thrust may harm the propulsion system by causing excessive wear leading to shorter propulsion unit service intervals and service life. The observer will also be needed to predict the motion of the vessel in situations where position or heading measurements become unavailable (dead reckoning).

- **Controller**: In a low speed application, the controller produces three demands; desired surge and sway force and desired yaw moment. Depending on the ongoing operation and selected modes, the controller considers the estimated states of the system, the reference trajectory, and the measured environmental conditions in the calculation of the demands. The internal controller logic governs the mode transitions between different types of operation, and it is also responsible for issuing alarms and warnings. The demands are usually the sum from a feedback controller and feed-forward terms. A conventional feedback controller is of PD-type using the low-frequency position and velocity estimates from the observer. Some kind of integral action is required to compensate for static environmental disturbances. The controller feed-forward normally consists of reference and wind feed-forward; the former improves tracking performance, and the latter compensates for wind

fluctuations and thus provides faster response to such disturbances.

- **Thrust allocation**: The allocation module maps the controller's force and moment demands into thruster set-points such as propeller speed, pitch ratio, and azimuth and rudder angles. It is important that the produced set-points do produce the expected demands and that this will be done in an "optimal" manner. In this setting optimal could refer to minimum power consumption or minimum azimuthing and rudder usage, objectives often in conflict which each other. A definite requirement is the interface with the ship's power management system in order to prevent power black out caused by high thrusting.

1.1.2 Background

While the history of ship autopilots dates back to the invention of the gyrocompass in 1908, the development of positioning control systems had to await the introduction of a proper POSREF. A local POSREF measures the distance, typically range and bearing relative to a certain fixed point. Integrated with the gyrocompass the northing and easting are easily identified. A global POSREF provides position measurements world wide.

A variety of local POSREFs exists based on different principles: There are mechanical systems such as taut wires, radio navigation systems like Decca and Loran-C, electromagnetic distance measuring systems such as Artemis, laser based systems (Fan Beam), and hydro-acoustic position reference systems (HPR). Satellite navigation systems such as GPS and GLONASS are global POSREFs. To increase the accuracy of satellite navigation, third party vendors provide local differential correction signals via radio or satellite link. By measuring the position of a known location, it is possible to remove uncertainty of the measured GPS or GLONASS position and obtain an accuracy of about 1 meter. This integration is commonly referred to as DGPS or differential GLONASS.

Marine Positioning Control

The first DP systems originating back in the 1960's relied on local POSREFs. They were implemented using individual conventional linear controllers in each degree of freedom combined with notch-filters to remove first order wave induced motion. A de-coupled approach like this have several disadvantages. First of all, uncritical notch-filtering introduce phase lag, and secondly integral action had to be quite slow due to disregarded couplings in the model.

The perhaps most significant development came in the mid 1970's with the application of Kalman filters and linear quadratic optimal controllers. This was a model based approach because the vessel's mathematical model was used to predict and estimate the motion. These systems were computationally demanding compared to the computer resources then available. Nevertheless, the standard was set, and it is fair to say that the leading manufacturers today still benefit from the results and

experiences achieved back then. Two academic teams were particularly involved, the norwegians led by Balchen (Balchen *et al.* 1976, Balchen *et al.* 1980, Sælid *et al.* 1983) and a british group headed by Mike Grimble (Grimble *et al.* 1980, Fung and Grimble 1983). Elaborations on those schemes are found in Sørensen *et al.* (1996) and Fossen *et al.* (1996).

The research covering positioning systems gained momentum in the 1990's. Renewed interest for the subject was shown by the application of alternative control strategies: Designs based on $\mathcal{H}_\infty$-control (Katebi *et al.* 1997, Donha and Tannuri 2001) was introduced, and controllers minimizing self-induced rolling and pitching were proposed (Sørensen and Strand 2000). New control strategies emerged in the wake of the progress made on nonlinear control, examples are designs for better handling of the inherent nonlinear characteristics of the dynamic model of the ship (Fossen and Grøvlen 1998, Fossen and Strand 1999, Aarset *et al.* 1998, Strand and Fossen 1999), but also more advanced techniques such as weather optimal position control (Fossen and Strand 2001) was proposed. Tannuri *et al.* (2001) presented a two-layered controller for moored vessels dedicated to minimize a general cost function punishing important operational parameters such as rolling, riser traction and fuel consumption. A common advantage of the nonlinear proposals is that the time required for tuning and calibration of a new installation was reduced considerably, because the complexity of the model and controller went down. Instead of performing online linearizations, the developed control algorithms exploited nonlinear characteristics, and they are considered to be simpler and more robust compared to their predecessors.

Thruster assisted PM systems based on Kalman filters and linear optimal control was studied in Nakamura *et al.* (1994). The nonlinear techniques developed for DP were in Sørensen *et al.* (1999) successfully applied to a full scale turret-anchored FPSO. Aamo and Fossen (1999) suggested a method for hybrid thruster and line tension control suited for oil exploration and production in deeper waters.

In the lower end of the scale, several manufacturers now offer manual joystick control systems with limited DP functionality (Källström and Theorén 1994, Terada *et al.* 1996).

General Improvements

In addition to these more structural advances, the positioning control systems as products have evolved significantly over the past two decades:

- **Computer resources**: During the past decades there has been a tremendous development of computer hardware and software. As a result, today's DP systems have become lighter, less expensive, and more reliable. The most striking feature is perhaps the improvements made on operator stations, graphical user interfaces, and on the advisory systems. A DP system can be regarded as a computerized integrated platform with nearly complete control over most parts of the ship.
- **Control algorithms and strategies**: Increased computational power has

provided the opportunity to implement more sophisticated control algorithms. More demanding control strategies such as model predictive control and online numerical optimization techniques have been commercialized.

- **Sensor technology**: The introduction of differentially corrected satellite navigation systems has made DP systems more versatile by expanding the range of operations in which a DP vessel can take part. The next step is the integration of inertial measurement units (IMU) and existing POSREF technology such that together they offer a more accurate navigation system. Such integrated systems are referred to as integrated navigation systems (INS). Integration of inertial measurements, that is linear accelerations and gyro rates, has received a great deal of attention lately. Another interesting solution is the integration with hydroacoustic POSREFs. The speed of sound in water is about 900 m/s, and this means that HPR systems suffer from large time delays in deep waters. Additionally, it is desirable to keep a low update frequency in order to extend the battery life of the transponders on the sea bottom. Aided by inertial measurements, however, high update frequency and position accuracy almost comparable to DGPS can be expected. The Kongsberg Maritime product HAINS is one such system.

1.2 Motivation

Since the design of positioning control systems for marine vehicles is a mature and much studied subject, the present work has sought to improve existing designs by taking advantage of recent developments in the surrounding technologies. It is no longer sufficient to focus on maintaining a prescribed position or track. Modern DP vessels must be able to solve various complicated operational tasks where the control objectives differ depending on the particular kind of operation and outside circumstances. For instance, depending on weather condition the objectives vary significantly: In fine weather it is desirable to focus on fuel efficiency while in harsh weather conditions the focus should be on positioning performance and safety for the crew and the equipment. For drilling and oil producing vessels yet another objective is to maintain production capability as long as possible by decreasing the rolling and pitching motion. These individual goals are usually in conflict, and the operator will have to settle for a trade-off between them. Intuitively, fuel efficiency suffers with improved positioning performance and vice versa.

One important question is whether new and improved sensor technology may be used to bridge, at least partially, some of these conflicting performance goals. Is it possible to achieve better positioning performance without simultaneously increase the propeller thrust? A positioned vessel is continuously exposed to time-varying disturbances, and with more knowledge about those disturbances, is it possible to better keep the desired position by applying thrust more wisely? An equally important alternative is how thrusting, particularly the peaks, can be reduced without sacrificing positioning performance. By reducing the peaks on propeller thrust, the amount of required electrical power available at any time is relaxed. Hence, the ship's overall fuel consumption goes down.

The main objective of this dissertation was to find an affirmative answer to those questions, and the basic idea was to introduce inertial measurements that had not been used actively in a marine control setting before. High performance inertial measurement units IMUs are becoming increasingly affordable. INS platforms integrating IMU and POSREF systems reproduce not only positions but also velocities and linear accelerations with great accuracy. It is likely that these types of systems will be delivered to future high-end DP vessels. However, practical challenges remain to be addressed, because there will still be a trade-off between increased performance on one side and increased cost due to instrument interfacing and additional hardware expenses on the other. The industrial impact the proposed methodology eventually would have depends on how well those challenges are met. Consequently, the theoretical findings had to be tested experimentally, and a new model ship had to be constructed for that particular purpose.

1.3 Contributions

The contribution of this dissertation is threefold:

1.3.1 Observer Design

The purpose of the observer is to reconstruct non-measured states of the system and to filter out the induced motion from the first order wave loads. Traditional designs cover position and heading measurements only since this is sufficient to reconstruct all states, for instance velocities, within the system. New and improved sensor technology calls for an update of the filter design: It should be possible to integrate velocity and acceleration signals.

Based on the identification of a commutation property between the Earth-fixed dynamics and the nonlinear kinematics, two model based observer designs based on the successful design of Fossen and Strand (1999) was proposed and implemented on the model ship Cybership II. The main feature of these observers is that they handle nearly all sensor configurations. Partial velocity and acceleration measurements can be exploited to improve the performance of the overall filter. For the first one (Lindegaard and Fossen 2001*a*, Lindegaard and Fossen 2001*b*), global exponential stability of the observer errors was proven by using a Lyapunov function of a certain structure. The second one (Lindegaard *et al.* 2002) is a more pragmatic approach relaxing the structural requirement by imposing a boundedness requirement for the yaw rate instead.

1.3.2 Controller Design

The main control design contribution is the deduction of a dynamic PID-inspired low speed tracking controller incorporating an additional acceleration term. This particular controller can be seen as a extension of conventional DP control laws with body-fixed gains. By showing that the kinematics can be removed from the

analysis and thereby the controller gain assignment, any one linear design tool can be used to find proper gains. In the implementation, the applied thrust is then found as the product of the gain matrix and a separate matrix containing the kinematics. The price paid is that the controllers are exponentially stable for bounded yaw rate $r_{\max}$. However, a conservative upper bound can be estimated numerically, and it seems that for a well-behaving controller this limit by far exceeds the physical limitations. Therefore, we could say that given proper gains, all controllers derived are uniformly globally exponentially stable. In addition, $r_{\max}$ can be included as a design criterion in the form of a linear matrix inequality (LMI) in a variety of LMI based state-feedback schemes.

All controllers are derived under full state feedback, but it also shown that substituting the actual states with their respective estimates from an asymptotically converging observer does not compromise stability.

It is shown that controllers utilizing measured acceleration are better suited than PID/PD-designs in attenuating slowly varying disturbances. The main advantage of acceleration feedback is that the closed-loop bandwidth can be kept constant while the acceleration term of the feedback law manipulates the mass of the system thus making it more inert, we are given an extra degree of freedom in the design. Experiments with Cybership II demonstrated that the positioning accuracy was increased when applying acceleration feedback without simultaneously increasing applied propeller thrust.

This material has been published in Lindegaard and Fossen (2003) while Lindegaard and Fossen (2002) is still under review.

1.3.3 Control Allocation

A control allocation algorithm for low speed marine vessels using propellers and rudders was derived by Lindegaard and Fossen (2003). Using rudders actively has advantages in a low-speed operation by decreasing the need for propeller power and fuel. However, at low speed a rudder is effective only for positive thrust. This complicates the thrust allocation problem which can no longer be solved by convex quadratic programming. In fact, the existence of local minima introduces discontinuities in the commanded thruster signals even if the desired control force is continuous. Discontinuous signals cause excessive wear on the thruster system and must be avoided. An analytic, 2-norm optimal method ensuring continuity of the solutions is proposed. Being analytic, however, its limitation is the capability of handling only configurations where one single thrust device is subject to sector constraints at a time. The fuel saving potential was illustrated experimentally with Cybership II. For this particular ship, the energy consumption was cut in half.

Chapter 2

Modeling of Marine Vessels

2.1 Introduction

In this chapter we first summarize the properties of the common 6 DOF dynamic model of craft at sea. In the first section the kinematics needed for studying marine craft is summarized. After a brief presentation of the kinematics and general notation, the low speed vessel model description of Fossen (1991) and Sagatun (1992) will be summarized in 6 DOF together with a new formulation of hydrostatic restoring forces. In addition, the 3 DOF model used in positioning control operations will be derived from the general 6 DOF model. The remaining sections discuss environmental forces experienced by a vessel in operation.

2.2 Notation and Kinematics

2.2.1 General Description

Dynamic motions have to be described with respect to some reference point or coordinate system. Because we are primarily interested in the dynamics of the vessel over a very limited area and operations where hydrodynamic and thruster applied forces are dominant, we may neglect the effects of the Earth's rotation and let the local geographic frame approximate the inertial frame.

These are the reference frames that will be used:

NED (n-frame) This is called North-East-Down $x_n y_n z_n$ that in its original definition is a tangent plane moving along with the vessel. Instead of the original definition, we consider it as Earth-fixed and use it as the inertial frame. This is also referred to as flat Earth navigation and is an approximation valid in smaller areas.

BODY (b-frame) The body frame $x_b y_b z_b$ is fixed to the vessel and hence moving along with it. Often, but not necessarily, is the b-frame located in the vessel's center of gravity.

VP (p-frame) The *vessel parallel* p-frame $x_p y_p z_p$ is a body-fixed frame just like the b-frame. Its orientation is horizontal like the n-frame but it has been rotated an angle ψ around its z-axis. For 3 DOF planar motion, the b- and p-frames coincide completely.

RP (d-frame) The *reference parallel* d-frame is fixed to the vessel with horizontal orientation and rotated an angle ψ_d around the z-axis. The angle ψ_d is the craft's desired heading angle, hence the name reference parallel.

The following notation will be used for describing position, linear velocities and angular velocities:

$\mathbf{p}^a_{cb}$	–	Distance (position) from point c to point b decomposed in the a-frame.
$\boldsymbol{\theta}_{cb}, \mathbf{q}_{cb}$	–	The orientation of frame b relative to c given in Euler angles and unit quaternions, respectively.
$\mathbf{v}^a_{cb}$	–	Linear velocity of point b relative to c decomposed in a.
$\boldsymbol{\omega}^a_{cb}$	–	Angular velocity of point b relative to c decomposed in a.
$\mathbf{f}^a$	–	A linear force decomposed in a.
$\mathbf{m}^a_b$	–	The moment about the point b decomposed in a.

A unit quaternion $\mathbf{q}$ is a singularity free alternative to Euler angles defined as

$$\mathbb{H}=\left\{\mathbf{q} \mid \mathbf{q}^T\mathbf{q}=1, \mathbf{q}=[\eta_q\ ,\ \boldsymbol{\varepsilon}_q^T]^T, \eta_q \in \mathbb{R}, \boldsymbol{\varepsilon}_q \in \mathbb{R}^3\right\} \tag{2.1}$$

It might be convenient to use more than one body frame. Then, the body-fixed frames are denoted b_i where i is a positive scalar. Often we will skip using b_i and simply say i, such that vectors with only one subscript means "with respect to n". For example $\mathbf{p}^n_i$ means the position of frame b_i with respect to n decomposed in n. Similarly, $\boldsymbol{\omega}^b_i$ means the rotation rate of frame b_i with respect to n decomposed in b_i.

The rotation from frame b to frame a is denoted $\mathbf{R}^a_b = \mathbf{R}(\boldsymbol{\theta}_{ab}) = \mathbf{R}(\mathbf{q}_{ab})$ such that for any vector decomposed in b, say $\mathbf{c}^b$, then decomposed in a becomes

$$\mathbf{c}^a = \mathbf{R}^a_b \mathbf{c}^b \tag{2.2}$$

Observe that the rotation $\mathbf{R}^a_b$ implicitly takes the orientation $\boldsymbol{\theta}_{ab}$ as input. The set of all 3×3 rotations is referred to as $SO(3)$, the Special Orthogonal group of order three.

Property 2.1 (Rotation Matrix) *A rotation matrix* $\mathbf{R} \in SO(3)$ *satisfies*

$$\mathbf{R}^{-1} = \mathbf{R}^T \tag{2.3}$$

$$\|\mathbf{R}\|_2 = \det(\mathbf{R}) = 1 \tag{2.4}$$

This property is fundamental for the analysis of the proposed observers in Chapter 4.

The cross-product of two vectors $\mathbf{c}, \mathbf{d} \in \mathbb{R}^3$ can be written

$$\mathbf{c} \times \mathbf{d} = \mathbf{S}(\mathbf{c})\mathbf{d} = -\mathbf{S}(\mathbf{d})\mathbf{c} \tag{2.5}$$

where $\mathbf{S} : \mathbb{R}^3 \to \mathbb{R}^{3\times 3}$ is a skew-symmetrical matrix

$$\mathbf{S}(\boldsymbol{\alpha}) = -\mathbf{S}^T(\boldsymbol{\alpha}) = \begin{bmatrix} 0 & -\alpha_3 & \alpha_2 \\ \alpha_3 & 0 & -\alpha_1 \\ -\alpha_2 & \alpha_1 & 0 \end{bmatrix} \tag{2.6}$$

Property 2.2 (Time Derivative of a Rotation) *The matrix differential equation of a rotation matrix* $\mathbf{R}_b^a$ *is*

$$\frac{d}{dt}\left(\mathbf{R}_b^a\right) \stackrel{\triangle}{=} \dot{\mathbf{R}}_b^a = \mathbf{R}_b^a \mathbf{S}(\boldsymbol{\omega}_{ab}^b) \tag{2.7}$$

In accordance with the literature, we follow the zyx-convention: The rotation from the n-frame to the b-frame is performed in three successive principal rotations about the z, y, and x-axis in terms of the Euler angles $\boldsymbol{\theta}_{nb} = [\phi, \theta, \psi]^T$, respectively

$$\mathbf{R}_b^n = \mathbf{R}(\boldsymbol{\theta}_{nb}) = \mathbf{R}_{z,\psi}\mathbf{R}_{y,\theta}\mathbf{R}_{x,\phi} \quad \Leftrightarrow \quad \mathbf{R}_n^b = \mathbf{R}^T(\boldsymbol{\theta}_{nb}) = \mathbf{R}_{x,\phi}^T\mathbf{R}_{y,\theta}^T\mathbf{R}_{z,\psi}^T \tag{2.8}$$

where, using $\mathrm{c}(\cdot) = \cos(\cdot)$ and $\mathrm{s}(\cdot) = \sin(\cdot)$,

$$\mathbf{R}_{x,\phi} = \begin{bmatrix} 1 & 0 & 0 \\ 0 & \mathrm{c}\phi & -\mathrm{s}\phi \\ 0 & \mathrm{s}\phi & \mathrm{c}\phi \end{bmatrix} \quad \mathbf{R}_{y,\theta} = \begin{bmatrix} \mathrm{c}\phi & 0 & \mathrm{s}\theta \\ 0 & 1 & 0 \\ -\mathrm{s}\theta & 0 & \mathrm{c}\theta \end{bmatrix} \quad \mathbf{R}_{z,\psi} = \begin{bmatrix} \mathrm{c}\psi & -\mathrm{s}\psi & 0 \\ \mathrm{s}\psi & \mathrm{c}\psi & 0 \\ 0 & 0 & 1 \end{bmatrix} \tag{2.9}$$

such that

$$\mathbf{R}_b^n = \begin{bmatrix} \mathrm{c}\psi\mathrm{c}\phi & \mathrm{s}\psi\mathrm{c}\phi + \mathrm{c}\psi\mathrm{s}\theta\mathrm{s}\phi & \mathrm{s}\psi\mathrm{s}\phi - \mathrm{c}\psi\mathrm{s}\theta\mathrm{c}\phi \\ -\mathrm{s}\psi\mathrm{c}\phi & \mathrm{c}\psi\mathrm{c}\phi - \mathrm{s}\psi\mathrm{s}\theta\mathrm{s}\phi & \mathrm{c}\psi\mathrm{s}\phi + \mathrm{s}\psi\mathrm{s}\theta\mathrm{c}\phi \\ \mathrm{s}\theta & -\mathrm{c}\theta\mathrm{s}\phi & \mathrm{c}\theta\mathrm{c}\phi \end{bmatrix} \tag{2.10}$$

2.2.2 Vessel Kinematics

Decomposed in the n-frame, the position of a body-fixed arbitrary point a is

$$\mathbf{p}_{na}^n = \mathbf{p}_{nb}^n + \mathbf{R}_b^n \mathbf{p}_{ba}^b \tag{2.11}$$

where $\mathbf{p}_{nb}^n$ is the position of the vehicle and $\mathbf{p}_{ba}^b$ is the position of the point a relative to the origin of the body. The time-derivative of $\mathbf{p}_{na}^n$ is the Earth-fixed velocity $\mathbf{v}_{na}^n$ given by

$$\dot{\mathbf{p}}_{na}^n \stackrel{\triangle}{=} \mathbf{v}_{na}^n = \mathbf{R}_b^n \mathbf{v}_{nb}^b - \mathbf{R}_b^n \mathbf{S}(\mathbf{p}_{ba}^b)\boldsymbol{\omega}_{nb}^b \tag{2.12}$$

If $\mathbf{p}_{ba}^b = \mathbf{0}$ we get the usual linear velocity relation

$$\dot{\mathbf{p}}_{na}^n = \mathbf{R}_b^n \mathbf{v}_{nb}^b \tag{2.13}$$

Property 2.2 contains the differential equation determining relation between the rotation rates in the n- and b-frames. However, in may applications it is convenient to find the Euler angles $\boldsymbol{\theta}_{nb}$ directly. It can be shown that the rotation rate relation is (Fossen 2002)

$$\dot{\boldsymbol{\theta}}_{nb} = \mathbf{T}_\theta \boldsymbol{\omega}_{nb}^b \tag{2.14}$$

where

$$\mathbf{T}_\theta = \begin{bmatrix} 1 & \sin\phi\tan\theta & \cos\phi\tan\theta \\ 0 & \cos\phi & -\sin\phi \\ 0 & \sin\phi/\cos\theta & \cos\phi/\cos\theta \end{bmatrix} \quad , \quad \theta \neq \pm\frac{\pi}{2} \tag{2.15}$$

Observe that $\mathbf{T}_\theta$ is singular for $\theta = \pm 90$ degrees. By using e.g. unit quaternions instead of Euler angles, the singularity can be avoided to the price of using 4 instead of 3 parameters.

Fossen (2002) suggests collecting the Earth-fixed position and orientation of a craft in a vector $\boldsymbol{\eta}$ and the body-fixed velocities in a vector $\boldsymbol{\nu}$ like this:

$$\boldsymbol{\eta} = \begin{bmatrix} \mathbf{p}_{nb}^n \\ \boldsymbol{\theta}_{nb} \end{bmatrix} \quad , \quad \boldsymbol{\nu} = \begin{bmatrix} \mathbf{v}_{nb}^b \\ \boldsymbol{\omega}_{nb}^b \end{bmatrix} \tag{2.16}$$

Using the above results

$$\dot{\boldsymbol{\eta}} = \mathbf{J}(\boldsymbol{\theta}_{nb})\boldsymbol{\nu} \tag{2.17}$$

where $\mathbf{J} : \mathbb{R}^3 \to \mathbb{R}^{6\times 6}$ is the block diagonal

$$\mathbf{J}(\boldsymbol{\theta}_{nb}) = \mathrm{Diag}(\mathbf{R}_b^n(\boldsymbol{\theta}_{nb}), \mathbf{T}_\theta(\boldsymbol{\theta}_{nb})) \tag{2.18}$$

2.3 6 DOF LF Model

The six DOF model description after Fossen (1991) and Sagatun (1992) is a well suited compact form of expressing marine vessel dynamics for control design. Using the $(\boldsymbol{\eta}, \boldsymbol{\nu})$-notation defined in (2.16) and the kinematics (2.17)-(2.18), the complete six DOF model can be written

$$\begin{aligned} \dot{\boldsymbol{\eta}} &= \mathbf{J}(\boldsymbol{\eta})\boldsymbol{\nu} \\ \mathbf{M}\dot{\boldsymbol{\nu}} + \mathbf{C}(\boldsymbol{\nu})\boldsymbol{\nu} + \mathbf{D}(\boldsymbol{\nu})\boldsymbol{\nu} + \mathbf{g}(\boldsymbol{\eta}) &= \boldsymbol{\tau}_{\text{thr}} + \boldsymbol{\tau}_{\text{env}} \end{aligned} \tag{2.19}$$

where $\mathbf{M} \in \mathbb{R}^{6\times 6}$ is the mass matrix, the sum of rigid-body mass and hydrodynamic added mass

$$\mathbf{M} = \mathbf{M}_{RB} + \mathbf{M}_A \tag{2.20}$$

Expressed in the b-system, the rigid body mass is

$$\mathbf{M}_{RB} = \mathbf{M}_{RB}^T = \begin{bmatrix} m\mathbf{I} & -m\mathbf{S}(\mathbf{r}_{bG}^b) \\ m\mathbf{S}(\mathbf{r}_{bG}^b) & \mathbf{I}_b \end{bmatrix} > 0 \tag{2.21}$$

where m is the rigid body mass, $\mathbf{r}_{bG}^b$ is the center of gravity, and $\mathbf{I}_b = \mathbf{I}_b^T$ is the rigid body inertia tensor with respect to the origin of the b-frame.

$$\mathbf{I}_b = \mathbf{I}_b^T = \begin{bmatrix} I_x & I_{xy} & I_{xz} \\ I_{xy} & I_y & I_{yz} \\ I_{xz} & I_{yz} & I_z \end{bmatrix} \tag{2.22}$$

2.3.1 Added Mass

In contrast to submerged volumes having constant added mass $\mathbf{M}_A$, the hydrodynamically added mass of surface vessels depends on the frequency of motion due to water surface effects. Considering a low-frequency description, we assume that $\mathbf{M}_A$ is constant and given as the limit when the frequency approaches zero

$$\mathbf{M}_A = \lim_{\omega \to 0} \mathbf{M}_A(\omega) \tag{2.23}$$

For vessels symmetric about the xz-plane (port/starboard symmetry),

$$\mathbf{M}_A = \begin{bmatrix} -X_{\dot{u}} & 0 & -X_{\dot{w}} & 0 & -X_{\dot{q}} & 0 \\ 0 & -Y_{\dot{v}} & 0 & -Y_{\dot{p}} & 0 & -Y_{\dot{r}} \\ -Z_{\dot{u}} & 0 & -Z_{\dot{w}} & 0 & -Z_{\dot{q}} & 0 \\ 0 & -K_{\dot{v}} & 0 & -K_{\dot{p}} & 0 & -K_{\dot{r}} \\ -M_{\dot{u}} & 0 & -M_{\dot{w}} & 0 & -M_{\dot{q}} & 0 \\ 0 & -N_{\dot{v}} & 0 & -N_{\dot{p}} & 0 & -N_{\dot{r}} \end{bmatrix} \tag{2.24}$$

At low speed, $\omega \to 0$, $\mathbf{M}_A = \mathbf{M}_A^T > 0$ and consequently, the mass $\mathbf{M}$ is symmetric and positive definite.

2.3.2 Coriolis and Centripetal Terms

The $\mathbf{C}(\cdot)$-matrix contains nonlinear terms due to Coriolis and centripetal effects. Coriolis and centripetal forces are workless forces in the sense that they neither introduce nor dissipate energy. The $\mathbf{C}$-matrix can always be formulated on a skew-symmetric form (Sagatun and Fossen 1991)

$$\mathbf{C}(\boldsymbol{\nu}) = -\mathbf{C}^T(\boldsymbol{\nu}) \tag{2.25}$$

and a typical representation is

$$\mathbf{C}(\boldsymbol{\nu}) = \begin{bmatrix} \mathbf{0} & -\mathbf{S}(\mathbf{M}_{11}\boldsymbol{\nu}_1 + \mathbf{M}_{12}\boldsymbol{\nu}_2) \\ -\mathbf{S}(\mathbf{M}_{11}\boldsymbol{\nu}_1 + \mathbf{M}_{12}\boldsymbol{\nu}_2) & -\mathbf{S}(\mathbf{M}_{12}^T\boldsymbol{\nu}_1 + \mathbf{M}_{22}\boldsymbol{\nu}_2) \end{bmatrix} \tag{2.26}$$

where $\mathbf{M}_{ij}$ represents the 3×3 partitions of $\mathbf{M}$

$$\mathbf{M} = \begin{bmatrix} \mathbf{M}_{11} & \mathbf{M}_{12} \\ \mathbf{M}_{12}^T & \mathbf{M}_{22} \end{bmatrix} \tag{2.27}$$

2.3.3 Damping Forces

On the vectorial form (2.19), the damping or drag forces are expressed using the matrix $\mathbf{D}(\boldsymbol{\nu})$. This matrix is often expressed as a sum of a constant and some velocity dependent term

$$\mathbf{D}(\boldsymbol{\nu}) = \mathbf{D}_L + \mathbf{D}_N(\boldsymbol{\nu}) \tag{2.28}$$

In this representation $\mathbf{D}_L$ supports linear damping forces while the latter $\mathbf{D}_N(\boldsymbol{\nu})$ represents nonlinear effects such as wave drift and turbulent viscous forces. A

vessel operating around zero speed and subject to small, continuous accelerations will experience potential damping proportional to the velocity. Therefore, for an actively positioned ship or vessels exposed to incoming waves, it is reasonable to assume that linear damping forces are indeed present and that $\mathbf{D}_L$ dominates over $\mathbf{D}_N(\boldsymbol{\nu})$ due to $|\boldsymbol{\nu}|$ being small. An un-accelerated vessel in calm waters, more or less regardless of speed, will mostly experience damping forces proportional to the square of the velocity. Those drag forces are better described by $\mathbf{D}_N(\boldsymbol{\nu})$.

Even though finding a universal $\mathbf{D}(\boldsymbol{\nu})$ is nontrivial, the damping forces are always dissipative

$$\boldsymbol{\nu}^T \left(\mathbf{D}(\boldsymbol{\nu}) + \mathbf{D}^T(\boldsymbol{\nu})\right) \boldsymbol{\nu} > 0 \quad , \quad \forall \quad \boldsymbol{\nu} \neq \mathbf{0} \tag{2.29}$$

2.3.4 Restoring Forces

The term $\mathbf{g}(\boldsymbol{\eta})$ in (2.19) contains restoring forces. By restoring forces we mean forces caused by a mooring system (Strand *et al.* 1998), mainly acting in the horizontal plane, and gravity and hydrostatic forces. The former will not be considered here, however, and therefore $\mathbf{g}(\boldsymbol{\eta})$ contains forces due to gravity and buoyancy only.

In Appendix C a new formulation of the restoring forces is developed, and those results are repeated here. This new formulation is exact and does not rely on any linearizations as long as the sides of the hull are vertical. For a typical rig this will be true. It also takes into account cross-couplings between rolling and pitching, an effect not considered by linearized approaches such as those based on metacentric height (Fossen 2002) or righting arms, the so-called $\overline{GZ}$-curves (Gillmer and Johnson 1982).

Let the displaced volume in equilibrium be denoted V_0. Observe that the vessel mass $m = \rho V_0$ where ρ is the density of water. For convenience, let the xy-plane of the b-frame coincide with the static water plane A_{wp}, thus at equilibrium the xy-planes of both the p- and b-frames coincide with A_{wp}; see Figure 2.1. The center of flotation, that is the geometric center of A_{wp}, then is

$$\mathbf{r}_{bf}^b = \frac{1}{A_{wp}} \begin{bmatrix} S_x^b \\ S_y^b \\ 0 \end{bmatrix} \tag{2.30}$$

$$S_x^b = \int_{A_{wp}} x_{ba}^b dS \tag{2.31}$$

$$S_y^b = \int_{A_{wp}} y_{ba}^b dS \tag{2.32}$$

where $\mathbf{r}_{ba}^b$ is the distance to some arbitrary point on A_{wp}. This means that $\mathbf{r}_{bf}^b$ is the geometrical center of the static water plane surface A_{wp}, that is $x_{bf}^b = S_x^b / A_{wp}$ and $y_{bf}^b = S_y^b / A_{wp}$ describe the respective longships and atwarthships positions relative to the origin of the b-frame.

The matrix $\mathbf{H}^b = \left(\mathbf{H}^b\right)^T$ is a constant matrix containing the moments of inertia

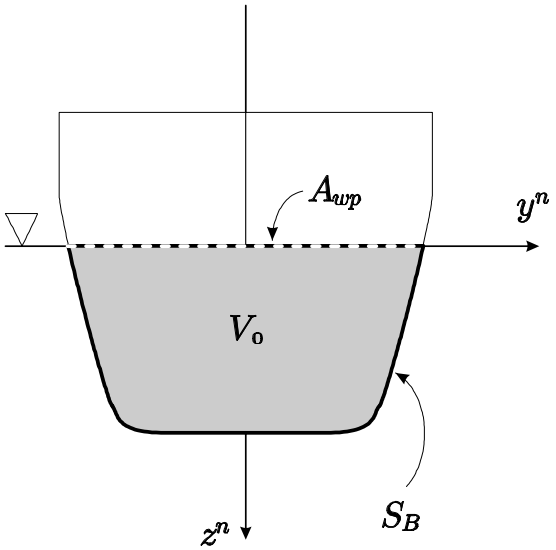

Figure 2.1: An yz-plane intersection of a neutrually buoyant vessel.

of the static water plane surface A_{wp}.

$$\mathbf{H}^b = \int_{A_{wp}} \mathbf{r}^b_{bs} \left(\mathbf{r}^b_{bs}\right)^T dS = \begin{bmatrix} S^b_{xx} & S^b_{xy} & 0 \\ S^b_{xy} & S^b_{yy} & 0 \\ 0 & 0 & 0 \end{bmatrix} \tag{2.33}$$

$$S^b_{xx} = \int_{A_{wp}} \left(x^b_{bs}\right)^2 dS \tag{2.34}$$

$$S^b_{xy} = \int_{A_{wp}} x^b_{bs} y^b_{bs} dS \tag{2.35}$$

$$S^b_{yy} = \int_{A_{wp}} \left(y^b_{bs}\right)^2 dS \tag{2.36}$$

The position of the center of gravity (CG) in vessel-fixed coordinates is called $\mathbf{r}^b_{bG}$. For rigid bodies, $\mathbf{r}^b_{bG}$ is a constant vector. The center of buoyancy (CB) $\mathbf{r}^b_{bB}$ defined as the geometrical center of the instantaneous submerged volume V is likely to change for surface vessels. For submerged vehicles, on the other hand, $\mathbf{r}^b_{bB}$ will always be constant. Nevertheless, we choose to define $\mathbf{r}^b_{bB}$ as the geometrical center of the statically displaced volume V_0.

$\mathbf{g}(\boldsymbol{\eta})$ can be written as

$$\mathbf{g}(\boldsymbol{\eta}) = -\begin{bmatrix} \mathbf{f}^b \\ \mathbf{m}^b \end{bmatrix} \tag{2.37}$$

where (C.41)

$$\begin{aligned} \mathbf{f}^b &= -\rho g A_{wp} \frac{\mathbf{R}_p^b \boldsymbol{\zeta} \boldsymbol{\zeta}^T}{\boldsymbol{\zeta}^T \mathbf{R}_b^p \boldsymbol{\zeta}} \left(\mathbf{r}_{nb}^n + \mathbf{R}_b^p \mathbf{r}_{bf}^b \right) \\ \mathbf{m}^b &= mg\mathbf{S}(\mathbf{r}_{bG}^b - \mathbf{r}_{bB}^b)\mathbf{R}_p^b \boldsymbol{\zeta} \\ &\quad + \frac{\rho g}{\boldsymbol{\zeta}^T \mathbf{R}_b^p \boldsymbol{\zeta}} \left(\mathbf{S}(\mathbf{R}_p^b \boldsymbol{\zeta}) \mathbf{H}^b - A_{wp} \mathbf{S}(\mathbf{r}_{bf}^b) \boldsymbol{\zeta}^T \mathbf{r}_{nb}^n \right) \mathbf{R}_p^b \boldsymbol{\zeta} \end{aligned} \tag{2.38}$$

where $\zeta = [0, 0, 1]^T$. Consequently, it is the heave position z_{nb}^n in $\mathbf{r}_{nb}^n = \boldsymbol{\eta}_1$ and the attitude $\boldsymbol{\theta}_{pb} = [\phi, \theta, 0]^T$ that determine $\mathbf{f}^b$ and $\mathbf{m}^b$. Notice that $\boldsymbol{\theta}_{pb}$ enters the rotation from the vessel parallel p-frame to the b-frame, $\mathbf{R}_p^b = \mathbf{R}^T(\boldsymbol{\theta}_{pb})$. From (2.10) we get that

$$\mathbf{R}_b^p = \mathbf{R}(\boldsymbol{\theta}_{pb}) = \begin{bmatrix} \cos\phi & \sin\theta\sin\phi & \sin\theta\cos\phi \\ 0 & \cos\phi & -\sin\phi \\ -\sin\theta & \cos\theta\sin\phi & \cos\theta\cos\phi \end{bmatrix} \tag{2.39}$$

because

$$\mathbf{R}_b^n = \mathbf{R}(\boldsymbol{\theta}_{nb}) = \mathbf{R}_{z,\psi}\mathbf{R}(\boldsymbol{\theta}_{pb}) \tag{2.40}$$

A Linearization for Surface Vessels

For neutrally buoyant vessels, that is for zero roll and pitch angles at equilibrium, a linearization of (2.38) can be derived for small inclinations, $\boldsymbol{\theta}_{pb} \approx \mathbf{0}$. As shown in Appendix C, the concept of metacentric heights is a result of this linearization.

More specifically, for a neutrally buoyant, xz-symmetric hull with approximately vertical sides, a linearization of the gravity and hydrostatic forces can be written

$$\mathbf{g}(\boldsymbol{\eta}) = \mathbf{G}\boldsymbol{\eta} \tag{2.41}$$

where $\mathbf{G} \in \mathbb{R}^{6\times 6}$ is partitioned as

$$\mathbf{G} = \begin{bmatrix} \mathbf{G}_{11} & \mathbf{G}_{12} \\ \mathbf{G}_{21} & \mathbf{G}_{23} \end{bmatrix} \tag{2.42}$$

and

$$\mathbf{G}_{11} = \rho g A_{wp} \mathrm{diag}(0, 0, 1) \tag{2.43}$$

$$\mathbf{G}_{12} = \rho g \begin{bmatrix} 0 & 0 & 0 \\ 0 & 0 & 0 \\ 0 & S_x^b & 0 \end{bmatrix} \tag{2.44}$$

$$\mathbf{G}_{21} = \mathbf{G}_{12}^T \tag{2.45}$$

$$\mathbf{G}_{22} = \rho g \mathrm{diag}(V_0 z_{BG}^b + S_{yy}^b, V_0 z_{BG}^b + S_{xx}^b, 0) \tag{2.46}$$

Using the definitions of transverse and longitudinal metacentric heights, that is GM_T and GM_L, respectively

$$GM_T \triangleq z_{GB}^b + \frac{1}{V_0} S_{yy}^b = \left(z_{bG}^b - z_{bB}^b \right) + \frac{1}{V_0} S_{yy}^b \tag{2.47}$$

$$GM_L \triangleq z_{GB}^b + \frac{1}{V_0} S_{xx}^b = \left(z_{bG}^b - z_{bB}^b \right) + \frac{1}{V_0} S_{xx}^b \tag{2.48}$$

$\mathbf{G}_{22}$ can be rewritten as

$$\mathbf{G}_{22} = \rho g V_0 \text{diag}(GM_T, GM_L, 0) \tag{2.49}$$

2.3.5 Thruster Forces

By a thruster we mean a device delivering a force of a magnitude F_i and direction α_i in the vessel's xy-plane. The force contributions along the x- and y-axis, denoted u_{ix} and u_{iy} respectively, constitute the *extended thrust* vector provided by thruster i

$$\mathbf{u}_i^b = \begin{bmatrix} u_{ix} \\ u_{iy} \end{bmatrix} \tag{2.50}$$

Considering also the tilting of the thruster, that is the angle between produced force and the xy-plane of the b-frame, we get an extended thrust in three dimensions

$$\bar{\mathbf{u}}_i^b = \begin{bmatrix} u_{ix} \\ u_{iy} \\ u_{iz} \end{bmatrix} = F_i \cos\mu_i \begin{bmatrix} \cos\alpha_i \\ \sin\alpha_i \\ \tan\mu_i \end{bmatrix} \tag{2.51}$$

where F_i is the generated force and $\mu_i \neq \pm\pi/2$ describes the tilt angle of the thruster. $\mu_i = 0$ means that force is produced along the x- and y-axis of the b-frame.

For simplicity, assume $\mu_i = 0$ for all i such that

$$\bar{\mathbf{u}}_i^b = \begin{bmatrix} u_{ix} \\ u_{iy} \\ 0 \end{bmatrix} \tag{2.52}$$

Assume further that thruster i is located at

$$\mathbf{r}_{bt_i}^b = \begin{bmatrix} x_{bt_i}^b & y_{bt_i}^b & z_{bt_i}^b \end{bmatrix}^T \tag{2.53}$$

which is the distance from the origin of the b-frame to the location of thruster i. Thus, the contribution $\boldsymbol{\tau}_i$ from each device is

$$\boldsymbol{\tau}_i = \begin{bmatrix} \bar{\mathbf{u}}_i^b \\ \mathbf{r}_{bt_i}^b \times \bar{\mathbf{u}}_i^b \end{bmatrix} = \begin{bmatrix} \mathbf{I} \\ \mathbf{S}(\mathbf{r}_{bt_i}^b) \end{bmatrix} \bar{\mathbf{u}}_i^b \tag{2.54}$$

Since the third element of $\bar{\mathbf{u}}_i^b$ is zero by assumption, we may instead consider

$$\begin{aligned} \boldsymbol{\tau}_i &= \begin{bmatrix} 1 & 0 \\ 0 & 1 \\ 0 & 0 \\ 0 & -z_{bt_i}^b \\ z_{bt_i}^b & 0 \\ -y_{bt_i}^b & x_{bt_i}^b \end{bmatrix} \begin{bmatrix} u_{ix} \\ u_{iy} \end{bmatrix} \\ &= \bar{\mathbf{B}}(\mathbf{r}_{bt_i}^b)\mathbf{u}_i \end{aligned} \tag{2.55}$$

Suppose that the z-coordinate of all thruster devices are identical, in other words that the thrusters are placed at the same depth z^b_{bt}. Then,

$$\tau = \sum_{i=1}^{n} \mathbf{B}(\mathbf{r}^b_{bt_i})\mathbf{u}_i \tag{2.56}$$

$$= \begin{bmatrix} \mathbf{B}(\mathbf{r}^b_{bt_1}) & \cdots & \mathbf{B}(\mathbf{r}^b_{bt_i}) \end{bmatrix} \begin{bmatrix} \mathbf{u}_i \\ \vdots \\ \mathbf{u}_n \end{bmatrix} \tag{2.57}$$

where

$$\mathbf{B}(\mathbf{r}^b_{bt_1}) = \begin{bmatrix} 1 & 0 & 0 & 0 & z^b_{bt} & -y^b_{bt_i} \\ 0 & 1 & 0 & -z^b_{bt} & 0 & x^b_{bt_i} \end{bmatrix}^T \tag{2.58}$$

This implies that the thrust-induced moments in roll and pitch are given as

$$\tau_4 = -z^b_{bt}\tau_2 \tag{2.59}$$

$$\tau_5 = z^b_{bt}\tau_1 \tag{2.60}$$

As we do not intend to assign propeller thrust in roll, pitch, and heave, this assumption is important because thrust generated roll and pitch moments are linear functions of sway and yaw thrust respectively regardless of how the thrust allocation modules operates. More precisely, for any $\boldsymbol{\tau}_{\text{3DOF}} = [\tau_1, \tau_2, \tau_6]^T$ the resulting propeller thrusts and moments will be given by

$$\boldsymbol{\tau} = \mathbf{B}_u \boldsymbol{\tau}_u \tag{2.61}$$

where

$$\mathbf{B}_u = \begin{bmatrix} 1 & 0 & 0 & 0 & z^b_{bt} & 0 \\ 0 & 1 & 0 & -z^b_{bt} & 0 & 0 \\ 0 & 0 & 0 & 0 & 0 & 1 \end{bmatrix}^T \tag{2.62}$$

2.4 3 DOF LF Model

A model in the horizontal plane describes the surge, sway, and yaw dynamics of a vessel. The motion in the vertical plane, that is heave, roll, and pitch, is neglected. From the general 6 DOF vessel model (2.19) the model in the horizontal plane is found by isolating the surge, sway and yaw elements and simultaneously setting heave, roll and, pitch to zero. The resulting model is described in terms of the position vector $\boldsymbol{\eta} = [x, y, \psi]^T$ containing North and East positions and heading respectively. Surge and sway velocity together with the yaw rate form the velocity vector $\boldsymbol{\nu} = [u, v, r]^T$. Then (Fossen 2002),

$$\dot{\boldsymbol{\eta}} = \mathbf{R}(\psi)\boldsymbol{\nu} \tag{2.63}$$

$$\mathbf{M}\dot{\boldsymbol{\nu}} + \mathbf{C}(\boldsymbol{\nu})\boldsymbol{\nu} + \mathbf{D}(\boldsymbol{\nu})\boldsymbol{\nu} + \mathbf{g}(\boldsymbol{\eta}) = \boldsymbol{\tau}_{\text{thr}} + \boldsymbol{\tau}_{\text{env}} \tag{2.64}$$

where the rotation is performed about the z-axis

$$\mathbf{R}(\psi) = \begin{bmatrix} \cos\psi & -\sin\psi & 0 \\ \sin\psi & \cos\psi & 0 \\ 0 & 0 & 1 \end{bmatrix} \tag{2.65}$$

Assuming xz-symmetry, the individual components in the velocity equation are

$$\mathbf{M} = \mathbf{M}_{RB} + \mathbf{M}_A = \begin{bmatrix} m - X_{\dot{u}} & 0 & 0 \\ 0 & m - Y_{\dot{v}} & m x_{bg}^b - Y_{\dot{r}} \\ 0 & m x_{bg}^b - N_{\dot{v}} & I_z - N_{\dot{r}} \end{bmatrix} \tag{2.66}$$

$$\begin{aligned} \mathbf{C}(\boldsymbol{\nu}) &= \mathbf{C}_{RB}(\boldsymbol{\nu}) + \mathbf{C}_A(\boldsymbol{\nu}) \\ &= \begin{bmatrix} 0 & 0 & -m_{22}v - m_{23}r \\ 0 & 0 & m_{11}u \\ m_{22}v + m_{23}r & -m_{11}u & 0 \end{bmatrix} \end{aligned} \tag{2.67}$$

As for the inertia matrix $\mathbf{M}$, surge is decoupled from sway and yaw

$$\mathbf{D}_L = \begin{bmatrix} -X_u & 0 & 0 \\ 0 & -Y_v & -Y_r \\ 0 & -N_v & -N_r \end{bmatrix} \tag{2.68}$$

The restoring term $\mathbf{g}(\boldsymbol{\eta})$ here contains mooring forces only. Since heave, roll, pitch are neglected, there will be no hydrostatic restoring forces.

2.5 Environmental Forces

This section describes the slowly-varying environmental forces $\boldsymbol{\tau}_{\text{env}}$ acting upon a surface vessel These are forces and moments due to ocean currents, wind, and wave drift. The latter effect will be described in detail using an approximation after Newman (1974), while ocean current and wind forces will only be briefly summarized. Rapid, purely oscillatory motion due to first order wave loads will not be addressed.

2.5.1 Ocean Current

A two-dimensional ocean current model is characterized by its velocity V_c and the Earth-fixed direction β_c it is running. Decomposed in the b-frame it can be written

$$u_c = V_c \cos(\beta_c - \psi) \tag{2.69}$$

$$v_c = V_c \sin(\beta_c - \psi) \tag{2.70}$$

The vessel now has a velocity relative to the fluid

$$\boldsymbol{\nu}_r = \begin{bmatrix} u - u_c & v - v_c & r \end{bmatrix}^T \tag{2.71}$$

in a horizontal plane model. Consequently, the effects of ocean currents may be included in the damping (drag) forces as functions of the relative velocity $\boldsymbol{\nu}_r$ rather than of $\boldsymbol{\nu}$ alone. However, because currents are steady phenomena, they contribute very little to the linear part of the drag so simply replacing $\mathbf{D}(\boldsymbol{\nu})\boldsymbol{\nu}$ with $\mathbf{D}(\boldsymbol{\nu}_r)\boldsymbol{\nu}_r$ would be inaccurate. Replacing $\boldsymbol{\nu}$ with $\boldsymbol{\nu}_r$ in the quadratic term is theoretically better

$$\mathbf{D}(\boldsymbol{\nu}, \boldsymbol{\nu}_r) = \mathbf{D}_L \boldsymbol{\nu} + \mathbf{D}_N(\boldsymbol{\nu}_r)\boldsymbol{\nu}_r \tag{2.72}$$

2.5.2 Wind

Similar to current, wind is characterized by a velocity V_w and an Earth-fixed propagation direction ψ_w. The Earth-fixed components are thus

$$\begin{bmatrix} u_w^n \\ v_w^n \end{bmatrix} = V_w \begin{bmatrix} \cos\psi_w \\ \sin\psi_w \end{bmatrix} \tag{2.73}$$

such that relative to the vessel itself, the onboard *experienced wind* is

$$u_r^b = V_w \cos(\psi_w - \psi) - u \tag{2.74}$$
$$v_r^b = V_w \sin(\psi_w - \psi) - v \tag{2.75}$$

The experienced incoming wind direction and velocity becomes

$$\gamma_r = \tan^{-1}(v_r^b/u_r^b) \tag{2.76}$$
$$V_r = \sqrt{(u_r^b)^2 + (v_r^b)^2} \tag{2.77}$$

While wind direction is slowly varying, or may even be constant for finite periods of time, the wind velocity is usually represented as the sum of a stationary and a rapidly fluctuating component with zero mean. The gust model is usually based on spectral approximations, see Fossen (2002) for a more detailed description.

The forces generated by the relative wind (V_r, γ_r) are based on wind coefficients obtained either analytically or experimentally. These coefficients are parameterized by the relative angle γ_r such that the wind generated forces and moments can be calculated as quadratic functions of the relative velocity. This horizontal plane formulation serves as an illustration

$$\boldsymbol{\tau}_{\text{wind}} = \frac{1}{2}\rho_a \begin{bmatrix} C_u(\gamma_r)A_T \\ C_v(\gamma_r)A_L \\ C_r(\gamma_r)A_L L \end{bmatrix} V_r^2 \tag{2.78}$$

Here ρ_a is the density of air, A_T and A_L are the transvere and lateral projected area, L is the ship length, and $C_u, C_v, C_r : \mathbb{R} \to \mathbb{R}$ are the wind coefficients in surge, sway and yaw.

2.5.3 Higher Order Wave Loads - Wave Drift

The notion *higher order* wave loads encompasses forces whose magnitudes are proportional to the square (or higher) of the waves' amplitudes. Due to the relatively low frequency content of these forces compared to the linear, purely oscillatory loads which oscillate with the wave frequency, higher order loads are often called *drift* forces. In this section we will briefly describe the source of such forces and discuss the importance of the slowly-varying components.

Wave drift forces are related to a structure's ability to cause waves (Faltinsen 1990). For craft with large surface piercing structures, the largest contribution of the horizontal drift forces is due to the relative vertical motion between the structure

and the waves (Aalbers *et al.* 2001). The incident waves are modified by the large structure resulting in non-zero drift forces due to the larger wave height on the upwind side of the hull. However, there are other contributions. One of them is the quadratic term in Bernoulli's equation, and for smaller surface piercing structures like semi-submersibles viscous effects proportional to the cube of the wave height will be significant (Faltinsen 1990).

The second order forces, static and slowly-varying, are often reconstructed in the time-domain using second-order transfer functions. Those transfer functions describe gain and phase shift of two harmonic signals of different frequencies. For instance, for $i = 1, 2$ let $u_k(t) = \mathrm{Re}(A_k e^{j\omega_k t})$ where $A_k \in \mathbb{C}$ describe magnitude and phase offset. Then, the output of a second-order transfer function of difference frequencies $H_{SV} : \mathbb{R}^2 \to \mathbb{C}$ is

$$y(t) = \mathrm{Re}\left(A_1 A_2^* H_{SV}(\omega_1, \omega_2) e^{j(\omega_1 - \omega_2)t}\right) \tag{2.79}$$

For simplicity disregard wave propagation direction. Thus, for a spectrum of waves represented by N frequencies the immediate wave height is

$$\zeta(t) = \mathrm{Re} \sum_{k=1}^{N} A_k e^{j\omega_k t} \tag{2.80}$$

and assuming $\omega_{k+1} > \omega_k$ for all k, the resulting slowly-varying drift force becomes

$$\mathbf{f}_{SV}^b(t) = \mathrm{Re} \sum_{k=1}^{N} \sum_{l=1}^{k} A_k A_l^* H_{SV}(\omega_k, \omega_l) e^{j(\omega_k - \omega_l)t} \tag{2.81}$$

Typically $N = 100$ is sufficient to describe a given sea state. Newman suggested that a reasonable approximation would be to replace $H_{SV}(\omega_k, \omega_l)$ with $H_{SV}(\omega_k, \omega_k)$ provided that the differences $|\omega_k - \omega_l|$ are sufficiently small (Newman 1974). As a consequence, the slowly-varying force $\mathbf{f}_{SV}^b$ can be adequately derived from the more simply obtainable wave drift coefficients $H_W(\omega) = H_{SV}(\omega, \omega)$ such that

$$\mathbf{f}_{SV}^b(t) = \mathrm{Re} \sum_{k=1}^{N} \sum_{l=1}^{k} A_k A_l^* H_W(\omega_k) e^{j(\omega_k - \omega_l)t} \tag{2.82}$$

$H_W(\omega_k)$ for craft similar to the supply vessel used in the experiments is reproduced in Figure 2.2.

An estimate of $\mathbf{f}_{SV}^b(t)$ based on Newman's approximation, by numerically reconstructing the wave conditions in the experiments presented in Chapter 6, can be seen in Figure 2.3. The magnitude of $\mathbf{f}_{SV}^b(t)$ is seen to be slowly varying compared to the incoming waves. This is verified by the power spectra in Figure 2.4 where the required bandwidth of a typical DP system is indicated. With a high wave group passing, as around $t = 60$ sec. in Figure 2.3, the drift force magnitude may rise to a level three times higher than the static drift.

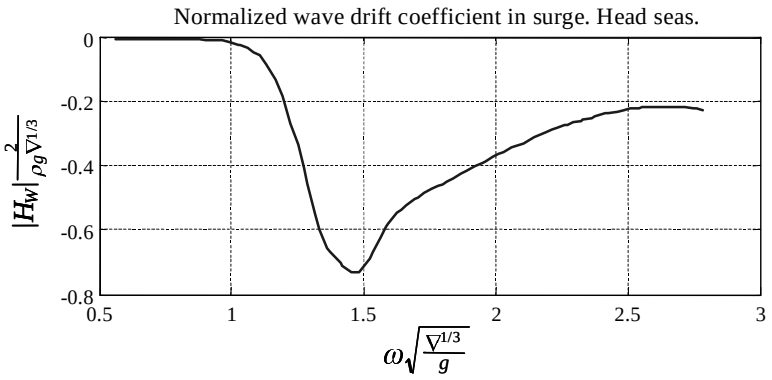

Figure 2.2: Normalized wave drift coefficient $H_W(\omega)$ in surge in head seas for a representative vessel. ∇ and ρ are the ship's displacement and the density of water, respectively.

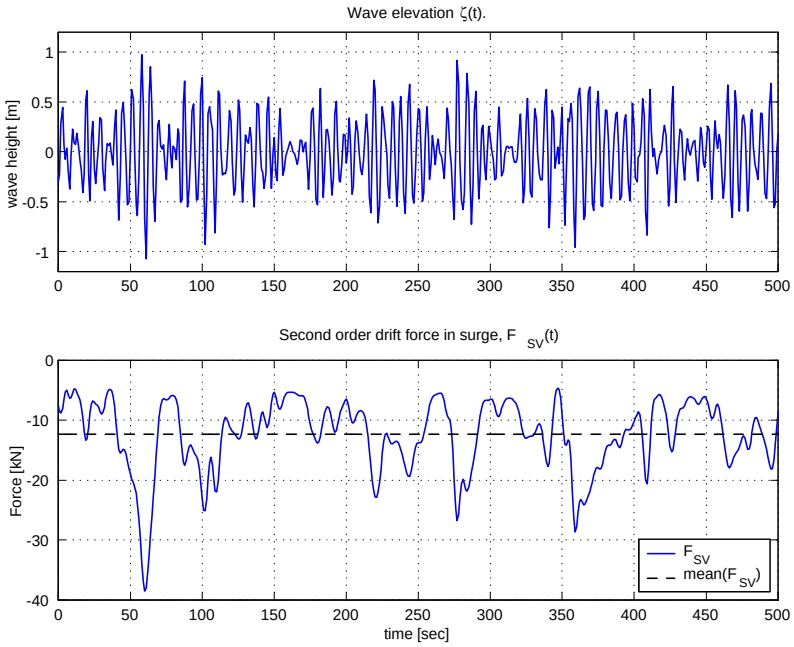

Figure 2.3: Top: Wave elevation $\zeta(t)$. Bottom: Resulting slowly varying drift forces $F_{SV}(t)$ according to Newman's approximation.

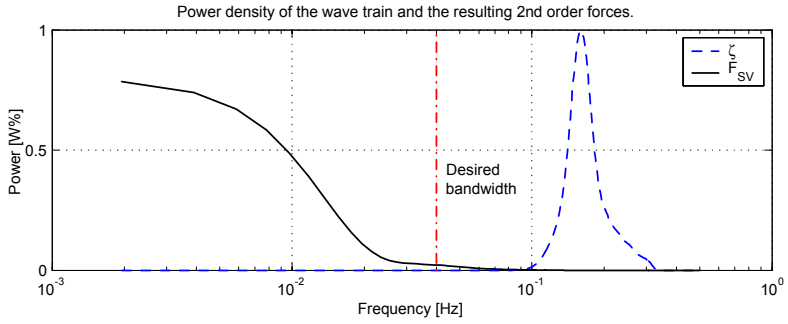

Figure 2.4: Power density of simulated wave drift forces (solid) compared to the density of the JONSWAP-distributed incoming waves (dashed).

Chapter 3

Inertial Measurements

3.1 Introduction

Over the years a variety of solutions and control strategies has been proposed to the DP control problem. A significant industrial contribution was the application of Kalman filters and optimal control (Balchen *et al.* 1976, Grimble *et al.* 1980, Balchen *et al.* 1980). These model based strategies separated the rapid, purely oscillatory (zero mean) motion caused by the first order, linear (i.e. proportional to the instantaneous wave height and with a frequency content equal to the incoming waves) wave loads, from the more slowly varying forces due to nonlinear wave effects, so called wave drift forces, wind and ocean currents. The applied thrust was then calculated from the estimated low-frequency motion thus reducing thruster modulation and wear and tear.

The objective of the DP system is therefore to counteract constant and the slowly-varying disturbances due to:

- Higher order wave loads (wave drift).
- Ocean currents.
- Wind forces (not wind gusts).

All these three components have stationary contributions, and some form of integral action will be required. Furthermore, the vessel's desired heading angle should be selected such that the power required to reject the constant force components is minimized. This can be achieved automatically by controlling the x- and y-positions provided that the vessel's reference point is located at a minimum distance fore of the centre of gravity (Pinkster and Nienhuis 1986). A more versatile and sophisticated concept called *weather optimal positioning control* (WOPC) was introduced by Fossen and Strand (2001).

It is not required to estimate the varying disturbances in order to stabilize the system. Disturbance feed-forward will be an optional feature attenuating deviations caused by varying disturbances. However, not all disturbance components are measurable. Estimating the dynamic wind forces can be done efficiently with a wind sensor and the knowledge of the ship's wind coefficients, and commercial DP systems include this "wind feed-forward" option. On the other hand, producing an estimate of the wave drift forces is non-trivial, and practical measures for handling these particular dynamic forces have not been explicitly taken until very recently. Even though PID-like control efficiently rejects constant disturbances, it is not the best option for attenuating varying disturbances in a second order mechanical system. This stems from the simple fact that a PID-controller, linear or nonlinear, cannot cope with the varying force disturbance due to the phase lag involved. After all, the control is calculated as a sum of the system's positions, integrated position errors and velocities. The resulting behavior will therefore be oscillatory in contrast to the case where the varying disturbance is completely cancelled out by an oppositely directed thrust force. Introducing more damping could theoretically reduce the amplitudes of the resulting motion, but due to wave-frequency residues in the low-frequency velocity estimate, increased damping simultaneously contributes to thruster modulation. There is therefore a practical limit for the derivative gain's magnitude.

In Aalbers *et al.* (2001) the authors proposed two "wave feed-forward" techniques to suppress the nonlinear wave effects. They illustrated the performance experimentally with a model ship. The wave drift forces were estimated by measuring the relative water motion around the waterline of the hull using ten probes. The estimated drift forces were, together with estimated wind forces, used directly in the PID feedback loop. For the same thrust power, the position deviations decreased. The method is, however, impractical because of the required number of wave probes and their robustness and expected length of life. It seems that such an installation could turn out to be expensive and somewhat unreliable.

An alternative method applicable to ships, or in fact to all mechanical systems, is to measure the accelerations. Active use of measured acceleration for control can be regarded as manipulating the system's mass. Negative acceleration feedback (AFB) increases the mass and positive feedback decreases it. By negative feedback the system is made virtually heavier as seen from the disturbances, thus their effects are attenuated and the positioning performance increases. In the opinion of the author, it seems more attractive to employ measured acceleration in positioning control of surface vessels to further suppress varying disturbances in general and slowly varying wave drift in particular rather than implementing a wave feed-forward approach (Aalbers *et al.* 2001) because:

- The sensor and engineering cost will be much lower. High-precision commercial inertial measurement units (IMUs) are becoming increasingly affordable and can be easily interfaced with existing control systems.

- The sensor equipment is intended for aerospace applications and is therefore extremely solid, reliable and robust.

- All kinds of slowly varying disturbances, not only wave drift, will be attenuated.

- Acceleration feedback is applicable to all kinds of vessels, in contrast to the first force estimation method proposed by Aalbers *et al.* (2001) which is primarily applicable to craft with large surface piercing structures such as tankers.

Active use of measured acceleration is well known in aerospace applications (Blakelock 1991) but is rarely applied in other areas like robotics and ship control simply because it is in general superfluous in stabilizing such systems. If, on the other hand, the system parameters are uncertain, the tracking performance and robustness may suffer. This is particularly evident in feedback linearization designs. Employing measured acceleration relaxes the need of an accurate model description because the right-hand side of Newton's second law

$$\sum_k F_k = ma \tag{3.1}$$

divided by the mass (and thereby the model itself) is actually being measured. Consequently, it seems plausible to expect improved robustness, tracking performance and disturbance rejection when AFB is constructively applied.

Using the acceleration in a feedback loop has been referred to as a *direct* approach (de Jager 1994) as opposed to *indirect* where the acceleration signal is used in an observer to improve the state estimates. de Jager (1994) recommended to consider using measured acceleration either directly or indirectly, but not in combination, and he reported increased tracking performance by counteracting uncertainty in the inertia matrix of a 2D Cartesian manipulator.

For rigid robots, Luo and Saridis (1985) suggested using a decentralized (diagonal) static linear controller for rigid robots assuming that joint positions, velocities and accelerations were available. Stability in the sense of Lyapunov and performance of this controller was later studied by Studenny and Bélanger (1984). In Kosuge *et al.* (1989) the authors suggest using low-pass filtered acceleration to improve the performance and robustness of a feedback linearization design of a two-link planar robot. The "disturbance" due to inaccurate model parameters introduced in the linearization was reduced in addition to the environmental disturbances. Complete disturbance cancellation can only be achieved as the acceleration gain tends towards infinity, and due to unmodeled dynamics, time delays, imperfect measurements, and other practical limitations, there will be an upper bound on the acceleration gain.

In low speed ship control, such as DP, a combined approach after de Jager's definition is almost inevitable due to the heavy notch filtering the observer has to perform. First order wave loads dominate the measured acceleration signal and direct application leads to thruster modulation and unbearable wear on the equipment. We let the notch filtered acceleration signal update both the state estimates and the control law. This particular combined approach proved to be successful.

3.1.1 Motivation: AFB in Mass-Damper Systems

Neglecting couplings and considering one degree of freedom (DOF) at a time, a ship at low speed can be regarded as a linear mass-damper system

$$m\ddot{x} = -d\dot{x} + u + w \tag{3.2}$$

where x and $v = \dot{x}$ are the states describing position and velocity,. u is the control and w is a disturbance. Isolating the velocity equation and defining $T_m = m/d$ we get the transfer function

$$h(s) = \frac{v}{w}(s) = \frac{1}{d}\frac{1}{(1 + T_m s)} \tag{3.3}$$

The idea is now to incorporate an acceleration term in the control u, that is let u be the sum

$$u = -h_a(s)\dot{v} + u_{PID} \tag{3.4}$$

where u_{PID} is to be designed later and $h_a(s)$ is some dynamic system. The effect of the negative acceleration term $-h_a(s)\dot{v}$ is increased mass, the system's *virtual mass* becomes $m_a(s) = m + h_a(s)$.

For attenuation of low-frequency disturbances, a suitable $h_a(s)$ could be a low-pass filter with a gain specified as a fraction of the original mass m

$$h_a(s) = \frac{\alpha m}{1 + T_f s} \tag{3.5}$$

For positive α's the mass increases to $(1 + \alpha)\, m$ for frequencies below $\omega_f = 1/T_f$ thus making the system virtually heavier and less influenced by varying disturbances. For high frequencies the mass is left unaltered because $|h_a(j\omega)| \to 0$ for $\omega \gg \omega_f$. The resulting transfer function for the velocity dynamics becomes

$$\frac{v}{u_{PID}}(s) = \frac{v}{w}(s) = \frac{1}{d}\frac{1 + T_f s}{(1 + T_m s)(1 + T_f s) + \alpha T_m s} \tag{3.6}$$

$$\approx \frac{\omega_a \omega_e}{d}\frac{1 + T_f s}{(s + \omega_a)(s + \omega_e)} \tag{3.7}$$

where

$$\omega_a = \frac{1}{T_m}\frac{1}{1 + \alpha} \quad , \quad \omega_e = \frac{1 + \alpha}{T_f} \tag{3.8}$$

The asymptotic Bode plots from force to velocity (Figure 3.1) with and without acceleration feedback show that, because the mechanical time constant has been increased by feedback, the magnitude decreases for frequencies $\omega_a < \omega < \omega_e$.

The "power", as given by the $\mathcal{L}_2$-induced norm, of the velocity v has been reduced for disturbances w in the frequency range $\omega_a < \omega < \omega_e$. For frequencies lower than ω_a, no reduction can be expected.

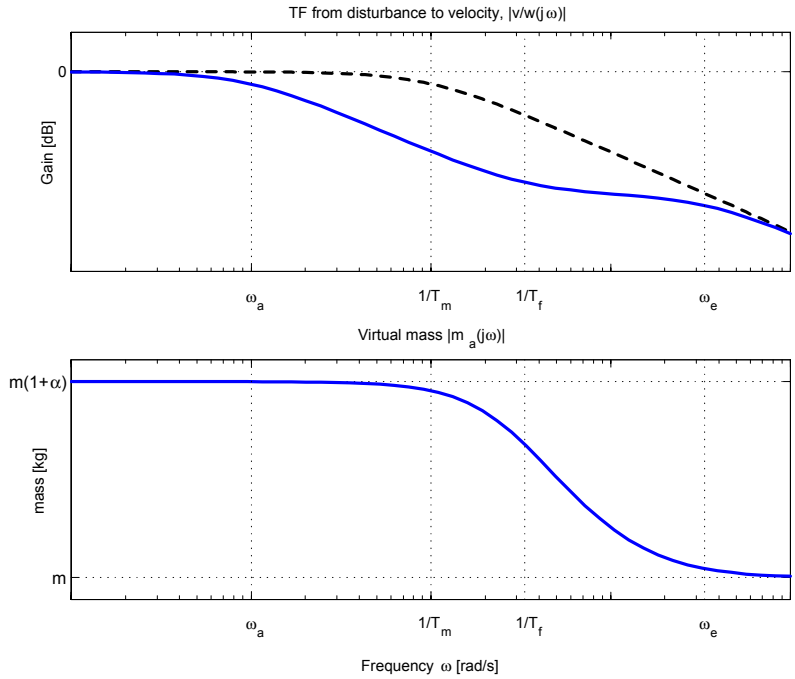

Figure 3.1: Top: Bode plot of $\frac{v}{w}(s)$ with (solid) and without (dashed) acceleration feedback. Bottom: The magnitude of virtual mass $m_a(s) = m + h_a(s)$.

3.2 Inertial Measurements

3.2.1 Angular Rates

When using high-precision gyro measurements it is required to take the Earth's rotation into account, the n-frame can no longer be regarded as the inertial frame. It is customary to express the rotations with respect to the ECI (Earth-centered inertial) i-frame which by definition does not rotate. The ECEF (Earth-centered Earth-fixed) frame is also located in the center of the Earth but rotates along with it.

An assumed error free gyro measures the rotation of the b-frame relative to the inertial ECI frame i.

$$\boldsymbol{\omega}^b_{\text{imu}} = \boldsymbol{\omega}^b_{ib} = \boldsymbol{\omega}^b_{ie} + \boldsymbol{\omega}^b_{en} + \boldsymbol{\omega}^b_{nb} \tag{3.9}$$

The second component can be ignored for marine applications, while the first can be ignored if it is below the gyro noise level which means that for high-precision gyros $\boldsymbol{\omega}^b_{ie}$ must be taken into consideration.

If the n-frame is fixed relative to the Earth, or as mentioned slowly-varying as in

marine operations, the gyro measurement is reduced to

$$\boldsymbol{\omega}^b_{\text{imu}} = \boldsymbol{\omega}^b_{ie} + \boldsymbol{\omega}^b_{nb} \tag{3.10}$$

3.2.2 Linear Accelerations

Consider now the n-frame as the inertial frame. Suppose the IMU is located at the distance $\mathbf{p}^b_{bI}$ from the origin of the body-fixed frame. In the inertial frame, the position of the IMU is then

$$\mathbf{p}^n_{nI} = \mathbf{p}^n_{nb} + \mathbf{R}^n_b \mathbf{p}^b_{bI} \tag{3.11}$$

and its velocity $\mathbf{v}^n_{nI} = \dot{\mathbf{p}}^n_{nI}$ is

$$\mathbf{v}^n_{nI} = \dot{\mathbf{p}}^n_{nb} + \mathbf{R}^n_b \mathbf{S}(\boldsymbol{\omega}^b_{nb})\mathbf{p}^b_{bI} = \mathbf{R}^n_b \left(\mathbf{v}^b_{nb} + \mathbf{S}(\boldsymbol{\omega}^b_{nb})\mathbf{p}^b_{bI}\right) \tag{3.12}$$

where we used that $\dot{\mathbf{R}}^n_b = \mathbf{R}^n_b \mathbf{S}(\omega^b_{nb})$. The acceleration $\mathbf{a}^n_{nI} = \ddot{\mathbf{p}}^n_{nI}$ is thus

$$\begin{aligned} \mathbf{a}^n_{nI} &= \ddot{\mathbf{p}}^n_{nb} + \mathbf{R}^n_b \left(\mathbf{S}^2(\boldsymbol{\omega}^b_{nb}) + \mathbf{S}(\dot{\boldsymbol{\omega}}^b_{nb})\right) \mathbf{p}^b_{bI} && (3.13)\\ &= \mathbf{R}^n_b \left(\mathbf{S}(\boldsymbol{\omega}^b_{nb})\mathbf{v}^b_{nb} + \dot{\mathbf{v}}^b_{nb}\right) + \mathbf{R}^n_b \left(\mathbf{S}^2(\boldsymbol{\omega}^b_{nb}) + \mathbf{S}(\dot{\boldsymbol{\omega}}^b_{nb})\right) \mathbf{p}^b_{bI} && (3.14) \end{aligned}$$

To avoid handling angular accelerations $\dot{\boldsymbol{\omega}}^b_{nb}$, let the accelerometer be located in the origin of the b-frame, i.e. $\mathbf{p}^b_{bI} = \mathbf{0}$. Since the acceleration measurements are decomposed in the b-frame, the assumed error free acceleration measurement $\mathbf{f}^b_{\text{imu}}$ consisting of the actual acceleration $\mathbf{a}^n_{nb}$ given by

$$\mathbf{a}^b_{nb} = \mathbf{R}^b_n \mathbf{a}^n_{nb} = \dot{\mathbf{v}}^b_{nb} + \mathbf{S}(\boldsymbol{\omega}^b_{nb})\mathbf{v}^b_{nb} \tag{3.15}$$

and gravity is written

$$\mathbf{f}^b_{\text{imu}} = \mathbf{a}^b_{nb} - \mathbf{R}^b_n \mathbf{g}^n \tag{3.16}$$

Here $\mathbf{g}^n = [0, 0, g]^T$ is the contribution from gravity. Notice the Coriolis effect $\mathbf{S}(\boldsymbol{\omega}^b_{nb})\mathbf{v}^b_{nb}$ caused by the rotation of the b-frame relative to the inertial n-frame. Observe that the gravity term could have been expressed using the vessel-parallell p-frame such that on component form

$$\mathbf{g}^b = \mathbf{R}^b_n \mathbf{g}^n = \mathbf{R}^b_p \mathbf{g}^p = \begin{bmatrix} -\sin\theta \\ \sin\phi\cos\theta \\ \cos\phi\cos\theta \end{bmatrix} g \tag{3.17}$$

because $\mathbf{g}^p = \mathbf{g}^n$.

In terms of the $\boldsymbol{\nu}$-vector, the error-free measured acceleration can be written as

$$\mathbf{f}^b_{\text{imu}} = \dot{\boldsymbol{\nu}}_1 + \mathbf{S}(\boldsymbol{\nu}_2)\boldsymbol{\nu}_1 - \mathbf{g}^b = \dot{\boldsymbol{\nu}}_1 + \boldsymbol{\nu}_2 \times \boldsymbol{\nu}_1 - \mathbf{g}^b \tag{3.18}$$

3.3 Compensators

The error-free measured acceleration (3.16) demonstrates that $\mathbf{y}^b_{\text{acc}} \neq \dot{\boldsymbol{\nu}}_1 = \dot{\mathbf{v}}^b_{nb}$. In order to construct a "measured" $\dot{\boldsymbol{\nu}}_1$ some kind of compensator has to be implemented:

$$\mathbf{y}_{\dot{\nu}_1} = \mathbf{f}^b_{\text{imu}} - \mathbf{S}(\hat{\boldsymbol{\omega}}^b_{nb})\hat{\mathbf{v}}^b_{nb} + \mathbf{R}(\hat{\boldsymbol{\theta}}_{pb})\mathbf{g}^p \approx \dot{\boldsymbol{\nu}}_1 \tag{3.19}$$

Even small roll and pitch angles will lead to gravity components in the acceleration measurements along the surge and sway axes. Those components will, because gravity is the dominating force acting upon the vessel, dominate. Consequently, accurate measurements of surge and sway acceleration require good roll and pitch measurements. An integrated navigation system estimates the position $\mathbf{p}^n_{nb}$, the orientation $\boldsymbol{\theta}_{nb}$ and the velocities $\mathbf{v}^b_{nb}$ and $\boldsymbol{\omega}^b_{nb}$. The compensator (3.19) can thus be realized using such systems.

An integrated navigation system is, however, not strictly required for gravity compensation. Below two different types of g-compensation are proposed and discussed, one static and one dynamic. The static compensator uses only acceleration measurements to remove the gravity forces, while the dynamic approach is an attitude observer also utilizing gyro measurements. However, neither the static nor the dynamic g-compensator is able to cancel the Coriolis component in

$$\mathbf{a}^b_{nb} = \dot{\boldsymbol{\nu}}_1 + \boldsymbol{\nu}_2 \times \boldsymbol{\nu}_1 \tag{3.20}$$

which means that unless the navigation system is able to accurately estimate $\boldsymbol{\nu}_1 = \mathbf{v}^b_{nb}$, this Coriolis effect cannot be removed and therefore isolating $\dot{\boldsymbol{\nu}}_1$ is generally speaking impossible and care must be taken when using the gravity compensated acceleration measurement in the control design.

Still, in positioning operations at sea, the need for such integrated systems can be relaxed as explained below.

3.3.1 Static Low-Speed Gravity Compensator

If we can assume that the velocities $\mathbf{v}^b_{nb}$ and $\boldsymbol{\omega}^b_{nb}$ are small, the error-free measured acceleration (3.16) can be approximated by

$$\mathbf{f}^b_{\text{imu}} \approx \dot{\mathbf{v}}^b_{nb} - \mathbf{R}^b_p \mathbf{g}^p \tag{3.21}$$

If the vessel is at complete rest

$$\mathbf{f}^b_{\text{imu}} = -\mathbf{R}^b_p \mathbf{g}^p \tag{3.22}$$

from which can solve for the roll and pitch angles as follows

$$\phi = \arctan\left(\frac{f_y}{f_z}\right) \quad , \quad f_z > 0 \tag{3.23}$$

$$\theta = \arctan\left(\frac{f_x}{\sqrt{f_z^2 + f_y^2}}\right) \tag{3.24}$$

where we used the individual components of the measured signal $\mathbf{f}_{imu}^b = [f_x, f_y, f_z]^T$. Provided the inclinations are small

$$\phi \approx -\frac{f_y}{g} \qquad \theta \approx \frac{f_x}{g} \tag{3.25}$$

and consequently, the roll and pitch errors $\delta\phi$ and $\delta\theta$ exhibit a similar dependence on the measurement errors δf_x and δf_y, that is

$$\delta\phi \approx -\frac{\delta f_y}{g} \qquad \delta\theta \approx \frac{\delta f_x}{g} \tag{3.26}$$

A 1 mg accelerometer error thus gives a static roll and pitch accuracy of 1 mrad ≈ 0.06 deg.

A successful g-compensation relies on good roll and pitch estimates (measurements). Suppose that the velocities are small in the sense that gravity forces dominate $\mathbf{S}(\boldsymbol{\omega}_{nb}^b)\mathbf{v}_{nb}^b$ such that (3.23)-(3.24) are reasonable approximations for roll and pitch. The accelerometers are contaminated with an error $\boldsymbol{\Delta}_{\text{acc}} = [\delta f_x, \delta f_y, \delta f_z]^T$ due to various effects. The error-free measured acceleration $\mathbf{f}_{\text{imu}}^b$ and the actual measured accelerations are

$$\begin{aligned} \mathbf{f}_{\text{imu}}^b &= \mathbf{a}^b - \mathbf{R}_p^b \mathbf{g}^p & (3.27)\\ \mathbf{y}_{\text{acc}}^b &= \mathbf{f}_{\text{imu}}^b + \boldsymbol{\Delta}_{\text{acc}} & (3.28) \end{aligned}$$

From the latter we can estimate $\mathbf{a}^b$ using the estimated roll and pitch angles $\hat{\boldsymbol{\theta}}_{pb} = [\hat{\phi}, \hat{\theta}, 0]^T$

$$\hat{\mathbf{a}}^b = \mathbf{y}_{\text{acc}}^b + \hat{\mathbf{R}}_p^b \mathbf{g}^p \tag{3.29}$$

The error $\tilde{\mathbf{a}}^b = \mathbf{a}^b - \hat{\mathbf{a}}^b$ is thus

$$\begin{aligned} \tilde{\mathbf{a}}^b &= \mathbf{f}_{\text{imu}}^b + \mathbf{R}_p^b \mathbf{g}^p - \left(\mathbf{f}_{\text{imu}}^b + \boldsymbol{\Delta}_{\text{acc}} + \hat{\mathbf{R}}_p^b \mathbf{g}^p\right) \\ &\approx \left(\mathbf{I} - \mathbf{S}(\boldsymbol{\theta}_{pb}) - \left(\mathbf{I} - \mathbf{S}(\hat{\boldsymbol{\theta}}_{pb})\right)\right) \mathbf{g}^p - \boldsymbol{\Delta}_{\text{acc}} \\ &= \mathbf{S}(\mathbf{g}^p)\tilde{\boldsymbol{\theta}}_{pb} - \boldsymbol{\Delta}_{\text{acc}} \end{aligned} \tag{3.30}$$

The linear approximations of the rotation matrices are valid for small inclinations. Taylor expansions of the roll and pitch components of the attitude error $\tilde{\boldsymbol{\theta}}_{pb} = \boldsymbol{\theta}_{pb} - \hat{\boldsymbol{\theta}}_{pb}$ are

$$\begin{aligned} \tilde{\phi} &\approx \frac{\delta f_y}{g} \\ \tilde{\theta} &\approx -\frac{\delta f_x}{g} \end{aligned}$$

Consequently, by inserting these errors into (3.30), we see that a g-compensator not only cancels out the gravity components but also removes the accelerometer error $\boldsymbol{\Delta}_{\text{acc}}$ on the x and y-axis

$$\tilde{\mathbf{a}}^b \approx -\begin{bmatrix} 0 & 0 & \delta f_z \end{bmatrix}^T \tag{3.31}$$

3.3.2 Dynamic Gravity Compensation

In order to measure dynamic roll and pitch accurately, a filter that integrates gyro and accelerometer measurements must be designed. This is often referred to as a vertical reference unit (VRU) and such can be implemented using a Kalman filter or an observer. Here the observer developed in Vik and Fossen (2001) is summarized and used as basis in a dynamic gravity compensation (DGC) scheme.

The "low-speed assumption" above that was required for using (3.23)-(3.24) as roll-pitch measurements is no longer applicable for vessels exposed to incoming waves. However, this requirement can be relaxed when employing angular velocity measurements.

The observer is written (Vik and Fossen 2001):

$$\dot{\hat{\mathbf{q}}} = \frac{1}{2}\mathbf{T}_{\hat{q}}(\hat{\mathbf{q}})\mathbf{R}(\tilde{\mathbf{q}})\left[\boldsymbol{\omega}^b_{\text{imu}} + \hat{\mathbf{b}}_{\text{gyro}} + \mathbf{K}_1\tilde{\boldsymbol{\varepsilon}_q}\,\text{sgn}(\tilde{\eta}_q)\right] - \frac{1}{2}\boldsymbol{\Xi}(\hat{\mathbf{q}})\boldsymbol{\omega}^n_{in} \tag{3.32}$$

$$\dot{\hat{\mathbf{b}}}_{\text{gyro}} = -\mathbf{T}^{-1}_{\text{gyro}}\hat{\mathbf{b}}_{\text{gyro}} + \frac{1}{2}\mathbf{K}_2\tilde{\boldsymbol{\varepsilon}}_q\,\text{sgn}(\tilde{\boldsymbol{\eta}}_q) \tag{3.33}$$

where $\hat{\mathbf{q}} \in \mathbb{H}$, is the four element unit quaternion

$$\mathbb{H}=\left\{\mathbf{q} \mid \mathbf{q}^T\mathbf{q}=1, \mathbf{q}=[\eta_q\ ,\ \boldsymbol{\varepsilon}_q^T]^T, \eta_q \in \mathbb{R}, \boldsymbol{\varepsilon}_q \in \mathbb{R}^3\right\} \tag{3.34}$$

$\boldsymbol{\omega}_{\text{imu}} \in \mathbb{R}^3$ is the angular velocity vector measured by the gyros, $\hat{\mathbf{b}}_{\text{gyro}} \in \mathbb{R}^3$ is the gyro bias, and $\boldsymbol{\omega}^n_{in} = \boldsymbol{\omega}^n_{ie} + \boldsymbol{\omega}^n_{en}$ where $\boldsymbol{\omega}^n_{ie}$ is the earth rate vector and $\boldsymbol{\omega}^n_{en}$ is the angular velocity due to the movement of the ship over the Earth. Computation of $\boldsymbol{\omega}^n_{ie}$ requires knowledge of true north. $\mathbf{T}_{\text{gyro}} \in \mathbb{R}^{3\times3}$ is a diagonal time constant matrix, and $\mathbf{K}_1 \in \mathbb{R}^{3\times3}$ and $\mathbf{K}_2 \in \mathbb{R}^{3\times3}$ are diagonal matrices. Finally,

$$\mathbf{T}_{\hat{q}}(\hat{q}) = \begin{bmatrix} -\hat{\boldsymbol{\varepsilon}}_q^T \\ \hat{\eta}_q\mathbf{I} + \mathbf{S}(\hat{\boldsymbol{\varepsilon}}_q) \end{bmatrix} \tag{3.35}$$

$$\boldsymbol{\Xi}(\hat{\mathbf{q}}) = \begin{bmatrix} -\hat{\boldsymbol{\varepsilon}}_q^T \\ \hat{\eta}_q\mathbf{I} - \mathbf{S}(\hat{\boldsymbol{\varepsilon}}_q) \end{bmatrix} \tag{3.36}$$

$\tilde{\boldsymbol{\varepsilon}}_q$ and $\tilde{\eta}_q$ are components of the quaternion error $\tilde{\mathbf{q}}$, which is computed from the estimated quaternion and a measurement quaternion derived from the accelerometer based attitude measurements (3.23)-(3.24). Since the accelerometer attitude measurement only needs to prevent the integrated gyro signal from drifting, the gains are usually chosen very small. The low gain means that horizontal accelerations have little influence on the roll and pitch measurements. Thus, these measurements can be used to compensate for the g-vector in the surge and sway acceleration measurements. Moreover, since the accelerometers are used for attitude computation, accelerometer bias will not influence the surge and sway measurements.

DGC is then carried out after (3.29), that is

$$\hat{\mathbf{a}}^b = \mathbf{y}^b_{\text{acc}} + \hat{\mathbf{R}}^b_p\mathbf{g}^p$$

where $\hat{\mathbf{R}}^b_p$ now reflects it is being calculated based on the VRU's attitude estimates $\hat{\mathbf{q}}$.

Figure 3.2 shows the measured and g-compensated acceleration in a static test using the Litton LN-200.

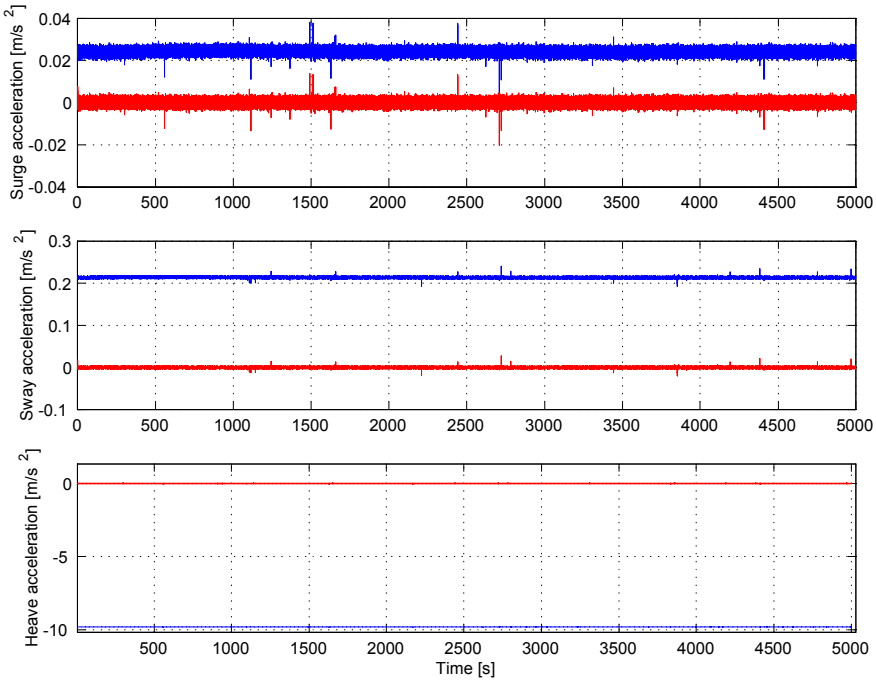

Figure 3.2: Measured and g-compensated accelerations. The noise level is about 120 μg (1σ), and the offset after compensation is a few μg on all three axes.

3.4 Positioning Control

In ship positioning, oscillatory motion caused by first order wave loads dominate the vessel's dynamic behavior. By separating the wave motion from the low-frequency dynamics, the body-fixed velocities and linear accelerations can be written as

$$\boldsymbol{\nu}^b_{nb} = \boldsymbol{\nu}^b_{LF} + \boldsymbol{\nu}^b_{WF} \tag{3.37}$$

$$\boldsymbol{\omega}^b_{nb} = \boldsymbol{\omega}^b_{LF} + \boldsymbol{\omega}^b_{WF} \tag{3.38}$$

where the subscripts now identify the low-frequency and and wave frequency parts instead of relative motion. The error-free acceleration measurement (3.16) can be written as

$$\begin{aligned} \mathbf{f}^b_{\text{imu}} &= \dot{\mathbf{v}}^b_{LF} + \dot{\mathbf{v}}^b_{WF} + \mathbf{S}(\boldsymbol{\omega}^b_{LF} + \boldsymbol{\omega}^b_{WF})\left(\mathbf{v}^b_{LF} + \mathbf{v}^b_{WF}\right) - \mathbf{R}^b_p \mathbf{g}^p \\ &= \dot{\mathbf{v}}^b_{LF} + \mathbf{S}(\boldsymbol{\omega}^b_{LF})\mathbf{v}^b_{LF} - \mathbf{R}^b_p \mathbf{g}^p + \mathbf{z}^b_{WF} \end{aligned} \tag{3.39}$$

where $\mathbf{z}_{WF}^b$ is a signal dominated by the linear wave induced motion

$$\mathbf{z}_{WF} = \mathbf{S}(\boldsymbol{\omega}_{LF}^b)\mathbf{v}_{WF}^b + \mathbf{S}(\boldsymbol{\omega}_{WF}^b)\left(\mathbf{v}_{LF}^b + \mathbf{v}_{WF}^b\right) \tag{3.40}$$

A reasonable assumption motivated by the small low-frequency velocities occurring in a positioning operation is:

A1 The Coriolis terms from the low-frequency motion can be neglected, that is

$$\mathbf{S}(\boldsymbol{\omega}_{LF}^b)\mathbf{v}_{LF}^b \approx \mathbf{0} \tag{3.41}$$

Hence, the measured acceleration can be approximated by

$$\mathbf{y}_{\text{acc}}^b \approx \dot{\mathbf{v}}_{LF}^b - \mathbf{R}_p^b \mathbf{g}^p + \mathbf{z}_{WF}^b + \boldsymbol{\Delta}_{\text{acc}} \tag{3.42}$$

which is the sum of the low-frequency acceleration, gravity contributions and some signal $\mathbf{z}_{WF}^b$ of a significantly higher frequency content than $\dot{\mathbf{v}}_{LF}^b$. Therefore, using a dynamic gravity compensator to remove $\mathbf{g}^b$ and $\boldsymbol{\Delta}_{\text{acc}}$ together with a wave filter (or observer) to remove the wave frequency components $\mathbf{z}_{WF}^b$ as depicted in Figure 3.3, it is at least in a positioning operation possible to isolate $\dot{\mathbf{v}}_{LF}^b = \dot{\boldsymbol{\nu}}_1$. Consequently, using $\dot{\boldsymbol{\nu}}_1$ in a low-speed control design is possible also without

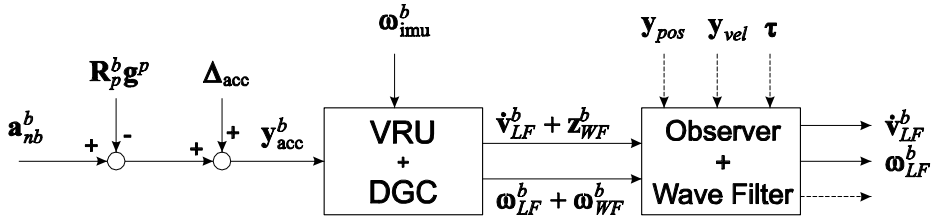

Figure 3.3: Realization of a g-compensation system and observer for reconstruction of the low-frequency body-fixed acceleration $\dot{\mathbf{v}}_{LF}^b$ and angular velocity $\boldsymbol{\omega}_{nb}^b$.

utilizing an integrated navigation system.

3.5 Conclusions

The active use of negative acceleration feedback has been briefly introduced by regarding it as a change of the system's mass. In order to utilize measured linear accelerations on surface vessels, some kind of dynamic compensation or preprocessing has to be performed in order to relate the measurement to the b-frame. By separating the low freqency motion from the wave induced motion (of relative high freqency content), it was demonstrated that a particular VRU with gravity compensation serves this purpose well as long as the vessel itself operates at low speed.

Chapter 4

Observer Design

4.1 Introduction

An observer filters available measurements to provide online estimates of the measured and unmeasured states within a system. In ship control, the most commonly needed states are the low-frequency (LF) parts of the positions, the heading, the velocities and stationary (or slowly varying) disturbances due to wind, ocean current and nonlinear wave effects. Based on those estimated states, the controller calculates its thrust demand. The three main objectives for the observer are:

- *State estimation:* To produce the state estimates from which the controller calculates its desired propeller thrust forces and moments.
- *Wave filtering:* The estimator should attenuate the fast, oscillatory motion due to first-order wave loads. It is useless trying to compensate this sinusoidal (zero mean) behavior, and doing so will only lead to excessive thruster system wear.
- *Handling dead-reckoning*: In the case of temporary sensor failure, the observer must for a period of time be able to adequately predict the motion of the ship such that the positioning operation can continue. This is a system redundancy requirement which is mandatory with the classification societies (Det Norske Veritas 1990).

The third objective implies that some kind of model based filter must be implemented.

Classic solutions to the DP problem of surface vessels are output-feedback designs using a state-estimator to filter out 1st-order wave induced motion from the LF positions while reconstructing LF velocities (Balchen *et al.* 1976, Balchen *et al.* 1980, Sælid *et al.* 1983, Grimble *et al.* 1980, Fung and Grimble 1983, Sørensen *et al.* 1996). All these were realized using linear stochastic theory (Kalman Filters),

but also $\mathcal{H}_\infty$-solutions been proposed (Katebi *et al.* 1997). Unfortunately, the linearization of the nonlinear kinematics implies that the results are only valid locally. However, if the nonlinearities satisfy a global Lipschitz-condition, a modification (Reif *et al.* 1999) of the extended Kalman filter ensures global exponential stability. Another approach with comparable performance is to utilize the model structure and let the observer "linearize" itself about the measured compass heading. As opposed to traditional extended Kalman-filters, the on-line explicit linearization is avoided, and global stability properties are more easily established since the nonlinear kinematics can be treated as a known time-varying block. Examples are the passivation designs (Fossen and Strand 1999, Strand and Fossen 1999), further extensions to higher order monotonic damping terms (Aamo *et al.* 2001), and non-dissipative linear damping terms (Lindegaard and Fossen 2001*b*).

As discussed previously, using the measured accelerations, we are able to better keep up with unmodeled disturbances like slowly varying wave forces which must be counteracted by the control system. Slowly varying wave induced forces is a phenomenon well known from nonlinear hydrodynamic theory (Faltinsen 1990), yet they are difficult to express in a form suited for controller design. However, feeding the measured accelerations uncritically into the closed loop system is not recommended due to the high-frequency, large amplitude oscillations caused by 1st-order wave loads. Therefore, some kind of notch filtering of the measured accelerations is required in order to remove the wave frequency components.

In this chapter we focus on extending the proven observer structure from Fossen and Strand (1999). More specifically, the contributions are:

- Identification of structural conditions unifying linear and nonlinear observer design for surface vessel at low speed: If some structural constraints are satisfied, the nonlinear kinematics can be disregarded in the stability analysis and linear design tools may be applied. While previous nonlinear observer designs either assumed a passive, and thus stable, vessel-fixed dynamics (Fossen and Grøvlen 1998, Fossen and Strand 1999, Strand and Fossen 1999, Loría *et al.* 2000, Aamo *et al.* 2001) or prescribed using non-diagonal observer gain matrices to handle the possibly unstable sway-yaw dynamics (Robertsson and Johansson 1998), we show that one can obtain uniform global exponential stability of the observer errors for all kinds of vessels using fixed, diagonal observer gains.
- Optional inclusion of velocity and acceleration measurements.

Common for all previously mentioned designs is that they are derived under the assumption that only the positions and compass heading were available for feedback. Today high performance inertial measurement units (IMU) are becoming increasingly affordable, and integrated navigation systems (INS) integrating IMU and GPS reproduce not only positions but also velocities and linear accelerations with great accuracy to a reasonable price. This development in sensor technology is reflected in the proposed designs.

Two different observers will be analyzed:

1. The first observer (Lindegaard and Fossen 2001*a*, Lindegaard and Fossen 2001*b*) contains one single wave model generating accelerations, velocities and positions. It requires position measurements, and the structure allows the inclusion of velocity and acceleration. Without acceleration measurements the resulting error dynamics is shown to be UGES provided that the wave model and selected observer gains satisfy the structural properties. With accelerations, a specific bound on the yaw rate $\dot{\psi}$ must be imposed and uniform *semi-global* exponential stability (USGES) can be guaranteed.

2. In the second observer (Lindegaard *et al.* 2002) the wave models for acceleration, velocity and position and treated as separate phenomena. This facilitates the tuning procedure significantly, and a particular tuning procedure based on pole placement is proposed. A similar structural constraint as for the first observer must also be assumed in this case, and USGES of the error dynamics is shown.

4.2 Common Model Description

The two observers are quite similar, the main difference between the two being in the implementation of the wave model used to filter out first order wave motion. This section discusses the LF model description used in both designs.

We consider the dynamics of a vessel in three degrees of freedom, the horizontal plane, and we choose to express the model in the Earth- and body-fixed coordinate frames. The body-fixed frame coincides with the principal axes of the vessel and it is rotated an angle ψ_y with respect to the Earth-fixed frame. This transformation of coordinates is represented by the orthogonal rotation matrix

$$\mathbf{R}(\psi_y) = \begin{bmatrix} \cos\psi_y & -\sin\psi_y & 0 \\ \sin\psi_y & \cos\psi_y & 0 \\ 0 & 0 & 1 \end{bmatrix} \tag{4.1}$$

and its time-derivative is $\dot{\mathbf{R}}(\alpha) \stackrel{\triangle}{=} \frac{d}{dt}(\mathbf{R}(\alpha)) = \dot{\alpha}\mathbf{S}\mathbf{R}(\alpha)$ where the skew-symmetric matrix $\mathbf{S} = -\mathbf{S}^T$ is given by

$$\mathbf{S} = \begin{bmatrix} 0 & -1 & 0 \\ 1 & 0 & 0 \\ 0 & 0 & 0 \end{bmatrix} \tag{4.2}$$

Let $\boldsymbol{\eta} = [x, y, \psi]^T$ be the LF position vector where x and y are the North and East positions respectively, and ψ being the LF heading. $\boldsymbol{\nu} = [u, v, r]^T$ contains the LF body-fixed velocities, i.e. surge, sway, and yaw. The LF ship model is assumed to satisfy:

A1 The orientation angle between the Earth-fixed and body-fixed frame is the

measured heading ψ_y such that:

$$\begin{aligned} \dot{\boldsymbol{\eta}} &= \mathbf{R}(\psi_y)\boldsymbol{\nu} \\ \dot{\mathbf{b}} &= -\mathbf{T}_b^{-1}\mathbf{b} + \mathbf{E}_b\mathbf{w}_b \\ \mathbf{M}\dot{\boldsymbol{\nu}} &= -\mathbf{G}\mathbf{R}^T(\psi_y)\boldsymbol{\eta} - \mathbf{D}\boldsymbol{\nu} + \boldsymbol{\tau} + \mathbf{R}^T(\psi_y)\mathbf{b} \end{aligned} \tag{4.3}$$

Here $\boldsymbol{\tau} \in \mathbb{R}^3$ is the applied thruster force, $\mathbf{M} = \mathbf{M}^T > 0$ is the sum of rigid body mass and hydrodynamic added mass, $\mathbf{D} \in \mathbb{R}^{3\times3}$ contains linear damping coefficients and $\mathbf{G} \in \mathbb{R}^{3\times3}$ describes the mooring forces. The bias forces $\mathbf{b} \in \mathbb{R}^3$ are modelled as Markov processes with a positive semi-definite diagonal matrix $\mathbf{T}_b \in \mathbb{R}^{3\times3}$ of time constants. $\mathbf{w}_b \in \mathbb{R}^3$ is a bounded disturbance signal, and $\mathbf{E}_b \in \mathbb{R}^{3\times3}$ is a gain factor.

In the following we will frequently utilize a commutation property between the Earth-fixed parameters and the rotation $\mathbf{R}(\alpha)$.

Property 4.1 *A matrix $\mathbf{A} \in \mathbb{R}^{3\times3}$ is said to* commute *with the rotation $\mathbf{R}(\alpha)$ if*

$$\mathbf{A}\mathbf{R}(\alpha) = \mathbf{R}(\alpha)\mathbf{A} \tag{4.4}$$

Examples of matrices $\mathbf{A}$ satisfying Property 4.1 are linear combinations $\mathbf{A} = a_1\mathbf{R}(\theta) + a_2\mathbf{I} + a_3\mathbf{k}^T\mathbf{k}$ for scalars a_i, θ and $\mathbf{k} = [0,0,1]^T$, the axis of rotation. Also note that since $\mathbf{R}(\alpha)$ is orthogonal, that is $\mathbf{R}^T(\alpha) = \mathbf{R}^{-1}(\alpha)$, Property 4.1 implies that

$$\mathbf{A} = \mathbf{R}^T(\alpha)\mathbf{A}\mathbf{R}(\alpha) = \mathbf{R}(\alpha)\mathbf{A}\mathbf{R}^T(\alpha) \tag{4.5}$$

Furthermore, if $\mathbf{A}$ is nonsingular, $\mathbf{A}^{-1}$ commutes with $\mathbf{R}(\alpha)$ too. That is

$$\mathbf{A}\mathbf{R}(\alpha) = \mathbf{R}(\alpha)\mathbf{A} \quad \overset{\mathbf{A} \text{ is nonsingular}}{\Longleftrightarrow} \quad \mathbf{A}^{-1}\mathbf{R}(\alpha) = \mathbf{R}(\alpha)\mathbf{A}^{-1} \tag{4.6}$$

4.3 Observer With Consistent Wave Model

In Section 4.3.1 below we describe the vessel model and some of its properties with attention given to how the individual measurements fit into the model framework. Section 4.3.2 concerns the filter design and stability analysis. An important part of this section is the discussion regarding structural properties: The structure of gain matrices updating the Earth-fixed error dynamics can not be selected arbitrarily. Section 4.3.3 presents some conclusions and remarks.

4.3.1 Complete Ship and Environment Models

The LF model is described by (4.3). Now, let $\mathbf{x}_w \in \mathbb{R}^{3n_w}$ describe the first order wave-induced motion where n_w denotes the number of states used to describe the wave frequency motion in each degree of freedom (DOF). Here we let the

WF model be expressed entirely in the Earth-fixed frame, and in accordance with Fossen and Strand (1999), we employ a linear wave model on the form

$$\dot{\mathbf{x}}_w = \mathbf{A}_w \mathbf{x}_w + \mathbf{E}_w \mathbf{w}_w \tag{4.7}$$

where $\mathbf{A}_w$ is assumed Hurwitz, $\mathbf{E}_w \in \mathbb{R}^{3n_w \times 3}$ is a gain matrix, and $\mathbf{w}_w \in \mathbb{R}^3$ is a zero-mean, bounded disturbance input. In a Kalman filter setting $\mathbf{w}_w$ should be a white, Gaussian process. We are ready to impose two additional model assumptions:

A2a For $\mathbf{D} = \{d_{ij}\} \quad i, j = 1, \cdots, 3$, the elements $d_{11}, d_{22} > 0$.

A3a The bias time constant matrix $\mathbf{T}_b$ and each 3×3 sub-block of $\mathbf{A}_w$ satisfies Property 4.1.

Note in Assumption A2a that there are no restrictions on neither d_{23}, d_{32} nor d_{33}. A2a is thus less restrictive than assuming $\mathbf{D} + \mathbf{D}^T > 0$ (Fossen and Strand 1999) and its interpretation is that separate surge and sway motions are dissipative. It does, however, include cases with potentially unstable sway/yaw dynamics (Robertsson and Johansson 1998). The last assumption, A3a, implies that the mean wave motion period, relative damping, and bias time constants in the North and East directions are identical. It should be emphasized that this is not as restrictive as it may sound since the dominating frequency of the first order wave induced motions will be approximately the same in surge and sway.

First Order Wave Motion

A suitable linear representation of the oscillatory motion caused by the 1st-order wave loads can be approximated by a set of three de-coupled linear transfer functions

$$h(s) = \frac{k_{wi} s}{\left(s^2 + 2\zeta_i \omega_{0i} s + \omega_{0i}^2\right)^2} \tag{4.8}$$

in each of the 3 DOF. The motivation for using a function of fourth order instead of other approximations, is that this choice ensures that the transfer functions between the excitation and positions, velocities as well as accelerations, will be strictly proper.

A minimal realization with $\mathbf{x}_w \in \mathbb{R}^{12}$ can in state-space be described by

$$\dot{\mathbf{x}}_w = \mathbf{A}_w \mathbf{x}_w + \mathbf{E}_w \mathbf{w}_w \tag{4.9}$$

$$\mathbf{A}_w = \begin{bmatrix} \mathbf{0} & \mathbf{I} & \mathbf{0} & \mathbf{0} \\ -\mathbf{\Omega} & -\mathbf{\Lambda} & \mathbf{0} & \mathbf{I} \\ \mathbf{0} & \mathbf{0} & \mathbf{0} & \mathbf{I} \\ \mathbf{0} & \mathbf{0} & -\mathbf{\Omega} & -\mathbf{\Lambda} \end{bmatrix}, \quad \mathbf{E}_w = \begin{bmatrix} \mathbf{0} \\ \mathbf{0} \\ \mathbf{0} \\ \mathrm{diag}\,(\mathbf{k}_w) \end{bmatrix}$$

where Ω and $\mathbf{\Lambda}$ are diagonal matrices holding the the wave motion resonance frequencies ω_{oi} and relative damping factors ζ_i, $i = 1, \cdots, 3$ for the North, East

and heading respectively like this

$$\mathbf{\Omega} = \text{diag}(\omega_{01}^2, \omega_{02}^2, \omega_{03}^2) \tag{4.10}$$
$$\mathbf{\Lambda} = \text{diag}(2\zeta_1\omega_{01}, 2\zeta_2\omega_{02}, 2\zeta_3\omega_{03}) \tag{4.11}$$

and $\mathbf{k}_w = [k_{w1}, k_{w2}, k_{w3}]^T$ is a gain vector. Assumption A3 requires $\omega_{01} = \omega_{02}$ and $\zeta_1 = \zeta_2$. The Earth-fixed wave induced position, velocity and acceleration can be extracted from $\mathbf{x}_w$ as follows

$$\mathbf{p}_w = \mathbf{C}_p\mathbf{x}_w, \quad \mathbf{v}_w = \mathbf{C}_v\mathbf{x}_w, \quad \mathbf{a}_w = \mathbf{C}_a\mathbf{x}_w \tag{4.12}$$

where $\mathbf{C}_p, \mathbf{C}_v, \mathbf{C}_a \in \mathbb{R}^{3\times 12}$

$$\mathbf{C}_p = \begin{bmatrix} \mathbf{I} & \mathbf{0} & \mathbf{0} & \mathbf{0} \end{bmatrix} \tag{4.13}$$
$$\mathbf{C}_v = \begin{bmatrix} \mathbf{0} & \mathbf{I} & \mathbf{0} & \mathbf{0} \end{bmatrix} \tag{4.14}$$
$$\mathbf{C}_a = \begin{bmatrix} -\mathbf{\Omega} & -\mathbf{\Lambda} & \mathbf{0} & \mathbf{I} \end{bmatrix} \tag{4.15}$$

Since $\frac{d}{dt}\left(\mathbf{R}^T\mathbf{v}_w\right) = \frac{d}{dt}\left(\mathbf{R}^T\right)\mathbf{v}_w + \mathbf{R}^T\dot{\mathbf{v}}_w = -\dot{\psi}_y\mathbf{R}^T\mathbf{S}\mathbf{v}_w + \mathbf{R}^T\mathbf{a}_w$, the experienced wave induced velocities and accelerations will in the body frame be given as

$$\mathbf{v}_w^b = \mathbf{R}^T(\psi_y)\mathbf{v}_w = \mathbf{R}^T(\psi_y)\mathbf{C}_v\mathbf{x}_w \tag{4.16}$$
$$\mathbf{a}_w^b = \mathbf{R}^T(\psi_y)\left(\mathbf{C}_a - \dot{\psi}_y\mathbf{S}\mathbf{C}_v\right)\mathbf{x}_w \tag{4.17}$$

The acceleration term depending on measured rotation rate $r_y = \dot{\psi}_y$ can be regarded as a Coriolis-like term.

Collect the Earth-fixed states in $\mathbf{x}_1 \in \mathbb{R}^{6+3n_w}$ and the body-fixed in $\mathbf{x}_2 \in \mathbb{R}^3$

$$\mathbf{x}_1 = \begin{bmatrix} \mathbf{x}_w^T & \boldsymbol{\eta}^T & \mathbf{b}^T \end{bmatrix}^T \tag{4.18}$$
$$\mathbf{x}_2 = \boldsymbol{\nu} \tag{4.19}$$

and define the block diagonal transformation matrix

$$\mathbf{T}(\psi_y) = \text{Diag}(\mathbf{R}^T\left(\psi_y\right), \cdots, \mathbf{R}^T\left(\psi_y\right), \mathbf{I}) \tag{4.20}$$

On compact form using Assumption A3 we get with $\mathbf{x} = [\mathbf{x}_1^T, \mathbf{x}_2^T]^T$ and $\mathbf{w} = [\mathbf{w}_w^T, \mathbf{w}_b^T]^T$

$$\dot{\mathbf{x}} = \mathbf{T}^T(\psi_y)\mathbf{A}\mathbf{T}(\psi_y)\mathbf{x} + \mathbf{B}\boldsymbol{\tau} + \mathbf{E}\mathbf{w} \tag{4.21}$$

where

$$\mathbf{A} = \begin{bmatrix} \mathbf{A}_w & \mathbf{0} & \mathbf{0} & \mathbf{0} \\ \mathbf{0} & \mathbf{0} & \mathbf{0} & \mathbf{I} \\ \mathbf{0} & \mathbf{0} & -\mathbf{T}_b^{-1} & \mathbf{0} \\ \mathbf{0} & -\mathbf{M}^{-1}\mathbf{G} & \mathbf{M}^{-1} & -\mathbf{M}^{-1}\mathbf{D} \end{bmatrix} \tag{4.22}$$

$$\mathbf{B} = \begin{bmatrix} \mathbf{0} \\ \mathbf{0} \\ \mathbf{0} \\ \mathbf{M}^{-1} \end{bmatrix}, \quad \mathbf{E} = \begin{bmatrix} \mathbf{E}_w & \mathbf{0} \\ \mathbf{0} & \mathbf{0} \\ \mathbf{0} & \mathbf{E}_b \\ \mathbf{0} & \mathbf{0} \end{bmatrix} \tag{4.23}$$

Measurements

We intend to cover all combinations of position, velocity and acceleration measurements. The positions are usually given in an Earth-fixed reference frame, while velocities and accelerations are given in a body-fixed coordinate system.

There might be cases where not all kinds of measurements are available, either due to sensor failure, or simply because that particular vessel was not equipped with that kind of instrument. Denote the measurements $\mathbf{y}$. We have that $\mathbf{y} \in \mathbb{R}^{n_y}$ where $3 \leq n_y \leq 8$ depending on the configuration. Define $\boldsymbol{\Upsilon}_2$ and $\boldsymbol{\Upsilon}_3$ as the projections extracting the measured velocities and accelerations respectively from the actual three DOF velocity and accelerations vectors. It is possible to measure all three velocities pretty accurately, which means that quite often $\boldsymbol{\Upsilon}_2 = \mathbf{I}$. While linear accelerations are easy to measure, the angular acceleration is not. Therefore, most likely only the accelerations in surge and sway are available and hence $n_{y_3} = 2$ and

$$\boldsymbol{\Upsilon}_3 = \begin{bmatrix} 1 & 0 & 0 \\ 0 & 1 & 0 \end{bmatrix} \tag{4.24}$$

Let $\mathbf{y}_1 \in \mathbb{R}^3$ contain the Earth-fixed positions and compass heading, $\mathbf{y}_2 \in \mathbb{R}^{n_{y_2}}$ the vessel-fixed velocities and $\mathbf{y}_3 \in \mathbb{R}^{n_{y_3}}$ accelerations. Then,

$$\begin{aligned}
\mathbf{y}_1 &= \boldsymbol{\eta} + \boldsymbol{\eta}_w = \boldsymbol{\eta} + \mathbf{C}_p \mathbf{x}_w && (4.25)\\
\mathbf{y}_2 &= \boldsymbol{\Upsilon}_2 \left(\boldsymbol{\nu} + \mathbf{R}^T \mathbf{C}_v \mathbf{x}_w \right) && (4.26)\\
\mathbf{y}_3 &= \boldsymbol{\Upsilon}_3 \left(\dot{\boldsymbol{\nu}} + \mathbf{a}_w^b \right) \\
&= \boldsymbol{\Upsilon}_3 \mathbf{M}^{-1} \left(-\mathbf{G}\mathbf{R}^T \boldsymbol{\eta} + \mathbf{R}^T \mathbf{b} - \mathbf{D}\boldsymbol{\nu} \right) + \boldsymbol{\Upsilon}_3 \mathbf{R}^T \left(\mathbf{C}_a - \dot{\psi}_y \mathbf{S}\mathbf{C}_v \right) \mathbf{x}_w && (4.27)
\end{aligned}$$

Compactly written

$$\mathbf{y} = \mathbf{C}_y(\psi_y, \dot{\psi}_y)\mathbf{x} + \mathbf{D}_y \boldsymbol{\tau} \tag{4.28}$$

where

$$\mathbf{C}_y(\psi_y, \dot{\psi}_y) = \begin{bmatrix} \mathbf{C}_p & \mathbf{I} & & \\ \boldsymbol{\Upsilon}_2 \mathbf{C}_v \mathbf{R}^T(\psi_y) & \mathbf{0} & & \\ \boldsymbol{\Upsilon}_3 (\mathbf{C}_a - \dot{\psi}_y \mathbf{S}\mathbf{C}_v) \mathbf{R}^T(\psi_y) & -\boldsymbol{\Upsilon}_3 \mathbf{M}^{-1} \mathbf{G} \mathbf{R}^T(\psi_y) & & \\ & & \mathbf{0} & \mathbf{0} \\ & & \mathbf{0} & \boldsymbol{\Upsilon}_2 \\ & & \boldsymbol{\Upsilon}_3 \mathbf{M}^{-1} \mathbf{R}^T(\psi_y) & -\boldsymbol{\Upsilon}_3 \mathbf{M}^{-1} \mathbf{D} \end{bmatrix}$$

$$\mathbf{D}_y = \begin{bmatrix} \mathbf{0} & \mathbf{0} & \mathbf{M}^{-T} \boldsymbol{\Upsilon}_3^T \end{bmatrix}^T \tag{4.30}$$

When only positions are available, $n_{y_2} = n_{y_3} = 0$, the model is reduced to the traditional DP observer problem.

In the stability analysis below it will be convenient to make an assumption on how the velocity and acceleration feedback is configured:

A4a Let $\boldsymbol{\Pi}_i = \boldsymbol{\Upsilon}_i^T \boldsymbol{\Upsilon}_i \in \mathbb{R}^{3\times 3}$, $i = 2, 3$. Valid configurations are those which allow $\boldsymbol{\Pi}_i$ to commute with $\mathbf{R}(\alpha)$, that is $\mathbf{R}(\alpha)\boldsymbol{\Pi}_i = \boldsymbol{\Pi}_i \mathbf{R}(\alpha)$ for all $\alpha \in \mathbb{R}$.

Objective

For the model (4.21) with output (4.28)-(4.30), under Assumptions A1, A2a, and A3a, we seek a deterministic, model based observer that is exponentially stable for all possible sensor combinations satisfying Assumption A4a.

4.3.2 Observer Design

By copying the system dynamics (4.21), the following observer is proposed:

$$\dot{\hat{\mathbf{x}}} = \mathbf{T}^T(\psi_y)\mathbf{A}\mathbf{T}(\psi_y)\hat{\mathbf{x}} + \mathbf{K}(\psi_y)\tilde{\mathbf{y}} \tag{4.31}$$

The estimated output is

$$\hat{\mathbf{y}} = \mathbf{C}_y(\psi_y, \dot{\psi}_y)\hat{\mathbf{x}} + \mathbf{D}_y\boldsymbol{\tau} \tag{4.32}$$

and hence when the estimation error is $\tilde{\mathbf{x}} = \mathbf{x} - \hat{\mathbf{x}}$,

$$\tilde{\mathbf{y}} = \mathbf{y} - \hat{\mathbf{y}} = \mathbf{C}_y(\psi_y, \dot{\psi}_y)\tilde{\mathbf{x}} \tag{4.33}$$

Although it somewhat restricts the flexibility, we suggest not to update the Earth-fixed estimates from the acceleration error $\tilde{\mathbf{y}}_3$ at this stage, because this would introduce transmission zeros. Therefore, this particular observer gain matrix $\mathbf{K}(\psi_y)$ with constant $\mathbf{K}_{1i} \in \mathbb{R}^{12\times 3}$, $\mathbf{K}_{2i} \in \mathbb{R}^{3\times 3}$, $\mathbf{K}_{3i} \in \mathbb{R}^{3\times 3}$ and $\mathbf{K}_{4i} \in \mathbb{R}^{3\times 3}$ is suggested

$$\mathbf{K}(\psi_y) = \begin{bmatrix} \mathbf{K}_{11} & \mathbf{K}_{12}\mathbf{R}(\psi_y)\boldsymbol{\Upsilon}_2^T & \mathbf{0} \\ \mathbf{K}_{21} & \mathbf{K}_{22}\mathbf{R}(\psi_y)\boldsymbol{\Upsilon}_2^T & \mathbf{0} \\ \mathbf{K}_{31} & \mathbf{K}_{32}\mathbf{R}(\psi_y)\boldsymbol{\Upsilon}_2^T & \mathbf{0} \\ \mathbf{K}_{41}\mathbf{R}^T(\psi_y) & \mathbf{K}_{42}\boldsymbol{\Upsilon}_2^T & \mathbf{K}_{43}\boldsymbol{\Upsilon}_3^T \end{bmatrix} \tag{4.34}$$

where the following assumption is made:

A5 Each 3×3 sub-block of the gain matrices $\mathbf{K}_{ji}$, $1 \leq j \leq 3$, $i = 1, 2$ commute with $\mathbf{R}(\alpha)$.

This implies that the gains in North and East must be identical. The body-fixed gain matrices $\mathbf{K}_{4i}$, $1 \leq i \leq 3$ can, however, be selected freely.

Error Dynamics

Since ψ_y is measured and the constant parameter matrix $\mathbf{A}$ is assumed known, we obtain:

$$\dot{\tilde{\mathbf{x}}} = \mathbf{T}^T(\psi_y)\mathbf{A}\mathbf{T}(\psi_y)\tilde{\mathbf{x}} - \mathbf{K}(\psi_y)\mathbf{C}_y(\psi_y, \dot{\psi}_y)\tilde{\mathbf{x}} \tag{4.35}$$

which can be written:

$$\dot{\tilde{\mathbf{x}}} = \mathbf{T}^T(\psi_y)\mathbf{A}_o(\dot{\psi}_y)\mathbf{T}(\psi_y)\tilde{\mathbf{x}} \tag{4.36}$$

Assumptions A3a, A4a, and A5 are sufficient requirements for this. Moreover, it can be shown that the resulting $\mathbf{A}_o$ can be written as

$$\mathbf{A}_o(\dot{\psi}_y) = \mathbf{A}_0 + \dot{\psi}_y \mathbf{A}_1 \tag{4.37}$$

$$\mathbf{A}_0 = \begin{bmatrix} \mathbf{A}_{0,11} & \mathbf{A}_{0,12} \\ \mathbf{A}_{0,21} & \mathbf{A}_{0,22} \end{bmatrix} \qquad \mathbf{A}_1 = \begin{bmatrix} \mathbf{0} & \mathbf{0} \\ \mathbf{A}_{1,21} & \mathbf{0} \end{bmatrix} \tag{4.38}$$

where $\mathbf{A}_{0,11} \in \mathbb{R}^{18\times 18}$, $\mathbf{A}_{0,12} \in \mathbb{R}^{18\times 3}$, $\mathbf{A}_{0,21} \in \mathbb{R}^{3\times 18}$, $\mathbf{A}_{0,22} \in \mathbb{R}^{3\times 3}$ and $\mathbf{A}_{1,21} \in \mathbb{R}^{3\times 18}$. Denote $\bar{\mathbf{K}}_{43} = \mathbf{I} - \mathbf{K}_{43}\mathbf{\Pi}_3$ such that $\mathbf{K}_{43}\mathbf{\Pi}_3 = \mathbf{I} - \bar{\mathbf{K}}_{43}$. Then:

$$\mathbf{A}_{0,11} = \begin{bmatrix} \mathbf{A}_w - \mathbf{K}_{11}\mathbf{C}_p - \mathbf{K}_{12}\mathbf{\Pi}_2\mathbf{C}_v & -\mathbf{K}_{11} & \mathbf{0} \\ -\mathbf{K}_{21}\mathbf{C}_p - \mathbf{K}_{22}\mathbf{\Pi}_2\mathbf{C}_v & -\mathbf{K}_{21} & \mathbf{0} \\ -\mathbf{K}_{31}\mathbf{C}_p - \mathbf{K}_{32}\mathbf{\Pi}_2\mathbf{C}_v & -\mathbf{K}_{31} & -\mathbf{T}_b^{-1} \end{bmatrix} \tag{4.39}$$

$$\mathbf{A}_{0,12} = \begin{bmatrix} -\mathbf{K}_{12}\mathbf{\Pi}_2 \\ \mathbf{I} - \mathbf{K}_{22}\mathbf{\Pi}_2 \\ -\mathbf{K}_{32}\mathbf{\Pi}_2 \end{bmatrix} \tag{4.40}$$

$$\mathbf{A}_{0,21} = \begin{bmatrix} -\left(\mathbf{K}_{41}\mathbf{C}_p + \mathbf{K}_{42}\mathbf{\Pi}_2\mathbf{C}_v + \left(\mathbf{I} - \bar{\mathbf{K}}_{43}\right)\mathbf{C}_a\right)^T \\ -\left(\mathbf{K}_{41} + \bar{\mathbf{K}}_{43}\mathbf{M}^{-1}\mathbf{G}\right)^T \\ -\left(\bar{\mathbf{K}}_{43}\mathbf{M}^{-1}\right)^T \end{bmatrix}^T \tag{4.41}$$

$$\mathbf{A}_{0,22} = \left[-\mathbf{K}_{42}\mathbf{\Pi}_2 - \bar{\mathbf{K}}_{43}\mathbf{M}^{-1}\mathbf{D}\right] \tag{4.42}$$

$$\mathbf{A}_{1,21} = \left(\mathbf{I} - \bar{\mathbf{K}}_{43}\right)\mathbf{S}\mathbf{C}_v \tag{4.43}$$

Stability Analysis

The form of the observer error dynamics (4.36) is very attractive because the known transformation $\mathbf{T}(\psi_y)$ can be eliminated from the analysis when Assumptions A3-A5 are employed. Although the eigenvalues of $\mathbf{T}^T\mathbf{A}_o(\dot{\psi}_y)\mathbf{T}$ are identical to the ones of $\mathbf{A}_o(\dot{\psi}_y)$ since $\mathbf{T}^T(s) = \mathbf{T}^{-1}(s)$ for all s, $\mathrm{Re}(\lambda_i(\mathbf{T}^T\mathbf{A}_o\mathbf{T})) < 0 \quad \forall \psi_y$ if and only if $\mathbf{A}_o$ is Hurwitz. In general, an eigenvalue analysis of a linear time-varying system will not be sufficient to prove stability (Khalil 1996). We have to find a Lyapunov function candidate to conclude on that.

The idea is to analyze the error-dynamics in the vessel-fixed coordinate system and selecting a quadratic Lyapunov function candidate $V = \mathbf{z}^T\mathbf{P}\mathbf{z}$ where the $\mathbf{P}$-matrix also satisfies some structural constraints. The following lemma will be useful in that respect (Lindegaard and Fossen 2001*b*).

Lemma 4.1 *Linear time-varying systems on the form*

$$\dot{\boldsymbol{\xi}}_1 = \bar{\mathbf{A}}_{11}\boldsymbol{\xi}_1 + \mathbf{H}(\phi)\bar{\mathbf{A}}_{12}\boldsymbol{\xi}_2 \tag{4.44a}$$

$$\dot{\boldsymbol{\xi}}_2 = \bar{\mathbf{A}}_{21}\mathbf{H}^T(\phi)\boldsymbol{\xi}_1 + \bar{\mathbf{A}}_{22}\boldsymbol{\xi}_2 \tag{4.44b}$$

$\boldsymbol{\xi}_1 \in \mathbb{R}^{n_1}$, $\boldsymbol{\xi}_2 \in \mathbb{R}^{n_2}$ *interconnected by a rotation* $\mathbf{H} : \mathbb{R} \to \mathbb{R}^{n_1 \times n_1}$ *and where* $\phi : \mathbb{R}_{\geq 0} \to \mathbb{R}$ *is a known signal and*

$$\bar{\mathbf{A}}_{11} = \mathbf{H}\bar{\mathbf{A}}_{11}\mathbf{H}^T \tag{4.45}$$

are uniformly globally exponentially stable (UGES) if there for a $\mathbf{Q} = \mathbf{Q}^T > 0$ *exists a structurally constrained* $\mathbf{P} = \mathbf{P}^T > 0$

$$\mathbf{P} = \begin{bmatrix} \mathbf{P}_{11} & \mathbf{P}_{12} \\ \mathbf{P}_{12}^T & \mathbf{P}_{22} \end{bmatrix} \quad , \quad \begin{aligned} \mathbf{P}_{11}\dot{\mathbf{H}}^T\mathbf{H} &= -\mathbf{H}^T\dot{\mathbf{H}}\mathbf{P}_{11} \\ \mathbf{H}^T\dot{\mathbf{H}}\mathbf{P}_{12} &= \mathbf{0} \end{aligned} \tag{4.46}$$

such that

$$\mathbf{P}\bar{\mathbf{A}} + \bar{\mathbf{A}}^T\mathbf{P} \leq -\mathbf{Q} \tag{4.47}$$

where $\bar{\mathbf{A}}$ *is the system matrix*

$$\bar{\mathbf{A}} = \begin{bmatrix} \bar{\mathbf{A}}_{11} & \bar{\mathbf{A}}_{12} \\ \bar{\mathbf{A}}_{21} & \bar{\mathbf{A}}_{22} \end{bmatrix} \tag{4.48}$$

The system matrix $\bar{\mathbf{A}}$ must be Hurwitz, otherwise no such $\mathbf{P}$ can be found.

Proof. Define $\boldsymbol{\xi} = [\boldsymbol{\xi}_1^T, \boldsymbol{\xi}_2^T]^T$. Because of the structural constrains (4.45) on $\bar{\mathbf{A}}_{11}$ we may write

$$\dot{\boldsymbol{\xi}} = \mathbf{T}^T(\phi)\bar{\mathbf{A}}\mathbf{T}(\phi)\boldsymbol{\xi} \tag{4.49}$$

where

$$\mathbf{T}(\phi) = \begin{bmatrix} \mathbf{H}^T(\phi) & \mathbf{0} \\ \mathbf{0} & \mathbf{I} \end{bmatrix} \tag{4.50}$$

Define $\mathbf{z} = \mathbf{T}(\phi)\boldsymbol{\xi}$. Since $\mathbf{H}^T(\phi)$ is a rotation, $|\mathbf{z}| = |\boldsymbol{\xi}|$. Now, abusing the notation slightly, $\dot{\mathbf{T}}(\phi) = \frac{d}{dt}(\mathbf{T}(\phi))$, we get

$$\begin{aligned} \dot{\mathbf{z}} &= \dot{\mathbf{T}}(\phi)\boldsymbol{\xi} + \mathbf{T}(\phi)\dot{\boldsymbol{\xi}} = \left(\dot{\mathbf{T}}(\phi) + \bar{\mathbf{A}}\mathbf{T}(\phi)\right)\boldsymbol{\xi} \\ &= \left(\dot{\mathbf{T}}(\phi)\mathbf{T}^T(\phi) + \bar{\mathbf{A}}\right)\mathbf{z} \end{aligned} \tag{4.51}$$

such that differentiating $V = \mathbf{z}^T\mathbf{P}\mathbf{z}$ along the trajectories yields

$$\begin{aligned} \dot{V} &= \mathbf{z}^T\mathbf{P}\dot{\mathbf{z}} + \mathbf{z}^T\mathbf{P}\dot{\mathbf{z}} \\ &= \mathbf{z}^T\left(\mathbf{P}\bar{\mathbf{A}} + \bar{\mathbf{A}}^T\mathbf{P}\right)\mathbf{z} + \mathbf{z}^T\left(\mathbf{P}\dot{\mathbf{T}}\mathbf{T}^T + \mathbf{T}\dot{\mathbf{T}}^T\mathbf{P}\right)\mathbf{z} \\ &\leq -\mathbf{z}^T\mathbf{Q}\mathbf{z} + \mathbf{z}^T\left(\mathbf{P}\dot{\mathbf{T}}\mathbf{T}^T + \mathbf{T}\dot{\mathbf{T}}^T\mathbf{P}\right)\mathbf{z} \end{aligned} \tag{4.52}$$

The structural constraints on $\mathbf{P}$ imply that the last term is zero and thus UGES is proven. ■

Even though this lemma indeed provides sufficient conditions for the elimination of the kinematics term and the dependence on the varying signal ψ_y, we still have to deal with the time-varying signal $\dot{\psi}_y$. Physically $\dot{\psi}_y$ describes the yaw rate of the vessel, and intuitively this quantity will be bounded even when exposed to incoming waves provided that the applied control is appropriate. Therefore, if a set of simultaneous Lyapunov inequalities are satisfied at the minimum and maximum of $\dot{\psi}_y$, the error dynamics (4.36) will be ULES. This is summarized in the following theorem.

Theorem 4.1 *Consider the observer (4.31)-(4.34) and let the Earth-fixed observer gains be selected according to Assumption A5. Assume that:*

$$\mathbf{A}_o(\delta) = \mathbf{A}_0 + \delta\mathbf{A}_1 \tag{4.53}$$

is Hurwitz for $\delta = 0$. If there exists a $\mathbf{P} = \mathbf{P}^T > 0$

$$\mathbf{P} = \begin{bmatrix} \mathbf{P}_{11} & \mathbf{P}_{12} \\ \mathbf{P}_{12}^T & \mathbf{P}_{22} \end{bmatrix} \tag{4.54}$$

where there are structural constraints on $\mathbf{P}_{11}$ and $\mathbf{P}_{12}$

$$\mathbf{P}_{11}\dot{\mathbf{H}}^T\mathbf{H} = -\mathbf{H}^T\dot{\mathbf{H}}\mathbf{P}_{11} \tag{4.55}$$
$$\mathbf{H}^T\dot{\mathbf{H}}\mathbf{P}_{12} = \mathbf{0} \tag{4.56}$$

and an $\varepsilon > 0$ such that for $\underline{\delta} = \min_t(\dot{\psi}_y)$ and $\bar{\delta} = \max_t(\dot{\psi}_y)$ the simultaneous Lyapunov inequalities are satisfied

$$\mathbf{P}\mathbf{A}_o(\underline{\delta}) + \mathbf{A}_o^T(\underline{\delta})\mathbf{P} \leq -\varepsilon\mathbf{I} \tag{4.57}$$
$$\mathbf{P}\mathbf{A}_o(\bar{\delta}) + \mathbf{A}_o^T(\bar{\delta})\mathbf{P} \leq -\varepsilon\mathbf{I} \tag{4.58}$$

the error-dynamics (4.36) is uniformly semi-globally exponentially stable (ULES).

Proof. $\mathbf{A}_o(0) = \mathbf{A}_0$ being Hurwitz is a straightforward requirement, likewise is the Lyapunov inequalities (4.57)-(4.58) sufficient for ensuring that for all $\delta \in [\underline{\delta}, \bar{\delta}] \subset \mathbb{R}$ since

$$f(\delta) = \mathbf{x}^T\left(\mathbf{P}\mathbf{A}_o(\delta) + \mathbf{A}_o^T(\delta)\mathbf{P}\right)\mathbf{x} \tag{4.59}$$

is linear in δ and thus convex such that if $f(\underline{\delta}), f(\bar{\delta}) \leq -\varepsilon$, $f(\delta) \leq -\varepsilon$ for any $\delta \in [\underline{\delta}, \bar{\delta}]$.

The rest of the proof consists of verifying that the error-dynamics can be expressed as (4.44) such that Lemma 4.1 can be employed. ■

Remark 4.1 *For configurations where only position and/or velocity feedback are used, $\mathbf{A}_1 = \mathbf{0}$ and the assumption of $\dot{\psi}_y$ being bounded is removed. The problem is thus reduced to finding a suitable $\mathbf{P} = \mathbf{P}^T > 0$ such that $\mathbf{P}\mathbf{A}_0 + \mathbf{A}_0^T\mathbf{P} \leq -\varepsilon\mathbf{I}$. In those cases, the observer is UGES.*

Remark 4.2 *This approach to handling the varying $\dot{\psi}_y$ is conservative in the sense that it guarantees exponential stability for arbitrarily fast variations in $\dot{\psi}_y$, i.e. as long as $\dot{\psi}_y$ is bounded there is no bound on $|\ddot{\psi}_y|$.*

The simultaneous Lyapunov inequalities can be represented as an LMI feasibility problem and hence solved using standard software packages: Find a $\mathbf{P} = \mathbf{P}^T > 0$ in accordance with the structural requirements such that

$$\begin{bmatrix} \mathbf{P}\mathbf{A}_o(\underline{\delta}) + \mathbf{A}_o^T(\underline{\delta})\mathbf{P} & \mathbf{0} \\ \mathbf{0} & \mathbf{P}\mathbf{A}_o(\bar{\delta}) + \mathbf{A}_o^T(\bar{\delta})\mathbf{P} \end{bmatrix} < 0 \tag{4.60}$$

4.3.3 Concluding Remarks

An existing nonlinear model-based observer with wave filtering capabilities for surface vessels has been extended to optionally include velocity and acceleration measurements. If the environmental model and some of the gain matrices satisfy certain structural properties, global exponential stability of the filter error dynamics can be concluded using a quadratic Lyapunov function with structural constraints. Once these model and gain constraints are satisfied, stability is determined by an eigenvalue analysis of the observer error's system matrix $\mathbf{A}_o(\delta)$. Without feedback from acceleration, the observer error is globally exponentially stable when $\mathbf{A}_o(0) = \mathbf{A}_0$ is Hurwitz. With acceleration feedback, on the other hand, the observer error will be exponentially stable semi-globally.

4.4 Simplified Observer

In the previous section we introduced a model based observer with wave filtering capabilities for surface vessels at low speed. Although this observer was the first model based integrated design that could incorporate partial velocity and acceleration measurements, there are two reasons why this design is unsuited from a practical point of view. At the core of these problems is the suggested model of first order wave induced motion:

1. The tuning procedure is much more complicated when velocity and/or acceleration measurements are included compared to the pole placement strategy used for position measurements. This is due to the fact that in the general case the observer gains enter non-affinely in the expressions describing the eigenvalue of the observer error-dynamics. One solution is to solve an algebraic Riccati equation (Kalman gains or $\mathcal{H}_\infty$-filtering techniques) either a priori or on-line, but having complete control of the notch-effects is almost impossible. As a consequence, it is very likely that the time spent tuning the DP system during sea-trials will increase.

2. A common wave model for all state derivatives could be fatal for the stability of the combined wave motion model if the individual measurements are out of synchronization with respect to each other. This occurs e.g. if the time-delays from the sensor system components are different.

Here we propose a model based observer where the wave models for position, velocity, and acceleration measurements are considered separately. The main idea is that wave induced acceleration is "uncorrelated" with the induced velocity, an assumption that is motivated more from engineering experience rather than from physics. Global exponential stability of the error dynamics may still be guaranteed using a structured $\mathbf{P}$ matrix. Still, we chose to trade global results in order to relax Assumption A2a and the need of a positive definite $\mathbf{T}_b$. With a bounded yaw rate the stability results will be valid only in a semi-global sense.

4.4.1 Complete Ship and Environment Model

As for the previously proposed observer, the LF vessel and bias models are described by (4.3). The by assumption uncorrelated wave induced positions, velocities, and accelerations respectively are given by

$$\dot{\mathbf{p}}_w = \mathbf{A}_{pw}\mathbf{p}_w + \mathbf{E}_{pw}\mathbf{w}_{pw} \tag{4.61}$$
$$\dot{\mathbf{v}}_w = \mathbf{A}_{vw}\mathbf{v}_w + \mathbf{E}_{vw}\mathbf{w}_{vw} \tag{4.62}$$
$$\dot{\mathbf{a}}_w = \mathbf{A}_{aw}\mathbf{a}_w + \mathbf{E}_{aw}\mathbf{w}_{aw} \tag{4.63}$$

where the order of each wave model number is arbitrary, but it is recommended to keep the order fairly low. Second or fourth order linear models are sufficient. Let m_p, m_v, m_a denote the order of the position, velocity and acceleration wave models respectively. Then $\mathbf{p}_w \in \mathbb{R}^{3m_p}$,$\mathbf{v}_w \in \mathbb{R}^{n_{y_2}\cdot m_v}$, $\mathbf{a}_w \in \mathbb{R}^{n_{y_3}\cdot m_a}$ describe the first order wave-induced positions, velocities and accelerations respectively. $\mathbf{A}_{pw} \in \mathbb{R}^{3m_p\times 3m_p}$, $\mathbf{A}_{vw} \in \mathbb{R}^{n_{y_2}\cdot m_v\times n_{y_2}\cdot m_v}$, $\mathbf{A}_{aw} \in \mathbb{R}^{n_{y_3}\cdot m_a\times n_{y_3}\cdot m_a}$ are assumed Hurwitz and describes the first order wave induced motion. The wave and bias models are driven by disturbances of appropriate dimensions.

In order to make use of the commutation properties, we have to assume

A2b The bias time constant matrix $\mathbf{T}_b$ and each 3×3 sub-block of $\mathbf{A}_{pw}$ satisfy Property 4.1.

Now, collect all the Earth-fixed states in $\mathbf{x}_1 \in \mathbb{R}^{6+3m_p}$ and stack the body-fixed ones into $\mathbf{x}_2 \in \mathbb{R}^{3+n_{y_2}\cdot m_v+n_{y_3}\cdot m_a}$

$$\mathbf{x}_1 = \begin{bmatrix} \mathbf{p}_w^T & \boldsymbol{\eta}^T & \mathbf{b}^T \end{bmatrix}^T \tag{4.64}$$
$$\mathbf{x}_2 = \begin{bmatrix} \mathbf{v}_w^T & \mathbf{a}_w^T & \boldsymbol{\nu}^T \end{bmatrix}^T \tag{4.65}$$

Let n denote the dimension of $\mathbf{x} = [\mathbf{x}_1^T, \mathbf{x}_2^T]^T$ and define the block diagonal transformation matrix $\mathbf{T} : \mathbb{R} \to \mathbb{R}^{n\times n}$

$$\mathbf{T}(\psi_y) = \mathrm{Diag}(\mathbf{R}^T(\psi_y), \cdots, \mathbf{R}^T(\psi_y), \mathbf{I}_{3+n_{y_2}\cdot m_v+n_{y_3}\cdot m_a}) \tag{4.66}$$

On compact form using Assumption A2b and $\mathbf{w} = [\mathbf{w}_{pw}^T, \mathbf{w}_b^T, \mathbf{w}_{vw}^T, \mathbf{w}_{aw}^T]^T$ we get

$$\dot{\mathbf{x}} = \mathbf{T}^T(\psi_y)\mathbf{A}\mathbf{T}(\psi_y)\mathbf{x} + \mathbf{B}\boldsymbol{\tau} + \mathbf{E}\mathbf{w} \tag{4.67}$$

where the parameters $\mathbf{A}$ have been separated from the rotation $\mathbf{R}(\psi_y)$. The model parameters in (4.67) are

$$\mathbf{A} = \begin{bmatrix} \mathbf{A}_{pw} & \mathbf{0} & \mathbf{0} & \mathbf{0} & \mathbf{0} & \mathbf{0} \\ \mathbf{0} & \mathbf{0} & \mathbf{0} & \mathbf{0} & \mathbf{0} & \mathbf{I} \\ \mathbf{0} & \mathbf{0} & -\mathbf{T}_b^{-1} & \mathbf{0} & \mathbf{0} & \mathbf{0} \\ \mathbf{0} & \mathbf{0} & \mathbf{0} & \mathbf{A}_{vw} & \mathbf{0} & \mathbf{0} \\ \mathbf{0} & \mathbf{0} & \mathbf{0} & \mathbf{0} & \mathbf{A}_{aw} & \mathbf{0} \\ \mathbf{0} & -\mathbf{M}^{-1}\mathbf{G} & \mathbf{M}^{-1} & \mathbf{0} & \mathbf{0} & -\mathbf{M}^{-1}\mathbf{D} \end{bmatrix} \tag{4.68}$$

$$\mathbf{B} = \begin{bmatrix} \mathbf{0} \\ \mathbf{0} \\ \mathbf{0} \\ \mathbf{0} \\ \mathbf{0} \\ \mathbf{M}^{-1} \end{bmatrix}, \quad \mathbf{E} = \begin{bmatrix} \mathbf{E}_{pw} & \mathbf{0} & \mathbf{0} & \mathbf{0} \\ \mathbf{0} & \mathbf{0} & \mathbf{0} & \mathbf{0} \\ \mathbf{0} & \mathbf{E}_b & \mathbf{0} & \mathbf{0} \\ \mathbf{0} & \mathbf{0} & \mathbf{E}_{vw} & \mathbf{0} \\ \mathbf{0} & \mathbf{0} & \mathbf{0} & \mathbf{E}_{aw} \\ \mathbf{0} & \mathbf{0} & \mathbf{0} & \mathbf{0} \end{bmatrix} \tag{4.69}$$

Measurements

Position and heading measurements are always required, and the number of velocity and acceleration measurements available are denoted $0 \leq n_{y_2} \leq 3$ and $0 \leq n_{y_3} \leq 3$, respectively. Let $\mathbf{y}_1 \in \mathbb{R}^3$, $\mathbf{y}_2 \in \mathbb{R}^{n_{y_2}}$ and $\mathbf{y}_3 \in \mathbb{R}^{n_{y_3}}$ describe the position, velocity and acceleration measurement vectors. We define the measurements as

$$\mathbf{y}_1 = \boldsymbol{\eta} + \mathbf{C}_{pw}\mathbf{p}_w \tag{4.70}$$
$$\mathbf{y}_2 = \boldsymbol{\Upsilon}_2\boldsymbol{\nu} + \mathbf{C}_{vw}\mathbf{v}_w \tag{4.71}$$
$$\mathbf{y}_3 = \boldsymbol{\Upsilon}_3\dot{\boldsymbol{\nu}} + \mathbf{C}_{aw}\mathbf{a}_w \tag{4.72}$$

where, $\boldsymbol{\Upsilon}_2$ and $\boldsymbol{\Upsilon}_3$ are projections isolating the components of the LF-model that are actually measured. Written compactly,

$$\mathbf{y} = \mathbf{C}_y(\psi_y)\mathbf{x} + \mathbf{D}_y\boldsymbol{\tau} \tag{4.73}$$

where

$$\mathbf{C}_y(\psi_y) = \begin{bmatrix} \mathbf{C}_{pw} & \mathbf{I} & & \\ \boldsymbol{\Upsilon}_2\mathbf{C}_v\mathbf{R}^T(\psi_y) & \mathbf{0} & & \\ \mathbf{0} & -\boldsymbol{\Upsilon}_3\mathbf{M}^{-1}\mathbf{G}\mathbf{R}^T(\psi_y) & & \\ & \mathbf{0} & \mathbf{0} & \mathbf{0} & \mathbf{0} \\ & \mathbf{0} & \boldsymbol{\Upsilon}_2 & \mathbf{C}_{vw} & \mathbf{0} \\ & -\boldsymbol{\Upsilon}_3\mathbf{M}^{-1}\mathbf{R}^T(\psi_y) & -\boldsymbol{\Upsilon}_3\mathbf{M}^{-1}\mathbf{D} & \mathbf{0} & \mathbf{C}_{aw} \end{bmatrix}$$

$$\mathbf{D}_y = \begin{bmatrix} \mathbf{0} & \mathbf{0} & \mathbf{M}^{-T}\boldsymbol{\Upsilon}_3^T \end{bmatrix}^T \tag{4.74}$$

Physically, however, it should be pointed out that the LF linear accelerations that are being measured is not $\dot{\boldsymbol{\nu}}$ as claimed in (4.72) since $\ddot{\boldsymbol{\eta}} \neq \dot{\boldsymbol{\nu}}$ when the Earth-fixed frame is considered as being the inertial frame. More specifically, considering the LF dynamics

$$\mathbf{y}_{3,LF} = \ddot{\boldsymbol{\eta}} = \dot{\psi}_y\mathbf{S}\mathbf{R}(\psi_y)\boldsymbol{\nu} + \mathbf{R}(\psi_y)\dot{\boldsymbol{\nu}} \tag{4.75}$$

which means that (4.72) is approximately correct for small angular rates. For large angular rates, however, an auxiliary pre-processor should be used to compensate for the Coriolis effect $\dot{\psi}_y\mathbf{S}\mathbf{R}(\psi_y)\boldsymbol{\nu}$. The need for an external processing unit will in fact always be there as discussed Section 3.3.

4.4.2 Observer Design

By duplicating the model dynamics and introducing a low-pass filter in order to achieve a certain roll-off effect, see (4.101), the following model based observer is proposed

$$\dot{\mathbf{a}}_f = \mathbf{T}_f^{-1}\left(-\mathbf{a}_f + \tilde{\mathbf{y}}_3\right) \tag{4.76}$$

$$\dot{\hat{\mathbf{x}}} = \mathbf{T}^T(\psi_y)\mathbf{A}\mathbf{T}(\psi_y)\hat{\mathbf{x}} + \mathbf{B}\boldsymbol{\tau} + \mathbf{K}(\psi_y)\tilde{\mathbf{y}} + \mathbf{K}_f\mathbf{a}_f \tag{4.77}$$

and its estimated output is

$$\hat{\mathbf{y}} = \mathbf{C}_y(\psi_y)\hat{\mathbf{x}} + \mathbf{D}_y\boldsymbol{\tau} \tag{4.78}$$

and hence when the estimation error is $\tilde{\mathbf{x}} = \mathbf{x} - \hat{\mathbf{x}}$, the output error is $\tilde{\mathbf{y}} = \mathbf{C}_y(\psi_y)\tilde{\mathbf{x}}$.

A pragmatic selection of observer gain matrices $\mathbf{K}(\psi_y)$ and $\mathbf{K}_f$ reducing interconnections is

$$\mathbf{K}(\psi_y) = \begin{bmatrix} \mathbf{K}_{11} & \mathbf{0} & \mathbf{0} \\ \mathbf{K}_{21} & \mathbf{0} & \mathbf{0} \\ \mathbf{K}_{31} & \mathbf{0} & \mathbf{0} \\ \mathbf{0} & \mathbf{K}_{42} & \mathbf{0} \\ \mathbf{0} & \mathbf{0} & \mathbf{K}_{53} \\ \mathbf{K}_{61}\mathbf{R}^T(\psi_y) & \mathbf{K}_{62} & \mathbf{0} \end{bmatrix} \tag{4.79}$$

$$\mathbf{K}_f = \begin{bmatrix} \mathbf{0} & \mathbf{0} & \mathbf{0} & \mathbf{0} & \mathbf{0} & \mathbf{K}_a^T \end{bmatrix}^T \tag{4.80}$$

In order to apply the concept of commutating matrices, we have to impose the following requirement on some of the gains:

A3b Each and every 3×3 block of $\mathbf{K}_{11}$, $\mathbf{K}_{21}$ and $\mathbf{K}_{31}$ commute with the rotation $\mathbf{R}(\psi_y)$ (Property 4.1).

A schematic drawing of this observer, without bias estimation, is given in Figure 4.1.

Stability Analysis

When Assumption A2b and A3b are satisfied, the rotations can be separated from the parameters. The observer error-dynamics can hence be rewritten on the compact form

$$\dot{\tilde{\mathbf{x}}} = \mathbf{T}^T(\psi_y)\mathbf{A}_o\mathbf{T}(\psi_y)\tilde{\mathbf{x}} + \mathbf{K}_f\mathbf{a}_f + \mathbf{E}_e\mathbf{w} \tag{4.81}$$

$$\dot{\mathbf{a}}_f = -\mathbf{T}_f^{-1}\mathbf{a}_f + \mathbf{T}_f^{-1}\mathbf{C}_3\mathbf{T}(\psi_y)\tilde{\mathbf{x}} \tag{4.82}$$

$$\mathbf{A}_o = \begin{bmatrix} \mathbf{A}_{11} & \mathbf{A}_{12} \\ \mathbf{A}_{21} & \mathbf{A}_{22} \end{bmatrix} \tag{4.83}$$

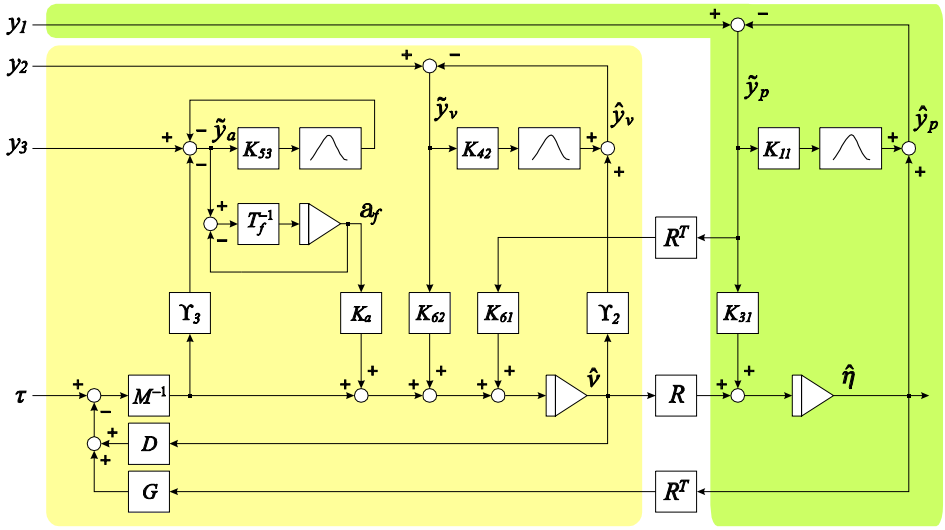

Figure 4.1: Observer with first order cut-off filter for acceleration. Bias estimation is not shown.

$$\mathbf{A}_{11} = \begin{bmatrix} \mathbf{A}_{pw} - \mathbf{K}_{11}\mathbf{C}_{pw} & -\mathbf{K}_{11} & \mathbf{0} \\ -\mathbf{K}_{21}\mathbf{C}_{pw} & -\mathbf{K}_{21} & \mathbf{0} \\ -\mathbf{K}_{31}\mathbf{C}_{pw} & -\mathbf{K}_{31} & -\mathbf{T}_b^{-1} \end{bmatrix} \tag{4.84}$$

$$\mathbf{A}_{12} = \begin{bmatrix} \mathbf{0} & \mathbf{0} & \mathbf{0} \\ \mathbf{0} & \mathbf{0} & \mathbf{I} \\ \mathbf{0} & \mathbf{0} & \mathbf{0} \end{bmatrix} \tag{4.85}$$

$$\mathbf{A}_{21} = \begin{bmatrix} \mathbf{0} & \mathbf{0} & \mathbf{0} \\ \mathbf{0} & \mathbf{0} & \mathbf{0} \\ -\mathbf{K}_{61}\mathbf{C}_{pw} & -\mathbf{M}^{-1}\mathbf{G} - \mathbf{K}_{61} & \mathbf{M}^{-1} \end{bmatrix} \tag{4.86}$$

$$\mathbf{A}_{22} = \begin{bmatrix} \mathbf{A}_{vw} - \mathbf{K}_{42}\mathbf{C}_{vw} & \mathbf{0} & -\mathbf{K}_{42}\boldsymbol{\Upsilon}_2 \\ \mathbf{0} & \mathbf{A}_{aw} - \mathbf{K}_{53}\mathbf{C}_{aw} & -\mathbf{K}_{53}\boldsymbol{\Upsilon}_3 \\ -\mathbf{K}_{62}\mathbf{C}_{vw} & \mathbf{0} & -\mathbf{M}^{-1}\mathbf{D} - \mathbf{K}_{62}\boldsymbol{\Upsilon}_2 \end{bmatrix} \tag{4.87}$$

$$\mathbf{C}_3 = \begin{bmatrix} \mathbf{0} & -\boldsymbol{\Upsilon}_3\mathbf{M}^{-1}\mathbf{G} & \boldsymbol{\Upsilon}_3\mathbf{M}^{-1} & -\boldsymbol{\Upsilon}_3\mathbf{M}^{-1}\mathbf{D} & \mathbf{0} & \mathbf{C}_{aw} \end{bmatrix} \tag{4.88}$$

Stacking (4.81)-(4.82) together into $\mathbf{z} \in \mathbb{R}^{n_z}$, more specifically $\mathbf{z} = [\tilde{\mathbf{x}}^T, \mathbf{a}_f^T]^T$, we then get

$$\dot{\mathbf{z}} = \mathbf{T}_z^T(\psi_y)\mathbf{A}_z\mathbf{T}_z(\psi_y)\mathbf{z} + \mathbf{E}_z\mathbf{w} \tag{4.89}$$

where $\mathbf{T}_z = \text{Diag}(\mathbf{T}, \mathbf{I}_{n_{y_3}})$ and

$$\mathbf{A}_z = \begin{bmatrix} \mathbf{A}_o & \mathbf{K}_f \\ \mathbf{T}_f^{-1}\mathbf{C}_3 & -\mathbf{T}_f^{-1} \end{bmatrix}, \quad \mathbf{E}_z = \begin{bmatrix} \mathbf{E}_e \\ \mathbf{0} \end{bmatrix} \tag{4.90}$$

We now state a robustness-like theorem for the stability of this filter. The limiting factor is the yaw rate $\dot{\psi}_y = r_y$, and we could just as well repeat using a $\mathbf{P}$-matrix of

a certain structure that commutes with $\mathbf{T}_z(\psi_y)$ in a quadratic Lyapunov function provided that Assumption A2b and A3b hold. Because the upper bound on $|r_y(t)|$ is likely to be larger than the physical limit, we assign an arbitrary $\mathbf{P}$. The advantage of an arbitrarily selected $\mathbf{P}$ is that there are no longer any restrictions on the selection of cross-terms. As a consequence we could have let $\|\mathbf{T}_b\| \to \infty$, then the bias is modelled as an open integrator and we obtain true integral action.

Before we state the theorem we need to introduce a skew-symmetric matrix $\mathbf{S}_z$ that appears when the rotation $\mathbf{T}_z(\psi_y)$ is differentiated.

$$\dot{\mathbf{T}}_z \triangleq \frac{d}{dt}\left(\mathbf{T}_z(\psi_y)\right) = \dot{\psi}_y \mathbf{S}_z \mathbf{T}_z(\psi_y) = \dot{\psi}_y \mathbf{T}_z(\psi_y)\mathbf{S}_z \tag{4.91}$$

In our case $\mathbf{S}_z = \text{Diag}(\mathbf{S}^T, ..., \mathbf{S}^T, \mathbf{0}_{n_z-12 x n_z-12})$ where $\mathbf{S}$ is given by (4.2).

Theorem 4.2 *The observer error dynamics (4.89) is exponentially stable for small $|r_y(t)| < r_{\max}$ (ULES) if and only if $\mathbf{A}_z$ is Hurwitz. Suppose an $r_{\max} > 0$ is explicitly given, then (4.89) is uniformly globally exponentially stable (UGES) if there exists a matrix $\mathbf{P} = \mathbf{P}^T > 0$ such that the following two LMIs are feasible for some $\varepsilon > 0$*

$$\begin{array}{rcl} \mathbf{P}\mathbf{A}_z + \mathbf{A}_z^T\mathbf{P} + \varepsilon\mathbf{I} & \leq & r_{\max}\left(\mathbf{P}\mathbf{S}_z + \mathbf{S}_z^T\mathbf{P}\right) \\ \mathbf{P}\mathbf{A}_z + \mathbf{A}_z^T\mathbf{P} + \varepsilon\mathbf{I} & \leq & -r_{\max}\left(\mathbf{P}\mathbf{S}_z + \mathbf{S}_z^T\mathbf{P}\right) \end{array} \tag{4.92}$$

Notice that stability can be characterized without dealing with the rotations $\mathbf{T}_z(\psi_y)$. However, there is a bound on the rotation rate $r_{\max}$ making the observer USGES due to observability.

Proof. Use the non-singular rotation $\mathbf{T}_z(\psi_y)$ as a mapping $\boldsymbol{\xi} = \mathbf{T}_z\mathbf{z}$. Then,

$$\begin{aligned} \dot{\boldsymbol{\xi}} &= \dot{\mathbf{T}}_z\mathbf{z} + \mathbf{T}_z\dot{\mathbf{z}} \\ &= \dot{\psi}_y\mathbf{S}_z\mathbf{T}_z\mathbf{z} + \mathbf{T}_z\mathbf{T}_z^T\mathbf{A}_z\mathbf{T}_z z \\ &= \left(\mathbf{A}_z + \dot{\psi}_y\mathbf{S}_z\right)\boldsymbol{\xi} \end{aligned} \tag{4.93}$$

Consider the Lyapunov function $V = \boldsymbol{\xi}^T\mathbf{P}\boldsymbol{\xi}$

$$\dot{V} = \boldsymbol{\xi}^T\left(\mathbf{P}\mathbf{A}_z + \mathbf{A}_z^T\mathbf{P}\right)\boldsymbol{\xi} + \dot{\psi}_y\boldsymbol{\xi}^T\left(\mathbf{P}\mathbf{S}_z + \mathbf{S}_z^T\mathbf{P}\right)\boldsymbol{\xi} \tag{4.94}$$

Since $\dot{V}$ is linear in $\dot{\psi}_y$ for fixed $\mathbf{P}$ and $\boldsymbol{\xi}$ it is also convex and it suffices to verify that $\dot{V} < 0$ at the boundaries of $\dot{\psi}_y$, namely $\pm r_{\max}$ since $-r_{\max} \leq \dot{\psi}_y \leq r_{\max}$ by assumption. We therefore have to make sure that

$$\dot{V}_1 = \dot{V}\Big|_{\dot{\psi}_y = r_{\max}} < 0 \tag{4.95}$$

$$\dot{V}_2 = \dot{V}\Big|_{\dot{\psi}_y = -r_{\max}} < 0 \tag{4.96}$$

Inserting the LMIs from (4.92) we get for $k = 1, 2$

$$\dot{V}_k \leq -\varepsilon\mathbf{I} \tag{4.97}$$

For small enough $r_{\max}$, there will always exist an $\varepsilon > 0$ if and only if $\mathbf{A}_z$ is Hurwitz. ■

This result could also be proven by the circle criterion, but the maximum allowable $r_{\max}$ is likely to be smaller due to the required SPR-property.

Notice that stability can be proven also for the limiting case $\mathbf{T}_b^{-1} = \mathbf{0}$. The passive design (Fossen and Strand 1999) and our previous version (Lindegaard and Fossen 2001*a*), on the other hand, require $\mathbf{T}_b^{-1} > 0$.

4.4.3 Observer Tuning

In this section we suggest models for the first order wave loads and then we suggest tuning rules that based on those models generate the desired frequency response between the measurements and the LF estimates.

For position, velocity, and acceleration measurements, $i = p, v, a$, a cascade of second order linear systems

$$\mathbf{A}_{iw} = \begin{bmatrix} \mathbf{0} & \mathbf{I} \\ -\mathbf{\Omega}_i & -\mathbf{\Lambda}_i \end{bmatrix} \quad , \quad \mathbf{C}_{iw} = \begin{bmatrix} \mathbf{0} & \mathbf{I} \end{bmatrix} \tag{4.98}$$

can be used to represent the wave induced motion whereby we obtain the desired wave filtering capability. Treat each DOF separated from the others by setting

$$\mathbf{\Omega}_i = \text{diag}(\omega_{i,1}^2, ..., \omega_{i,n_{y_i}}^2) \tag{4.99}$$

$$\mathbf{\Lambda}_i = \text{diag}(2\zeta_{i,1}\omega_{i,1}, ..., 2\zeta_{i,n_{y_i}}\omega_{i,n_{y_i}}) \tag{4.100}$$

where $\omega_{i,k} > 0$ is the resonance frequency and $\zeta_{i,k} > 0$ is the relative damping factor which determines the width of the spectrum.

Depending on the number $p_i = m_i/2$, where $i = p, v, a$ of second order models in cascade, the desired transfer function between any measurement and the LF estimate is

$$h_{d_i}(s) = \omega_{c,k} \frac{\left(s^2 + 2\zeta_{i,k}\omega_{i,k}s + \omega_{i,k}^2\right)^{p_i}}{\left(s^2 + 2\delta_{i,k}\zeta_{i,k}\omega_{i,k}s + \omega_{i,k}^2\right)^{p_i}(\omega_{c,k} + s)} \quad i = p, v, a \tag{4.101}$$

which is a notch-filter, with center frequency at $\omega_{i,k}$, the wave model resonance, and notch "width" given by $\delta_{i,k} \geq 1$, in series with a low-pass filter that guarantees a certain roll-off for frequencies larger than $\omega_{c,k}$. In order to achieve good performance, the roll-off frequency $\omega_{c,k}$ should be larger than the resonance frequency of the notch-filter, that is $\omega_{c,k} \geq \omega_{i,k}$.

Wave Model Gains

We apply a same pole-placement technique to find observer gains for position and velocity innovation. If we were dealing with second order wave models, the

tuning rules from Fossen and Strand (1999) apply. However, due to the increasing power of the wave frequency components in the velocity and acceleration signal, we suggest using a fourth order wave model, at least for acceleration, in order to achieve satisfactory wave filtering capabilities. We were in fact unable to get good results for acceleration using second order models. Below, we therefore present the extension of Fossen and Strand (1999) to fourth order models.

Consider the surge dynamics being updated from position measurements. We aim to find the elements to put in $\mathbf{K}_{11}$ and $\mathbf{K}_{31}$ in order to create the desired notch and roll-off $h_{d_i}(s)$ in (4.101)

$$\frac{\hat{\eta}_i}{y_{1,i}}(s) = h_{d_i}(s) \tag{4.102}$$

This can be obtained one degree of freedom at the time by defining $\alpha_{p,i} = \omega_{p,i}^2 > 0$ and $\beta_{p,i} = 2\zeta_{p,i}\omega_{p,i} > 0$ and letting

$$\mathbf{A}_{pw,i} = \begin{bmatrix} 0 & 1 & 0 & 0 \\ -\alpha_{p,i} & -\beta_{p,i} & 0 & 1 \\ 0 & 0 & 0 & 1 \\ 0 & 0 & -\alpha_{p,i} & -\beta_{p,i} \end{bmatrix} \tag{4.103}$$

$$\bar{\mathbf{C}}_{pw,i} = \begin{bmatrix} 1 & 0 & 0 & 0 \end{bmatrix} \tag{4.104}$$

and selecting observer gains according to

$$\mathbf{k}_{11,i} = \mathbf{L}_i^{-1}\mathbf{c}_i \tag{4.105}$$

$$k_{31,i} = \omega_{c,i} \tag{4.106}$$

where

$$\mathbf{L}_i = \begin{bmatrix} 1 & 0 & 0 & 0 \\ 2\beta_{p,i} & 1 & 0 & 0 \\ \alpha_{p,i} + \beta_{p,i}^2 & \beta_{p,i} & 0 & 1 \\ \beta_{p,i} & 1 & -1 & 0 \end{bmatrix} \tag{4.107}$$

$$\mathbf{c}_i = \begin{bmatrix} 2\beta_{p,i}\left(\delta_{p,i} - 1\right) \\ \beta_{p,i}^2\left(\delta_{p,i}^2 - 1\right) + 2\beta_{p,i}\left(\delta_{p,i} - 1\right)\omega_{c,i} \\ \alpha_{p,i}\beta_{p,i}\left(\delta_{p,i} - 1\right) + \beta_{p,i}^2\left(\delta_{p,i}^2 - 1\right)\omega_{c,i} \\ 2\beta_{p,i}\left(\delta_{p,i} - 1\right)\omega_{c,i} \end{bmatrix} \tag{4.108}$$

ensures that the specified notch-effect and roll-off is indeed acquired. The gains $\mathbf{K}_{31}$ and $\mathbf{K}_{61}$, the gains from position innovation which update the bias and LF velocity, can be selected freely as long as $\mathbf{A}_z$ remains Hurwitz.

The very same approach can be applied to assign values to $\mathbf{K}_{42}$, $\mathbf{K}_{62}$ in order to obtain a notch-effect for the velocity measurements.

Acceleration Gains

The acceleration part of the filter possesses another feature as well. Measuring the acceleration could be regarded as an alternative to using a model based observer

because the model actually *estimates* the acceleration while an accelerometer *measures* it. The gain $\mathbf{K}_f$ serves as a weight factor determining how much emphasis we should put on the model. When $\mathbf{K}_f = \mathbf{0}$ we choose not to utilize acceleration feedback to update the filter at all and when $\mathbf{K}_f = 1$, the LF model description is completely disregarded for low frequencies.

The low-pass filter between acceleration innovation $\tilde{\mathbf{y}}_3$ and $\dot{\hat{\boldsymbol{\nu}}}$ takes care of the roll-off. The filter constants $\mathbf{T}_f$ should therefore be selected as

$$\mathbf{T}_f^{-1} = \text{diag}(\omega_{c,1}, ..., \omega_{c,n_{y3}}) \tag{4.109}$$

Next, to obtain the desired notch-filtering around the resonance frequency, select

$$\mathbf{K}_{53} = \begin{bmatrix} \mathbf{0} \\ \text{diag}(\delta_{a,1}, ..., \delta_{a,n_{y3}}) \end{bmatrix} \tag{4.110}$$

4.4.4 Experiments

The experiment was carried out with "Cybership II", and the dynamic compensator scheme presented in Chapter 2 was implemented.

Based on the principle of certainty of equivalence, an observer-feedback PID-like tracking controller on the form

$$\dot{\boldsymbol{\xi}} = \hat{\boldsymbol{\eta}} - \boldsymbol{\eta}_d \tag{4.111}$$

$$\begin{aligned} \boldsymbol{\tau} = & -\mathbf{K}_i \mathbf{R}^T(\hat{\psi})\boldsymbol{\xi} - \mathbf{K}_p \mathbf{R}^T(\hat{\psi})\left(\hat{\boldsymbol{\eta}} - \boldsymbol{\eta}_d\right) \\ & -\mathbf{K}_d\left(\hat{\boldsymbol{\nu}} - \boldsymbol{\nu}_d\right) \end{aligned} \tag{4.112}$$

was used to keep the boat on the position $\boldsymbol{\eta}_d = [-0.3, 0, 0]^T$, $\boldsymbol{\nu}_d = \mathbf{0}$. The controller and the thrust allocation algorithm is described and analyzed in Lindegaard and Fossen (2003).

From $t \approx 20$ seconds and onwards, the model ship was exposed to JONSWAP-distributed irregular head waves. The peak period and significant wave height were set to $T_s = 0.75$ and $H_{1/3} = 0.02$ meters respectively.

Time series plots of the measured positions (dotted) and their respective LF estimates are reproduced in Figure 4.2 together with the observer's surge bias estimate. Notice that the surge bias converges towards the controller's I-term, that is the mean of applied surge propeller force τ_1. A large wave slammed into the vessel at $t \approx 115$ generating a temporary drift off in East and heading because the vessel had a small offset angle at the time of the impact. The slow oscillations are due to nonlinear wave effects and not to the first order induced motion. Figure 4.3 shows g-compensated measurements of the surge and sway accelerations. Here, the wave frequency motion (first order wave loads) dominate the picture. But as the empirical transfer functions (Figure 4.4) of the measured signals and the state derivatives show, for low frequencies the estimated LF-accelerations are excellent, because they follow the measured signals at frequencies below $f = 0.1$ Hz. As required, frequency components around the wave frequency peak $f = 1/T_s = 1.33$ Hz have been successfully attenuated.

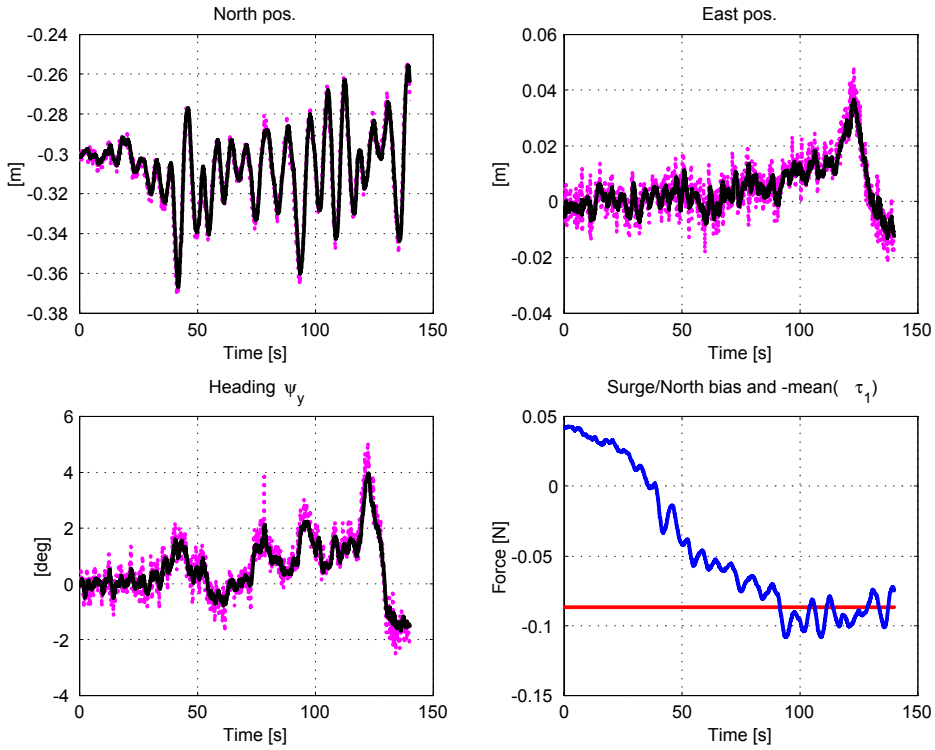

Figure 4.2: Top left, measured (dotted) and LF estimated North position. Top right, measured (dotted) and LF estimated East position. Bottom left, measured (dotted) and LF estimated heading. Bottom right, estimated bias and mean of applied thrust thrust τ_1.

4.4.5 Concluding Remarks

A simple model based state estimator for surface vessels with wave filtering capabilities has been proposed and analyzed along with an intuitive tuning procedure. For bounded yaw rate, the observer error dynamics was shown to be exponentially stable. Inertial measurements, that is linear accelerations and yaw rate, were included in the filter to improve performance. Due to the acceleration measurement ambiguity, a g-compensation system had to be utilized in order to remove gravity components from the linear acceleration terms.

Experimental results with a model ship performing a DP operation as it was exposed to incoming irregular waves illustrated the performance of the filter. Empirically calculated frequency responses between available measurements and estimated low frequency positions, velocities and accelerations documented that the desired notch filtering of first order wave induced motion was achieved.

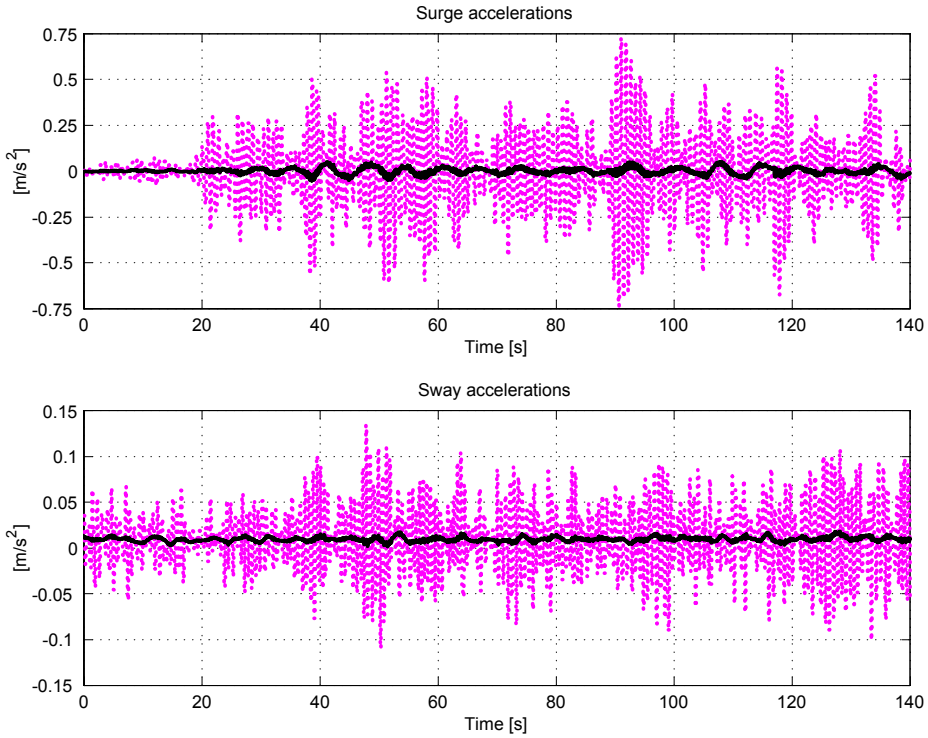

Figure 4.3: g-compensated surge and sway accelerations. Measurements (dotted) and LF estimates (solid).

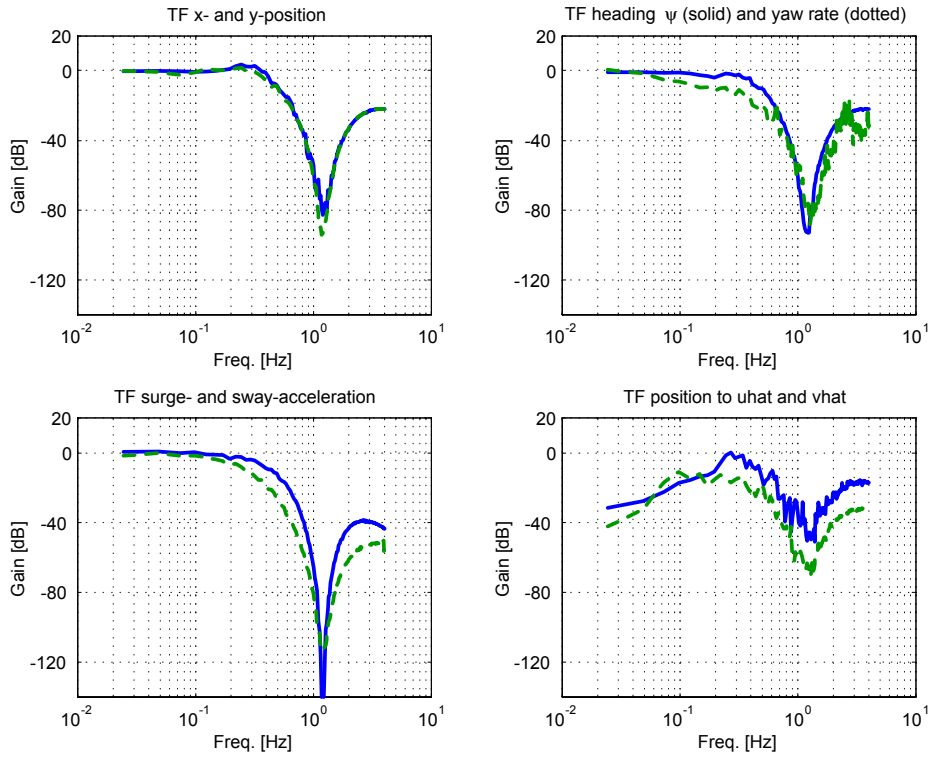

Figure 4.4: Top left, TF from measured North (solid) and East (dotted) position to their respective LF estimates. Top right, TF from measured heading (solid) and yaw rate (dotted) to LF estimates. Bottom left, TF from measured surge (solid) and sway (acceleration) to LF estimates. Bottom left, TF from North position to surge velocity (solid) and from East to sway (dotted).

Chapter 5

Controller Design

5.1 Introduction

Problems of motion control can be classified into three groups (Encarnação and Pascoal 2001):

- *Point stabilization*: The objective is to stabilize and keep a vehicle at a specified point and orientation.
- *Trajectory tracking*: The task of making a vehicle track a reference trajectory parameterized in time.
- *Path following*: The vehicle is required to converge to and follow a desired path without an implicit speed assignment.

Trajectory tracking is the most commonly implemented control approach in commercial DP systems today. This chapter focuses on both linear and nonlinear control strategies for low speed tracking and positioning control (point stabilization) of fully or overactuated surface vessels in the horizontal plane. Whenever the desired velocities are zero, the desired trajectory collapses into a single point and the tracking controller becomes a positioning controller. There are, however, operations where starting time and encountered delays are of minor concern. An intuitive example is way-point tracking, the task of following a path of specified way-points in the horizontal plane. Furthermore, more typical DP operations like pipe lying and dredging are also likely to benefit from a control strategy with less attention to time constraints.

Path following is typically applied to underactuated ships in transit, and many recent developments have been reported: In Zhang *et al.* (2000) the authors addressed the problem of following straight lines, and to achieve this a new output combining the cross-track error and the heading angle was defined. Asymptotic stability to the path was shown by the use of sliding mode control. Another redefinition emulating that of an experienced helmsman was proposed by Pettersen and

Lefeber (2001); the desired heading was defined as a function of the cross-track error. A more flexible alternative is the introduction of a Serret-Frenet frame to represent the cross-track and heading error (Encarnação *et al.* 2000, Encarnação and Pascoal 2000, Skjetne and Fossen 2001). The advantage is that the path can be regarded as a more general smooth curve in the plane rather than consist of straight lines.

Underactuated trajectory tracking and stabilization has received a lot of attention, see Do *et al.* (2002) and references therein. A natural consequence of the ship being underactuated is that geometric restrictions apply on the reference trajectory. More specifically, the desired yaw velocity must be persistently excitative.

A method combining trajectory tracking and path following was proposed in Hindman and Hauser (1996). Suppose a desired path $\boldsymbol{\eta}_d : \mathbb{R}_{\geq 0} \to \mathbb{R}^n$ is given and that it is a continuous function of the path variable $\theta \geq 0$. The basic idea is to determine θ by projecting the current state of the vehicle onto the reference trajectory. This returns the appropriate trajectory "time" given the current state of the system. Under some geometrical path conditions, it is shown that feeding $\boldsymbol{\eta}_d(\theta)$ instead of $\boldsymbol{\eta}_d(t)$ into an already existing tracking controller guarantees convergence to the path. This procedure, however, requires a path specification for the full state, and it is applicable to feedback linearizable systems. An output maneuvering extension to Hindman and Hauser (1996) was proposed in Encarnação and Pascoal (2001). By employing backstepping (Krstić *et al.* 1995), the need for time derivatives of $\boldsymbol{\eta}_d$, the full path specification, was relaxed. This approach is well suited for mechanical systems such as ships, but it is less fitted for systems of relative degree higher than two due to the need of higher order derivatives of the path variable θ. Recently, Skjetne *et al.* (2003) proposed a more general robust maneuvering design for systems on strict feedback form which tackles the relative degree restriction.

Trajectory tracking is geometrically speaking relatively simple compared to path following, and the above described methods unifying tracking and path following promise increased flexibility of the controllers derived in this chapter. We extend existing DP designs (Strand 1999, Berge 1999) and provide ideas and suggestions to improve and facilitate the design and implementation of observer feedback positioning control systems. Ships suited for traditional dynamic positioning operations are usually overactuated. This means that the desired thrust $\boldsymbol{\tau}$ can almost always be satisfied. In fact, due to propeller rate and thrust magnitude constraints, there are indeed practical limits, but it is assumed that these issues can be disregarded or at least addressed elsewhere. The control laws will be derived assuming full state feedback. Later substituting the state variables with their respective low frequency estimates, the so called principle of *certainty of equivalence*, we show that the combination of an observer and controller stabilizes the entire closed loop system. Results from the study of nonlinear cascaded systems will be used in the analysis.

These are the main objectives of this chapter:

1. Derive a simple yet flexible framework for low speed trajectory tracking of fully actuated surface vessels. First, a method separating the nonlinear

kinematics from the otherwise linear closed-loop dynamics will be proposed. This type of design, which has many similarities to more conventional PID-compatible schemes, is attractive because one can apply any linear design tool to shape the error-dynamics. Some examples will be given. The method called *commutating design* will be described in Section 5.3. A generalization to more nonlinear ship models (higher velocities) is given in Section 5.5.

2. To refine the already derived framework in order to incorporate acceleration terms in the controller (Section 5.4).

5.2 Trajectory Generation

The desired position or trajectory of a DP vessel is usually given with respect to the so called center of rotation (COR), about which any rotation of the vessel should be conducted. The COR is a freely selectable fixed point inside or outside the physical boundaries of the ship, and its coordinates will be assumed given relative to the body-fixed b-frame. This section derives some basic kinematic relations between the desired trajectory given in Earth-fixed coordinates (n-frame) and the transformation into the b-frame which is the reference frame where the DP controller operates.

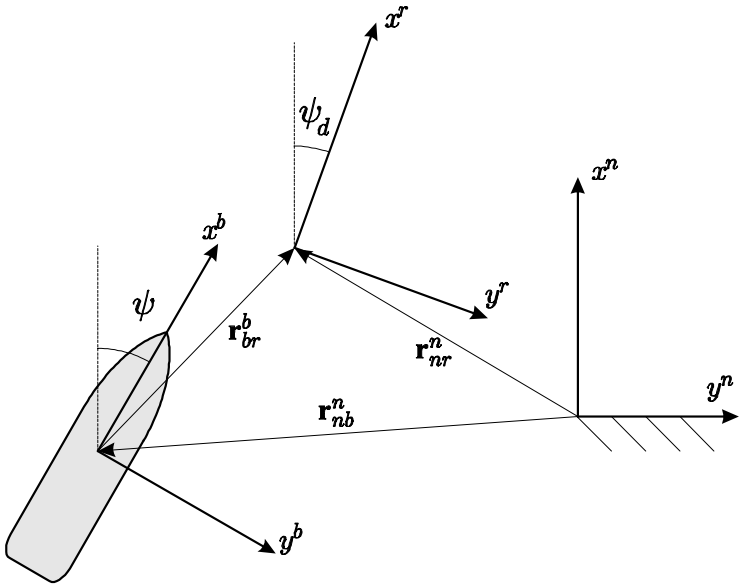

Figure 5.1: Definition of the Earth-fixed position of center of rotation $\mathbf{r}^n_{nr}$ and its relation to the position of the vessel $\mathbf{r}^n_{nb}$.

Let $\mathbf{r}^b_{br} = [x^b_{br}, y^b_{br}]^T$ denote the position of the COR relative the the b-frame. The desired Earth-fixed position and heading of the COR is given by $\boldsymbol{\eta}_{dr}(t) =$

$[({}^d\mathbf{r}^n_{nr}(t))^T, \psi_d(t)]^T$ where again ${}^d\mathbf{r}^n_{nr} = [{}^d x^n_{nr}, {}^d y^n_{nr}]^T$ is the distance in the horizontal plane from the n-frame to the desired position of the COR. Observe that the desired heading $\psi_d(t)$ of the COR is identical to the desired heading of the ship. According to Figure 5.1 the desired position of the b-frame is given by

$$ {}^d\mathbf{r}^n_{nb} = {}^d\mathbf{r}^n_{nr} - \bar{\mathbf{R}}(\psi_d)\mathbf{r}^b_{br} \tag{5.1} $$

where the rotation $\bar{\mathbf{R}}(\psi_d)$ is defined as

$$ \bar{\mathbf{R}}(\psi_d) = \begin{bmatrix} \cos\psi_d & -\sin\psi_d \\ \sin\psi_d & \cos\psi_d \end{bmatrix} \tag{5.2} $$

Frequently, it is dersirable to let the vessel rotate about some other point than CG. For instance when deploying a device on the sea bed using a crane, the ship should rotate about the crane head rather than CG. Consider Figure 5.2 where a 180 deg change of heading instructs the DP controller to move the vessel on a circular arc while turning rather than revolving about the center of the b-frame.

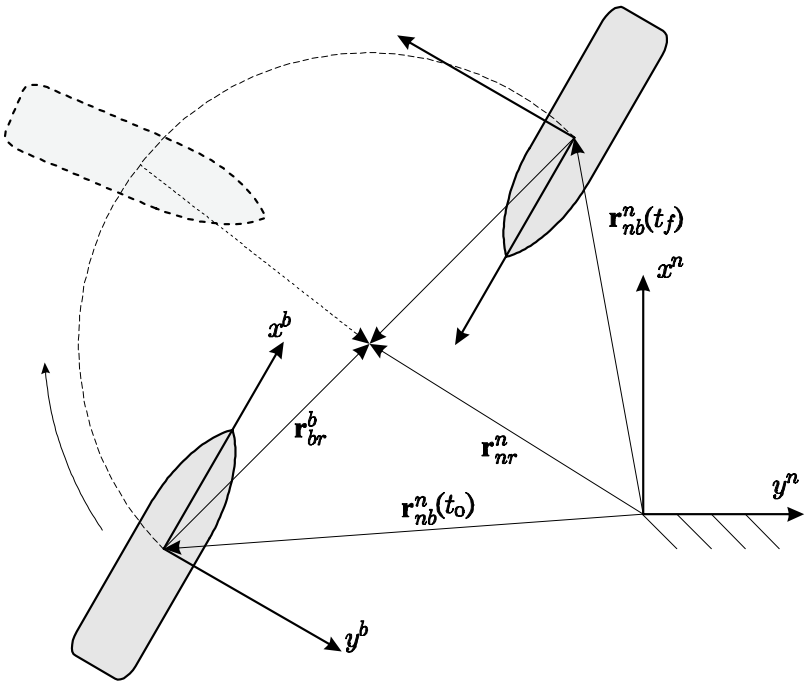

Figure 5.2: Change of heading 180 deg about the COR: The ship is moved from $\mathbf{r}^n_{nb}(t_0)$ towards $\mathbf{r}^n_{nb}(t_f)$ while turning.

The Earth-fixed velocity and acceleration of the COR are denoted $\dot{\boldsymbol{\eta}}_{dr}(t) = [({}^d\dot{\mathbf{r}}^n_{nr}(t))^T, r_d(t)]^T$ and $\ddot{\boldsymbol{\eta}}_{dr}(t) = [({}^d\ddot{\mathbf{r}}^n_{nr}(t))^T, \dot{r}_d(t)]^T$ respectively. Desired velocity and acceleration of

the b-frame decomposed in the n-frame are found by differentiating ${}^d\mathbf{r}^n_{nb}$.

$$\begin{aligned} {}^d\dot{\mathbf{r}}^n_{nb} &= {}^d\dot{\mathbf{r}}^n_{nr} - r_d\bar{\mathbf{R}}(\psi_d)\bar{\mathbf{S}}\mathbf{r}^b_{br} && (5.3)\\ {}^d\ddot{\mathbf{r}}^n_{nb} &= {}^d\ddot{\mathbf{r}}^n_{nr} - \dot{r}_d\bar{\mathbf{R}}(\psi_d)\bar{\mathbf{S}}\mathbf{r}^b_{br} - r_d^2\bar{\mathbf{R}}(\psi_d)\bar{\mathbf{S}}^2\mathbf{r}^b_{br} \\ &= {}^d\ddot{\mathbf{r}}^n_{nr} - \dot{r}_d\bar{\mathbf{R}}(\psi_d)\bar{\mathbf{S}}\mathbf{r}^b_{br} + r_d^2\bar{\mathbf{R}}(\psi_d)\mathbf{r}^b_{br} && (5.4)\end{aligned}$$

Here

$$\bar{\mathbf{S}} = \begin{bmatrix} 0 & -1 \\ 1 & 0 \end{bmatrix} \tag{5.5}$$

The desired speed and acceleration along the trajectory should not exceed neither the physical nor the imposed limitations of the ship. Considering these limitations in an Earth-fixed setting is difficult, but the control will be regained when expressing the trajectory in a reference parallell frame, the d-frame: When the vessel tracks the desired trajectory perfectly, the velocities in the d-frame will be exactly those of the vessel itself (b-frame). The desired velocity is

$$\begin{aligned} {}^d\mathbf{v}^d_{nb} &\triangleq \bar{\mathbf{R}}^T(\psi_d){}^d\dot{\mathbf{r}}^n_{nb} \\ &= \bar{\mathbf{R}}^T(\psi_d){}^d\dot{\mathbf{r}}^n_{nr} - r_d\bar{\mathbf{S}}\mathbf{r}^b_{br} \end{aligned} \tag{5.6}$$

and for the acceleration we have

$$\begin{aligned} {}^d\dot{\mathbf{v}}^d_{nb} &= \frac{d}{dt}\left({}^d\mathbf{v}^d_{nb}\right) \\ &= \bar{\mathbf{R}}^T(\psi_d){}^d\ddot{\mathbf{r}}^n_{nr} - r_d\bar{\mathbf{R}}^T(\psi_d)\bar{\mathbf{S}}{}^d\dot{\mathbf{r}}^n_{nr} - \dot{r}_d\bar{\mathbf{S}}\mathbf{r}^b_{br} && (5.7)\end{aligned}$$

The translation and rotation of the d-frame can thus be regarded as a virtual ship, yet the motion does not need to be that of a numerical ship model.

To summarize, suppose the COR is located at $\mathbf{r}^b_{br} = [x^b_{br}, y^b_{br}, 0]^T$, and once a smooth, Earth-fixed reference trajectory for the COR is given, $\boldsymbol{\eta}_{dr} : \mathbb{R}_{\geq 0} \to \mathbb{R}^3$, $\dot{\boldsymbol{\eta}}_{dr} : \mathbb{R}_{\geq 0} \to \mathbb{R}^3$, and $\ddot{\boldsymbol{\eta}}_{dr} : \mathbb{R}_{\geq 0} \to \mathbb{R}^3$, the desired trajectory for the orgin of the vessel will be given by

$$\begin{aligned} \boldsymbol{\eta}_d &= \boldsymbol{\eta}_{dr} - \mathbf{R}(\psi_d)\mathbf{r}^b_{br} && (5.8)\\ \boldsymbol{\nu}_d &= \mathbf{R}^T(\psi_d)\dot{\boldsymbol{\eta}}_{dr} - r_d\mathbf{S}\mathbf{r}^b_{br} && (5.9)\\ \dot{\boldsymbol{\nu}}_d &= \mathbf{R}^T(\psi_d)\ddot{\boldsymbol{\eta}}_{dr} - r_d\mathbf{R}^T(\psi_d)\mathbf{S}\dot{\boldsymbol{\eta}}_{dr} - \dot{r}_d\mathbf{S}\mathbf{r}^b_{br} && (5.10)\end{aligned}$$

Observe that this trajectory satisfies $\dot{\boldsymbol{\eta}}_d = \mathbf{R}(\psi_d)\boldsymbol{\nu}_d$. The corresponding velocities $\boldsymbol{\nu}_d(t) = [u_d, v_d, r_d]^T$ and accelerations $\dot{\boldsymbol{\nu}}_d(t) = [\dot{u}_d, \dot{v}_d, \dot{r}_d]^T$ are thus decomposed in the reference parallel d-frame.

5.3 Commutating Control

From a practical point of view it is important that the tuning procedure for the DP controller is intuitive. There is usually little time available for detailed tuning,

and still the adjustments made during a short sea trial have to perform well in weather conditions ranging from calm sea to the more extreme. During the limited time available personnel with limited theoretic background make decisions influencing the vessel's positioning performance for many years to come. Computer simulations do provide an acceptable initial tuning, but some modifications are almost always needed. If a controller gain adjustment does result in a predictable behavior of the vessel, it is likely that the engineer is confident that the tuning is acceptable, the overall procedure takes less time, and the customer eventually gets satisfied.

Here we elaborate on nonlinear PID-like tracking controllers simply because such controllers are readily interpreted and analyzed. Low speed vessel tracking and positioning control can be accomplished with relatively simple means, such as PID-control, and in a critical situation where understanding of physics is needed experimenting with other approaches may not be advisable. The price we pay for concentrating on such straightforward controllers is that stability can only be guaranteed for bounded yaw rates. However, the resulting upper bound $r_{\max}$ for a well-behaving controller usually exceeds the physical limitations for the ship. A definite advantage is that we can incorporate static or dynamic feedback from acceleration directly within the derived framework. The derived controllers are linear in the sense that their respective terms are bounded linearly in the error variables. They are nonlinear in the sense that the kinematics is included.

5.3.1 Full State Feedback PID Tracking Control

The motivation for studying PID or even PD in detail is to show how different linear design techniques can be applied in DP control. Similarly to the observer design, it is possible to separate the kinematics from the design procedure and later include these rotations again when implementing the controller. Finding the controller's gains themselves is a task which may be performed without considering the kinematics at all.

The objective is to track a given smooth trajectory $(\boldsymbol{\eta}_d(t), \boldsymbol{\nu}_d(t), \dot{\boldsymbol{\nu}}_d(t))$. Let the position error $\boldsymbol{\eta}_e$ be given in the Earth-fixed n-frame and the velocity and acceleration error in the b-frame, that is

$$\begin{aligned} \boldsymbol{\eta}_e &= \boldsymbol{\eta} - \boldsymbol{\eta}_d && (5.11)\\ \boldsymbol{\nu}_e &= \boldsymbol{\nu} - \mathbf{R}^T(\psi_e)\boldsymbol{\nu}_d && (5.12)\\ \dot{\boldsymbol{\nu}}_e &= \dot{\boldsymbol{\nu}} - \dot{\psi}_e \mathbf{S}^T \mathbf{R}^T(\psi_e)\boldsymbol{\nu}_d - \mathbf{R}^T(\psi_e)\dot{\boldsymbol{\nu}}_d && (5.13) \end{aligned}$$

Observe that in DP $\boldsymbol{\nu}_d = \dot{\boldsymbol{\nu}}_d = \mathbf{0}$ such that

$$\begin{aligned} \boldsymbol{\eta}_e &= \boldsymbol{\eta} - \boldsymbol{\eta}_d \\ \boldsymbol{\nu}_e &= \boldsymbol{\nu} \\ \dot{\boldsymbol{\nu}}_e &= \dot{\boldsymbol{\nu}} \end{aligned}$$

The low-speed ship model considered is

$$\dot{\boldsymbol{\eta}} = \mathbf{R}(\psi)\boldsymbol{\nu} \tag{5.14}$$
$$\mathbf{M}\dot{\boldsymbol{\nu}} + \mathbf{D}_L\boldsymbol{\nu} = \boldsymbol{\tau} + \mathbf{R}^T(\psi)\mathbf{w} \tag{5.15}$$

where $\mathbf{w} = \mathbf{w}_b + \mathbf{R}(\psi)\mathbf{w}_{sv}$ is an disturbance consisting of a constant bias $\mathbf{w}_b$ and a slowly varying term $\mathbf{w}_{sv}$. The former will be attenuated be integral action. During the design we will, however, let $\mathbf{w} = \mathbf{0}$ in order to simplify the stability analysis.

A controller with respective proportional, integral, and derivative gains $\mathbf{K}_p, \mathbf{K}_i, \mathbf{K}_d \in \mathbb{R}^{3\times 3}$ can be formulated as

$$\dot{\boldsymbol{\xi}} = \boldsymbol{\eta}_e \tag{5.16}$$
$$\boldsymbol{\tau} = -\mathbf{K}_i\mathbf{R}^T(\psi)\boldsymbol{\xi} - \mathbf{K}_p\mathbf{R}^T(\psi)\boldsymbol{\eta}_e - \mathbf{K}_d\boldsymbol{\nu}_e + \boldsymbol{\tau}_{\text{rff}} \tag{5.17}$$

where $\psi_e = \psi - \psi_d$. Notice that the first three terms form the PID feedback control while the latter term $\boldsymbol{\tau}_{\text{rff}}$ is the reference feed-forward given by

$$\boldsymbol{\tau}_{\text{rff}} = \mathbf{D}_L\mathbf{R}^T(\psi_e)\boldsymbol{\nu}_d + \mathbf{M}\left(\dot{\psi}_e\mathbf{S}^T\mathbf{R}^T(\psi_e)\boldsymbol{\nu}_d + \mathbf{R}^T(\psi_e)\dot{\boldsymbol{\nu}}_d\right) \tag{5.18}$$

Also note that the gains $\mathbf{K}_i$ and $\mathbf{K}_p$ have been put to the left of $\mathbf{R}^T(\psi)$ making them body-fixed gains. This makes more sense to an operator than having them on the right of $\mathbf{R}^T(\psi)$ (Loría *et al.* 2000) because the compass heading $\psi(t)$ should not influence the convergence rates. The drawback of doing this is that energy-based stability proofs can no longer be applied directly.

By inserting $\boldsymbol{\tau}$ into (5.15) we get

$$\mathbf{M}\Big(\dot{\boldsymbol{\nu}} - \dot{\psi}_e\mathbf{S}^T\mathbf{R}^T(\psi_e)\boldsymbol{\nu}_d + \mathbf{R}^T(\psi_e)\dot{\boldsymbol{\nu}}_d\Big) = -\mathbf{K}_i\mathbf{R}^T(\psi)\boldsymbol{\xi} - \mathbf{K}_p\mathbf{R}^T(\psi)\boldsymbol{\eta}_e - (\mathbf{K}_d + \mathbf{D}_L)\,\boldsymbol{\nu}_e$$

Consequently, the velocity error dynamics can be written

$$\mathbf{M}\dot{\boldsymbol{\nu}}_e = -\mathbf{K}_i\mathbf{R}^T(\psi)\boldsymbol{\xi} - \mathbf{K}_p\mathbf{R}^T(\psi)\boldsymbol{\eta}_e - (\mathbf{K}_d + \mathbf{D}_L)\,\boldsymbol{\nu}_e \tag{5.19}$$

By collecting the states $\mathbf{x}_e = [\boldsymbol{\xi}^T, \boldsymbol{\eta}_e^T, \boldsymbol{\nu}_e^T]^T$ and simultaneously considering the slowly varying disturbance $\mathbf{w}_{sv}$ only, we may now rewrite the closed-loop dynamics on the compact form

$$\dot{\mathbf{x}}_e = \mathbf{T}^T(\psi)\mathbf{A}_c\mathbf{T}(\psi)\mathbf{x}_e + \mathbf{B}\mathbf{w}_{sv} \tag{5.20}$$

where $\mathbf{T}(\psi)$ is defined as the block-diagonal $\mathbf{T}(\psi) = \text{Diag}(\mathbf{R}^T(\psi), \mathbf{R}^T(\psi), \mathbf{I})$ and

$$\mathbf{A}_c = \mathbf{A} - \mathbf{B}\mathbf{K} = \begin{bmatrix} \mathbf{0} & \mathbf{I} & \mathbf{0} \\ \mathbf{0} & \mathbf{0} & \mathbf{I} \\ -\mathbf{M}^{-1}\mathbf{K}_i & -\mathbf{M}^{-1}\mathbf{K}_p & -\mathbf{M}^{-1}\left(\mathbf{D}_L + \mathbf{K}_d\right) \end{bmatrix} \tag{5.21}$$
$$\mathbf{B} = \begin{bmatrix} \mathbf{0} & \mathbf{0} & \mathbf{M}^{-T} \end{bmatrix}^T \tag{5.22}$$
$$\mathbf{K} = \begin{bmatrix} \mathbf{K}_i & \mathbf{K}_p & \mathbf{K}_d \end{bmatrix} \tag{5.23}$$

Due to the pair $(\mathbf{B}, \mathbf{A})$ being controllable, we have complete control over the eigenvalues of $\mathbf{A}_c$ by assigning appropriate gains $\mathbf{K}_p$, $\mathbf{K}_i$, and $\mathbf{K}_d$. Similarly to

the observer design, the eigenvalues of $\mathbf{T}^T(\psi)\mathbf{A}_c\mathbf{T}(\psi)$ are constant for all ψ and equal to the ones of $\mathbf{A}_c$ because $\mathbf{T}^T(\psi) = \mathbf{T}^{-1}(\psi)$. The applied control $\boldsymbol{\tau}$ is using these definitions written as

$$\boldsymbol{\tau} = -\mathbf{K}\mathbf{T}(\psi)\mathbf{x}_e + \boldsymbol{\tau}_{\text{rff}} \tag{5.24}$$

where the gain $\mathbf{K} \in \mathbb{R}^{3\times 9}$ is given by (5.23) and $\boldsymbol{\tau}_{\text{rff}}$ by (5.18).

We have deliberately left out a Coriolis term in the controller (5.24) compensating for the time-derivative of $\mathbf{R}(\psi)$ that would have allowed us to establish global stability properties. The limiting factor is thus the rotation rate $\dot{\psi} = r$. Nevertheless, uniform local exponential stability (ULES) can be verified for bounded $r(t)$, that is $|r(t)| \leq r_{\max}$. Notice also that $\lim_{t\to\infty} \mathbf{x}_e(t) = \mathbf{0}$ does not imply that $\psi \to 0$ but rather $\psi \to \psi_d$ even though ψ occurs in error dynamics $\dot{\mathbf{x}}_e = \mathbf{T}^T(\psi)\mathbf{A}_c\mathbf{T}(\psi)\mathbf{x}_e$.

Theorem 5.1 *Consider the system (5.14)-(5.15) controlled by (5.24). Suppose* $|r(t)| \leq r_{\max}$ *and* $\mathbf{w}_{sv} = \mathbf{0}$ *for all* $t \geq t_0$. *The origin* $\mathbf{x}_e = \mathbf{0}$ *of (5.20) is uniformly locally exponentially stable provided* $r_{\max} > 0$ *is sufficiently small and if and only if* $\mathbf{K}_p, \mathbf{K}_d, \mathbf{K}_i \in \mathbb{R}^{3\times 3}$ *are chosen such that* $\mathbf{A}_c$ *as defined by (5.21) is Hurwitz. If* $r_{\max}$ *is larger than any physical upper limit for* $|r(t)|$, *(5.20) is said to be uniformly globally exponentially stable.*

Proof. The necessity of $\mathbf{A}_c$ being Hurwitz is well known. For proving sufficiency, define $\mathbf{z} = \mathbf{T}(\psi)\mathbf{x}_e$. By $\dot{\mathbf{T}}(\psi)$ we hereby mean $\frac{d}{dt}(\mathbf{T}(\psi))$. Then,

$$\dot{\mathbf{z}} = \dot{\mathbf{T}}\mathbf{x}_e + \mathbf{T}\dot{\mathbf{x}}_e = \dot{\mathbf{T}}\mathbf{T}^T\mathbf{z} + \mathbf{A}_c\mathbf{T}\mathbf{x}_e = (\mathbf{A}_c + r\mathbf{S}_T)\,\mathbf{z} \tag{5.25}$$

where $\mathbf{S}_T = \text{Diag}(\mathbf{S}^T, \mathbf{S}^T, 0)$. If and only if $\mathbf{A}_c$ is Hurwitz there exists a $\mathbf{P} = \mathbf{P}^T > 0$ such that

$$\mathbf{P}\mathbf{A}_c + \mathbf{A}_c^T\mathbf{P} = -\mathbf{Q} \tag{5.26}$$

for a given $\mathbf{Q} = \mathbf{Q}^T > 0$.

Consider the radially unbounded storage function $V(\mathbf{x}_e, \psi) = \mathbf{x}_e^T\mathbf{T}^T(\psi)\mathbf{P}\mathbf{T}(\psi)\mathbf{x}_e = \mathbf{z}^T\mathbf{P}\mathbf{z}$. Differentiated along the trajectories we get

$$\begin{aligned}
\dot{V} &= \dot{\mathbf{z}}^T\mathbf{P}\mathbf{z} + \mathbf{z}^T\mathbf{P}\dot{\mathbf{z}} \\
&= \mathbf{z}^T\left(\mathbf{A}_c^T\mathbf{P} + \mathbf{P}\mathbf{A}_c + r\left(\mathbf{P}\mathbf{S}_T + \mathbf{S}_T^T\mathbf{P}\right)\right)\mathbf{z} \\
&\leq -\mathbf{z}^T\mathbf{Q}\mathbf{z} + 2r_{\max}\lambda_{\max}(\mathbf{P})\,|\mathbf{z}|^2 \\
&= -\left(\lambda_{\min}(\mathbf{Q}) - 2r_{\max}\lambda_{\max}(\mathbf{P})\right)|\mathbf{x}_e|^2
\end{aligned} \tag{5.27}$$

which is negative definite provided that $r_{\max}$ is small enough. ■

If it is known a priori that $r(t) \in \mathcal{L}_2 \cap \mathcal{L}_\infty$, convergence to zero can be shown no matter how large $\sup_{t\geq 0} r(t)$ actually is. On the other hand, if we do not in advance know that $r(t) \to 0$, an efficient but admittedly conservative method for estimating $r_{\max} > 0$ is solving a generalized eigenvalue problem (Boyd *et al.* 1994) as explained in the following Corollary:

Corollary 5.1 *For a given* $\mathbf{A}_c$*, a yaw rate bound* $r_{\max} > 0$ *that guarantees exponential stability of (5.20) can be found be solving the following generalized eigenvalue problem in the decision variables* $\mathbf{P}$ *and* λ

$$\begin{array}{ll} \textit{minimize} & \lambda \\ \textit{subject to} & \left\{ \begin{array}{rcl} \mathbf{P} = \mathbf{P}^T > 0, \quad \lambda > 0 & & \\ \mathbf{P}\mathbf{S}_T + \mathbf{S}_T^T\mathbf{P} & < & -\lambda\left(\mathbf{A}_c^T\mathbf{P} + \mathbf{P}\mathbf{A}_c\right) \\ -\mathbf{P}\mathbf{S}_T - \mathbf{S}_T^T\mathbf{P} & < & -\lambda\left(\mathbf{A}_c^T\mathbf{P} + \mathbf{P}\mathbf{A}_c\right) \end{array} \right. \end{array} \tag{5.28}$$

where $r_{\max} = 1/\lambda$.

Proof. From the proof of Theorem 5.1 we note that if

$$g(r) = \lambda_{\max}\left(\mathbf{A}_c^T\mathbf{P} + \mathbf{P}\mathbf{A}_c + r\left(\mathbf{P}\mathbf{S}_T + \mathbf{S}_T^T\mathbf{P}\right)\right) < 0$$

for all $t \geq t_0$ then (5.20) is exponentially stable. As $g(r)$ is linear in r it suffices to show $g(-r_{\max}) < 0$ and $g(r_{\max}) < 0$, and the constraints in (5.28) therefore ensures $g(r) < 0$ for all $|r(t)| \leq r_{\max}$. ■

Observe that Corollary 5.1 yields a conservative $r_{\max}$ because it allows infinitely fast changes in $r(t)$, that is unbounded $|\dot{r}(t)|$, as long as $|r(t)| < r_{\max}$. Still, finding this $r_{\max}$ given any Hurwitz $\mathbf{A}_c$ is a relatively simple task using available software packages like Matlab's LMI Toolbox (Gahinet *et al.* 1995).

5.3.2 LMI Control Strategies

Yet another feature of the LMIs given by Corollary 5.1 is that it may be combined by LMI based control synthesis methods in order to provide state-feedback controllers rendering the closed loop globally exponentially stable for any specified $r_{\max}$. This section briefly explores how LMI synthesis provides a state feedback $\mathbf{K}$ resulting in a globally exponentially stable closed loop dynamics for any given $r_{\max}$.

First, we briefly summarize three common and widely applicable kinds of LMI control strategies that may be used separately or in combination, those being $\mathcal{H}_\infty$, $\mathcal{H}_2$, and pole-clustering. When applied together, we say that the resulting control is multiobjective. Using the more general description of a linear plant

$$\mathbf{H}\left\{ \begin{array}{rl} \dot{\mathbf{x}} & = \mathbf{A}\mathbf{x} + \mathbf{B}\mathbf{u} + \mathbf{E}\mathbf{w} \\ \mathbf{z}_\infty & = \mathbf{C}_\infty\mathbf{x} + \mathbf{D}_{\infty w}\mathbf{w} + \mathbf{D}_{\infty u}\mathbf{u} \\ \mathbf{z}_2 & = \mathbf{C}_2\mathbf{x} + \mathbf{D}_{2u}\mathbf{u} \end{array} \right. \tag{5.29}$$

where $\mathbf{z}_\infty \in \mathbb{R}^{n_\infty}$ and $\mathbf{z}_2 \in \mathbb{R}^{n_2}$ are the outputs used in the $\mathcal{H}_\infty$ and $\mathcal{H}_2$ cost criteria, respectively. Let $\mathbf{A} \in \mathbb{R}^{n\times n}$ and $\mathbf{B} \in \mathbb{R}^{n\times m}$ be the nominal model, and without any further discussion on model scaling, we assume that $\mathbf{E} \in \mathbb{R}^{n\times p}$, $\mathbf{C}_\infty \in \mathbb{R}^{n_\infty\times n}$, $\mathbf{D}_{\infty w} \in \mathbb{R}^{n_\infty\times p}$, $\mathbf{D}_{\infty u} \in \mathbb{R}^{n_\infty\times m}$, $\mathbf{C}_2 \in \mathbb{R}^{n_2\times n}$, and $\mathbf{D}_{2u} \in \mathbb{R}^{n_\infty\times m}$ are properly scaled. The control objective is to compute a state-feedback controller

$$\mathbf{u} = -\mathbf{K}\mathbf{x} \tag{5.30}$$

that fulfills certain specifications on the closed-loop behavior. These closed loop design criteria can be cast as convex optimization problems satisfying certain LMIs. The following summary is taken from a variety of sources (Boyd *et al.* 1994, Chilali and Gahinet 1996, Scherer *et al.* 1997).

$\mathcal{H}_\infty$-Control

Let $\mathbf{H}_{wz_\infty}(s)$ denote the closed loop realization between $\mathbf{w}$ and $\mathbf{z}_\infty$. Minimization of the $\mathcal{H}_\infty$-gain γ from $\mathbf{w}$ to $\mathbf{z}_\infty$ can be cast as an LMI optimization problem in the matrix variables $\mathbf{X}_\infty \in \mathbb{R}^{n\times n}$ and $\mathbf{Y} \in \mathbb{R}^{m\times n}$ (with $\mathbf{X}_\infty = \mathbf{X}_\infty^T > 0$) and $\mathbf{Y}$ while minimizing $\gamma > 0$ in the following LMI

$$\begin{bmatrix} \mathbf{A}\mathbf{X}_\infty + \mathbf{X}_\infty\mathbf{A}^T + \mathbf{B}\mathbf{Y} + \mathbf{Y}^T\mathbf{B}^T & \mathbf{E} & \mathbf{X}_\infty\mathbf{C}_\infty^T + \mathbf{Y}^T\mathbf{D}_{\infty u}^T \\ \mathbf{E}^T & -\gamma^2\mathbf{I} & \mathbf{D}_{\infty w}^T \\ \mathbf{C}_\infty\mathbf{X}_\infty + \mathbf{D}_{\infty u}\mathbf{Y} & \mathbf{D}_{\infty w} & -\mathbf{I} \end{bmatrix} < 0 \quad (5.31)$$

This inequality is known as the bounded real lemma. Provided that (5.31) is feasible, it is guaranteed that the $\mathcal{H}_\infty$ gain is below γ, that is $\|\mathbf{H}_{wz_\infty}(s)\|_\infty < \gamma$, when applying the state-feedback matrix

$$\mathbf{K} = -\mathbf{Y}\mathbf{X}_\infty^{-1} \quad (5.32)$$

A prerequisite for this method to complete successfully is that the pair $(\mathbf{A}, \mathbf{B})$ is controllable and $(\mathbf{A}, \mathbf{C}_\infty)$ is observable. This means that for the augmented integral control to work, the augmented state $\boldsymbol{\xi}$ must be reflected in the output matrix $\mathbf{C}_\infty$. The $\mathcal{H}_\infty$ performance is convenient to enforce robustness to model uncertainty, and it is a direct measure for the $\mathcal{L}_2$ gain from disturbance $\mathbf{w} \in \mathcal{L}_2$ to the respective output $\mathbf{z}_\infty \in \mathcal{L}_2$.

$\mathcal{H}_2$-Control

Let $\mathbf{H}_{wz_2}(s)$ denote the closed loop realization between $\mathbf{w}$ and $\mathbf{z}_2$. Then, $\|\mathbf{H}_{wz_2}(s)\|_2 < \varepsilon$ if there exist $\mathbf{X}_2 = \mathbf{X}_2^T < 0$, $\mathbf{Y} \in \mathbb{R}^{m\times n}$, and $\mathbf{Z} \in \mathbb{R}^{n\times n_2}$ such that the following LMIs are feasible

$$\begin{aligned} \begin{bmatrix} \mathbf{A}\mathbf{X}_2 + \mathbf{X}_2\mathbf{A}^T + \mathbf{B}\mathbf{Y} + \mathbf{Y}^T\mathbf{B}^T & \mathbf{E} \\ \mathbf{E}^T & -\mathbf{I} \end{bmatrix} &< 0 \\ \begin{bmatrix} -\mathbf{X}_2 & \mathbf{X}_2\mathbf{C}_2^T \\ \mathbf{C}_2\mathbf{X}_2 & -\mathbf{Z} \end{bmatrix} &< 0 \\ \mathrm{Trace}(\mathbf{Z}) &< \varepsilon^2 \end{aligned} \quad (5.33)$$

Consequently, the state-feedback $\mathbf{u} = -\mathbf{K}\mathbf{x}$, where $\mathbf{K}$ is defined similarly to (5.32) as $\mathbf{K} = -\mathbf{Y}\mathbf{X}_2^{-1}$, guarantees that the $\mathcal{H}_2$-gain from $\mathbf{w}$ to $\mathbf{z}_\infty$ is below ε.

Pole Clustering

Assigning closed loop poles of a linear system can be seen as a tool for specifying a minimum decay rate. This technique may also be used to ensure a minimum closed

loop damping factor or a maximum bandwidth in order to avoid fast dynamics and high frequency gain in the controller.

In order to describe convex regions in the complex plane in which the poles are supposed to be put, we follow the definitions of Chilali and Gahinet (1996):

Definition 5.1 *A subset $\mathcal{D}$ of the complex plane $\mathbb{C}$ is called an LMI region if there exist a symmetric matrix $\boldsymbol{\alpha} \in \mathbb{R}^{n_\mathcal{D} \times n_\mathcal{D}}$ and a matrix $\boldsymbol{\beta} \in \mathbb{R}^{n_\mathcal{D} \times n_\mathcal{D}}$ such that*

$$\mathcal{D} = \{z \in \mathbb{C} : \quad \mathbf{F}_\mathcal{D} < 0\} \tag{5.34}$$

with

$$\mathbf{F}_\mathcal{D}(z) = \boldsymbol{\alpha} + z\boldsymbol{\beta} + \bar{z}\boldsymbol{\beta}^T < 0 \tag{5.35}$$

where $\bar{z}$ is the complex conjugate of z.

An LMI region is convex and symmetric about the real axis. Furthermore, LMI regions are invariant under set intersection: The intersection of two LMI regions $\mathcal{D}_1$ and $\mathcal{D}_2$ is also an LMI region with the characteristic function

$$\mathbf{F}_{\mathcal{D}_1 \cap \mathcal{D}_2}(z) = \mathrm{Diag}(\mathbf{F}_{\mathcal{D}_1}(z), \mathbf{F}_{\mathcal{D}_2}(z)) \tag{5.36}$$

As a consequence, an arbitrary region consisting of the intersection of conic curves, vertical strips, and/or horizontal strips can be expressed in terms of LMI regions.

Definition 5.2 *A matrix $\mathbf{A}$ is said to be $\mathcal{D}$-stable if all its eigenvalues lie in $\mathcal{D}$.*

We may now summarize this for control synthesis purposes by the following theorem (Chilali and Gahinet 1996):

Theorem 5.2 *Let $\boldsymbol{\alpha} \in \mathbb{R}^{n_\mathcal{D} \times n_\mathcal{D}}$ be a real symmetric matrix and $\boldsymbol{\beta} \in \mathbb{R}^{n_\mathcal{D} \times n_\mathcal{D}}$. Then $\mathbf{A}_{cl} = \mathbf{A} - \mathbf{BK}$ has all its eigenvalues in the LMI region (5.35) if and only if a real, symmetric, positive definite $\mathbf{X} \in \mathbb{R}^{n \times n}$ and a real $\mathbf{Y} \in \mathbb{R}^{m \times n}$ exist such that the LMI*

$$\boldsymbol{\alpha} \otimes \mathbf{X} + \boldsymbol{\beta} \otimes \mathbf{V} + \boldsymbol{\beta}^T \otimes \mathbf{V}^T < 0 \tag{5.37}$$

where $\otimes$ is the Kronecker product and

$$\mathbf{V} = \mathbf{AX} + \mathbf{BY} \tag{5.38}$$

$$\mathbf{K} = -\mathbf{YX}^{-1} \tag{5.39}$$

is feasible.

Observe that this is a generalization of Lyapunov stability for linear systems, that is the eigenvalues of $\mathbf{A}_c$ having negative real part (Hurwitz), because the left half complex plane is described by $\alpha = 0$ and $\beta = 1$. Then, Theorem 5.2 simply states that

$$\mathbf{A}_c\mathbf{X} + \mathbf{X}\mathbf{A}_c^T < 0 \tag{5.40}$$

For more examples of various LMI regions and how to construct them, please refer to Chilali and Gahinet (1996).

Stability For a Prescribed $r_{\max}$

Let us now recast the results from Corollary 5.1 into a set of LMIs that can be included with other LMIs in a state feedback synthesis procedure. For the sake of clarity, this result is formulated as a Theorem.

Theorem 5.3 *Suppose the system (5.14)-(5.15) is to track a sufficiently smooth trajectory $\boldsymbol{\eta}_d(t) = [x_d(t), y_d(t), \psi_d(t)]^T$ by using the controller (5.16)-(5.17). If there for a specified $r_{\max} > 0$ exist matrices $\mathbf{X} = \mathbf{X}^T > 0$ and $\mathbf{Y} \in \mathbb{R}^{m \times n}$ such that*

$$\begin{aligned} \mathbf{A}\mathbf{X} + \mathbf{X}\mathbf{A}^T + \mathbf{B}\mathbf{Y} + \mathbf{Y}^T\mathbf{B}^T + r_{\max}\left(\mathbf{S}_T\mathbf{X} + \mathbf{X}\mathbf{S}_T^T\right) &< 0 \\ \mathbf{A}\mathbf{X} + \mathbf{X}\mathbf{A}^T + \mathbf{B}\mathbf{Y} + \mathbf{Y}^T\mathbf{B}^T - r_{\max}\left(\mathbf{S}_T\mathbf{X} + \mathbf{X}\mathbf{S}_T^T\right) &< 0 \end{aligned} \tag{5.41}$$

is feasible, then the state feedback gain $\mathbf{K} = -\mathbf{Y}\mathbf{X}^{-1}$ guarantees uniform (global) exponential stability of $\mathbf{x}_e$.

Proof. Revisiting Theorem 5.1 we remember that the exponential stability of $\mathbf{x}_e$ is equivalent to the existence of a $\mathbf{P} = \mathbf{P}^T > 0$ such that for all $r(t) < r_{\max}\ \forall t \geq 0$

$$(\mathbf{A} - \mathbf{B}\mathbf{K})^T\mathbf{P} + \mathbf{P}(\mathbf{A} - \mathbf{B}\mathbf{K}) + r\left(\mathbf{P}\mathbf{S}_T + \mathbf{S}_T^T\mathbf{P}\right) < 0 \tag{5.42}$$

Pre- and post-multiplying with $\mathbf{P}^{-1}$ and substituting $\mathbf{Y} = -\mathbf{K}\mathbf{P}^{-1}$ we get

$$\mathbf{A}\mathbf{X} + \mathbf{B}\mathbf{Y} + \mathbf{X}\mathbf{A}^T + \mathbf{Y}^T\mathbf{B}^T + r\left(\mathbf{S}_T\mathbf{X} + \mathbf{X}\mathbf{S}_T^T\right) < 0 \tag{5.43}$$

Negative definiteness is ensured by (5.41) since this inequality is convex in r. ■

As for the other LMI criteria above, in a control synthesis procedure we end up searching for a $\mathbf{X} = \mathbf{X}^T > 0$ and a $\mathbf{Y}$. Consequently, (5.41) can be combined with any suitable LMI design criterion, that being $\mathcal{H}_\infty$, $\mathcal{H}_2$, pole clustering or combinations of those, to obtain globally exponentially stable tracking controllers for all $r_{\max}$.

5.4 Acceleration Feedback

Having established the PID control framework we are now ready to expand the state feedback control synthesis above with additional acceleration feedback. The proposed controller and the certainty equivalence realization are particular contributions of this thesis.

5.4.1 Dynamic Acceleration Feedback

First, let us consider the velocity and acceleration dynamics. Suppose that measured acceleration $\mathbf{y}_a \in \mathbb{R}^{n_{y_a}}$ where $1 \leq n_{y_a} \leq 3$ is given in the b-frame and let

$\mathbf{\Pi} \in \mathbb{R}^{n_{y_a} \times 3}$ be the projection extracting those available accelerations $\mathbf{y}_a = \mathbf{\Pi}\dot{\boldsymbol{\nu}}$. Let the applied control $\boldsymbol{\tau}$ be

$$\begin{aligned} \dot{\mathbf{a}}_f &= \mathbf{A}_f \mathbf{a}_f + \mathbf{B}_f \left(\mathbf{y}_a - \mathbf{\Pi} \left(\dot{\psi}_e \mathbf{S}^T \mathbf{R}^T(\psi_e) \boldsymbol{\nu}_d + \mathbf{R}^T(\psi_e) \dot{\boldsymbol{\nu}}_d \right) \right) \\ \boldsymbol{\tau} &= \boldsymbol{\tau}_{\text{PID}} - \mathbf{K}_a \mathbf{a}_f \end{aligned} \tag{5.44}$$

where $\mathbf{a}_f \in \mathbb{R}^{n_a}$ is the filtered acceleration error described by the $\mathbf{A}_f \in \mathbb{R}^{n_a \times n_a}$ and $\mathbf{B}_f \in \mathbb{R}^{n_a \times n_{y_a}}$ matrices. $\boldsymbol{\tau}_{\text{PID}}$ is to be determined shortly. The velocity error dynamics can be written

$$\mathbf{M}\dot{\boldsymbol{\nu}}_e = -\mathbf{D}\boldsymbol{\nu}_e + \boldsymbol{\tau}_{\text{PID}} - \mathbf{K}_a \mathbf{a}_f + \mathbf{w} \tag{5.45}$$

At low frequencies $\mathbf{a}_f \approx \mathbf{y}_a - \mathbf{\Pi} \left(\dot{\psi}_e \mathbf{S}^T \mathbf{R}^T(\psi_e) \boldsymbol{\nu}_d + \mathbf{R}^T(\psi_e) \dot{\boldsymbol{\nu}}_d \right) = \mathbf{\Pi}\boldsymbol{\nu}_e$ which means that the acceleration feedback term $\mathbf{K}_a \mathbf{a}_f$ can be regarded as a change in the system's mass. Taking the position error dynamics into account, we get

$$\begin{aligned} \dot{\boldsymbol{\eta}}_e &= \mathbf{R}(\psi)\boldsymbol{\nu}_e \\ (\mathbf{M} + \mathbf{K}_a \mathbf{\Pi})\, \dot{\boldsymbol{\nu}}_e &= -\mathbf{D}\boldsymbol{\nu}_e + \boldsymbol{\tau}_{\text{PID}} + \mathbf{w} \end{aligned} \tag{5.46}$$

Next, we want to find a PID-like control law $\boldsymbol{\tau}_{\text{PID}}$ for the system (5.46). As in Section 5.3 integral action is obtained by integrating the position deviation and assign gains $\mathbf{K}_i \in \mathbb{R}^{3\times3}$, $\mathbf{K}_p \in \mathbb{R}^{3\times3}$, $\mathbf{K}_d \in \mathbb{R}^{3\times3}$. Applying the very same PID-controller as in (5.16)-(5.17), that is

$$\begin{aligned} \dot{\boldsymbol{\xi}} &= \boldsymbol{\eta}_e \\ \boldsymbol{\tau}_{\text{PID}} &= -\mathbf{K}_i \mathbf{R}^T(\psi)\boldsymbol{\xi} - \mathbf{K}_p \mathbf{R}^T(\psi)\boldsymbol{\eta}_e - \mathbf{K}_d \boldsymbol{\nu}_e + \boldsymbol{\tau}_{\text{rff}} \end{aligned} \tag{5.47}$$

where the reference feed-forward $\boldsymbol{\tau}_{\text{rff}}$ is defined by (5.18). Collecting the states into $\mathbf{x}_e = [\boldsymbol{\xi}^T, \boldsymbol{\eta}_e^T, \boldsymbol{\nu}_e^T, \mathbf{a}_f^T]^T \in \mathbb{R}^{9+n_a}$, we can by defining the block-diagonal $\mathbf{T} : \mathbb{R} \to \mathbb{R}^{(9+n_a)\times(9+n_a)}$ as follows

$$\mathbf{T}(\alpha) = \text{Diag}(\mathbf{R}^T(\alpha), \mathbf{R}^T(\alpha), \mathbf{I}_{3+n_a}) \tag{5.48}$$

and letting $\mathbf{B}_M = \mathbf{B}_f \mathbf{\Pi} \mathbf{M}^{-1}$ express the complete error-dynamics on the compact form

$$\dot{\mathbf{x}}_e = \mathbf{T}^T(\psi)\mathbf{A}_c\mathbf{T}(\psi)\mathbf{x}_e + \mathbf{E}\mathbf{w} \tag{5.49}$$

where

$$\mathbf{A}_c = \begin{bmatrix} \mathbf{0} & \mathbf{I} & \mathbf{0} & \mathbf{0} \\ \mathbf{0} & \mathbf{0} & \mathbf{I} & \mathbf{0} \\ -\mathbf{M}^{-1}\mathbf{K}_i & -\mathbf{M}^{-1}\mathbf{K}_p & -\mathbf{M}^{-1}(\mathbf{D}+\mathbf{K}_d) & -\mathbf{M}^{-1}\mathbf{K}_a \\ -\mathbf{B}_M\mathbf{K}_i & -\mathbf{B}_M\mathbf{K}_p & -\mathbf{B}_M(\mathbf{D}+\mathbf{K}_d) & \mathbf{A}_f - \mathbf{B}_M\mathbf{K}_a \end{bmatrix} \tag{5.50}$$

$$\mathbf{E} = \begin{bmatrix} \mathbf{0} & \mathbf{0} & \mathbf{I} & \mathbf{B}_M^T \end{bmatrix}^T \tag{5.51}$$

The system parameters and controller gains have been isolated in the matrix $\mathbf{A}_c$, and due to controllability the eigenvalues of $\mathbf{A}_c$ are freely assignable.

Theorem 5.1 and Corollary 5.1 can now be employed to establish stability properties for (5.49).

5.4.2 Controller Tuning

One of the main objectives of this thesis was to illustrate that constructive use of measured acceleration could improve performance of DP systems compared to PID or PD designs irrespective of their design philosophy. A reasonable way to do this is to assign more or less identical poles to the resulting closed-loop systems. The method is described in this section.

Step 1: Acceleration Feedback.

A first-order low-pass filter was used to remove high-frequency noise components from the two acceleration signals available, surge- and sway-acceleration. Thus, we let $\mathbf{K}_a \in \mathbb{R}^{3\times 2}$ and

$$\mathbf{A}_f = -\mathbf{B}_f = \text{diag}(-1/T_f, -1/T_f) \tag{5.52}$$

$$\mathbf{\Pi} = \begin{bmatrix} 1 & 0 & 0 \\ 0 & 1 & 0 \end{bmatrix} \tag{5.53}$$

where the filter constant T_f was selected so small

$$T_f \ll \min\left(\frac{m_{11}}{d_{11}}, \frac{m_{22}}{d_{22}}\right) \tag{5.54}$$

that the acceleration feedback term could be regarded as a direct manipulation of the mass (5.46), that is $\mathbf{M}_a = \mathbf{M} + \mathbf{K}_a\mathbf{\Pi}$.

Step 2: PID-control.

When the rotations are disregarded, we are left with finding a state-feedback control $\mathbf{u} = -\mathbf{K}\mathbf{x}$ to the system

$$\dot{\mathbf{x}}_e = \mathbf{A}\mathbf{x}_e + \mathbf{B}\mathbf{u} \tag{5.55}$$

where

$$\mathbf{A} = \begin{bmatrix} \mathbf{0} & \mathbf{I} & \mathbf{0} \\ \mathbf{0} & \mathbf{0} & \mathbf{I} \\ \mathbf{0} & \mathbf{0} & \mathbf{M}_a^{-1}\mathbf{D} \end{bmatrix} \quad , \quad \mathbf{B} = \begin{bmatrix} \mathbf{0} \\ \mathbf{0} \\ \mathbf{M}_a^{-1} \end{bmatrix} \tag{5.56}$$

When the gain matrix $\mathbf{K} \in \mathbb{R}^{3\times 9}$ is partitioned as follows

$$\mathbf{K} = \begin{bmatrix} \mathbf{K}_i & \mathbf{K}_p & \mathbf{K}_d \end{bmatrix} \tag{5.57}$$

the closed loop dynamics can be written as, remember that $\boldsymbol{\eta} \in \mathbb{R}^3$ is the position vector,

$$\ddot{\boldsymbol{\eta}} + 2\mathbf{\Lambda}\mathbf{\Omega}\dot{\boldsymbol{\eta}} + \mathbf{\Omega}^2\boldsymbol{\eta} + \bar{\mathbf{K}}_i \int_0^t \boldsymbol{\eta}(s)ds = \mathbf{w} \tag{5.58}$$

which we recognize as a second order dynamic system with integral action.

$$2\mathbf{\Lambda}\mathbf{\Omega} = \mathbf{M}_a^{-1}(\mathbf{D} + \mathbf{K}_d) \tag{5.59}$$

$$\mathbf{\Omega}^2 = \mathbf{M}_a^{-1}\mathbf{K}_p \tag{5.60}$$

$$\bar{\mathbf{K}}_i = \mathbf{M}_a^{-1}\mathbf{K}_i \tag{5.61}$$

If $\bar{\mathbf{K}}_i = \mathbf{0}$ the matrices $\mathbf{\Omega}, \mathbf{\Lambda} \in \mathbb{R}^{3\times 3}$ determine the natural frequency and relative damping respectively. In this study we de-coupled the individual degrees of freedom by the following selection of gains

$$\mathbf{\Omega} = \text{diag}(\omega_1, \omega_2, \omega_3) \tag{5.62}$$
$$\mathbf{\Lambda} = \text{diag}(\zeta_1, \zeta_2, \zeta_3) \tag{5.63}$$
$$\bar{\mathbf{K}}_i = \text{diag}(k_{i1}, k_{i2}, k_{i3}) \tag{5.64}$$

Consequently, for a constant selection $\mathbf{\Omega}$, $\mathbf{\Lambda}$ and $\bar{\mathbf{K}}_i$, acceleration feedback control as defined in Step 1 does not influence the system's tracking capabilities.

5.4.3 Output Feedback

This section discusses the extension of the state-feedback controller (5.44), (5.47) to output-feedback by using an observer with wave filtering capabilities. Global asymptotic stability of the complete system is established using Theorem A.2. This analysis is valid for any commutating design following the algorithm outlined in Section 5.3. For a more specific treatment of a simpler PID-controller please see Lindegaard and Fossen (2003).

Observer review

The main objective of the implemented observer is to reconstruct the system's LF states and accelerations

$$\mathbf{x}_o = [\hat{\boldsymbol{\eta}}^T, \hat{\boldsymbol{\nu}}^T, \hat{\dot{\boldsymbol{\nu}}}^T]^T \tag{5.65}$$

based on measured positions and other types of sensor data, that is in particular (partial) velocity and acceleration feedback. Note the difference between $\hat{\dot{\boldsymbol{\nu}}}$, the estimated acceleration, and $\dot{\hat{\boldsymbol{\nu}}}$, the differential equation used to update the estimated velocity $\hat{\boldsymbol{\nu}}$.

In Lindegaard *et al.* (2002) an observer for low-speed ship applications was proposed and discussed. Based on the same stability arguments as the state-feedback controller in Section four, that is for bounded yaw rate, the observer error

$$\tilde{\mathbf{x}}_o = \mathbf{x}_o - [\boldsymbol{\eta}^T, \boldsymbol{\nu}^T, \dot{\boldsymbol{\nu}}^T]^T \tag{5.66}$$

was shown to converge exponentially to zero

$$|\tilde{\mathbf{x}}_o(t)| \leq k\,|\tilde{\mathbf{x}}_o(0)| \exp(-\gamma t) \quad , \quad t \geq 0 \tag{5.67}$$

for some $k, \gamma > 0$.

Observer-Feedback Control

Based on the principle of certainty equivalence, an observer-feedback controller is realized substituting the actual states in the state-feedback controller (5.44) and

(5.47) by their estimated values $\hat{\boldsymbol{\eta}}$, $\hat{\boldsymbol{\nu}}$, and $\hat{\dot{\boldsymbol{\nu}}}$. A new set of error variables following the definitions (5.11)-(5.13) are thus

$$\begin{aligned}
\hat{\boldsymbol{\eta}}_e &= \hat{\boldsymbol{\eta}} - \boldsymbol{\eta}_d && (5.68)\\
\hat{\boldsymbol{\nu}}_e &= \hat{\boldsymbol{\nu}} - \mathbf{R}^T(\hat{\psi}_e)\boldsymbol{\nu}_d && (5.69)\\
\hat{\dot{\boldsymbol{\nu}}}_e &= \hat{\dot{\boldsymbol{\nu}}} - \left(\hat{r}_e \mathbf{S}^T \mathbf{R}^T(\hat{\psi}_e)\boldsymbol{\nu}_d + \mathbf{R}^T(\hat{\psi}_e)\dot{\boldsymbol{\nu}}_d\right)\\
&= \hat{\dot{\boldsymbol{\nu}}} - \left((\hat{r} - r_d)\,\mathbf{S}^T \mathbf{R}^T(\hat{\psi} - \psi_d)\boldsymbol{\nu}_d + \mathbf{R}^T(\hat{\psi} - \psi_d)\dot{\boldsymbol{\nu}}_d\right) && (5.70)
\end{aligned}$$

The proposed observer-feedback controller with dynamic acceleration feedback for (5.14)-(5.15) is

$$\begin{aligned}
\dot{\boldsymbol{\xi}} &= \hat{\boldsymbol{\eta}}_e\\
\dot{\mathbf{a}}_f &= \mathbf{A}_f \mathbf{a}_f + \mathbf{B}_f \boldsymbol{\Pi} \hat{\dot{\boldsymbol{\nu}}}_e && (5.71)\\
\hat{\boldsymbol{\tau}} &= -\mathbf{K}_i \mathbf{R}^T(\hat{\psi})\boldsymbol{\xi} - \mathbf{K}_p \mathbf{R}^T(\hat{\psi})\hat{\boldsymbol{\eta}}_e - \mathbf{K}_d \hat{\boldsymbol{\nu}}_e - \mathbf{K}_a \mathbf{a}_f + \hat{\boldsymbol{\tau}}_{\text{rff}}
\end{aligned}$$

where the reference feed-forward is given by

$$\hat{\boldsymbol{\tau}}_{\text{rff}} = \mathbf{D}_L \mathbf{R}^T(\hat{\psi}_e)\boldsymbol{\nu}_d + \mathbf{M}\left((\hat{r} - r_d)\,\mathbf{S}^T \mathbf{R}^T(\hat{\psi}_e)\boldsymbol{\nu}_d + \mathbf{R}^T(\hat{\psi}_e)\dot{\boldsymbol{\nu}}_d\right) \qquad (5.72)$$

Notice that in the rotations we have substituted ψ with $\hat{\psi}$ and consequently state estimates appear non-affinely in the control $\hat{\boldsymbol{\tau}}$. Due to the linear bound of $\|\mathbf{R}(\psi) - \mathbf{I}\|$ and the inherent linear characteristics of the system, using (5.71) instead of (5.44) and (5.47) does not compromise the asymptotic stability established for state-feedback control. This can be summarized as follows

Theorem 5.4 *Consider the system (5.14)-(5.15) for which there exists an observer whose errors $\tilde{\mathbf{x}}_o(t)$ converge asymptotically to zero (5.67). The observer-feedback control (5.71)-(5.72) will guarantee UGAS of $\mathbf{x}_e = [\boldsymbol{\xi}^T, \boldsymbol{\eta}_e^T, \boldsymbol{\nu}_e^T, \mathbf{a}_f^T]^T$ provided that*

1. *The gains $\mathbf{K}_i, \mathbf{K}_p, \mathbf{K}_d, \mathbf{K}_a$ are selected such that $\mathbf{A}_c$ as defined by (5.50) is Hurwitz.*
2. *Maximum yaw rate $r_{\max}$ calculated by Corollary 5.1 does not exceed the physical bound, $|r(t)| \leq r_{\max}$.*

The formal proof is given in Appendix B.1.

5.5 Nonlinear Control

The main objective of this section is to identify the lacking terms in the commutation based controller that if included would have guaranteed global exponential

stability of the tracking error. A second objective is to show the similarities between controllers formulated in a reference parallel frame and our two-frame based design. Using integrator backstepping (Krstić *et al.* 1995), we demonstrate that, under some restrictions, reference parallel control (Strand 1999) is equal to body fixed control (Berge 1999). Furthermore, the derived tracking controller

- Considers Coriolis, centripetal, and nonlinear damping terms, while it does not directly cancel any of these forces.
- Handles smooth, time-varying trajectories.
- Implements "true" integral action in the sense that the position deviation updates the controller's integral action.

5.5.1 Model Description

Consider a 3 DOF model with Coriolis $\mathbf{C}(\boldsymbol{\nu}) = -\mathbf{C}^T(\boldsymbol{\nu})$ and nonlinear damping $\mathbf{D}(\boldsymbol{\nu}) = \mathbf{D}_L + \mathbf{D}_N(\boldsymbol{\nu})$

$$\begin{aligned} \dot{\boldsymbol{\eta}} &= \mathbf{R}(\psi)\boldsymbol{\nu} \\ \mathbf{M}\dot{\boldsymbol{\nu}} &= -\mathbf{C}(\boldsymbol{\nu})\boldsymbol{\nu} - \mathbf{D}(\boldsymbol{\nu})\boldsymbol{\nu} + \boldsymbol{\tau} + \mathbf{w} \end{aligned} \tag{5.73}$$

A smooth reference trajectory is assumed given in the *reference parallel* d-frame according to (5.8)-(5.10).

5.5.2 State Feedback Backstepping Control

Backstepping is a constructive design procedure for the control of nonlinear systems on feedback form. The original state variables are transformed into a new set of variables, the errors $\mathbf{z}$, for which a stabilizing controller is derived stepwise together with a block diagonal Lyapunov function. There is, however, no dominating general method for obtaining controller integral action, yet this can be implemented by introducing an additional "step" (Aarset *et al.* 1998, Strand 1999) or parameter adaptation (Godhavn *et al.* 1997, Berge 1999, Fossen *et al.* 2001). The first alternative complicates the derived controller (backstepping controllers tend to be comparatively complicated and an additional step increases the complexity even more). In a parameter adaptation setting, the "integrator" will be updated by a combination of the states. For example, in mechanical systems this means that the integral action is updated by a sum of the position and velocity errors in contrast to conventional linear control where only position error is used. The advantage of such designs is that the integral gain can be chosen arbitrarily large due to a relative degree of one between the controller and the constructed output updating this integrator. On the other hand, the close connection between a linear controller and a backstepping controller becomes less obvious.

We suggest yet another method for obtaining integral action in the tracking of ships: The idea is to augment the position error with an extra integrator such that

two steps will be sufficient. As a result, "true" integral action, in the sense of it is being updated by the position error alone, is achieved At the same time controller complexity is reduced, at least when expressed in the **z**-variables, compared to a three step method.

The objective is to follow the sufficiently smooth reference trajectory $\boldsymbol{\eta}_d, \boldsymbol{\nu}_d, \dot{\boldsymbol{\nu}}_d : \mathbb{R}_{\geq 0} \to \mathbb{R}^3$ where $\dot{\boldsymbol{\eta}}_d = \mathbf{R}(\psi_d)\boldsymbol{\nu}_d$. Let the position error $\mathbf{e}$ be given in the d-frame

$$\mathbf{e} = \mathbf{R}^T(\psi_d)\left(\boldsymbol{\eta} - \boldsymbol{\eta}_d\right) = \mathbf{R}^T(\psi_d)\boldsymbol{\eta}_e \tag{5.74}$$

such that

$$\begin{aligned} \dot{\mathbf{e}} &= -\dot{\psi}_d \mathbf{S}\mathbf{R}^T(\psi_d)\boldsymbol{\eta}_e + \mathbf{R}^T(\psi_d)\left(\mathbf{R}(\psi)\boldsymbol{\nu} - \mathbf{R}(\psi_d)\boldsymbol{\nu}_d\right) \\ &= -\dot{\psi}_d \mathbf{S}\mathbf{e} + \mathbf{R}(\psi_e)\boldsymbol{\nu}_e \end{aligned} \tag{5.75}$$

where the heading error is $\psi_e = \psi - \psi_d$. A kind of integral action performed in the Earth-fixed frame can be augmented as follows:

$$\dot{\boldsymbol{\xi}} = -\boldsymbol{\Lambda}\boldsymbol{\xi} + \mathbf{C}_{11}^T \mathbf{R}(\psi_d)\mathbf{e} \tag{5.76}$$

The matrix $\mathbf{C}_{11} \in \mathbb{R}^{3 \times n_\xi}$ is a projection used to isolate the components of $\mathbf{e}$ that is subject to integral action. $\boldsymbol{\Lambda} \in \mathbb{R}^{n_\xi \times n_\xi}$ should be diagonal and contain the inverse of some large time constants. The larger these constants are the closer we get to true integral action in the sense that $\boldsymbol{\xi}$ becomes an open integrator. For the purpose of a simpler analysis we let $\boldsymbol{\Lambda}$ be non-zero as this allows us to establish exponential stability more easily.

Theorem 5.5 below confirms that the tracking error $\left[\mathbf{e}^T, \boldsymbol{\nu}_e^T\right]$ where $\boldsymbol{\nu}_e = \boldsymbol{\nu} - \mathbf{R}^T(\psi_e)\boldsymbol{\nu}_d$ is UGES. It also provides conditions on how the individual gain matrices should be selected such that reference parallel (Strand 1999) control becomes identical to body-fixed control (Berge 1999).

Theorem 5.5 *Assume that there exist symmetric and positive definite* $\boldsymbol{\Delta}_1 \in \mathbb{R}^{n_\xi \times n_\xi}$, $\boldsymbol{\Delta}_2 \in \mathbb{R}^{3\times 3}$ *where* $\boldsymbol{\Delta}_2$ *commutes with* $\mathbf{R}(\psi)$ *and* $\mathbf{C}_{11}\boldsymbol{\Delta}_1$ *is selected such that*

$$\mathbf{R}(\psi)\mathbf{C}_{11}\boldsymbol{\Delta}_1 = \mathbf{C}_{11}\boldsymbol{\Delta}_1\mathbf{C}_{11}^T\mathbf{R}(\psi)\mathbf{C}_{11} \tag{5.77}$$

Applying the controller

$$\begin{aligned} \dot{\boldsymbol{\xi}} &= -\boldsymbol{\Lambda}\boldsymbol{\xi} + \mathbf{C}_{11}^T\mathbf{R}(\psi_d)\mathbf{e} \\ \boldsymbol{\tau} &= -\mathbf{K}_i(\boldsymbol{\nu})\mathbf{R}^T(\psi)\boldsymbol{\xi} - \mathbf{K}_p(\boldsymbol{\nu},\psi)\mathbf{R}^T(\psi_e)\mathbf{e} - \mathbf{K}_d\boldsymbol{\nu}_e + \boldsymbol{\tau}_{\text{rff}} \end{aligned} \tag{5.78}$$

where the gains are

$$\begin{aligned} \mathbf{K}_i(\boldsymbol{\nu}) &= \left(\mathbf{C}(\boldsymbol{\nu}) + \mathbf{D}(\boldsymbol{\nu}) + \mathbf{C}_2 + r\mathbf{M}\mathbf{S}^T\right)\boldsymbol{\Delta}_2^{-1}\mathbf{C}_{11}\boldsymbol{\Delta}_1\mathbf{C}_{11}^T \\ &\quad -\mathbf{M}\boldsymbol{\Delta}_2^{-1}\mathbf{C}_{11}\boldsymbol{\Delta}_1\boldsymbol{\Lambda}\mathbf{C}_{11}^T \qquad (5.79) \\ \mathbf{K}_p(\boldsymbol{\nu},\psi) &= \boldsymbol{\Delta}_2 + \left(\mathbf{C}(\boldsymbol{\nu}) + \mathbf{D}(\boldsymbol{\nu}) + \mathbf{C}_2\right)\mathbf{C}_{12} \\ &\quad +\mathbf{M}\boldsymbol{\Delta}_2^{-1}\mathbf{R}^T(\psi)\mathbf{C}_{11}\boldsymbol{\Delta}_1\mathbf{C}_{11}^T\mathbf{R}(\psi) + r\mathbf{M}\mathbf{C}_{12}\mathbf{S}^T \qquad (5.80) \\ \mathbf{K}_d &= \mathbf{C}_2 + \mathbf{M}\mathbf{C}_{12} \qquad (5.81) \end{aligned}$$

and the reference feed-forward is

$$\boldsymbol{\tau}_{\text{rff}} = \left(\mathbf{C}(\boldsymbol{\nu}) + \mathbf{D}(\boldsymbol{\nu})\right)\mathbf{R}^T(\psi_e)\boldsymbol{\nu}_d + \mathbf{M}\frac{d}{dt}\left(\mathbf{R}^T(\psi_e)\boldsymbol{\nu}_d\right) \tag{5.82}$$

yields uniform global exponential stability of $\mathbf{x}_e = \left[\boldsymbol{\xi}^T, \boldsymbol{\eta}_e^T, \boldsymbol{\nu}_e^T\right]^T = \mathbf{0}$ *whenever* $\mathbf{C}_{12} \in \mathbb{R}^{3\times 3}$, $\mathbf{C}_2 \in \mathbb{R}^{3\times 3}$, *and* $\boldsymbol{\Lambda} \in \mathbb{R}^{n_\xi \times n_\xi}$ *are selected such that*

$$\boldsymbol{\Delta}_1\boldsymbol{\Lambda} + \boldsymbol{\Lambda}^T\boldsymbol{\Delta}_1 > 0 \tag{5.83}$$

$$\boldsymbol{\Delta}_2\mathbf{C}_{12} + \mathbf{C}_{12}^T\boldsymbol{\Delta}_2 > 0 \tag{5.84}$$

$$\mathbf{D}(\boldsymbol{\nu}) + \mathbf{D}^T(\boldsymbol{\nu}) + \mathbf{C}_2 + \mathbf{C}_2^T > 0 \tag{5.85}$$

The proof is given in Appendix B.2.

If all positions are subject to integral action $\mathbf{C}_{11} = \mathbf{I}$, the gains are reduced to

$$\mathbf{K}_i(\boldsymbol{\nu}) = \left(\mathbf{C}(\boldsymbol{\nu}) + \mathbf{D}(\boldsymbol{\nu}) + \mathbf{C}_2\right)\boldsymbol{\Delta}_2^{-1}\boldsymbol{\Delta}_1 - \mathbf{M}\boldsymbol{\Delta}_2^{-1}\boldsymbol{\Delta}_1\boldsymbol{\Lambda} + r\mathbf{M}\boldsymbol{\Delta}_2^{-1}\boldsymbol{\Delta}_1\mathbf{S}^T \tag{5.86}$$

$$\mathbf{K}_p(\boldsymbol{\nu}) = \boldsymbol{\Delta}_2 + \left(\mathbf{C}(\boldsymbol{\nu}) + \mathbf{D}(\boldsymbol{\nu}) + \mathbf{C}_2\right)\mathbf{C}_{12} + \mathbf{M}\boldsymbol{\Delta}_2^{-1}\boldsymbol{\Delta}_1 + r\mathbf{M}\mathbf{C}_{12}\mathbf{S}^T \tag{5.87}$$

$$\mathbf{K}_d = \mathbf{C}_2 + \mathbf{M}\mathbf{C}_{12} \tag{5.88}$$

Considering now the low speed model (5.15) and $\mathbf{C}_{11} = \mathbf{I}$, the following gains should be used

$$\mathbf{K}_i(r) = \left(\mathbf{D}_L + \mathbf{C}_2\right)\boldsymbol{\Delta}_2^{-1}\boldsymbol{\Delta}_1 - \mathbf{M}\boldsymbol{\Delta}_2^{-1}\boldsymbol{\Delta}_1\boldsymbol{\Lambda} + r\mathbf{M}\boldsymbol{\Delta}_2^{-1}\mathbf{S}^T\boldsymbol{\Delta}_1 \tag{5.89}$$

$$\mathbf{K}_p(r) = \boldsymbol{\Delta}_2 + \left(\mathbf{D}_L + \mathbf{C}_2\right)\mathbf{C}_{12} + \mathbf{M}\boldsymbol{\Delta}_2^{-1}\boldsymbol{\Delta}_1 + r\mathbf{M}\mathbf{C}_{12}\mathbf{S}^T \tag{5.90}$$

$$\mathbf{K}_d = \mathbf{C}_2 + \mathbf{M}\mathbf{C}_{12} \tag{5.91}$$

and the same reference feed-forward as for the commutating designs (5.18). From (5.89)-(5.90) the missing yaw rate dependent terms needed for establishing UGES are clearly visible. Since $\mathbf{R}^T(\psi_e)\mathbf{e} = \mathbf{R}^T(\psi)\boldsymbol{\eta}_e$ and $\mathbf{R}(\psi_d)\mathbf{e} = \boldsymbol{\eta}_e$, we immediately recognize that (5.78) is the very same controller as (5.17) apart from that the gains are selected according to a different strategy.

It is also worth emphasizing that the yaw rate dependendent gains, those are $\mathbf{M}\boldsymbol{\Delta}_2^{-1}\boldsymbol{\Delta}_1\mathbf{S}^T$ and $\mathbf{M}\mathbf{C}_{12}\mathbf{S}^T$ in (5.89) and (5.90) respectively, can be kept small while simultaneoulsy increasing the sum of the constant terms in $\mathbf{K}_p$ and $\mathbf{K}_d$. In other words, in accordance with the commutating controller (5.24), this leads to higher bounds of $r_{\max}$ if the yaw rate components in $\mathbf{K}_i(r)$ and $\mathbf{K}_p(r)$ were to be neglected.

5.5.3 Output Feedback

Even though the state feedback controller derived by backstepping guarantees global exponential stability of the tracking error, it cannot be used directly in a certainty equivalence kind of output feedback control setting. In fact, the restriction experienced with the commutation based designs, the bounded yaw rate

$|r(t)| \leq r_{\max}$, is indeed relaxed, but the price paid is significant: The error in the compass heading estimate $\tilde{\psi}$ in combination with the nonlinear terms of the proportional and integral gains excludes employing the results on cascaded systems in establishing asymptotic stability of the closed loop system. The interconnection term between the observer errors Σ_2 and the tracking errors Σ_1 is no longer linearly bounded in the states of Σ_1.

In Aarset *et al.* (1998) the authors used observer backstepping to avoid using $\tilde{\psi} = 0$, but this contradicts the separation principle in the sense that the resulting controller tuning depends on the observer. Another approach is pursued for more general Euler-Lagrange systems (Loría and Panteley 1999, Aamo *et al.* 2001) where ψ is assumed measured and available for feedback. Neglecting the linearly wave induced motion and thus using ψ_y (the measured heading angle) in the derived controller (5.78), this procedure would be globally asymptotically stable here as well. In the following we are, however, going to analyze a certainty equivalence design to point out the $\tilde{\psi}$-dependency and then suppose $\tilde{\psi} = 0$ to eliminate the conflicting terms.

Prerequisites

First we summarize some of the properties of the Coriolis and damping matrices needed in the forthcoming analysis.

- The Coriolis and centripetal matrix is linear in its argument, that is for $\mathbf{a}$,$\mathbf{b} \in \mathbb{R}^3$
$$\mathbf{C}(\mathbf{a} + \mathbf{b}) = \mathbf{C}(\mathbf{a}) + \mathbf{C}(\mathbf{b}) \tag{5.92}$$
As a consequence, it is bounded linearly in the argument as well: There exist positive scalars c_m,$c_M > 0$ such that
$$c_m \left|\mathbf{a}\right| \leq \left\|\mathbf{C}(\mathbf{a})\right\| \leq c_M \left|\mathbf{a}\right| \tag{5.93}$$

- The damping is linear plus quadratic throughout the entire velocity range $\mathbf{D}(\boldsymbol{\nu}) = \mathbf{D}_L + \mathbf{D}_N(\boldsymbol{\nu})$. Then, for any $\mathbf{a} \in \mathbb{R}^3$ there are bounds d_m and d_M such that
$$d_m \left|\mathbf{a}\right| \leq \left\|\mathbf{D}_N(\mathbf{a})\right\| \leq d_M \left|\mathbf{a}\right| \tag{5.94}$$
Assume furthermore that the error in $\mathbf{D}_N$ defined as
$$\mathbf{D}_{err}(\mathbf{a}, \mathbf{b}) = \mathbf{D}_N(\mathbf{a} - \mathbf{b}) - \mathbf{D}_N(\mathbf{a}) \tag{5.95}$$
is bounded linearly in $\mathbf{b}$. More specifically for some $d_{err} > 0$ the following holds
$$\left\|\mathbf{D}_{err}(\mathbf{a}, \mathbf{b})\right\| \leq d_{err} \left|\mathbf{b}\right| \tag{5.96}$$

Remark 1 *In the scalar case it is known that*

$$|a - b| - |a| \leq |b| \quad \forall a, b \in \mathbb{R}$$

which means that (5.96) at least covers any diagonal $\mathbf{D}_N$*.*

Define

$$\begin{aligned} \mathbf{N}(\boldsymbol{\nu}) &= \mathbf{C}(\boldsymbol{\nu}) + \mathbf{D}(\boldsymbol{\nu}) && (5.97) \\ \mathbf{N}_{err}(\boldsymbol{\nu}, \tilde{\boldsymbol{\nu}}) &= \mathbf{D}_{err}(\boldsymbol{\nu}, \tilde{\boldsymbol{\nu}}) - \mathbf{C}(\tilde{\boldsymbol{\nu}}) && (5.98) \end{aligned}$$

then

$$\mathbf{N}(\hat{\boldsymbol{\nu}}) = \mathbf{N}(\boldsymbol{\nu}) + \mathbf{N}_{err}(\boldsymbol{\nu}, \tilde{\boldsymbol{\nu}}) \tag{5.99}$$

From the assumptions above we see that

$$|\mathbf{N}_{err}(\boldsymbol{\nu}, \tilde{\boldsymbol{\nu}})| \leq (d_{err} + c_M)\,|\tilde{\boldsymbol{\nu}}| \tag{5.100}$$

Observe when disregarding Coriolis and quadratic damping that $\mathbf{N}(\boldsymbol{\nu}) = \mathbf{D}_L$ and thus $\mathbf{N}_{err}(\boldsymbol{\nu}, \tilde{\boldsymbol{\nu}}) = \mathbf{0}$.

Observer-Feedback Control

The proposed observer feedback controller is obtained by substituting the state variables with their estimated counterparts (certainty of equivalence), and without loss of generality, integral action is applied in all three DOFs.

Let position and velocity error be defined by (5.68) and (5.69) respectively. The position error decomposed in the reference parallel frame is thus

$$\hat{\mathbf{e}} = \mathbf{R}^T(\psi_d)\hat{\boldsymbol{\eta}}_e = \mathbf{e} - \mathbf{R}^T(\psi_d)\tilde{\boldsymbol{\eta}} \tag{5.101}$$

The controller reads

$$\begin{aligned} \dot{\boldsymbol{\xi}} &= -\boldsymbol{\Lambda}\boldsymbol{\xi} + \mathbf{R}(\psi_d)\hat{\mathbf{e}} \\ \hat{\boldsymbol{\tau}} &= -\mathbf{K}_i(\hat{\boldsymbol{\nu}})\mathbf{R}^T(\hat{\psi})\boldsymbol{\xi} - \mathbf{K}_p(\hat{\boldsymbol{\nu}})\mathbf{R}^T(\hat{\psi}_e)\hat{\mathbf{e}} - \mathbf{K}_d\hat{\boldsymbol{\nu}}_e + \hat{\boldsymbol{\tau}}_{\text{rff}} \end{aligned} \tag{5.102}$$

where the reference feed-forward is

$$\hat{\boldsymbol{\tau}}_{\text{rff}} = \mathbf{N}(\hat{\boldsymbol{\nu}})\mathbf{R}^T(\hat{\psi}_e)\boldsymbol{\nu}_d + \mathbf{M}\left(\hat{r}_e\mathbf{S}^T\mathbf{R}^T(\hat{\psi}_e)\boldsymbol{\nu}_d + \mathbf{R}^T(\hat{\psi}_e)\dot{\boldsymbol{\nu}}_d\right) \tag{5.103}$$

and the gains are

$$\begin{aligned} \mathbf{K}_i(\hat{\boldsymbol{\nu}}) &= (\mathbf{N}(\hat{\boldsymbol{\nu}}) + \mathbf{C}_2)\,\boldsymbol{\Delta}_2^{-1}\boldsymbol{\Delta}_1 - \mathbf{M}\boldsymbol{\Delta}_2^{-1}\boldsymbol{\Delta}_1\boldsymbol{\Lambda} + \hat{r}\mathbf{M}\boldsymbol{\Delta}_2^{-1}\boldsymbol{\Delta}_1\mathbf{S}^T && (5.104) \\ \mathbf{K}_p(\hat{\boldsymbol{\nu}}) &= \boldsymbol{\Delta}_2 + (\mathbf{N}(\hat{\boldsymbol{\nu}}) + \mathbf{C}_2)\,\mathbf{C}_{12} + \mathbf{M}\boldsymbol{\Delta}_2^{-1}\boldsymbol{\Delta}_1 + \hat{r}\mathbf{M}\mathbf{C}_{12}\mathbf{S}^T && (5.105) \\ \mathbf{K}_d &= \mathbf{C}_2 + \mathbf{M}\mathbf{C}_{12} && (5.106) \end{aligned}$$

Theorem 5.6 *Consider a sufficiently smooth reference trajectory* $\boldsymbol{\eta}_d, \boldsymbol{\nu}_d, \dot{\boldsymbol{\nu}}_d : \mathbb{R}_{\geq 0} \to \mathbb{R}^3$ *where* $\dot{\boldsymbol{\eta}}_d = \mathbf{R}(\psi_d)\boldsymbol{\nu}_d$*, and assume there exists an observer with asymptotically converging states* $\mathbf{x}_o$*. The controller (5.102)-(5.106) guarantees UGAS of the tracking error* $\left[\mathbf{e}^T, \boldsymbol{\nu}_e^T\right]^T$ *provided that* $\tilde{\psi} = 0$ *and the gains are selected according to Theorem 5.5.*

The proof is given in Appendix B.3.

Remark 2 *Admittedly, by imposing bounds on the velocity vector $\boldsymbol{\nu}$ and the estimated heading error $\tilde{\psi}$ it would be possible to establish asymptotic stability by a completion of the squares in the derivative of the Lyapunov function derived under state-feedback. This, however, contradicts the objective of obtaining UGAS under observer feedback. Instead we settled for $\tilde{\psi} = 0$ (ψ is perfectly measured).*

Separating the linear control terms from the nonlinear ones can be done by introducing the following definitions:

$$\begin{aligned}
\mathbf{G}_i &= \mathbf{C}_2\boldsymbol{\Delta}_2^{-1}\boldsymbol{\Delta}_1 - \mathbf{M}\boldsymbol{\Delta}_2^{-1}\boldsymbol{\Delta}_1\boldsymbol{\Lambda} && (5.107)\\
\mathbf{X}_{i1} &= \mathbf{C}_2\boldsymbol{\Delta}_2^{-1}\boldsymbol{\Delta}_1 && (5.108)\\
\mathbf{X}_{i2} &= \mathbf{M}\boldsymbol{\Delta}_2^{-1}\boldsymbol{\Delta}_1\mathbf{S}^T && (5.109)\\
\mathbf{G}_p &= \boldsymbol{\Delta}_2 + \mathbf{C}_2\mathbf{C}_{12} + \mathbf{M}\boldsymbol{\Delta}_2^{-1}\boldsymbol{\Delta}_1 && (5.110)\\
\mathbf{X}_p &= \mathbf{M}\mathbf{C}_{12}\mathbf{S}^T && (5.111)
\end{aligned}$$

The gains are thus given as

$$\begin{aligned}
\mathbf{K}_i(\hat{\boldsymbol{\nu}}) &= \mathbf{G}_i + \mathbf{N}(\hat{\boldsymbol{\nu}})\mathbf{X}_{i1} + \hat{r}\mathbf{X}_{i2} && (5.112)\\
\mathbf{K}_p(\hat{\boldsymbol{\nu}}) &= \mathbf{G}_p + \mathbf{N}(\hat{\boldsymbol{\nu}})\mathbf{C}_{12} + \hat{r}\mathbf{X}_p && (5.113)\\
\mathbf{K}_d &= \mathbf{C}_2 + \mathbf{M}\mathbf{C}_{12} && (5.114)
\end{aligned}$$

where the $\mathbf{G}_i \in \mathbb{R}^{3\times3}$ and $\mathbf{G}_p \in \mathbb{R}^{3\times3}$ are the constant (linear control) gains. The terms requiring $\tilde{\psi} = 0$ are the nonlinear factors of $\mathbf{K}_i(\hat{\boldsymbol{\nu}})$ and $\mathbf{K}_p(\hat{\boldsymbol{\nu}})$. It should be noted that even though $\hat{\boldsymbol{\tau}}_{\text{rff}}$ indeed contains $\mathbf{N}(\hat{\boldsymbol{\nu}})$, for this term alone it is not necessary to assume $\tilde{\psi} = 0$ because $|\boldsymbol{\nu}_d|$ is known to be bounded.

Chapter 6

Experiments with Acceleration Feedback

6.1 Introduction

This chapter deals with the theoretical expectations and the actual results from the experimens conducted with Cybership II. The main objective of these experiments was to use measured linear acceleration in order to better attenuate the unknown slowly varying wave drift forces. As these forces significantly deteriorates positioning performance, it was important to investigate theoretically and experimentally that negative acceleration feedback (AFB) could serve as a suitable tool to improve the performance without sacrifying thruster usage.

The chapter is organized as follows: First, we compare our acceleration augmented controller (Section 5.4) with a traditional PID-controller assigning the very same closed loop eigenvalues to either one of them. Possible theoretical improvements are examined in a state-feedback setting in terms of operator norms such as induced $\mathcal{L}_2$ and the "energy to peak" norm. Due to the rotations being separated from the otherwise linear closed loop model, tools applicable for linear system analysis were used for this purpose. Next, the actual experiments are documented together with the environmental conditions used. Finally we draw the conclusions.

6.2 State-Feedback Performance

The controller in Section 5.4 was implemented with three different acceleration gains (Table 6.1). Otherwise the identical closed-loop performance characteristics, that is $\mathbf{\Omega}$ and $\mathbf{\Lambda}$ as defined (5.62)-(5.63) were kept constant.

	$\mathbf{K}_a$	$r_{\max}$ [deg/s]
Standard PID	0	670
Low AFB	$\begin{bmatrix} \gamma_{l1} m_{11} & 0 & 0 \\ 0 & \gamma_{l2} m_{22} & 0 \end{bmatrix}^T$	780
High AFB	$\begin{bmatrix} \gamma_{h1} m_{11} & 0 & 0 \\ 0 & \gamma_{h2} m_{22} & 0 \end{bmatrix}^T$	590

Table 6.1: Acceleration gains. The scalars m_{ij} indicate the entries of the mass matrix $\mathbf{M}$

$$\mathbf{\Omega} = \text{diag}(1.2, 0.7, 0.8) \tag{6.1}$$
$$\mathbf{\Lambda} = \mathbf{I} \tag{6.2}$$
$$\mathbf{K}_i = 0.02\mathbf{I} \tag{6.3}$$

Notice that $\bar{\mathbf{K}}_i$ was not constant, but due to the integral gain's small magnitude this had no significant influence on the characteristics around the system's bandwidth. The resulting model-scale yaw rate bounds $r_{\max}$ calculated according to Corollary 5.1 are also reproduced in Table 6.1, and those values exceed the physical limit by a factor of 10.

The structure of $\mathbf{M}$ and $\mathbf{D}$ together with the separation of the kinematics motivates a separate analysis of the North-surge dynamics. Thus we are allowed to compare the resulting North-surge motion of the three controllers in order to illustrate performance. Figure 6.1 and 6.2 show the transfer functions $h_{xw_1}(s)$ and $h_{\tau_1 w_1}(s)$, those being the frequency responses from surge-disturbance w_1 to position x and applied surge thrust τ_1 respectively. Here, as in the experiments, we have used $\gamma_{l1} = 0.78$, $\gamma_{h1} = 2.0$. Figure 6.1 demonstrates that disturbances having frequencies within the range $\omega \in (10^{-3}, 2)$ rad/s are effectively attenuated using acceleration feedback.

For the high gain acceleration controller disturbances was reduced by 66%, or -10 dB. Table 6.2 documents that the energy content of position as well as applied

	$\|h_{xw_1}\|_2$	$\|h_{\tau_1 w_1}\|_2$	$\|h_{xw_1}\|_{2\infty}$	$\|h_{\tau_1 w_1}\|_{2\infty}$
Standard PID	1	1	1	1
Low AFB	0.56	0.95	0.56	1.30
High AFB	0.34	0.92	0.33	1.65

Table 6.2: Normalized induced gains from surge disturbance to surge position and surge thrust.

thrust decreases (slightly) using acceleration feedback. Moreover, the worst case peak of the position, and thereby velocity, also decreases. A drawback is that the peak in applied thrust may increase as indicated by $\|h_{\tau_1 w_1}\|_{2\infty}$.

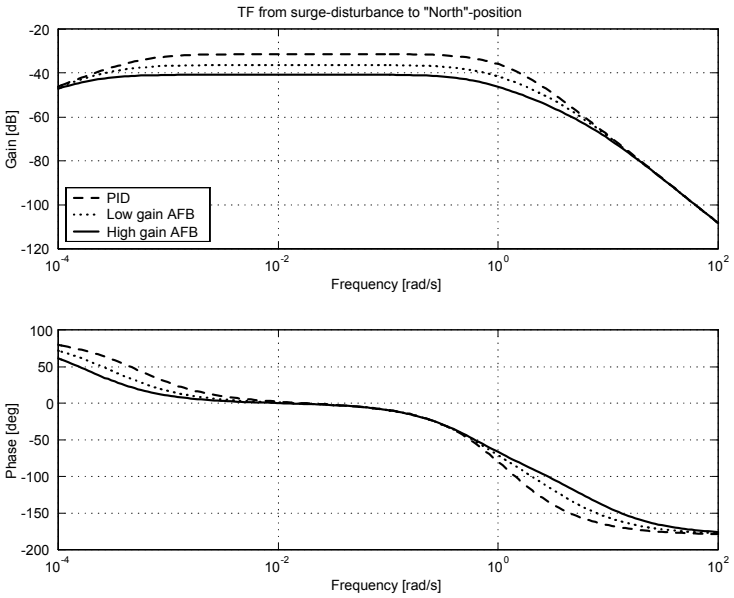

Figure 6.1: Model scale Bode plot of $h_{xw_1}(s)$ for the three implemented controllers.

6.3 Experimental Results

6.3.1 Environmental Conditions

No wind or current forces were applied during the experiments. Instead the boat was exposed only to incoming waves after a JONSWAP distribution with a significant wave height $H_s = 2$ cm and mean period $T_s = 0.75$ sec, that is $\omega = 2\pi/T_s = 8.38$ rad/s. In full-scale this corresponds to sea state code 4 (moderate) $H_s = 1.4$ m and $T_s = 0.75\sqrt{70} \approx 6.3$ sec, that is $f_s = 0.16$ Hz, see Figure 6.3. Sea state code 4 is the most frequently experienced condition worldwide as well as in the North Atlantic (Price and Bishop 1974). The lack of wind and current forces ensures that the experienced slowly varying motion is excited by nonlinear wave effects.

Due to the irregular wave pattern, it was impossible to exactly repeat the conditions in two experiments in succession. The validity of the results is therefore based on performing long test runs. The recorded test runs were 30 min, from which we extracted 20 min for presentation purposes. In full-scale this corresponds to analyzing time series up to 2 hours and 47 minutes long. In order to claim validity, this seems sufficient.

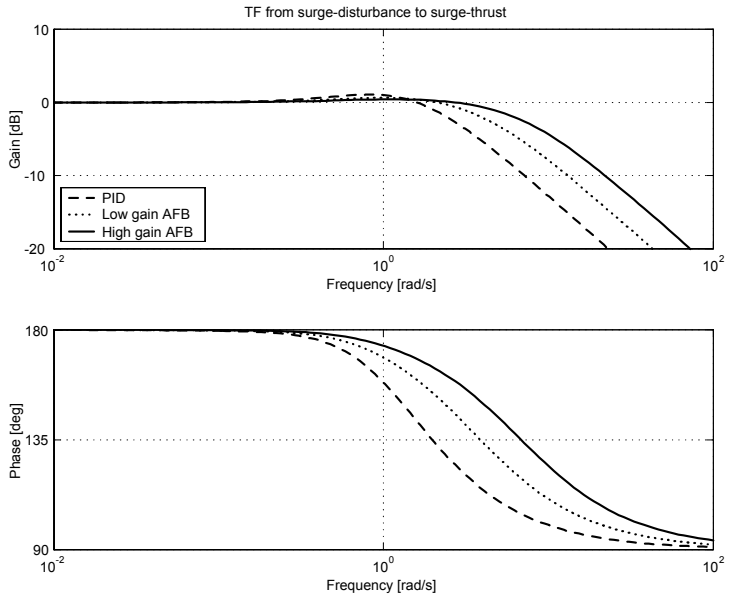

Figure 6.2: Model scale Bode plot of $h_{\tau_1 w_1}(s)$ for the three implemented controllers.

6.3.2 Documented Performance

The ship was to maintain the desired position $\boldsymbol{\eta}_d = [0, 0, 0]^T$ while being exposed to irregular, head waves. The incoming waves would be tangential to the centerline of the vessel provided that its heading $\psi = 0$, and hence wave drift would be experienced mostly longships. Therefore, acceleration feedback was only implemented in surge in order to attenuate those unknown slowly varying disturbances, and the following acceleration gains (see Table 6.1) were used

$$\begin{array}{lll} \text{Low AFB}: & \gamma_{l1} = 0.78 & \gamma_{l2} = 0.0 \\ \text{High AFB}: & \gamma_{h1} = 2.0 & \gamma_{h2} = 0.0 \end{array} \tag{6.4}$$

As commented above, comparing the time-series plots for the three individual acceleration gain settings is useless. We therefore chose to reproduce a representative time slot from the data recorded with the high gain AFB controller in full scale. In Figure 6.4 the measured and LF estimate of the North position is plotted along with the measured and LF estimated surge acceleration. Notice that since $\psi \approx 0$ the position and acceleration are, as expected, 180 degrees out of phase. This is most easily seen around $t = 8000$ sec. The large amplitudes of the measured acceleration, due to the first order wave induced motion, still has little influence on the LF estimate, which is an example of a well-functioning observer. Had the observer estimates been corrupted with wave frequency components, it would have caused thruster modulation immediately. The measured and LF estimated East position are given in Figure 6.5 together with sway acceleration. Measured and

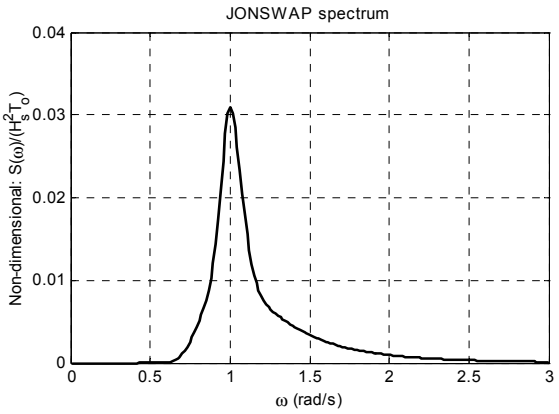

Figure 6.3: Plot showing the full-scale equivalent JONSWAP wave spectrum for $H_s = 1.4$ m, $T_s = 6.3$ sec, and peakedness $\gamma = 3.3$.

LF estimated heading and yaw rate are plotted in Figure 6.6.

For comparison of the energy content in recorded time-series data the RMS-gain is a relevant performance parameter together with empirical mean $\bar{y}$ and standard deviation s_y. The experiments documented that by using the estimated low-frequency acceleration in the output-feedback controller, the positioning performance increased for practically the same amount of consumed surge thrust power, see Table 6.3. A graphical illustration of the resulting performance enhancements are given in Figure 6.8: The ellipses to the left represent standard deviation of the North and East-positions for the three implemented controllers. The RMS-norms of the corresponding applied surge and sway thrust to the right show that for approximately the some amount of thrust, the positioning accuracy in North/surge improved significantly using acceleration feedback. As AFB was not enabled in East/sway, the three controllers performed equally well.

	s_x	$\|x\|_{RMS}$	s_{τ_1}	$\|\tau_1\|_{RMS}$	$\bar{\tau}_1$
Standard PID	1.0	1.0	1.0	1.0	1.0
Low AFB	0.86	0.86	0.96	0.96	1.04
High AFB	0.83	0.82	0.99	0.99	1.02

Table 6.3: Empircal performance indicators normalized with respect to values obtained with regular PID-control.

6.3.3 Comments

It may be argued that the position deviations are large for this moderate sea state code. The amplitudes could have been made smaller if the controller had applied more damping. But this in turn requires a greater accuracy in the velocity estimates, and it can in fact degrade performance if the observer is loosely

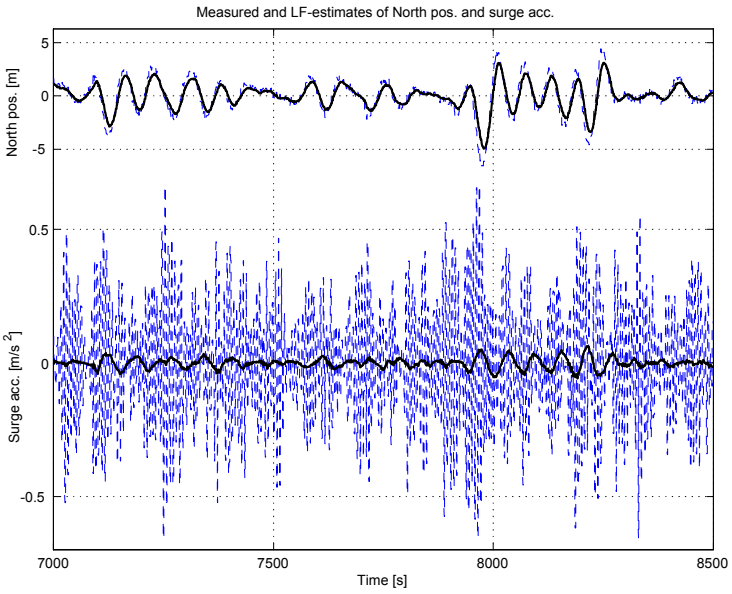

Figure 6.4: Top: Measured (dotted) and LF-estimated (solid) North position. Bottom: Measured (dotted) and LF-estimated (solid) surge acceleration.

tuned. In fact, we found it difficult to add more damping without destabilizing the surge-dynamics. However, since the closed loop relative damping was constant, a comparison between the two could still be made.

From the empirical standard deviation s_x we see that the idealized performance enhancements found in the state-feedback analysis could not be reached. The signal transmission delays and phase lag caused by the observer as well as by other factors altogether degraded the performance. Nevertheless, the concept seems to be promising since s_x was reduced significantly using acceleration feedback while $\|\tau_1\|_{RMS}$ was kept constant.

6.4 Conclusions and Recommendations

We have suggested using measured acceleration to increase the performance in positioning operations of surface vessels. The advantages of this concept has been motivated by and illustrated through state-feedback analysis of the low-frequency dynamics of the vessel model. Theoretically it is possible to attenuate a disturbance's influence and obtain improved positioning and simultaneously lower applied thrust force. As a consequence, the fuel consumption (and gas emission) is likely to go down while the safety of the operation is improved.

Due to the purely oscillatory first order wave loads, a state-observer with wave filtering capabilities is required in order to prevent thruster modulation. Although

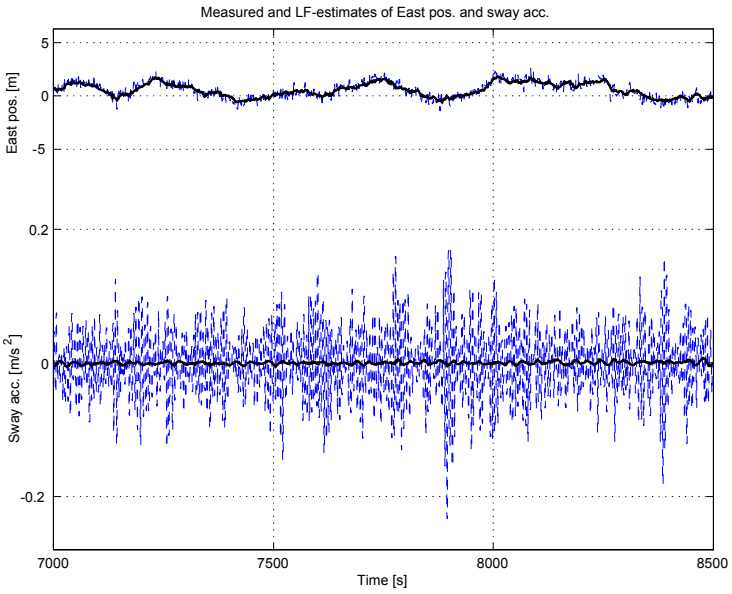

Figure 6.5: Top: Measured (dotted) and LF-estimated (solid) East position. Bottom: Measured (dotted) and LF-estimated (solid) sway acceleration.

this somewhat deteriorates the performance, the experiments validate that the positioning performance does improve with acceleration feedback for practically the same applied thrust. It is likely to assume that further testing and alternative controller structures can provide even better results.

Using measured acceleration actively in dynamic positioning operations is a cost effective method to reduce operational cost and increase the safety and positioning performance.

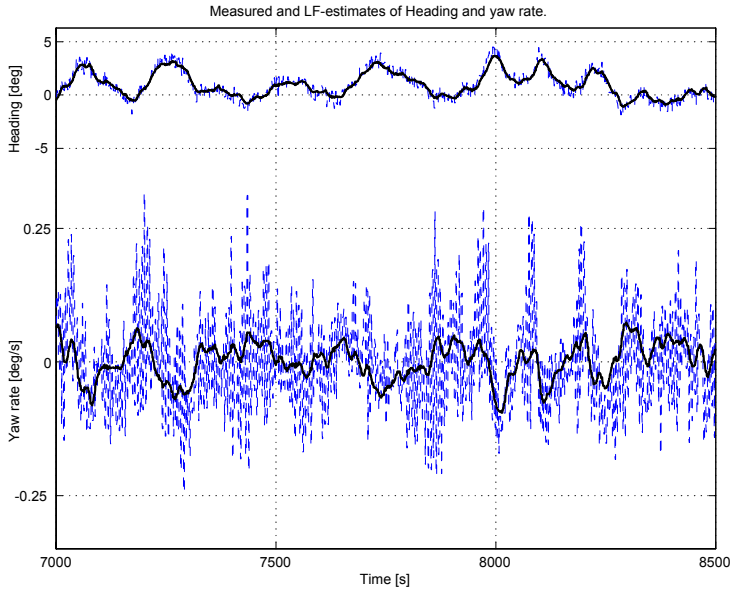

Figure 6.6: Top: Measured (dotted) and LF-estimated (solid) heading Bottom: Measured (dotted) and LF-estimated (solid) yaw rate.

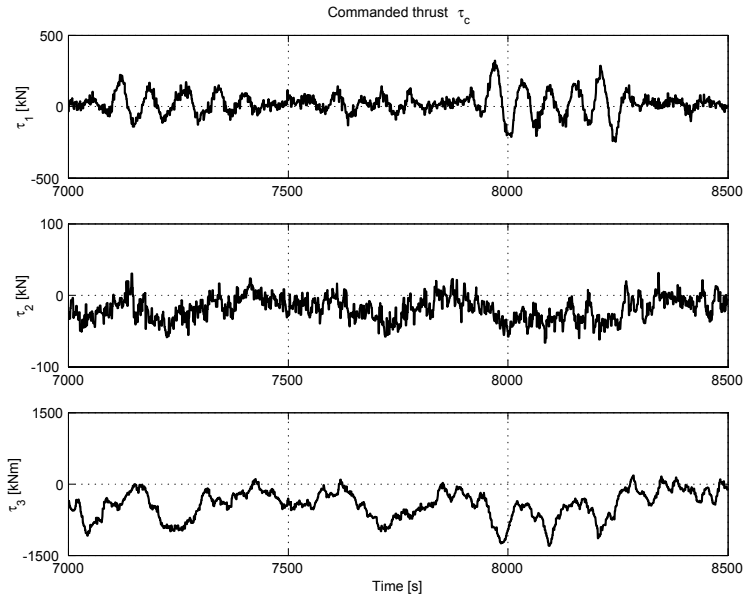

Figure 6.7: Commanded thrust $\boldsymbol{\tau}$. Observe the different y-axis scalings.

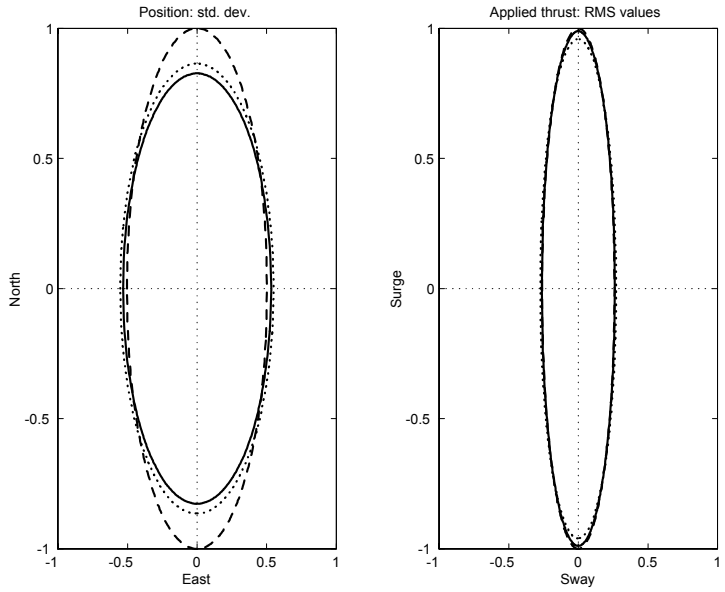

Figure 6.8: Comparison of position standard deviations (s_x, s_y) and RMS-norms of applied thrust ($\|\tau_1\|_{RMS}, \|\tau_2\|_{RMS}$) for standard PID-control (dashed), low gain AFB (dotted) and high gain AFB (solid).

Chapter 7

Thrust Allocation with Rudders

7.1 Introduction

The main contribution of this chapter is a thrust and rudder (control) allocation algorithm for marine vessels. This is a challenging problem since a ship at zero speed with a main propeller and a single rudder produces lift (sideforce) for positive propeller revolutions only. Rudder forces are approximately zero when the propeller is reversed. The rudder force is also limited to a small sector due to rudder angle saturation.

Optimal thrust allocation in station-keeping has been addressed previously (Jenssen 1981, Lindfors 1993, Sørdalen 1997*a*, Sørdalen 1997*b*, Berge and Fossen 1997), while simultaneous thrust and rudder allocation for ships at zero speed has received less attention. Since operating a rudder servo is relatively inexpensive compared to operating a propeller, this gives a large fuel saving potential. This solution is well known in practice since experienced captains use a non-zero rudder angle (for positive thrust) in station-keeping and docking to produce additional forces in the transverse direction. In this chapter a constrained rudder/propeller control allocation algorithm is derived.

For ships with more control inputs than controllable degrees of freedom (DOF), it is possible to find an "optimal" distribution of control forces $\mathbf{F} \in \mathbb{R}^p$ provided that the demand is attainable. Here p is the number of actuators/propulsive devices which can be operated individually. The commanded generalized force (forces and moments), $\boldsymbol{\tau}_c$, is generated by a higher-level controller, for instance a dynamic positioning system. In this context a higher-level controller may be any arbitrary automatic control law (Figure 7.1) or, alternativly, a joystick operator manually commanding surge and sway forces as well as a yaw moment (Figure 7.2). Regardless of the source of commanded forces, the control allocation (CA) algorithm is responsible for calculating an "optimal" solution of actuator set-points

that at all times satisfy the presumed attainable commanded generalized force signal.

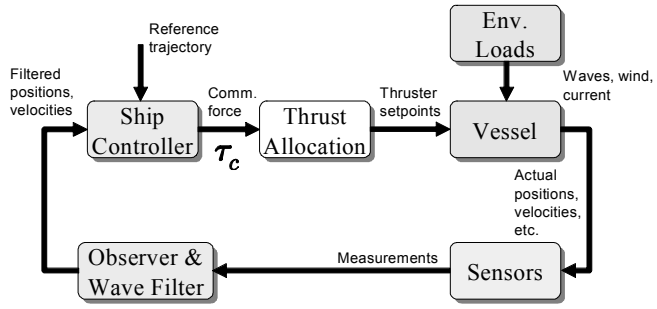

Figure 7.1: Overview of an automatic ship control system with a high level controller.

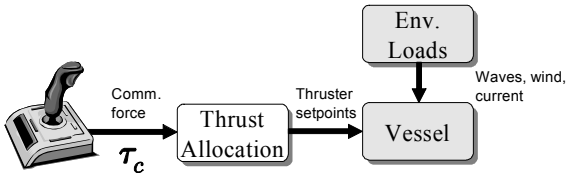

Figure 7.2: Overview of a manual joystick control system.

In general, CA is a dynamic nonlinear optimization problem since there are sector limitations for operation of the rudders and the rotatable thrusters (azimuth thrusters). This problem can be solved using nonlinear optimization techniques (Nocedal and Wright 1999) e.g. quadratic programming (QP), see Lindfors (1993). An alternative method using the singular value decomposition and a filtering scheme to control the azimuth directions has been proposed in Sørdalen (1997*b*) and, with results from sea trials, in Sørdalen (1997*a*). A similar technique using the damped least squares algorithm has been reported in Berge and Fossen (1997).

Compared to advanced controller and filter design, the allocation part of ship control has received less attention (Sørdalen 1997*b*). This seems unfortunate, because the performance of an automatic control system will suffer if the CA module is poorly designed. Moreover, the design of the allocation module is the decisive element determining the costs, in terms of energy consumption, of obtaining the desired level of performance. A more efficient CA algorithms requires less power, reduces fuel consumption, and decreases gas emissions.

While the mentioned CA schemes for ships perform an unconstrained optimization, the aerospace community has addressed constrained CA methods for quite some time. The two most frequently reported strategies are Durham's tailor-made generalized inverses (Durham 1993, Durham 1994*a*, Durham 1994*b*, Durham 1999*b*,

Durham 1999*a*, Bordignon and Durham 1995*a*) and actuator daisy chaining (Berg *et al.* 1996, Buffington and Enns 1996, Buffington *et al.* 1998). The set of admissible controls is usually an n-dimensional rectangle, as in the tailor-made inverses, and the controls can be selected independently of each other. These methods do not apply to ships with rotatable thrusters or rudders. Neither is the set of admissible controls necessarily convex, nor will the controls be independent. Another difference between an aircraft and a ship is how a universal cost criterion should be defined. For a ship at low speed it is an obvious goal to minimize the total thrust force (and thereby fuel consumption), while for a cruising airplane the cost in terms of energy of using the passive control surfaces is of minor importance, although drag minimization has been considered (Durham *et al.* 1996).

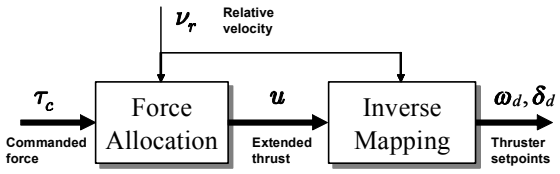

Figure 7.3: The thrust allocation problem seen as a two-step process.

The control allocation problem arises in cases where there are more actuators than DOFs, or more precisely when the decision variables $\mathbf{u}$ outnumber the equality constraints. An algorithm can be divided into two steps as described in Figure 7.3. In the first step, called force allocation, the commanded generalized force $\boldsymbol{\tau}_c$ is distributed out to each one of the p available actuators. The decision made at this stage determines how "good" the algorithm is. The second step deals with finding which actuator set-points will generate the desired forces $\mathbf{F}$. This step is called "inverse mapping" because it must solve the inverse of the actuator models. The vessel's velocity relative to the fluid $\boldsymbol{\nu}_r$ is considered an auxiliary signal that must be accounted for since rudder forces greatly depend on surge velocity. Evidently, the thrust models used in the second step influence the domain of $\mathbf{u}$. For low speed applications, as considered in this chapter, the ship's relative velocity $\boldsymbol{\nu}_r$ may be neglected.

The thrust allocation problem is an optimization problem with several requirements to consider. For instance, the algorithm must take into account the capacity of each thrust device and it must avoid "singular solutions" (Sørdalen 1997*b*, Johansen *et al.* 2003) that produce unacceptably large thrust magnitudes. Furthermore, finding a suitable solution must take a minimum of time and computational effort because the implementation runs on a real-time platform often with limited resources. More sophisticated algorithms should include support for thrusters with a preferred thrusting direction (many thrust devices are more effective when producing positive thrust than negative) and also take into account the dynamic constraints of the propulsion system, e.g. a rotatable thruster cannot rotate arbitrarily fast (rate saturation). Those issues will, however, not be addressed here.

A topic related to saturation handling is to the determine attainable thrust set

(Durham 1993, Durham 1994*a*, Durham 1994*b*), that is all combinations of $\boldsymbol{\tau}_c$ that the thruster system can provide. Limitations will be imposed by the maximum capacity of each device (box constraints), but also by the amount of available power on the power buses on which the thrusters are connected. If rate limitations are to be handled, the current states influence the attainable thrust, too. By analyzing the attainable set before sending the demand $\boldsymbol{\tau}_c$ to the force allocation module (Figure 7.3), or at least taking it into account in the allocation itself, we are given the opportunity to analyze and modify the demand in light of the limitations. The desired $\boldsymbol{\tau}_c$ should be checked for attainability. If it is not attainable, explicit action must be taken because if the actuators are individually limited after the inverse mapping, overall control of the resulting thrust may be lost. In such cases one approach could be to give preference to some of the controllable DOFs in the $\boldsymbol{\tau}_c$-vector and to modify the other ones such that $\boldsymbol{\tau}_c$ eventually becomes attainable. In aerospace applications the set of attainable thrust is convex (Durham 1994*a*, Durham 1994*b*) simplifying such priority considerations significantly. This is, however, not the case for ships with sector restricted rotatable thrusters or propeller-rudder pairs. Because of this non-convexity, we assume that $\boldsymbol{\tau}_c$ is always attainable.

7.2 Problem Statement

7.2.1 Notation and Definitions

Consider a vessel with p actuators. Actuators denote rotatable or fixed propellers, waterjets, and other devices capable of producing a propulsive force. A main propeller equipped with a rudder is considered a rotatable device. Passive devices such as standalone rudders and flaps are to be considered as actuators at non-zero velocities, while at velocities near zero they should not.

Assume there are p_r rotatable and p_f fixed force devices such that $p = p_r + p_f$. Notice that a rotatable actuator has two controls, one for the direction and one for force amplitude. For the rotatable and fixed actuators this yields $n_r = 2p_r$ and $n_f = p_f$ number of decision variables respectively. In sum there are $n = n_r + n_f$ decision variables. Let q denote the number of DOFs under consideration, and if $n > q$ the vessel is said to be *overactuated*. From now on we shall consider *surge*, *sway* and *yaw* only, thus $q = 3$.

Each thruster k is located at

$$\mathbf{r}_k = \begin{bmatrix} l_{k,x} & l_{k,y} \end{bmatrix}^T \tag{7.1}$$

with respect to the origin of the vessel-fixed coordinate system and can produce a force F_k in a direction α_k. The x-axis points forward and the y-axis to the right (starboard). The difference between the rotatable thrusters numbered $1 \leq k \leq p_r$ and fixed thrusters $p_r + 1 \leq k \leq p$ is that the direction α_k can be manipulated.

Let $F_k^{\max} > 0$ be the maximum thrust force such that the *normalized thrust* ρ_k

defined as

$$\rho_k = \frac{1}{F_k^{\max}} F_k \tag{7.2}$$

satisfies $|\rho_k| \leq 1$ for all k. Define $\mathcal{I}$ as a subset of $\mathbb{R}$

$$\mathcal{I} = \{x \in \mathbb{R} \,|-1 \leq x \leq 1\} \tag{7.3}$$

Then $\rho_k \in \mathcal{I}$ and $\boldsymbol{\rho} \in \mathcal{I}^p$.

The sum of *generalized forces* on the vessel $\boldsymbol{\tau} \in \mathbb{R}^3$ is

$$\boldsymbol{\tau} = \underbrace{\bar{\mathbf{A}}(\boldsymbol{\alpha})}_{\substack{\text{configuration}\\ \text{matrix}}} \underbrace{\bar{\mathbf{F}}\boldsymbol{\rho}}_{\text{thrust}} \tag{7.4}$$

where

$$\bar{\mathbf{A}}(\boldsymbol{\alpha}) = \begin{bmatrix} \cos\alpha_1 & \cdots & \cos\alpha_p \\ \sin\alpha_1 & & \sin\alpha_p \\ -l_{1,y}\cos\alpha_1 + l_{1,x}\sin\alpha_1 & \cdots & -l_{p,y}\cos\alpha_p + l_{p,x}\sin\alpha_p \end{bmatrix} \tag{7.5}$$

$$\bar{\mathbf{F}} = \text{diag}\{F_1^{\max}, \cdots, F_p^{\max}\} \tag{7.6}$$

The vessel is said to be in a *singular configuration* if $\bar{\mathbf{A}}(\boldsymbol{\alpha})$ looses rank due to a poor selection of $\boldsymbol{\alpha}$.

Let $\mathbf{u} \in \mathcal{I}^n$ denote the control vector where the normalized thrust ρ_k for each thruster has been decomposed in the horizontal plane according to:

$$u_{k,x} = \rho_k \cos\alpha_k \quad , \quad u_{k,y} = \rho_k \sin\alpha_k \tag{7.7}$$

The decomposition $\mathbf{u}$ is called *extended thrust*. Let $\boldsymbol{\Pi}_k$ be a projection that extracts the extended thrust vector $\mathbf{u}_k$ of thruster k from $\mathbf{u}$ according to

$$\mathbf{u}_k = \boldsymbol{\Pi}_k \mathbf{u} \tag{7.8}$$

For rotatable thrusters $\mathbf{u}_k \in \mathcal{I}^2$, $1 \leq k \leq p_r$ and for fixed thrusters $p_r + 1 \leq k \leq p$ we have $u_k = \rho_k \in \mathcal{I}$.

Most likely an extended thrust $\mathbf{u}_k$ is confined to a domain of $\mathcal{I}^2$ (or $\mathcal{I}$), e.g. an azimuth thruster could be restricted to thrust only inside a predefined sector. Let each extended thrust $\mathbf{u}_k$ be confined to the domain $\mathcal{D}_k$, that is for $k \in [1, p_r]$ we have $\mathcal{D}_k \subset \mathcal{I}^2$, and for $k > p_r$ $\mathcal{D}_k \subset \mathcal{I}$.

Using the concept of extended thrust, the generalized thrust vector $\boldsymbol{\tau}$ becomes

$$\boldsymbol{\tau} = \mathbf{B}\mathbf{F}_u\mathbf{u} \tag{7.9}$$

where $\mathbf{B} \in \mathbb{R}^{3\times n}$ consists of $\mathbf{B}_r \in \mathbb{R}^{3\times n_r}$ and $\mathbf{B}_f \in \mathbb{R}^{3\times n_f}$

$$\mathbf{B} = \begin{bmatrix} \mathbf{B}_r & \mathbf{B}_f \end{bmatrix} \tag{7.10}$$

$$\mathbf{B}_r = \begin{bmatrix} 1 & 0 & \cdots & 1 & 0 \\ 0 & 1 & \cdots & 0 & 1 \\ -l_{1,y} & l_{1,x} & \cdots & -l_{n_r,y} & l_{n_r,x} \end{bmatrix} \tag{7.11}$$

$$\mathbf{B}_f = \begin{bmatrix} \cos\alpha_{p_r+1} & \cdots & \cos\alpha_p \\ \sin\alpha_{p_r+1} & \cdots & \sin\alpha_p \\ -l_{p_r+1,y}\cos\alpha_{p_r+1} + l_{p_r+1,x}\sin\alpha_{p_r+1} & \cdots & -l_{p,y}\cos\alpha_p + l_{p,x}\sin\alpha_p \end{bmatrix} \tag{7.12}$$

Notice that $\mathbf{B}$ is a constant matrix of rank q (here $q = 3$) whenever the craft is overactuated. The matrix $\mathbf{F}_u \in \mathbb{R}^{n\times n}$ is a diagonal matrix with corresponding values of $F_k^{\max}$ along the diagonal. Define:

$$\mathbf{A} = \mathbf{B}\mathbf{F}_u \tag{7.13}$$

A control vector $\mathbf{u}$ (extended thrust) is called *feasible* if the linear constraint

$$\mathbf{f} = \mathbf{A}\mathbf{u} - \boldsymbol{\tau}_c = \mathbf{0} \tag{7.14}$$

and each and every $\mathbf{u}_k = \boldsymbol{\Pi}_k\mathbf{u}$ lies in its domain $\mathcal{D}_k$.

Let the columns in the matrix N be an orthonormal basis of the null-space $\mathcal{N}(\mathbf{A})$. Then, $\mathbf{A}\mathbf{N} = \mathbf{0}$. The null-space $\mathcal{N}(\mathbf{A})$ and row-space of $\mathbf{A}$, denoted $\mathcal{R}(\mathbf{A}^T)$, are orthogonal subspaces of $\mathbb{R}^n$.

The *generalized inverse* of a matrix $\mathbf{A}$, using a symmetric and positive definite weight matrix $\mathbf{W} = \mathbf{W}^T > 0$, is defined as:

$$\mathbf{A}^\dagger = \mathbf{W}^{-1}\mathbf{A}^T\left(\mathbf{A}\mathbf{W}^{-1}\mathbf{A}^T\right)^{-1} \tag{7.15}$$

such that the unconstrained solution:

$$\mathbf{u}_* = \mathbf{A}^\dagger\boldsymbol{\tau}_c \tag{7.16}$$

is the optimal solution, in a weighed 2-norm sense, that is

$$\mathbf{u}_*^T\mathbf{W}\mathbf{u}_* \le \mathbf{u}^T\mathbf{W}\mathbf{u} \quad \forall \quad \{\mathbf{u}\in\mathbb{R}^n \,|\mathbf{A}\mathbf{u} - \boldsymbol{\tau}_c = \mathbf{0}\} \tag{7.17}$$

Moreover, $\mathbf{u}_* \in \mathcal{R}(\mathbf{W}^{-1}\mathbf{A}^T)$.

If $\mathbf{W} = \mathbf{I}$, we get the *pseudo-inverse*

$$\mathbf{A}^+ = \mathbf{A}^T\left(\mathbf{A}\mathbf{A}^T\right)^{-1} \tag{7.18}$$

such that $\mathbf{u}_* \in \mathcal{R}(\mathbf{A}^T)$. Without loss of generality, we use $\mathbf{A}^+$ instead of $\mathbf{A}^\dagger$ in calculating the unconstrained solution.

7.2.2 Problem Introduction

The main objective is to find a feasible control vector $\mathbf{u}$ (extended thrust) that is optimal with respect to some cost function quadratic in $\mathbf{u}$.

Quadratic cost functions are attractive candidates because when the domains $\mathcal{D}_k$ are described by linear inequalities the problem is a general quadratic program (QP). Quadratic programs can be solved in a finite number of iterations and are

consequently quite predictable which again makes them well suited for real-time implementation. Unfortunately, a propeller-rudder device requires a non-convex domain $\mathcal{D}_k$ because these propulsive devices are unable to produce lateral forces without simultaneously generating significant longitudinal forces.

It is reasonable to assume that the rudder is capable of producing lift for positive thrust force (forward). For negative longitudinal force the rudder can be regarded as inactive, thus the attainable set shrinks to a thin line. Typically the physically attainable thrust region resembles a twisted circular sector, represented by the grid in Figure 7.4. Notice that the negative x-axis is also a part of the attainable set. For convenience, the grid is approximated by an inscribed circular sector so that the feasible set $\mathcal{D}_k$ is given by this sector element and the negative x-axis.

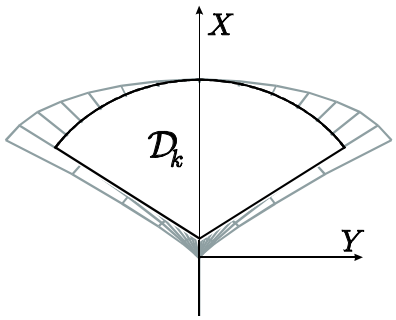

Figure 7.4: The physically attainable thrust region (grid) for a propeller-rudder pair. An inscribed circular sector and the negative x-axis together serve as the feasible region $\mathcal{D}_k$.

Even though a sequential QP (SQP) or a sequential linearly constrained (SLC) method does find a solution, careless utilization of any numerical method can lead to unintended results:

1. An SQP method solves a sequence of QP problems and is therefore more computationally demanding than a single QP. Moreover, if the iteration sequence is interrupted or preempted due to CPU time limitations, the current solution may not be optimal.

2. The non-convex inequality constraints for the propeller-rudder couple introduce a discontinuity in the mapping from $\boldsymbol{\tau}_c \rightarrow \mathbf{u}$ if the optimal solution is to be used at all times. However, infinitesimal changes in $\boldsymbol{\tau}_c$ should never lead to discontinuous extended thrust $\mathbf{u}$.

This second situation is illustrated in Figure 7.5: The optimal unconstrained solution for thruster k, that is $\mathbf{u}_{*,k}$, is marked with a cross and the dotted cost curves illustrate the cost involved getting the solution into the feasible domain $\mathcal{D}_k$. The two circles mark feasible solutions with identical cost. Since the unconstrained solution $\mathbf{u}_{*,k}$ lies slightly above the *equicost line* (dashed) the uppermost solution

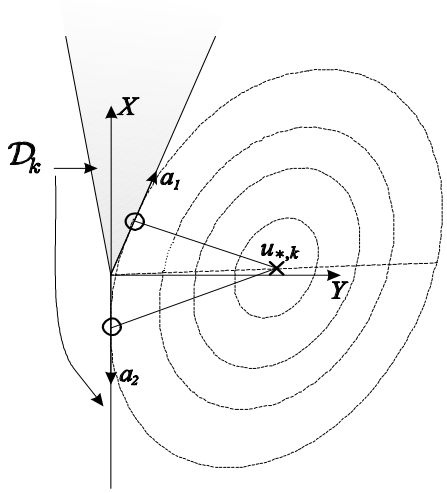

Figure 7.5: Illustration of a discontinuous mapping from τ_c to extended thrust vector u.

is selected. Once $\mathbf{u}_{*,k}$ crosses the equicost, the lower solution becomes optimal. Hence, the mapping is discontinuous and this will again cause undesired propeller and rudder angle chattering. It is therefore of paramount importance to avoid introducing this discontinuity.

7.3 Force Allocation

The proposed algorithm is analytic and requires no iterations whatsoever. This means that some assumptions have to be made:

1. Only one thruster, thruster k, with sector constraints is supported.
2. Thrust force magnitude constraints (box constraints) are not considered.

Due to the feasible region being non-convex, problems may arise if re-allocation is applied uncritically should one or more of the thrust devices saturate. Re-allocating by looping through all possible configurations (Bordignon and Durham 1995*b*) can also be time-consuming. Still, our method is 2-norm optimal, it does avoid rudder-chattering, and it does produce continuous solutions. The two latter properties have, as far as we know, not been considered elsewhere, but any CA algorithm for ships should, in our opinion, support them.

Assumption 1 is the key to handle sector constraints analytically and to ensure continuity. The disadvantage is that for configurations where several thrusters are subject to sector constraints, some sub-optimal modification must be made, for

instance by handling one thruster at a time and keeping the others at a fixed angle. This particular approach was pursued here since our ship model was equipped with two propeller-rudder pairs. As a consequence, one rudder only could be used at any one time.

Thruster saturation is not covered according to Assumption 2. Traditionally, iterative solvers distribute possible overshoot from the saturated thrusters onto the remaining ones provided that the demand $\boldsymbol{\tau}_c$ is attainable. Without saturation handling, however, we are not guaranteed to obtain the desired $\boldsymbol{\tau}_c$ even when it is attainable. But as long as $\boldsymbol{\tau}_c$ is comparatively small with respect to the attainable set, no thruster should saturate and the box constraints can be disregarded. It should be noted that explicit, non-iterative, off-line pre-computed schemes do handle box-constraints (Johansen *et al.* 2002), but they do not support non-convex constraints.

The algorithm for finding a feasible extended thrust vector $\mathbf{u}$ is solved in two steps in order to maximize computational performance. First, an unconstrained solution is found. If this 2-norm optimal solution lies outside the feasible domain $\mathcal{D}$, we need to determine the minimum accumulated cost translating the solution from $\mathbf{u}_*$ towards the domain $\mathcal{D}$.

7.3.1 Unconstrained

The first step in the allocation of extended thrust $\mathbf{u}$ is achieved by simply employing the pseudo-inverse in order to minimize the 2-norm of $\mathbf{u}$.

$$\mathbf{u}_* = \mathbf{A}^+ \boldsymbol{\tau}_c \tag{7.19}$$

If $\mathbf{u}_* \notin \mathcal{D}$, Figure 7.5 indicates that simply projecting the $\mathbf{u}_*$ onto $\mathcal{D}$ one is not guaranteed to find the minimum cost $\mathbf{u} \in \mathcal{D}$. We have to consider the actual cost accumulated of traversing the null-space $\mathcal{N}(\mathbf{A})$. This is the topic of the next subsection.

7.3.2 Sector Constraints

Assume that thrust device k is restricted in a domain $\mathcal{D}_k \subset \mathbb{R}^2$ as illustrated in Figure 7.5 and that the pseudo-inverse solution $\mathbf{u}_*$ has already been found. Since $\mathbf{u}_*$ satisfies the linear equality constraint (7.14), we may add any linear combination of the columns in $\mathbf{N}$ denoted $\delta\mathbf{u} = \mathbf{N}\boldsymbol{\sigma}$ where $\boldsymbol{\sigma}$ is a vector of appropriate dimension, and still have a solution satisfying the linear equality constraint.

$$\mathbf{u} = \mathbf{u}_* + \delta\mathbf{u} = \mathbf{u}_* + \mathbf{N}\boldsymbol{\sigma} \tag{7.20}$$

The objective is now to find the optimal $\boldsymbol{\sigma}$ which renders $\mathbf{u}$ feasible and minimizes $|\mathbf{u}| \geq |\mathbf{u}_*|$. We have

$$\begin{aligned} |\mathbf{u}|^2 &= (\mathbf{u}_* + \mathbf{N}\boldsymbol{\sigma})^T (\mathbf{u}_* + \mathbf{N}\boldsymbol{\sigma}) \\ &= |\mathbf{u}_*|^2 + |\boldsymbol{\sigma}|^2 \end{aligned} \tag{7.21}$$

where we have used that $\mathbf{u}_* \in \mathcal{R}(\mathbf{A}^T)$ such that $\mathbf{N}^T\mathbf{u}_* = \mathbf{0}$ and $\mathbf{N}^T\mathbf{N} = \mathbf{I}$ since $\mathbf{N}$ is an orthonormal basis. Consequently, we seek a vector $\boldsymbol{\sigma}$ with minimum 2-norm.

Consider device number k. We have to find an increment $\delta\mathbf{u}_k$ such that $\mathbf{u}_k \in \mathcal{D}_k$

$$\mathbf{u}_k = \mathbf{u}_{*,k} + \delta\mathbf{u}_k, \quad \delta\mathbf{u}_k = \boldsymbol{\Pi}_k\mathbf{N}\boldsymbol{\sigma} \tag{7.22}$$

Once again the pseudo-inverse is applicable because it minimizes the 2-norm. Hence,

$$\boldsymbol{\sigma} = (\boldsymbol{\Pi}_k\mathbf{N})^+ \delta\mathbf{u}_k \tag{7.23}$$

is the solution we are looking for, but we have yet to determine $\delta\mathbf{u}_k$.

Once $\mathbf{u}_k$ enters the feasible region spanned by $\mathbf{a}_1$ and $\mathbf{a}_2$ (Figure 7.5), it is going to be parallel to one linear boundary curve $\mathbf{a}_i \in \mathbb{R}^2$. Consequently, we have reached the minimum when $\mathbf{u}_k || \mathbf{a}_i$, which can be rephrased as a linear constraint because any $\mathbf{a}_i$ is a design parameter. By letting $\mathbf{a} = \mathbf{a}_i$ and using the inner product we get the constraint

$$f_s = \mathbf{a}_\perp^T\mathbf{u}_k = \mathbf{a}_\perp^T(\mathbf{u}_{*,k} + \delta\mathbf{u}_k) = 0 \tag{7.24}$$

where $\mathbf{a}_\perp$ is orthogonal to $\mathbf{a}$, that is $\mathbf{a}^T\mathbf{a}_\perp = 0$. Later, in Section 7.3.4 we focus on determining which boundary vector $\mathbf{a}$ to use.

Define the Lagrangian

$$\begin{aligned} L &= \frac{1}{2}\boldsymbol{\sigma}^T\boldsymbol{\sigma} + \lambda f_s \\ &= \frac{1}{2}(\delta\mathbf{u}_k)^T\mathbf{W}_k\delta\mathbf{u}_k + \lambda\left(\mathbf{a}_\perp^T\mathbf{u}_{*,k} + \mathbf{a}_\perp^T\delta\mathbf{u}_k\right) \end{aligned} \tag{7.25}$$

where it can be shown that

$$\mathbf{W}_k = \left(\boldsymbol{\Pi}_k\mathbf{N}\mathbf{N}^T\boldsymbol{\Pi}_k\right)^{-1} \tag{7.26}$$

is positive definite as long as $\dim\mathcal{N}(\mathbf{A}) \geq 2$. In other words, $\mathbf{N}$ must have at least two columns. It must be pointed out that only the inverse $\mathbf{W}_k^{-1}$ will be utilized and not $\mathbf{W}_k$ itself. Since we only have to calculate

$$\mathbf{W}_k^{-1} = \boldsymbol{\Pi}_k\mathbf{N}\mathbf{N}^T\boldsymbol{\Pi}_k \tag{7.27}$$

we may disregard the dimension of the null-space causing a singular $\mathbf{W}_k$.

If $\dim\mathcal{N}(\mathbf{A}) \geq 2$, this reduces to an unconstrained QP problem trivially solved using the generalized inverse. The minimum solution is found by minimizing L

$$\frac{\partial L}{\partial\delta\mathbf{u}_k} = \mathbf{W}_k\delta\mathbf{u}_k + \mathbf{a}_\perp\boldsymbol{\lambda} = \mathbf{0} \tag{7.28}$$

$$\delta\mathbf{u}_k = -\mathbf{W}_k^{-1}\mathbf{a}_\perp\boldsymbol{\lambda} \tag{7.29}$$

Since the constrained solution is parallel to $\mathbf{a}$, by using (7.24)

$$\boldsymbol{\lambda} = \left(\mathbf{a}_\perp^T\mathbf{W}_k^{-1}\mathbf{a}_\perp\right)^{-1}\mathbf{a}_\perp^T\mathbf{u}_{*,k} \tag{7.30}$$

the optimal solution is

$$\delta\mathbf{u}_k = -\mathbf{W}_k^{-1}\mathbf{a}_\perp \left(\mathbf{a}_\perp^T\mathbf{W}_k^{-1}\mathbf{a}_\perp\right)^{-1}\mathbf{a}_\perp^T\mathbf{u}_{*,k} \tag{7.31}$$

For all thrust devices together, the optimal increment $\delta\mathbf{u}$ is obtained by combining (7.20), (7.23) and (7.31)

$$\delta\mathbf{u} = \mathbf{N}\left(\mathbf{\Pi}_k\mathbf{N}\right)^+\delta\mathbf{u}_k \tag{7.32}$$

and hence for the modified extended thrust, assuming that $\mathbf{u} \in \mathcal{D}$

$$\begin{aligned}\mathbf{u} &= \mathbf{u}_* - \mathbf{N}\left(\mathbf{\Pi}_k\mathbf{N}\right)^+\mathbf{W}_k^{-1}\mathbf{a}_\perp\left(\mathbf{a}_\perp^T\mathbf{W}_k^{-1}\mathbf{a}_\perp\right)^{-1}\mathbf{a}_\perp^T\mathbf{u}_{*,k}\\ &= \left(\mathbf{I} - \mathbf{N}\mathbf{N}^T\mathbf{\Pi}_k^T\mathbf{a}_\perp\left(\mathbf{a}_\perp^T\mathbf{W}_k^{-1}\mathbf{a}_\perp\right)^{-1}\mathbf{a}_\perp^T\mathbf{\Pi}_k\right)\mathbf{u}_*\end{aligned} \tag{7.33}$$

Note that $\mathbf{W}_k^{-1}$, $\mathbf{N}$ and $\mathbf{\Pi}_k$ are constant matrices. Even if the sector bound $\mathbf{a}$, or equivalently $\mathbf{a}_\perp$ varies in time, no time-consuming matrix operations need to be performed on-line, because $\mathbf{a}_\perp^T\mathbf{W}_k^{-1}\mathbf{a}_\perp$ is a non-negative scalar.

7.3.3 Sector Constraint with Rudder Anti-Chat

In order to remove rudder chattering around zero, we propose to translate the sector constraint a distance $\mathbf{r}^o \in \mathbb{R}^2$, or more specifically, slightly along the x-axis as shown in Figure 7.6. This modification ensures that the rudder will not be used unless the actuator thrust is above some positive threshold. Furthermore, the transition from zero rudder angle to maximum deflection will be continuous, because rudder will be applied gradually as the required thrust along the x-axis increases.

The distance between the origin of the original O-frame and the origin of the translated B-frame is denoted $\mathbf{r}^o$ when it is decomposed in the O-frame. Then, a point $\mathbf{c}^b$ in the B-frame is in the O-frame given as $\mathbf{c}^o = \mathbf{r}^o + \mathbf{c}^b$. Thus, the optimal unconstrained solution decomposed in the B-frame is $\mathbf{u}_*^b = \mathbf{u}_*^o - \mathbf{r}^o$.

We may now perform the adjustment due to the sector constraint in the B-frame instead of in the O-frame, because $\delta\mathbf{u}_k^b = \delta\mathbf{u}_k^o$ since the coordinate systems are linearly translated and not rotated with respect to each other. The basic results from the previous section can therefore be applied. More specifically, the cost $\mathbf{W}_k$ as given in (7.26) serves as the weight in the Lagrangian

$$L = \frac{1}{2}\left(\delta\mathbf{u}_k^b\right)^T\mathbf{W}_k\delta\mathbf{u}_k^b + \lambda\left(\mathbf{a}_\perp^T\mathbf{u}_{*,k}^b + \mathbf{a}_\perp^T\delta\mathbf{u}_k^b\right) \tag{7.34}$$

where it must be noted that $\mathbf{a}_\perp$ is now given in the B-frame. The minimum cost adjustment is

$$\delta\mathbf{u}_k^b = -\mathbf{W}_k^{-1}\mathbf{a}_\perp\left(\mathbf{a}_\perp^T\mathbf{W}_k^{-1}\mathbf{a}_\perp\right)^{-1}\mathbf{a}_\perp^T\mathbf{u}_{*,k}^b \tag{7.35}$$

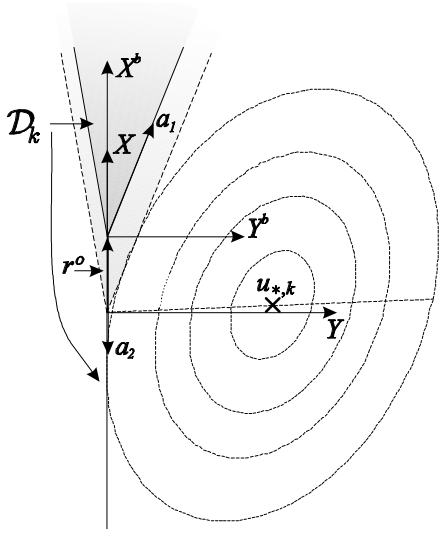

Figure 7.6: Translating the sector constraint of thruster k: Defintion of the B-frame.

and the optimal constrained solution $\mathbf{u}^b$ and $\mathbf{u}^o$ given in the B- and O-frames are

$$\mathbf{u}^b = \mathbf{u}_*^b + \mathbf{N}\left(\mathbf{\Pi}_k\mathbf{N}\right)^+ \delta\mathbf{u}_k^b \tag{7.36}$$

$$\mathbf{u}^o = \mathbf{u}_*^o + \mathbf{N}\left(\mathbf{\Pi}_k\mathbf{N}\right)^+ \delta\mathbf{u}_k^b \tag{7.37}$$

A more detailed calculation reveals that

$$\begin{aligned}\mathbf{u}^o = &\left(\mathbf{I} - \mathbf{N}\mathbf{N}^T\mathbf{\Pi}_k\mathbf{a}_\perp\left(\mathbf{a}_\perp^T\mathbf{W}_k^{-1}\mathbf{a}_\perp\right)^{-1}\mathbf{a}_\perp^T\mathbf{\Pi}_k\right)\mathbf{u}_* \\ &+\mathbf{N}\left(\mathbf{\Pi}_k\mathbf{N}\right)^+\mathbf{W}_k^{-1}\mathbf{a}_\perp\left(\mathbf{a}_\perp^T\mathbf{W}_k^{-1}\mathbf{a}_\perp\right)^{-1}\mathbf{a}_\perp^T\mathbf{r}^o\end{aligned} \tag{7.38}$$

where we notice that the first term is exactly the same as (7.33), that is when the B-frame coincides with the O-frame, and that the contribution from the translation $\mathbf{r}^o$ appears as an additional linear term.

7.3.4 The Equicost Line

In case $\mathbf{u}_{*,k} \notin \mathcal{D}_k$, we have to decide which of the two nearest boundaries of the feasible domain $\mathcal{D}_k$ we should approach, see Figure 7.6. Assume that $\mathbf{a}_1, \mathbf{a}_2 \in \mathbb{R}^2$ are two vectors defining the boundaries of $\mathcal{D}_k$. We seek the unit vector $\mathbf{e}_l$ describing the *equicost line*. That is, for any point on $\mathbf{e}_l$, say $\mathbf{p} = c\mathbf{e}_l$, where $c \in \mathbb{R}$ is an arbitrary scalar, the costs of approaching $\mathbf{a}_1$ and $\mathbf{a}_2$ are identical.

From the results in the two previous sections we know that

$$\delta\mathbf{p}_1 = \mathbf{W}_k^{-1}(\mathbf{a}_1)_\perp \left((\mathbf{a}_1)_\perp^T \mathbf{W}^{-1}(\mathbf{a}_1)_\perp\right)^{-1} (\mathbf{a}_1)_\perp^T \mathbf{p} \tag{7.39}$$

$$\delta\mathbf{p}_2 = \mathbf{W}_k^{-1}(\mathbf{a}_2)_\perp \left((\mathbf{a}_2)_\perp^T \mathbf{W}^{-1}(\mathbf{a}_2)_\perp\right)^{-1} (\mathbf{a}_2)_\perp^T \mathbf{p} \tag{7.40}$$

are the optimal steps towards $\mathbf{a}_1$ and $\mathbf{a}_2$ respectively. The costs involved are $i = 1, 2$

$$\begin{aligned} J_i &= (\delta\mathbf{p}_i)^T \mathbf{W}_k \delta\mathbf{p}_i \\ &= \mathbf{p}^T \left((\mathbf{a}_i)_\perp \left((\mathbf{a}_i)_\perp^T \mathbf{W}^{-1}(\mathbf{a}_i)_\perp\right)^{-1} (\mathbf{a}_i)_\perp^T\right) \mathbf{p} \end{aligned} \tag{7.41}$$

and in order to find the equicost line we require $J_1 = J_2$ or $\Delta J = J_1 - J_2 = 0$. Hence,

$$\Delta J = \mathbf{p}^T \mathbf{L} \mathbf{p} = 0 \quad \Leftrightarrow \quad \mathbf{e}_l^T \mathbf{L} \mathbf{e}_l = 0 \tag{7.42}$$

where $\mathbf{L} = \mathbf{L}^T$ is given by

$$\mathbf{L} = \begin{bmatrix} L_{11} & L_{12} \\ L_{12} & L_{22} \end{bmatrix} = \frac{(\mathbf{a}_1)_\perp (\mathbf{a}_1)_\perp^T}{(\mathbf{a}_1)_\perp^T \mathbf{W}_k^{-1} (\mathbf{a}_1)_\perp} - \frac{(\mathbf{a}_2)_\perp (\mathbf{a}_2)_\perp^T}{(\mathbf{a}_2)_\perp^T \mathbf{W}_k^{-1} (\mathbf{a}_2)_\perp}$$

Expanding this expression using $\mathbf{e}_l = [x, y]^T$ we obtain the two linear curves where the hyperbola $z = \mathbf{e}_l^T \mathbf{L} \mathbf{e}_l$ intersects the xy-plane, that is

$$L_{11}x^2 + 2L_{12}xy + L_{22}y^2 = 0 \tag{7.43}$$

Using polar coordinates $\mathbf{e}_l = [\cos\theta, \sin\theta]^T$ we get four solutions

$$\theta = \arctan\left(-\frac{L_{12}}{L_{22}} \pm \sqrt{\left(\frac{L_{12}}{L_{22}}\right)^2 - \frac{L_{11}}{L_{22}}}\right) + j\pi \tag{7.44}$$

where $j = 0, 1$. From this the correct solution is selected, namely the one lying in the sector spanned by $\mathbf{a}_1$ and $\mathbf{a}_2$. Observe that for this method to be valid, $|L_{22}| > 0$, the infeasible sector has to be less than 180 degrees wide. For propeller/rudder pairs this will always be the case.

7.3.5 Restore Continuity

We have already predicted that crossing the equicost line could introduce a discontinuity in $\mathbf{u}_k^b$ even if the commanded thrust force $\boldsymbol{\tau}_c$ is continuous. In this section, we propose a remedy for this situation; a solution $\mathbf{u}_k^b$ that does not necessarily minimize the 2-norm. The idea is outlined in Figure 7.7. If $\mathbf{u}_{*,k}^b$ is situated inside the sector surrounding the equicost line, we drive $\mathbf{u}_k^b$ to a point closer to the origin (the intersection between $\mathbf{a}_1$ and $\mathbf{a}_2$). Unlike the procedure given above, we now follow the solid arrows instead of the dotted lines. Consequently, if $\mathbf{u}_{*,k}^b$ lies exactly on the equicost, the desired $\mathbf{u}_k^b$ should be zero and continuity will be restored. Figure 7.8 shows more details: Having already calculated the constrained optimal

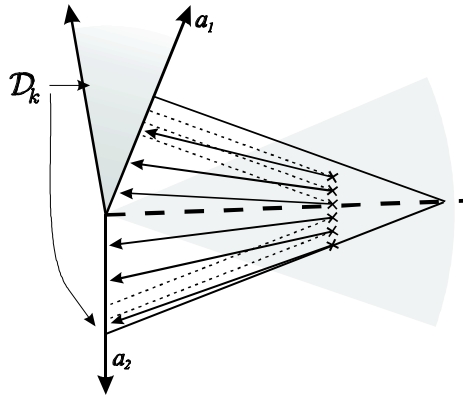

Figure 7.7: Translation of $\mathbf{u}^b_{*,k}$ without loss of continuity.

solution $\mathbf{u}^b_k$, marked with a circle, we now force it towards the origin increasing the cost.

Decompose $\mathbf{u}^b_{*,k}$ onto the unit vectors $\mathbf{e}_l$ and $\mathbf{e}_\delta$. $\mathbf{e}_l$ is parallel to the equicost line and

$$\mathbf{e}_\delta = \frac{\delta \mathbf{u}^b_k}{\left|\delta \mathbf{u}^b_k\right|} \tag{7.45}$$

$\mathbf{e}_l$ and $\mathbf{e}_\delta$ define a (not necessarily orthogonal) basis for $\mathbb{R}^2$ such that

$$\mathbf{c} = [e_l | e_\delta]^{-1} \mathbf{u}^b_{*,k} \tag{7.46}$$

yields

$$\mathbf{u}^b_{*,k} = \mathbf{c}_1 \mathbf{e}_l + \mathbf{c}_2 \mathbf{e}_\delta \tag{7.47}$$

The distance between the equicost line and $\mathbf{u}^b_{*,k}$ is

$$\mathbf{b} = \mathbf{u}^b_{*,k} + \delta \mathbf{u}^b_k - c_1 \mathbf{e}_l \tag{7.48}$$

so that the ratio

$$\gamma = \frac{c_2}{|\mathbf{b}|} \tag{7.49}$$

defines the location of $\mathbf{u}^b_{*,k}$ along the line $\mathbf{b}$. A γ close to zero means that $\mathbf{u}^b_{*,k}$ is close to the equicost line, and we need to force $\mathbf{u}^b_k$ toward the origin. The strategy is: Introduce a design parameter $0 < \gamma_r < 1$ and a continuous, non-decreasing weighing function $f : \mathbb{R}_{\geq 0} \to [0, 1]$. Besides (7.35) we now use

$$\Delta \mathbf{u}^b_k = \left(f\left(\gamma/\gamma_r\right) - 1\right) \mathbf{u}^b_{*,k} + f\left(\gamma/\gamma_r\right) \delta \mathbf{u}^b_k \tag{7.50}$$

$$\mathbf{u}^b_k = \mathbf{u}^b_{*,k} + \Delta \mathbf{u}^b_k = f\left(\gamma/\gamma_r\right) \left(\mathbf{u}^b_{*,k} + \delta \mathbf{u}^b_k\right) \tag{7.51}$$

The width of the sector is determined by γ_r. Outside of the sector, $f\left(\gamma/\gamma_r\right) = 1$ and $\Delta \mathbf{u}^b_k = \delta \mathbf{u}^b_k$. The optimal but discontinuous solution corresponds to $\gamma_r \to 0$ or $f(s) = 1$ for all $s \geq 0$. Figure 7.9 shows three weighing function alternatives.

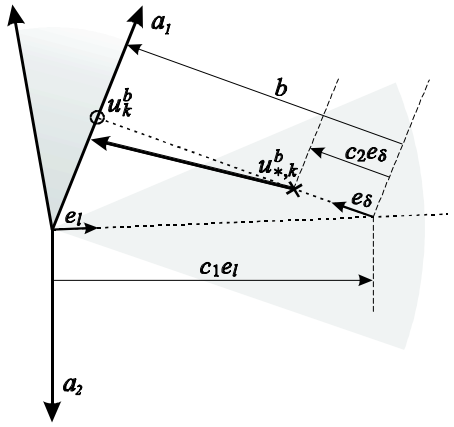

Figure 7.8: Detailed picture of restored continuity and definition of basis vectors $\mathbf{e}_l$ and $\mathbf{e}_\delta$.

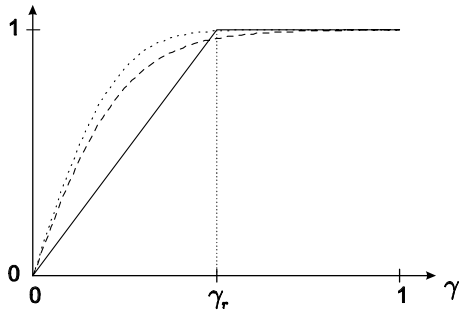

Figure 7.9: Weighing functions: $f_1(s) = \text{sat}(s)$ (solid), $f_2(s) = \tanh(2s)$ (dashed) and $f_3(s) = \text{erf}(2s)$ (dotted).

7.3.6 Proposed Algorithm

The force allocation procedure can be summarized by the following sequence of operations:

1. $\mathbf{u}_* = \mathbf{A}^+ \boldsymbol{\tau}_c$.
2. If $\mathbf{u}_* \in \mathcal{D}$ then terminate.
3. Approaching $\mathcal{D}$.
   - Assume thruster k such that $\mathbf{u}_{*,k} \notin \mathcal{D}_k$.
   - $\mathbf{u}_*^b = \mathbf{u}_* - \mathbf{r}^o$.
   - Find equicost line $\mathbf{e}_l$ and determine towards which boundary $\mathbf{a}_i$ of $\mathcal{D}_k$ we should go. Call it $\mathbf{a}$.

- $\delta \mathbf{u}_k^b = -\mathbf{W}_k^{-1}\mathbf{a}_\perp \left(\mathbf{a}_\perp^T \mathbf{W}_k^{-1}\mathbf{a}_\perp\right)^{-1} \mathbf{a}_\perp^T \mathbf{u}_{*,k}^b$

4. If $\dim(\mathcal{N}(\mathbf{A})) > 1$

   - Restore continuity of the mapping $\boldsymbol{\tau}_c \rightarrow \mathbf{u}^b$
   - $\mathbf{e}_\delta = \delta \mathbf{u}_k^b / \left|\delta \mathbf{u}_k^b\right|$
   - $\mathbf{c} = \left[\mathbf{e}_l | \mathbf{e}_\delta\right]^{-1} \mathbf{u}_{*,k}^b$
   - $\mathbf{b} = \mathbf{u}_{*,k}^b + \delta \mathbf{u}_k^b - c_1 \mathbf{e}_l$
   - $\gamma = c_2 / \left|\mathbf{b}\right|$
   - $\Delta \mathbf{u}_k^b = \left(f\left(\gamma/\gamma_r\right) - 1\right) \mathbf{u}_{*,k}^b + f\left(\gamma/\gamma_r\right) \delta \mathbf{u}_k^b$

5. If $\dim \mathcal{N}(\mathbf{A}) = 1$

   - $\Delta \mathbf{u}_k^b = \delta \mathbf{u}_k^b$

6. For all thrusters

   - $\mathbf{u}^b = \mathbf{u}_*^b + \mathbf{N}\left(\boldsymbol{\Pi}_k \mathbf{N}\right)^+ \Delta \mathbf{u}_k^b$
   - $\mathbf{u}^o = \mathbf{u}^b + \mathbf{r}^o$

If the dimension of the null-space of $\mathbf{A}$ is 1, it is futile to perform step 4 (Restore continuity). Likewise, the concept of the equicost line does not apply.

7.4 Experimental Results

The experiment was performed in the Guidance, Navigation and Control (GNC) Laboratory at NTNU with the model ship Cybership II (CS2). This vessel is equipped with three propulsive devices: In the bow there is a small two-bladed RPM-controlled tunnel-thruster capable to produce a sway force, and at the stern there are two RPM-controlled main propellers with rudders. See Appendix E.2.2 for a complete description of the low speed model and thruster/rudder models for CS2.

7.4.1 Output Feedback Control

The observer presented in Section 4.3 was implemented using position and heading measurements only. Together with the PID-like controller

$$\begin{aligned} \dot{\boldsymbol{\xi}} &= \hat{\boldsymbol{\eta}} - \boldsymbol{\eta}_d \\ \hat{\boldsymbol{\tau}} &= -\mathbf{K}_i \mathbf{R}^T(\psi)\boldsymbol{\xi} + \mathbf{K}_p \mathbf{R}^T(\psi)\left(\hat{\boldsymbol{\eta}} - \boldsymbol{\eta}_d\right) \\ &\quad + \mathbf{K}_d\left(\hat{\boldsymbol{\nu}} - \boldsymbol{\nu}_d\right) + \mathbf{D}\boldsymbol{\nu}_d + \mathbf{M}\dot{\boldsymbol{\nu}}_d \end{aligned} \tag{7.52}$$

asymptotic stability of the closed loop was guaranteed by Theorem 5.4.

7.4.2 Experiment Description

The main objective of the experiments was to compare the energy consumption with and without the active use of rudders during a positioning operation: Move 30 cm sideways while maintaining a fixed heading. This operation is particularly energy consuming when the rudders are not to be used because the ship is unable to produce lateral forces in the stern.

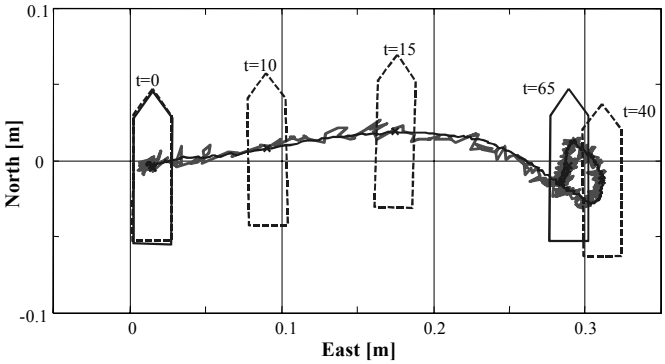

Figure 7.10: Operation overview.

In order to emphasize the differences, at $t = 2$ the desired position changed from $\boldsymbol{\eta}_d = [0, 0, 0]^T$ to $\boldsymbol{\eta}_d = [0, 0.30, 0]^T$ in a step-response fashion, see Figure 7.10. In full-scale 30 cm corresponds to approximately 20 meters. The observer's low frequency estimate is the smooth mean of the measured position.

The applied step in desired position $\boldsymbol{\eta}_d$ suggested that the integral action should be turned off, $\mathbf{K}_i = \mathbf{0}$. Otherwise, the integrator would build up uncorrectly resulting in a large overshoot. Furthermore, the proportional and derivative gains had to be small enough to avoid magnitude saturation of the thrusters. The remaining two gain matrices were selected as

$$\mathbf{K}_p = \text{diag}(0.5, 0.8, 0.5) \tag{7.53}$$

$$\mathbf{K}_d = \text{diag}(8, 6, 1) \tag{7.54}$$

Inwards rudder deflection was allowed. Consequently, the port propeller/rudder pair was allowed to have a lateral component pointing port while the starboard propeller/rudder had a component pointing in the starboard direction. Two solutions were calculated at each sample. In the first one, $\mathbf{u}_1$, the port rudder was allowed to be used while the starboard rudder was fixed at zero degrees, and in the second one, $\mathbf{u}_2$, the starboard rudder was deflected and the port rudder set at zero degrees. Finally, we selected the solution with minimum 2-norm, that is $|\mathbf{u}_i|$ for $i = 1, 2$.

The feasible sector was varied in four steps from zero to a maximum of 32 degrees, more specifically

$$\boldsymbol{\alpha}_{\max} = \begin{bmatrix} 0 & 10 & 20 & 32 \end{bmatrix}^T \quad [\text{deg}] \tag{7.55}$$

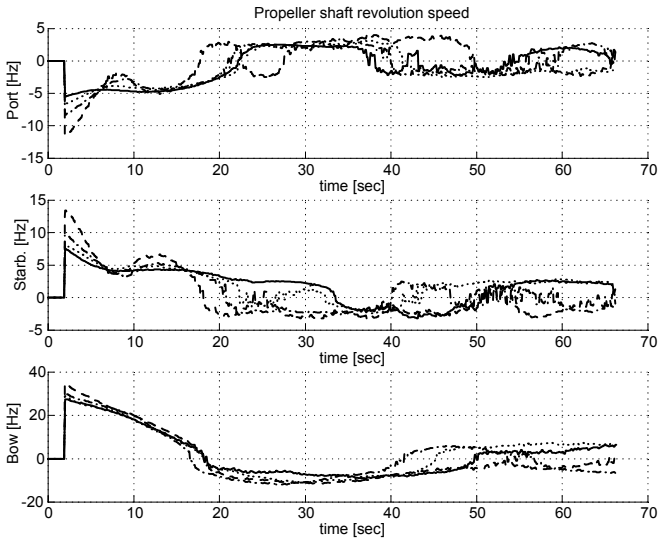

Figure 7.11: Propeller shaft speeds ω_i for feasible sector widths $\alpha_{\max} = 0$ (dashed), $\alpha_{\max} = 10$ (dash-dotted), $\alpha_{\max} = 20$ (dotted) and $\alpha_{\max} = 32$ deg (solid).

In order to attenuate rudder chattering around zero, the following $\mathbf{r}^o$ was used for both main propellers

$$\mathbf{r}^o = \begin{bmatrix} 1.5 & 0 \end{bmatrix}^T \quad [\text{mN}] \tag{7.56}$$

Figure 7.11 shows the applied propeller revolution speed for all four test runs. The dashed lines denote $\alpha_{\max} = 0$, the dash-dotted lines $\alpha_{\max} = 10$, the dotted lines $\alpha_{\max} = 20$, and the solid lines represent $\alpha_{\max} = 32$ degrees. Figure 7.12 is a close-up of Figure 7.11. The applied rudder angles are plotted in Figure 7.13. Notice that since the rudders were deflected inwards, the port rudder is always negative while the starboard rudder is always positive.

Absorbed hydrodynamic power is proportional to the cube of the shaft speed. We assumed that the efficiency factor was constant so that applied electrical power was proportional to hydrodynamic power. Figure 7.14 show normalized power, in fractions of the maximum equal to 1, for all four test runs. Thus, we may compare individual runs without having an exact power model available. The main propellers' energy consumption defined as the integral of normalized power is reproduced in Figure 7.15, and the normalized power and energy consumption for the bow thruster is plotted in Figure 7.16.

7.4.3 Comments

The responses in terms of tracking the desired position were very similar for all four test runs, and consequently the applied thrust forces $\boldsymbol{\tau}_c$ were almost indistinguishable. Time series plots of the positions and thrust forces are not shown.

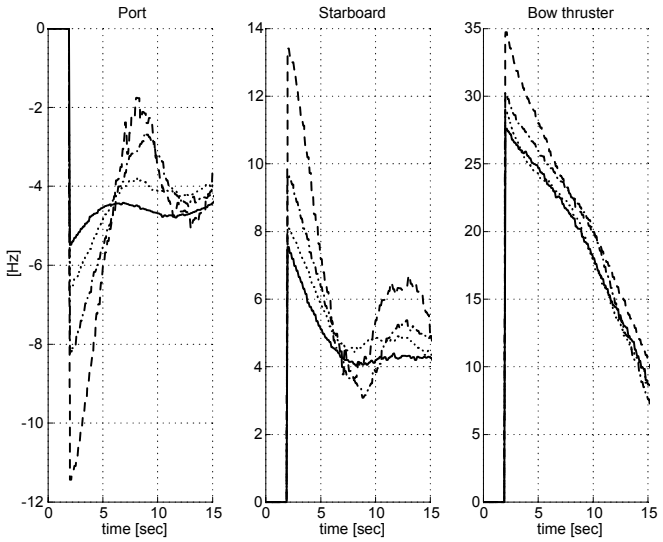

Figure 7.12: Propeller shaft speeds ω_i during the first 15 seconds of operation. $\alpha_{\max} = 0$ (dashed), $\alpha_{\max} = 10$ (dash-dotted), $\alpha_{\max} = 20$ (dotted), $\alpha_{\max} = 32$ deg (solid).

When the force allocation algorithm is allowed to use the rudders to generate sway forces in the stern, the power and energy consumption for all three propellers decrease significantly. For $\alpha_{\max} = 32$ degrees, the peak in required power for the main propellers is being reduced to only 15% of that required for $\alpha_{\max} = 0$. The peak of the bow thruster's power consumption is reduced by around 50%. When the ship approaches its new position, the differences are less pronounced.

The rudder anti-chattering option, this is a non-zero $\mathbf{r}^o$, works satisfactorily. If this functionality is turned off, the rudder angle set-points would switch between zero and maximum rudder deflection. Measurement noise residues in $\boldsymbol{\tau}_c$ spuriously creates an impression of oscillatory rudder behavior (Figure 7.13).

7.5 Concluding Remarks

We have introduced a force allocation algorithm for a sector-restricted thrust device such as a propeller-rudder pair. Handling sector constraints is non-trivial, because the optimization problem is no longer convex and local minima exist. The proposed force allocation method is a three-step algorithm that avoids rudder chattering and ensures a continuous mapping between the commanded thrust force and the extended thrust.

Experiments with a model ship confirmed that using rudders actively has a great potential in terms of improving energy efficiency.

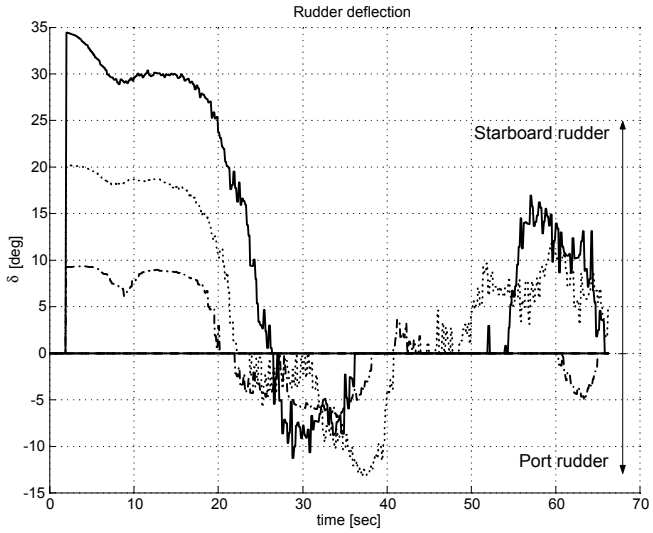

Figure 7.13: Rudder angles. $\alpha_{\max} = 0$ (dashed), $\alpha_{\max} = 10$ (dash-dotted), $\alpha_{\max} = 20$ (dotted), $\alpha_{\max} = 32$ deg (solid).

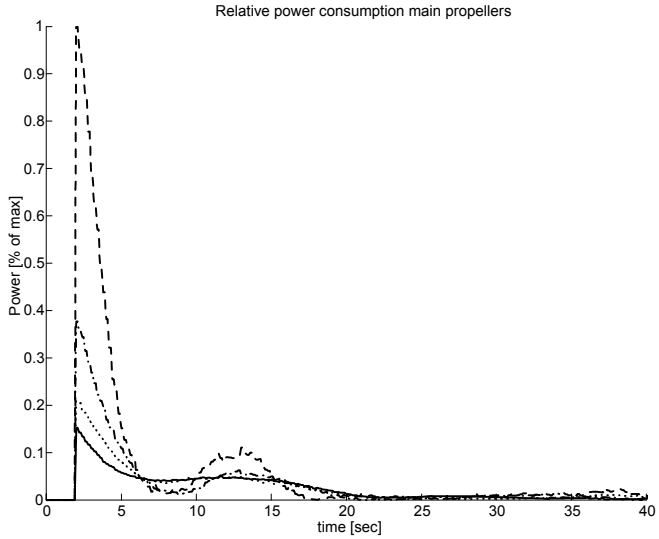

Figure 7.14: Normalized power consumption for the main propellers. $\alpha_{\max} = 0$ (dashed), $\alpha_{\max} = 10$ (dash-dotted), $\alpha_{\max} = 20$ (dotted), $\alpha_{\max} = 32$ deg (solid).

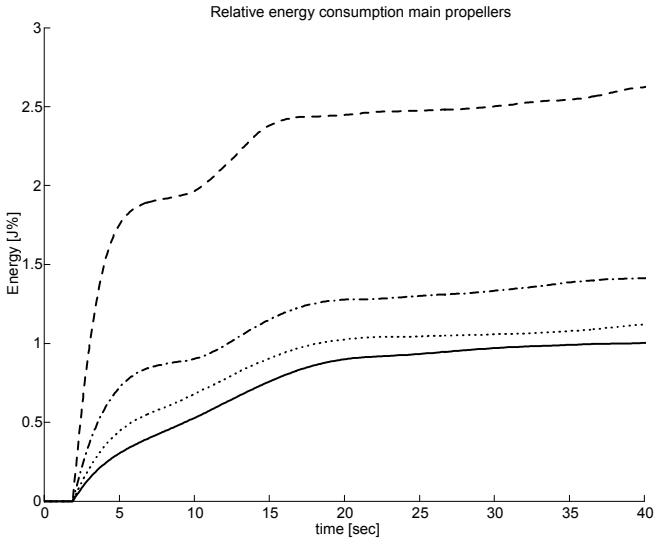

Figure 7.15: Consumed energy for the main propellers, given as integrated normalized power. $\alpha_{\max} = 0$ (dashed), $\alpha_{\max} = 10$ (dash-dotted), $\alpha_{\max} = 20$ (dotted), $\alpha_{\max} = 32$ deg (solid).

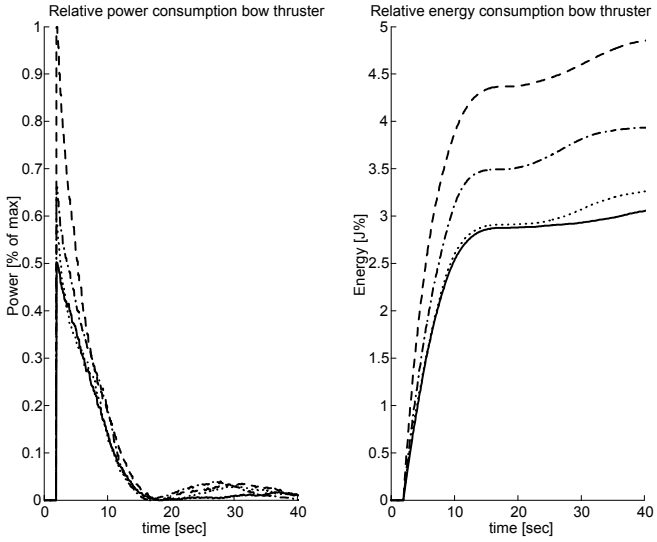

Figure 7.16: Normalized power and energy consumption of the bow thruster. $\alpha_{\max} = 0$ (dashed), $\alpha_{\max} = 10$ (dash-dotted), $\alpha_{\max} = 20$ (dotted), $\alpha_{\max} = 32$ deg (solid).

Bibliography

Aalbers, A. B., R. F. Tap and J. A. Pinkster (2001). An application of dynamic positioning control using wave feed forward. *Int. Journal of Robust and Nonlinear Control* **11**, 1207–1237.

Aamo, O. M. and T. I. Fossen (1999). Controlling line tension in thruster assisted mooring systems. In: *Proc. of the 1999 IEEE Int. Conf. on Control Applications (CCA'99)*. Honolulu, Hawaii. pp. 1104–1109.

Aamo, O. M., M. Arcak, T. I. Fossen and P. V. Kokotović (2001). Global output tracking control of a class of Euler-Lagrange systems with monotonic nonlinearities in the velocities. *Int. Journal of Control* **74**(7), 649–658.

Aarset, M. F., J. P. Strand and T. I. Fossen (1998). Nonlinear vectorial observer backstepping with integral action and wave filtering for ships. In: *Proc. of IFAC Conf. On Control Applications in Marine Systems (CAMS '98)*. Fukuoka, Japan. pp. 83–88.

Abbot, I. H. and A. E. von Doenhoff (1959). *Theory of Wing Sections*. Dover Publications. New York, NY.

Bachmayer, R., L. L. Whitcomb and M. A. Grosenbaugh (2000). An accurate four-quadrant nonlinear dynamical model for marine thrusters: Theory and experimental validation. *IEEE J. of Oceanic Engineering* **25**(1), 146–159.

Balchen, J. G., N. A. Jenssen and S. Sælid (1976). Dynamic positioning using Kalman filtering and optimal control theory. In: *IFAC/IFIP Symposium on Automation in Offshore Oil Field Operation*. Amsterdam, Holland. pp. 183–186.

Balchen, J. G., N. A. Jenssen, E. Mathisen and S. Sælid (1980). A dynamic positioning system based on Kalman filtering and optimal control. *Modeling Identification and Control* **1**(3), 135–163.

Berg, J. M., K. D. Hammet, C. A. Schwartz and S. S. Banda (1996). An analysis of the destabilizing effect of daisy chained rate-limited actuators. *IEEE Trans. on Control Systems Technology* **4**(2), 171–176.

Berge, S. P. (1999). Nonlinear Way-Point Tracking Control and Docking of Ships. PhD thesis. Dept. of Engineering Cybernetics, Norwegian University of Science and Technology. Trondheim, Norway.

Berge, S. P. and T. I. Fossen (1997). Robust Control Allocation of Overactuated Ships: Experiments With a Model Ship. In: *Proc. of the 4th IFAC Conf. on Manoeuvring and Control of Marine Craft*. Brijuni, Croatia. pp. 166–171.

Blakelock, J. H. (1991). *Automatic Control of Aircraft and Missiles*. second ed.. John Wiley & Sons, Inc.

Blanke, M., K.-P. Lindegaard and T. I. Fossen (2000). Dynamic model for thrust generation of marine propellers. In: *Proc. of the 5th IFAC Conf. on Manoeuvering and Control of Marine Craft (MCMC'2000)*. pp. 363–368.

Bordignon, K. A. and W. C. Durham (1995*a*). Closed-Form Solutions to Constrained Control Allocation Problem. *AIAA Journal of Guidance, Control and Dynamics* **18**(5), 1000–1007.

Bordignon, K. A. and W. C. Durham (1995*b*). Null-space augmented solutions to constrained control allocation problems. In: *Proc. of the 1995 AIAA Guidance, Navigation and Control Conf. (AIAA-95-3209)*. Vol. 0. Baltimore, MD.

Boyd, S., L. El Ghaoui, E. Feron and V. Balakrishnan (1994). *Linear Matrix Inequalities in System and Control Theory*. Society for Industrial and Applied Mathematics SIAM. Philadelphia, PA.

Breslin, J. P. and P. Andersen (1994). *Hydrodynamics of Ship Propellers*. Cambrigde University Press.

Brix, J. (1993). *Manoeuvring Technical Manual*. Seehafen Verlag. Hamburg, Germany.

Buffington, J. M. and D. F. Enns (1996). Lyapunov stability analysis of daisy chain control allocation. *AIAA Journal of Guidance, Control and Dynamics* **19**(6), 1226–1230.

Buffington, J. M., D. F. Enns and A. R. Teel (1998). Control allocation and zero dynamics. *AIAA Journal of Guidance, Control and Dynamics* **21**(3), 458–464.

Carlton, J. S. (1994). *Marine Propellers and Propulsion*. Butterworth-Heinemann.

Chilali, M. and P. Gahinet (1996). H_∞ design with pole placement constraints: An LMI approach. *IEEE Trans. on Automatic Control* **41**(3), 358–367.

de Jager, B. (1994). Acceleration assisted tracking control. *IEEE Control Systems Magazine* **14**(5), 20–27.

Det Norske Veritas (1990). *Rules for Classification of Ships Newbuildings, Special Equipment and Systems, Part 6 Ch. 7: Dynamic Positioning Systems*.

Do, K. D., Z. P. Jiang and J. Pan (2002). Universal controllers for stabilization and tracking of underactuated ships. *Systems & Control Letters* **47**, 299–317.

Donha, D. C. and E. A. Tannuri (2001). Non-linear semi-submersible positioning system design using an H_∞ controller. In: *Proc. of the 5th IFAC Conf. on Control Applications in Marine Systems (CAMS2001)*. Glasgow, UK.

Durham, W. C. (1993). Constrained Control Allocation. *AIAA Journal of Guidance, Control and Dynamics* **16**(4), 717–725.

Durham, W. C. (1994*a*). Attainable Moments for the Constrained Control Allocation Problem. *AIAA Journal of Guidance, Control and Dynamics* **17**(6), 1371–1373.

Durham, W. C. (1994*b*). Constrained Control Allocation: Three Moment Problem. *AIAA Journal of Guidance, Control and Dynamics* **17**(2), 330–336.

Durham, W. C. (1999*a*). Computationally efficient control allocation. *AIAA Journal of Guidance, Control and Dynamics* **24**(3), 519–524.

Durham, W. C. (1999*b*). Efficient, Near-Optimal Control Allocation. *AIAA Journal of Guidance, Control and Dynamics* **22**(2), 369–372.

Durham, W. C., J. G. Bolling and K. A. Bordignon (1996). Minimum drag control allocation. *AIAA Journal of Guidance, Control and Dynamics* **19**(1), 30–36.

Encarnação, P., A. Pascoal and M. Arcak (2000). Path following for autonomous marine craft. In: *Proc. of the 5th IFAC Conf. on Manoevering and Control of Marine Craft*. Aalborg, Denmark. pp. 117–122.

Encarnação, P. and A. Pascoal (2000). 3D path following for autonomous underwater vehicle. In: *Proc. of the 39th IEEE Conf. on Decision and Control*. Sydney, Australia. pp. 2977–2982.

Encarnação, P. and A. Pascoal (2001). Combined trajectory tracking and path following: An application to the coordinated control of autonomous marine craft. In: *Proc. of the 40th IEEE Conf. on Decision and Control*. Orlando, FL. pp. 964–969.

Faltinsen, O. M. (1990). *Sea Loads on Ships and Offshore Structures*. Cambridge University Press.

Fossen, T. I. (1991). Nonlinear Modelling and Control of Underwater Vehicles. PhD thesis. Dept. of Engineering Cybernetics, The Norwegian Institute of Technology.

Fossen, T. I. (2002). *Marine Control Systems: Guidance, Navigation and Control of Ships, Rigs and Underwater Vehicles*. Marine Cybernetics AS. Trondheim, Norway.

Fossen, T. I., A. Loria and A. Teel (2001). A Theorem for UGAS and ULES of (Passive) Nonautonomous Systems: Robust Control of Mechanical Systems and Ships. *Intl. Journal of Robust and Nonlinear Control* **11**, 95–108.

Fossen, T. I. and Å. Grøvlen (1998). Nonlinear output feedback control of dynamically positioned ships using vectorial observer backstepping. *IEEE Trans. on Control Systems Technology* **6**(1), 121–128.

Fossen, T. I. and J. P. Strand (1999). Passive nonlinear observer design for ships using Lyapunov methods: Experimental results with a supply vessel. *Automatica* **35**(1), 3–16.

Fossen, T. I. and J. P. Strand (2001). Nonlinear passive weather optimal positioning control (WOPC) system for ships and rigs: Experimental results. *Automatica* **37**(5), 701–715.

Fossen, T. I. and M. Blanke (2000). Nonlinear output feedback control of underwater vehicle propellers using feedback from estimated axial flow velocity. *IEEE J. of Oceanic Engineering* **25**(2), 241–255.

Fossen, T. I., S. I. Sagatun and A. J. Sørensen (1996). Identification of dynamically positioned ships. *Control Engineering Practice* **4**(3), 369–376.

Fung, P. T.-K. and M. J. Grimble (1983). Dynamic ship positioning using a self-tuning Kalman filter. *IEEE Trans. on Automatic Control* **28**(3), 339–349.

Gahinet, P., A. Nemirovski, A. J. Laub and M. Chilali (1995). *LMI Control Toolbox*. The Mathworks Inc.

Gillmer, T. C. and B. Johnson (1982). *Introduction to Naval Architecture*. Naval Institute Press. Annapolis, MD.

Godhavn, J.-M., T. I. Fossen and S. P. Berge (1997). Non-linear and adaptive backstepping designs for tracking control of ships. *Intl. Journal of Adaptive Control and Signal Processing* **12**, 649–670.

Greenberg, M. D. (1972). Nonlinear actuator disk theory. *Zeitschrift für Flugwissenschaften* **20**(3), 90–98.

Greenberg, M. D. and S. R. Powers (1970). Nonlinear actuator disk theory and flow field calculations, including nonuniform loading. Technical report. NASA Contractor Report, CR-1672.

Grimble, M. J., R. J. Patton and D. A. Wise (1980). The design of dynamic positioning control systems using stochastic optimal control theory. *Optimal Control Applications and Methods* **1**, 167–202.

Healey, A. J., S. M. Rock, S. Cody, D. Miles and J. P. Brown (1995). Toward an inproved understanding of thruster dynamics for underwater vehicles. *IEEE J. of Oceanic Engineering* **20**(4), 354–361.

Hindman, R. and J. Hauser (1996). Maneuver modified trajectory tracking. In: *Int. Symp. Mathematical Theory Networks and Systems*. St. Louis, MO, USA.

Janković, M., R. Sepulchre and P. V. Kokotović (1996). Constructive Lyapunov stabilization of nonlinear cascade systems. *IEEE Trans. on Automatic Control* **41**(12), 1723–1736.

Jenssen, N. A. (1981). Estimation and Control in Dynamic Positioning of Vessels. PhD thesis. Dept. of Engineering Cybernetics, Norwegian University of Science and Technology.

Johansen, T. A., T. I. Fossen and P. Tøndel (2002). Efficient optimal constrained control allocation via multi-parametric programming. *Submitted to AIAA J. of Guidance, Control and Dynamics*.

Johansen, T. A., T. I. Fossen and S. P. Berge (2003). Constrained nonlinear control allocation with singularity avoidance using sequential quadratic programming. *Submitted to IEEE Trans. on Control Systems Technology*.

Källström, C. G. and K. Theorén (1994). Dynamic compensation system. In: *Proc. of the 3rd IEEE Conf. on Control Applications (CCA'94)*. New York, NY. pp. 1093–1098.

Katebi, M. R., M. J. Grimble and Y. Zhang (1997). H_∞ robust control design for dynamic ship positioning. In: *IEE Proc. on Control Theory and Applications*. pp. 110–120.

Khalil, H. K. (1996). *Nonlinear Systems*. second ed.. Prentice-Hall.

Kosuge, K., M. Umetsu and K. Furuta (1989). Robust linearization and control of robot arm using acceleration feedback. In: *Proc. of the IEEE Int. Conf. On Control and Applications, ICCON '89*. pp. 161–165.

Krstić, M., I. Kanellakopoulos and P. Kokotović (1995). *Nonlinear and Adaptive Control Design*. John Wiley & Sons.

Lindegaard, K.-P. and T. I. Fossen (2001*a*). A model based wave filter for surface vessels using position, velocity and partial acceleration feedback. In: *Proc. of the 40th IEEE Conf. on Decision and Control*. Orlando, FL.

Lindegaard, K.-P. and T. I. Fossen (2001*b*). On global model based observer designs for surface vessels. In: *Proc. of the 5th IFAC Conf. On Control Applications in Marine Systems, CAMS2001*. Glasgow, UK.

Lindegaard, K.-P. and T. I. Fossen (2002). Increasing performance of dynamically positioned vessels by acceleration feedback: Experimental results. Submitted to Automatica, October 6 2002.

Lindegaard, K.-P. and T. I. Fossen (2003). Fuel efficient rudder and propeller control allocation for marine craft: Experiments with a model ship. *IEEE Trans. on Control Systems Technology*. To appear.

Lindegaard, K.-P., B. Vik and T. I. Fossen (2002). Experimental results with a simplified model based wave filter with inertial sensor feedback for surface vessels. In: *Proc. of the 10th Mediterranean Conference on Control & Automation*. Lisbon, Portugal.

Lindfors, I. (1993). Thrust allocation method for the dynamic positioning system. In: *Proc. of the 10th International Ship Control Systems Symposium (SCSS'93)*. Ottawa, Canada. pp. 3.93–3.106.

Loría, A. and E. Panteley (1999). A separation principle for a class of Euler-Lagrange systems. In: *New Directions in Nonlinear Observer Design* (H. Nijmeijer and T. I. Fossen, Eds.). pp. 229–247. Springer.

Loría, A., T. I. Fossen and E. Panteley (2000). A separation principle for dynamic positioning of ships: Theoretical and experimental results. *IEEE Trans. on Control Systems Technology* **8**(2), 332–343.

Luo, G. and G. N. Saridis (1985). L-Q design of PID controllers for robot arms. *IEEE J. of Robotics and Automation* **1**(3), 152–158.

Molland, A. F. and S. R. Turnock (1993). Wind tunnel investigation of the influence of propeller loading on ship rudder performance. *Trans. of RINA, the Royal Institution of Naval Architects* **135**, 105–120.

Molland, A. F. and S. R. Turnock (1994). Prediction of ship rudder-propeller interaction at low speeds and in four quadrants of operation. In: *Proc. of the Conference on Manouevring and Control of Marine Craft, MCMC'94.* pp. 319–333.

Molland, A. F. and S. R. Turnock (1996). A compact computational method for predicting forces on a rudder in a propeller slipstream. *Trans. of RINA, the Royal Institution of Naval Architects* **138**, 227–244.

Molland, A. F., S. R. Turnock and P. A. Wilson (1996). Performance of an enhanced rudder force prediction model in a ship manoeuvring simulator. In: *Proc. of the International Conference on Marine Simulation and Ship Manoeuvrability, MARSIM'96.* Copenhagen, Denmark. pp. 425–434.

Munk, M. M. (1922). Notes on propeller design - II: The distribution of thrust over a propeller blade. Technical report. NACA Technical Note No. 94. Accessed June 23 2003: http://naca.larc.nasa.gov/reports/1922/naca-tn-94/.

Nakamura, M., W. Koterayama, H. Kajiwara and T. Mitamura (1994). Application of a dynamic positioning system to a moored floating platform. In: *Proc. of the 4th International Offshore and Polar Engineering Conference.* The International Society of Offshore and Polar Engineers. Osaka, Japan. pp. 190–197.

Newman, J. N. (1974). Second-order, slowly-varying forces on vessels in irregular waves. In: *Proc. Int. Symp. Dynamics of Marine Vehicles and Structures in Waves.* pp. 182–186.

Newman, J. N. (1977). *Marine Hydrodynamics.* The MIT Press.

Nocedal, J. and S. J. Wright (1999). *Numerical Optimization.* Springer-Verlag. New York, NY.

Panteley, E. and A. Loria (1998). On global uniform asymptotic stability of nonlinear time-varying non-autonomous systems in cascade. *Systems & Control Letters* **33**(2), 131–138.

Pettersen, K. Y. and E. Lefeber (2001). Way-point tracking control of ships. In: *Proc. of the 40th IEEE Conf. on Decision and Control.* Orlando, FL. pp. 940–945.

Pinkster, J. A. and U. Nienhuis (1986). Dynamic positioning of large tankers at sea. In: *Proc. of the Offshore Technology Conference (OTC'86).* Houston, TX.

Prandtl, L. (1923). Applications of modern hydrodynamics to aeronautics. Technical report. NACA Report No. 116. Accessed June 23 2003: http://naca.larc.nasa.gov/reports/1923/naca-report-116/.

Price, W. G. and R. E. D. Bishop (1974). *Probalistic Theory of Ship Dynamics*. Chapman and Hall. London.

Reif, K., F. Sonnemann and R. Unbehauen (1999). Nonlinear state observation using H_∞-filtering Riccati design. *IEEE Trans. on Automatic Control* **44**(1), 203–208.

Robertsson, A. and R. Johansson (1998). Comments on "nonlinear output feedback control of dynamically positioned ships using vectorial observer backstepping". *IEEE Trans. on Control Systems Technology* **6**(3), 439–441.

Sælid, S., N. A. Jensen and J. G. Balchen (1983). Design and analysis of a dyanmic positioning system based on Kalman filtering and optimal control. *IEEE Trans. on Automatic Control* **28**(3), 331–339.

Sagatun, S. I. (1992). Modeling and Control of Underwater Vehicles: A Lagrangian Approach. PhD thesis. Dept. of Engineering Cybernetics, The Norwegian Institute of Technology.

Sagatun, S. I. and T. I. Fossen (1991). Lagrangian formulation of underwater vehicle's dynamics. In: *Proc. of the IEEE International Conference on Systems, Man and Cybernetics*. Charlottesville, VA.

Scherer, C. and S. Weiland (2000). Linear matrix inequalities in control. Lecture notes accessed June 23 2003: http://www.cs.ele.tue.nl/SWeiland/lmi.pdf.

Scherer, C., P. Gahinet and M. Chilali (1997). Multiobjective output-feedback control via LMI optimization. *IEEE Trans. on Automatic Control* **42**(7), 896–911.

Shouji, K., T. Ishiguro and S. Mizoguchi (1990). Hydrodynamic forces by propeller and rudder interaction at low speed. In: *Proceedings of the Intl. Conference on Marine Simulation and Ship Manoeuvrability, MARSIM & ICSM 90*. Tokyo, Japan. pp. 369–376.

Shuster, M. D. and S. D. Oh (1981). Three-axis attitude determination from vector observations. *AIAA Journal of Guidance and Control* **4**(1), 70–77.

Skjetne, R., T. I. Fossen and P. Kokotović (2003). Robust output maneuvering for a class of nonlinear systems. *Automatica*. Submitted May 7th, 2002, accepted May 15th, 2003.

Skjetne, Roger and Thor I. Fossen (2001). Nonlinear maneuvring and control of ships. In: *Proc. MTS/IEEE Oceans 2001*. Honolulu, Hawaii. pp. 1808–1815.

Sørdalen, O. J. (1997*a*). Full Scale Sea Trials with Optimal Thrust Allocation. In: *Proc. of the 4th IFAC Conf. on Manoeuvring and Control of Marine Craft (MCMC'97)*. Brijuni, Croatia. pp. 150–155.

Sørdalen, O. J. (1997*b*). Optimal thrust allocation for marine vessels. *Control Engineering Practice* **5**(9), 1223–1231.

Sørensen, A. J. and J. P. Strand (2000). Positioning of small-waterplane-area marine constructions with roll and pitch damping. *J. of Control Engineering Practice* **8**(2), 205–213.

Sørensen, A. J., J. P. Strand and T. I. Fossen (1999). Thruster assisted position mooring system for turret-anchored FPSOs. In: *Proc. of the 1999 IEEE Int. Conf. on Control Applications (CCA'99)*. Honolulu, Hawaii. pp. 1110–1117.

Sørensen, A. J., S. I. Sagatun and T. I. Fossen (1996). Design of a dynamic positioning system using model-based control. *J. of Control Engineering Practice* **4**(3), 359–368.

Strand, J. P. (1999). Nonlinear Position Control Systems Design for Marine Vessels. PhD thesis. Dept. of Eng. Cybernetics, Norwegian University of Science and Technology, Trondheim, Norway.

Strand, J. P., A.J. Sørensen and T. I. Fossen (1998). Design of automatic thruster assisted position mooring systems for ships. *Modeling, Identification and Control* **19**(2), 65–71.

Strand, J. P. and T. I. Fossen (1999). Nonlinear passive observer design for ships with adaptive wave filtering. In: *New Directions in Nonlinear Observer Design* (H. Nijmeijer and T. I. Fossen, Eds.). pp. 113–134. Springer-Verlag, London.

Studenny, J. and P. R. Bélanger (1984). Robot manipulator control using acceleration feedback. In: *Proc. of the 23rd IEEE Conf. on Decision and Control*. Las Vegas, NV.

Tannuri, E. A., C. P. Pesce and D. C. Donha (2001). Assisted dynamic positioning system for a FPSO based on minimization of a cost function. In: *Proc. of the 5th IFAC Conf. On Control Applications in Marine Systems, CAMS2001*. Glasgow, UK.

Terada, Y., H. Ojima and Y. Wada (1996). Development of an advanced joystick control system for ship maneuvring. In: *Proc. of the Japan-USA Symposium on Flexible Automation*. New York, NY. pp. 387–390.

Tsai, R. Y. (1987). A versatile camera calibration technique for high-accuracy 3D machine vision metrology using off-the-shelf TV cameras and lenses. *IEEE J. of Robotics and Automation* **3**(4), 323–344.

van Lammeren, W. P. A., J. D. van Manen and M. W. C. Oosterveld (1969). The Wageningen B-screw series. *Trans. on SNAME* **77**, 269–317.

Vik, B. and T. I. Fossen (2001). Nonlinear observer design for integration of GPS and inertial navigation systems. In: *Proc. of the 40th IEEE Conf. on Decision and Control*. Orlando, FL.

Whitcomb, L. L. and D. R. Yoerger (1999). Preliminary experiments in model-based thruster control for underwater vehicle positioning. *IEEE J. of Oceanic Engineering* **24**(4), 495–506.

White, F. M. (1999). *Fluid Mechanics*. fourth ed.. WCB McGraw-Hill.

Yoerger, D. R., J. G. Cooke and J.-J. E. Slotine (1990). The influence of thruster dynamics on underwater vehicle behavior and their incorporation into control system design. *IEEE J. of Oceanic Engineering*.

Zhang, R., Y. Chen, Z. Sun, F. Sun and X. Hu (2000). Path control of a surface ship in restricted waters using sliding mode. *IEEE Trans. on Control Systems Technology* **8**(4), 722–732.

Appendix A

Notation and Mathematical Results

This appendix is dedicated to establishing the notation used and various definitons, lemmas and theorems needed and referred to throughout the text.

A.1 Notation

For vectors $\mathbf{v} \in \mathbb{R}^n$ its Euclidean norm will be denoted $|\mathbf{v}|$. For matrices $\mathbf{A} \in \mathbb{R}^{m\times n}$ we use $\|\mathbf{A}\| = \sup_{|\mathbf{x}|=1} |\mathbf{A}\mathbf{x}| = [\lambda_{\max}(\mathbf{A}^T\mathbf{A})]^{1/2}$. A square matrix $\mathbf{A} \in \mathbb{R}^{n\times n}$ is said to be Hurwitz if its eigenvalues are in the open left-half plane, $\mathrm{Re}(\lambda_i(\mathbf{A})) < 0$ where $\lambda_i(\mathbf{A})$ is the i-th eigenvalue of $\mathbf{A}$. For a square, symmetric matrix $\mathbf{A} = \mathbf{A}^T \in \mathbb{R}^{n\times n}$, $\lambda_{\min}(\mathbf{A}) = \min_i \lambda_i(\mathbf{A})$ and $\lambda_{\max}(\mathbf{A}) = \max_i \lambda_i(\mathbf{A})$.

Let $\mathcal{L}_p$ be the set of all piecewise continuous functions $\mathbf{u} : [0,\infty) \to \mathbb{R}^n$ being p-integrable on $[0,\infty)$, that is $\int_0^\infty |\mathbf{u}(t)|^p < \infty$. The norm on $\mathcal{L}_p$ is

$$\|\mathbf{u}(t)\|_p = \left(\int_0^\infty |\mathbf{u}(t)|^p\right)^{\frac{1}{p}} \tag{A.1}$$

and in the limit $\|\mathbf{u}(t)\|_\infty = \sup_{t\geq 0} |\mathbf{u}(t)|$.

A dynamic system Σ described by

$$\Sigma : \begin{array}{l} \dot{\mathbf{x}} = \mathbf{f}(\mathbf{x},\mathbf{u}) \\ \mathbf{y} = \mathbf{h}(\mathbf{x},\mathbf{u}) \end{array} \tag{A.2}$$

exited by an external input $\mathbf{u}$ and with output $\mathbf{y}$ is represented by the operator $\mathbf{H}_{yu}$. The $\mathcal{L}_2$-induced norm $\|\mathbf{H}_{yu}\|_2$ is the ratio between the energy content of the system's output and input signals and is defined as

$$\|\mathbf{H}_{yu}\|_2 = \sup_{0<\|u\|_2<\infty} \frac{\|\mathbf{y}\|_2}{\|\mathbf{u}\|_2} \tag{A.3}$$

The induced $\mathcal{L}_2$-$\mathcal{L}_\infty$-norm, the "energy to peak" norm, is

$$\|\mathbf{H}_{yu}\|_{2\infty} = \sup_{0<\|u\|_2<\infty} \frac{\|\mathbf{y}\|_\infty}{\|\mathbf{u}\|_2} \tag{A.4}$$

If Σ is a linear system

$$\dot{\mathbf{x}} = \mathbf{A}\mathbf{x} + \mathbf{B}\mathbf{u} \tag{A.5}$$
$$\mathbf{y} = \mathbf{C}\mathbf{x} + \mathbf{D}\mathbf{u} \tag{A.6}$$

we let $\mathbf{H}_{yu}(s)$ describe the transfer matrix $\mathbf{H}_{yu}(s) = \mathbf{C}(s\mathbf{I}-\mathbf{A})^{-1}\mathbf{B}+\mathbf{D}$. Then, the $\mathcal{L}_2$-induced norm $\|\mathbf{H}_{yu}\|_2$ is equivalent to the $\mathcal{H}_\infty$-norm of $\mathbf{H}_{yu}(s)$, see Corollary A.2.

Let $\mathbf{y}$ be a sequence of N entries, hence $\mathbf{y} \in \mathbb{R}^N$. The empirical mean $\bar{y}$ and standard deviation s_y are defined as

$$\bar{y} = \frac{1}{N}\sum_{k=1}^{N} y_k \tag{A.7}$$

$$s_y = \left(\frac{1}{N-1}\sum_{k=1}^{N}(y_k - \bar{y})^2\right)^{\frac{1}{2}} \tag{A.8}$$

and the RMS-gain of $\mathbf{y}$ is defined as

$$\|\mathbf{y}\|_{RMS} = \left(\frac{1}{N}\sum_{k=1}^{N}|y_k|^2\right)^{\frac{1}{2}} \tag{A.9}$$

A.2 Lyapunov Stability

A continuous function $\alpha : \mathbb{R}_{\geq 0} \to \mathbb{R}_{\geq 0}$ is said to be of class $\mathcal{K}$ ($\alpha \in \mathcal{K}$) if it is strictly increasing and $\alpha(0) = 0$. If in addition $\alpha(s) \to \infty$ as $s \to \infty$ then $\alpha \in \mathcal{K}_\infty$. Consider the time-varying nonlinear system

$$\dot{\mathbf{x}} = \mathbf{f}(t, \mathbf{x}) + \mathbf{g}(t, \mathbf{x})\mathbf{w} \tag{A.10}$$

where $\mathbf{x} \in \mathbb{R}^n$ is the state and $\mathbf{w} : \mathbb{R}_{\geq 0} \to \mathbb{R}^q$ is a disturbance. The standard Lyapunov theorem on uniform global asymptotic stability (UGAS) and uniform global exponential stability (UGES) for the nominal system $\dot{\mathbf{x}} = \mathbf{f}(t, \mathbf{x})$ is characterized by the following theorem (Khalil 1996).

Theorem A.1 *Let $\mathbf{x} = 0$ be an equilibrium point of the unperturbed ($\mathbf{w} = 0$) system (A.10). Suppose there exists a continuously differentiable function $V : \mathbb{R}_{\geq 0} \times \mathbb{R}^n \to \mathbb{R}_{\geq 0}$ and class $\mathcal{K}_\infty$ functions $\alpha_1, \alpha_2, \alpha_3$ such that $\forall\ t \geq 0$, $\mathbf{x} \in \mathbb{R}^n$ the following holds*

$$a_1(|\mathbf{x}|) \leq V(t, \mathbf{x}) \leq \alpha_2(|\mathbf{x}|) \tag{A.11}$$

$$\frac{\partial V}{\partial t} + \frac{\partial V}{\partial \mathbf{x}}\mathbf{f}(t, \mathbf{x}) \leq -\alpha_3(|\mathbf{x}|) \tag{A.12}$$

Then $\mathbf{x} = 0$ *is UGAS. If* $\alpha_1(|\cdot|) = c_1|\cdot|^p$, $\alpha_2(|\cdot|) = c_2|\cdot|^p$ *and* $\alpha_3(|\cdot|) = c_3|\cdot|^p$ *for some positive* c_1, c_2, c_3 *and* p, *then* $\mathbf{x} = 0$ *is UGES.*

In proving stability of the proposed observer-feedback system we shall employ a slightly modified version of Theorem 3 from Panteley and Loria (1998).

Theorem A.2 *Consider the cascaded system*

$$\Sigma_1 \quad : \quad \dot{\mathbf{x}}_1 = \mathbf{f}_1(t, \mathbf{x}_1) + \mathbf{g}(t, \mathbf{x}) \tag{A.13}$$
$$\Sigma_1 \quad : \quad \dot{\mathbf{x}}_2 = \mathbf{f}_2(t, \mathbf{x}_2) \tag{A.14}$$

where $\mathbf{g}(t, x) = 0$ *whenever* $\mathbf{x}_2 = 0$ *and the origin* $\mathbf{x}_1 = 0$ *of* $\dot{\mathbf{x}}_1 = \mathbf{f}_1(t, \mathbf{x}_1)$ *is UGAS. If the origin* $\mathbf{x}_2 = 0$ *of (A.14) is UGAS and the assumptions A1 and A2 below are satisfied, then the cascaded system (A.13)-(A.14) is UGAS.*

A1 The function $\mathbf{g}(t, \mathbf{x})$ satisfies the following bound

$$|\mathbf{g}(t, \mathbf{x})| \leq \theta_1(|\mathbf{x}_2|) + \theta_2(|\mathbf{x}_2|)|\mathbf{x}_1| \tag{A.15}$$

where $\theta_i : \mathbb{R}_{\geq 0} \to \mathbb{R}_{\geq 0}$ for $i = 1, 2$ are continuous and $\theta_i(0) = 0$.

A2 The nominal part of Σ_1, $\dot{\mathbf{x}}_1 = \mathbf{f}_1(t, \mathbf{x}_1)$, is UGAS with a Lyapunov function $V(t, \mathbf{x}_1)$ satisfying the following: There exist functions α_1,α_2,$\alpha_3 \in \mathcal{K}_\infty$ and an $\alpha_4 \in \mathcal{K}$ such that

$$\alpha_1(|\mathbf{x}_1|) \leq V(t, \mathbf{x}_1) \leq \alpha_2(|\mathbf{x}_1|) \tag{A.16}$$
$$\frac{\partial V}{\partial t} + \frac{\partial V}{\partial \mathbf{x}_1} f_1(t, \mathbf{x}_1) \leq -\alpha_3(|\mathbf{x}_1|) \tag{A.17}$$
$$\left|\frac{\partial V}{\partial \mathbf{x}_1}\right| \leq \alpha_4(|\mathbf{x}_1|) \tag{A.18}$$

where $\alpha_4(|\mathbf{x}_1|)$ is such that there exist constants $b_*, k_* > 0$ and $\kappa \geq 0$ satisfying

$$\alpha_4(|\mathbf{x}_1|)|\mathbf{x}_1| \leq b_* \alpha_1(|\mathbf{x}_1|) \quad \forall\, |\mathbf{x}_1| \geq \kappa \tag{A.19}$$
$$k_* \alpha_4(|\mathbf{x}_1|)|\mathbf{x}_1| \leq \alpha_3(|\mathbf{x}_1|) \quad \forall \mathbf{x}_1 \in \mathbb{R}^n \tag{A.20}$$

Remark A.1 *The formulation of Theorem A.2 differs from Theorem 3 in Panteley and Loria (1998) in two ways. First, in Panteley and Loria (1998) the authors used* $\mathbf{g}(t, \mathbf{x})\mathbf{x}_2$ *instead of the more general form* $\mathbf{g}(t, \mathbf{x})$ *to point out its* $\mathbf{x}_2$*-dependency. Secondly, inspired by Janković* et al. *(1996) we have used the growth condition (A.15) instead of* $|\mathbf{g}(t, \mathbf{x})| \leq \theta(|\mathbf{x}_2|)|\mathbf{x}_1|$. *These modifications are straightforward, however, in the sense that they do not interfere with the original result.*

A.3 Dissipativity

The definitions and theorems in this section is taken from Boyd *et al.* (1994) and Scherer and Weiland (2000).

Consider a continuous, time-invariant dynamical system Σ described by (A.2) where $\mathbf{x}$ takes on values in a state-space $\mathbb{X} \subset \mathbb{R}^n$, $\mathbf{u}$ is the input $\mathbf{u} \in \mathbb{U} \subset \mathbb{R}^m$ and $\mathbf{y}$ the output $\mathbf{y} \in \mathbb{Y} \subset \mathbb{R}^p$. Let $\mathbf{x}(t_0) = \mathbf{x}(0)$ be the initial state and assume that the state $\mathbf{x}$ and output $\mathbf{y}$ are uniquely defined for all $t \geq t_0$ and that they depend on $\mathbf{u}$ in a causal way. The system Σ generates outputs $\mathbf{y}$ from the inputs $\mathbf{u}$ and the initial condition $\mathbf{x}(t_0)$. Let

$$s : \mathbb{U} \times \mathbb{Y} \to \mathbb{R} \tag{A.21}$$

be a mapping that is locally integrable in t. The mapping s will be referred to as the supply function or the supply rate.

Definition A.1 (Dissipativity) *The system Σ with supply rate s is said to be* dissipative *if there exists a non-negative function $V : \mathbb{X} \to \mathbb{R}$ such that*

$$V(\mathbf{x}(t_0)) + \int_{t_0}^{t_1} s(\mathbf{u}(t), \mathbf{y}(t))dt \geq V(\mathbf{x}(t_1)) \tag{A.22}$$

for all $t_0 \leq t_1$ and all trajectories $(\mathbf{u}, \mathbf{x}, \mathbf{y})$ which satisfy (A.2).

Definition A.2 (Passivity) *A system Σ that is dissipative with respect to the supply rate $s = \mathbf{u}^T\mathbf{y} + \mathbf{y}^T\mathbf{u}$ is said to be* passive.

A.3.1 Linear Dissipative Systems with Quadratic Supply Rates

Consider a linear system on compact form

$$\begin{bmatrix} \dot{\mathbf{x}} \\ \mathbf{y} \end{bmatrix} = \begin{bmatrix} \mathbf{A} & \mathbf{B} \\ \mathbf{C} & \mathbf{D} \end{bmatrix} \begin{bmatrix} \mathbf{x} \\ \mathbf{u} \end{bmatrix} \tag{A.23}$$

with state space $\mathbb{X} \in \mathbb{R}^n$, input space $\mathbb{U} \in \mathbb{R}^m$ and output space $\mathbb{Y} \in \mathbb{R}^p$. The general quadratic supply function $s : \mathbb{U} \times \mathbb{Y} \to \mathbb{R}$ is defined by

$$s(\mathbf{u}, \mathbf{y}) = \begin{bmatrix} \mathbf{y} \\ \mathbf{u} \end{bmatrix}^T \mathbf{Q} \begin{bmatrix} \mathbf{y} \\ \mathbf{u} \end{bmatrix} \tag{A.24}$$

where

$$\mathbf{Q} = \begin{bmatrix} \mathbf{Q}_{yy} & \mathbf{Q}_{yu} \\ \mathbf{Q}_{yu}^T & \mathbf{Q}_{uu} \end{bmatrix} \tag{A.25}$$

is symmetric.

Theorem A.3 *Suppose the system (A.23) is controllable and let the supply rate s be defined by (A.24). Then, the following statements are equivalent:*

1. (Σ, s) *is dissipative.*
2. (Σ, s) *admits a quadratic storage function* $V(\mathbf{x}) = \mathbf{x}^T\mathbf{P}\mathbf{x}$ *with* $\mathbf{P} = \mathbf{P}^T \geq 0$.
3. *There exists a* $\mathbf{P} = \mathbf{P}^T \geq 0$ *such that*

$$\mathbf{F} = -\begin{bmatrix} \mathbf{PA} + \mathbf{A}^T\mathbf{P} & \mathbf{PB} \\ \mathbf{B}^T\mathbf{P} & \mathbf{0} \end{bmatrix} + \begin{bmatrix} \mathbf{C} & \mathbf{D} \\ \mathbf{0} & \mathbf{I} \end{bmatrix}^T \begin{bmatrix} \mathbf{Q}_{yy} & \mathbf{Q}_{yu} \\ \mathbf{Q}_{yu}^T & \mathbf{Q}_{uu} \end{bmatrix} \begin{bmatrix} \mathbf{C} & \mathbf{D} \\ \mathbf{0} & \mathbf{I} \end{bmatrix} \geq 0 \tag{A.26}$$

4. *For all* $\omega \in \mathbb{R}$ *with* $\det(j\omega I - \mathbf{A}) \neq 0$, *the transfer function* $\mathbf{H}(j\omega) = \mathbf{C}(j\omega\mathbf{I} - \mathbf{A})^{-1}\mathbf{B} + \mathbf{D}$ *satisfies*

$$\begin{bmatrix} \mathbf{H}(j\omega) \\ \mathbf{I} \end{bmatrix}^* \begin{bmatrix} \mathbf{Q}_{yy} & \mathbf{Q}_{yu} \\ \mathbf{Q}_{yu}^T & \mathbf{Q}_{uu} \end{bmatrix} \begin{bmatrix} \mathbf{H}(j\omega) \\ \mathbf{I} \end{bmatrix} \geq 0 \tag{A.27}$$

Moreover, if one of the above statements holds, then $V(\mathbf{x}) = \mathbf{x}^T\mathbf{P}\mathbf{x}$ *is a quadratic storage function if and only if* $\mathbf{P} \geq 0$ *and* $\mathbf{F}(\mathbf{P}) \geq 0$

We are primarily interested in "passive" systems, and for those systems the supply rate is defined to be $s = \mathbf{y}^T\mathbf{u} + \mathbf{u}^T\mathbf{y}$, thus

$$\mathbf{Q} = \begin{bmatrix} \mathbf{Q}_{yy} & \mathbf{Q}_{yu} \\ \mathbf{Q}_{yu}^T & \mathbf{Q}_{uu} \end{bmatrix} = \begin{bmatrix} \mathbf{0} & \mathbf{I} \\ \mathbf{I} & \mathbf{0} \end{bmatrix} \tag{A.28}$$

and applying the previous theorem to this type of systems yields the celebrated "positive real lemma" or the "Kalman-Yakubovich-Popov lemma".

Corollary A.1 (Kalman-Yakubovich-Popov) *Suppose* Σ *described by (A.23) is controllable and has transfer function* $\mathbf{H}(j\omega) = \mathbf{C}(j\omega\mathbf{I} - \mathbf{A})^{-1}\mathbf{B} + \mathbf{D}$ *and let* $s = \mathbf{y}^T\mathbf{u} + \mathbf{u}^T\mathbf{y}$ *be a supply rate. The following statements are equivalent:*

1. (Σ, s) *is passive.*
2. *The system of linear matrix inequalities*

$$\mathbf{P} = \mathbf{P}^T \geq 0 \tag{A.29}$$

$$\begin{bmatrix} \mathbf{PA} + \mathbf{A}^T\mathbf{P} & \mathbf{PB} - \mathbf{C}^T \\ \mathbf{B}^T\mathbf{P} - \mathbf{C} & -\mathbf{D} - \mathbf{D}^T \end{bmatrix} \leq 0 \tag{A.30}$$

   is feasable.

3. *For all* $\omega \in \mathbb{R}$ *with* $\det(j\omega\mathbf{I} - \mathbf{A}) \neq 0$, $\mathbf{H}(j\omega) + \mathbf{H}(j\omega)^* \geq 0$.

Moreover, $V(\mathbf{x}) = \mathbf{x}^T\mathbf{P}\mathbf{x}$ *is a quadratic storage function if and only if* $\mathbf{P}$ *satisfies the above system of LMIs.*

Remark 3 *It is also worth noting that for strictly proper systems,* $\mathbf{D} = \mathbf{0}$, *the cross-term* $-\mathbf{PB} + \mathbf{C}^T$ *has got to be zero, i.e.*

$$\mathbf{PB} = \mathbf{C}^T \tag{A.31}$$

Corollary A.2 (Bounded Real) *Suppose Σ described by (A.23) is controllable and has transfer function $\mathbf{H}(j\omega) = \mathbf{C}(j\omega\mathbf{I} - \mathbf{A})^{-1}\mathbf{B} + \mathbf{D}$ and let $s = \gamma^2\mathbf{u}^T\mathbf{u} - \mathbf{y}^T\mathbf{y}$ be its supply rate. Then the following statements are equivalent:*

1. *(Σ, s) is dissipassive.*
2. *The system of linear matrix inequalities*

$$\mathbf{P} = \mathbf{P}^T \geq 0 \tag{A.32}$$

$$\begin{bmatrix} \mathbf{P}\mathbf{A} + \mathbf{A}^T\mathbf{P} + \mathbf{C}^T\mathbf{C} & \mathbf{P}\mathbf{B} + \mathbf{C}^T\mathbf{D} \\ \mathbf{B}^T\mathbf{P} + \mathbf{D}^T\mathbf{C} & \mathbf{D}^T\mathbf{D} - \gamma^2\mathbf{I} \end{bmatrix} \leq 0 \tag{A.33}$$

   is feasable.

3. *For all $\mathbf{u} \in \mathcal{L}_2$*

$$\sup_{\mathbf{u}\in\mathcal{L}_2} \frac{\|\mathbf{y}\|_2}{\|\mathbf{u}\|_2} < \gamma \tag{A.34}$$

4. *The $\mathcal{H}_\infty$-norm of $\mathbf{H}(\omega)$ is bounded by γ*

$$\|\mathbf{H}\|_\infty = \sup_{\omega\in\mathbb{R}} \sigma_{\max}(\mathbf{H}(\omega)) < \gamma \tag{A.35}$$

5. *For all $\omega \in \mathbb{R}$ with $\det(j\omega\mathbf{I} - \mathbf{A}) \neq 0$, $\mathbf{H}(j\omega)^*\mathbf{H}(j\omega) \leq \gamma^2\mathbf{I}$.*

Moreover, $V(\mathbf{x}) = \mathbf{x}^T\mathbf{P}\mathbf{x}$ is a quadratic storage function if and only if $\mathbf{P}$ satisfies the above system of LMIs.

Appendix B

Detailed Proofs

B.1 Proof of Theorem 5.4

The proof is outlined as follows: First we show that under observer-feedback the resulting closed loop system can be written on a cascaded form where Σ_1 is the state-feedback system perturbed by the observer-error dynamics Σ_2. From Theorem 5.1 we already have an LFC for the nominal Σ_1, and consequently if the perturbation $\mathbf{g}(t, \mathbf{x})$ satisfies the bounds given by Theorem A.2, the proof will be complete.

Part 1:

To repeat, the proposed observer-feedback controller for (5.14)-(5.15) was given by (5.71)-(5.72):

$$\begin{aligned} \dot{\boldsymbol{\xi}} &= \hat{\boldsymbol{\eta}}_e \\ \dot{\mathbf{a}}_f &= \mathbf{A}_f \mathbf{a}_f + \mathbf{B}_f \boldsymbol{\Pi} \hat{\dot{\boldsymbol{\nu}}}_e \\ \hat{\boldsymbol{\tau}} &= -\mathbf{K}_i \mathbf{R}^T(\hat{\psi}) \boldsymbol{\xi} - \mathbf{K}_p \mathbf{R}^T(\hat{\psi}) \hat{\boldsymbol{\eta}}_e - \mathbf{K}_d \hat{\boldsymbol{\nu}}_e - \mathbf{K}_a \mathbf{a}_f + \hat{\boldsymbol{\tau}}_{\text{rff}} \end{aligned}$$

where

$$\hat{\boldsymbol{\tau}}_{\text{rff}} = \mathbf{D}_L \mathbf{R}^T(\hat{\psi}_e) \boldsymbol{\nu}_d + \mathbf{M} \left((\hat{r} - r_d) \, \mathbf{S}^T \mathbf{R}^T(\hat{\psi}_e) \boldsymbol{\nu}_d + \mathbf{R}^T(\hat{\psi}_e) \dot{\boldsymbol{\nu}}_d \right)$$

The rotations involved are rewritten as

$$\mathbf{R}^T(\hat{\psi}) = \mathbf{R}^T(\psi - \tilde{\psi}) = \mathbf{R}^T(\psi) + \mathbf{R}^T(\psi) \left(\mathbf{R}(\tilde{\psi}) - \mathbf{I} \right) \tag{B.1}$$

$$\mathbf{R}^T(\hat{\psi}_e) = \mathbf{R}^T(\psi - \tilde{\psi} - \psi_d) = \mathbf{R}^T(\psi_e) + \mathbf{R}^T(\psi_e) \left(\mathbf{R}(\tilde{\psi}) - \mathbf{I} \right) \tag{B.2}$$

We are now ready to study the error variables $\hat{\boldsymbol{\eta}}_e$, $\hat{\boldsymbol{\nu}}_e$, and $\hat{\dot{\boldsymbol{\nu}}}_e$ further. The objective is to rewrite each one as the errors between the actual state and reference trajectory, the very same error variables used in the original state-feedback controller. To save space, subscripts denote function arguments for the rotations, that

is $\mathbf{R}_a \stackrel{\triangle}{=} \mathbf{R}(a)$. For position we get

$$\hat{\boldsymbol{\eta}}_e = \hat{\boldsymbol{\eta}} - \boldsymbol{\eta}_d = \boldsymbol{\eta} - \tilde{\boldsymbol{\eta}} - \boldsymbol{\eta}_d = \boldsymbol{\eta}_e - \tilde{\boldsymbol{\eta}} \tag{B.3}$$

and for the velocity deviation

$$\begin{aligned} \hat{\boldsymbol{\nu}}_e &= \hat{\boldsymbol{\nu}} - \mathbf{R}_{\hat{\psi}_e}^T \boldsymbol{\nu}_d \\ &= \boldsymbol{\nu}_e - \tilde{\boldsymbol{\nu}} - \mathbf{R}_{\psi_e}^T \left(\mathbf{R}_{\tilde{\psi}} - \mathbf{I}\right) \boldsymbol{\nu}_d \end{aligned} \tag{B.4}$$

and finally for the acceleration we get

$$\begin{aligned} \hat{\dot{\boldsymbol{\nu}}}_e &= \hat{\dot{\boldsymbol{\nu}}} - \left(\hat{r}_e \mathbf{S}^T \mathbf{R}_{\hat{\psi}_e}^T \boldsymbol{\nu}_d + \mathbf{R}_{\hat{\psi}_e}^T \dot{\boldsymbol{\nu}}_d\right) \\ &= \dot{\boldsymbol{\nu}} - \tilde{\dot{\boldsymbol{\nu}}} - \left((r - r_d - \tilde{r})\, \mathbf{S}^T \left(\mathbf{R}_{\psi_e}^T + \mathbf{R}_{\psi_e}^T (\mathbf{R}_{\tilde{\psi}} - \mathbf{I})\right) \boldsymbol{\nu}_d\right) \\ &\quad - \left(\mathbf{R}_{\psi_e}^T + \mathbf{R}_{\psi_e}^T (\mathbf{R}_{\tilde{\psi}} - \mathbf{I})\right) \dot{\boldsymbol{\nu}}_d \\ &= \underbrace{\dot{\boldsymbol{\nu}} - \left(r_e \mathbf{S}^T \mathbf{R}_{\psi_e}^T \boldsymbol{\nu}_d + \mathbf{R}_{\psi_e}^T \dot{\boldsymbol{\nu}}_d\right)}_{\dot{\boldsymbol{\nu}}_e} - \tilde{\dot{\boldsymbol{\nu}}} \\ &\quad - \left(r_e \mathbf{S}^T \mathbf{R}_{\psi_e}^T (\mathbf{R}_{\tilde{\psi}} - \mathbf{I}) \boldsymbol{\nu}_d - \tilde{r} \mathbf{S}^T \mathbf{R}_{\psi_e}^T \mathbf{R}_{\tilde{\psi}} \boldsymbol{\nu}_d + \mathbf{R}_{\psi_e}^T (\mathbf{R}_{\tilde{\psi}} - \mathbf{I}) \dot{\boldsymbol{\nu}}_d\right) \end{aligned} \tag{B.5}$$

Consequently, for the feedback part $\hat{\boldsymbol{\tau}}_{\text{fb}}$ of $\hat{\boldsymbol{\tau}} = \hat{\boldsymbol{\tau}}_{\text{fb}} + \hat{\boldsymbol{\tau}}_{\text{rff}}$ we get

$$\begin{aligned} \hat{\boldsymbol{\tau}}_{\text{fb}} &= -\mathbf{K}_i \mathbf{R}_{\hat{\psi}}^T \boldsymbol{\xi} - \mathbf{K}_p \mathbf{R}_{\hat{\psi}}^T \hat{\boldsymbol{\eta}}_e - \mathbf{K}_d \tilde{\boldsymbol{\nu}}_e - \mathbf{K}_a \mathbf{a}_f \\ &= -\mathbf{K}_i \left(\mathbf{R}_{\psi}^T + \mathbf{R}_{\psi}^T (\mathbf{R}_{\tilde{\psi}} - \mathbf{I})\right) \boldsymbol{\xi} - \mathbf{K}_p \left(\mathbf{R}_{\psi}^T + \mathbf{R}_{\psi}^T (\mathbf{R}_{\tilde{\psi}} - \mathbf{I})\right) (\boldsymbol{\eta}_e - \tilde{\boldsymbol{\eta}}) \\ &\quad - \mathbf{K}_d \left(\boldsymbol{\nu}_e - \tilde{\boldsymbol{\nu}} - \mathbf{R}_{\psi_e}^T (\mathbf{R}_{\tilde{\psi}} - \mathbf{I}) \boldsymbol{\nu}_d\right) - \mathbf{K}_a \mathbf{a}_f \\ &= -\mathbf{K}_i \mathbf{R}_{\psi}^T \boldsymbol{\xi} - \mathbf{K}_p \mathbf{R}_{\psi}^T \boldsymbol{\eta}_e - \mathbf{K}_d \boldsymbol{\nu}_e - \mathbf{K}_a \mathbf{a}_f \\ &\quad - \mathbf{K}_i \mathbf{R}_{\psi}^T (\mathbf{R}_{\tilde{\psi}} - \mathbf{I}) \boldsymbol{\xi} - \mathbf{K}_p \mathbf{R}_{\psi}^T (\mathbf{R}_{\tilde{\psi}} - \mathbf{I}) \boldsymbol{\eta}_e + \mathbf{K}_p \left(\mathbf{R}_{\psi}^T + \mathbf{R}_{\psi}^T (\mathbf{R}_{\tilde{\psi}} - \mathbf{I})\right) \tilde{\boldsymbol{\eta}} \\ &\quad + \mathbf{K}_d \left(\tilde{\boldsymbol{\nu}} + \mathbf{R}_{\psi_e}^T (\mathbf{R}_{\tilde{\psi}} - \mathbf{I}) \boldsymbol{\nu}_d\right) \\ &= \boldsymbol{\tau}_{\text{fb}} - \mathbf{K}_i \mathbf{R}_{\psi}^T (\mathbf{R}_{\tilde{\psi}} - \mathbf{I}) \boldsymbol{\xi} - \mathbf{K}_p \mathbf{R}_{\psi}^T (\mathbf{R}_{\tilde{\psi}} - \mathbf{I}) \boldsymbol{\eta}_e \\ &\quad + \mathbf{K}_p \mathbf{R}_{\psi}^T \mathbf{R}_{\tilde{\psi}} \tilde{\boldsymbol{\eta}} + \mathbf{K}_d \left(\tilde{\boldsymbol{\nu}} + \mathbf{R}_{\psi_e}^T (\mathbf{R}_{\tilde{\psi}} - \mathbf{I}) \boldsymbol{\nu}_d\right) \end{aligned} \tag{B.6}$$

The reference feed-forward $\hat{\boldsymbol{\tau}}_{\text{rff}} = \hat{\boldsymbol{\tau}}_{\text{vff}} + \hat{\boldsymbol{\tau}}_{\text{aff}}$ enters both $\hat{\boldsymbol{\tau}}$ and the $\mathbf{a}_f$-dynamics. The velocity and acceleration parts, denoted $\hat{\boldsymbol{\tau}}_{\text{vff}}$ and $\hat{\boldsymbol{\tau}}_{\text{aff}}$ respectively, are

$$\begin{aligned} \hat{\boldsymbol{\tau}}_{\text{vff}} &= \mathbf{D}_L \mathbf{R}_{\hat{\psi}_e}^T \boldsymbol{\nu}_d \\ &= \mathbf{D}_L \mathbf{R}_{\psi_e}^T \boldsymbol{\nu}_d + \mathbf{D}_L \mathbf{R}_{\psi_e}^T (\mathbf{R}_{\tilde{\psi}} - \mathbf{I}) \boldsymbol{\nu}_d \\ &= \boldsymbol{\tau}_{\text{vff}} + \mathbf{D}_L \mathbf{R}_{\psi_e}^T (\mathbf{R}_{\tilde{\psi}} - \mathbf{I}) \boldsymbol{\nu}_d \end{aligned} \tag{B.7}$$

$$
\begin{aligned}
\hat{\boldsymbol{\tau}}_{\text{aff}} &= \mathbf{M}\left((\hat{r}-r_d)\,\mathbf{S}^T\mathbf{R}_{\tilde{\psi}_e}^T\boldsymbol{\nu}_d+\mathbf{R}_{\tilde{\psi}_e}^T\dot{\boldsymbol{\nu}}_d\right)\\
&= \mathbf{M}\Big[r_e\mathbf{S}^T\left(\mathbf{R}_{\psi_e}^T+\mathbf{R}_{\psi_e}^T(\mathbf{R}_{\tilde{\psi}}-\mathbf{I})\right)\boldsymbol{\nu}_d-\tilde{r}\mathbf{S}^T\left(\mathbf{R}_{\psi_e}^T+\mathbf{R}_{\psi_e}^T(\mathbf{R}_{\tilde{\psi}}-\mathbf{I})\right)\boldsymbol{\nu}_d\\
&\quad+\left(\mathbf{R}_{\psi_e}^T+\mathbf{R}_{\psi_e}^T(\mathbf{R}_{\tilde{\psi}}-\mathbf{I})\right)\dot{\boldsymbol{\nu}}_d\Big]\\
&= \underbrace{\mathbf{M}\left(r_e\mathbf{S}^T\mathbf{R}_{\psi_e}^T\boldsymbol{\nu}_d+\mathbf{R}_{\psi_e}^T\dot{\boldsymbol{\nu}}_d\right)}_{\boldsymbol{\tau}_{\text{aff}}}\\
&\quad+\mathbf{M}\left(r_e\mathbf{S}^T\mathbf{R}_{\psi_e}^T(\mathbf{R}_{\tilde{\psi}}-\mathbf{I})\boldsymbol{\nu}_d-\tilde{r}\mathbf{S}^T\mathbf{R}_{\psi_e}^T\mathbf{R}_{\tilde{\psi}}\boldsymbol{\nu}_d+\mathbf{R}_{\psi_e}^T(\mathbf{R}_{\tilde{\psi}}-\mathbf{I})\dot{\boldsymbol{\nu}}_d\right) \quad \text{(B.8)}
\end{aligned}
$$

and for the $\mathbf{a}_f$-dynamics

$$
\begin{aligned}
\dot{\mathbf{a}}_f &= \mathbf{A}_f\mathbf{a}_f+\mathbf{B}_f\boldsymbol{\Pi}\hat{\dot{\boldsymbol{\nu}}}_e\\
&= \mathbf{A}_f\mathbf{a}_f+\mathbf{B}_f\boldsymbol{\Pi}\left(\dot{\boldsymbol{\nu}}_e-\tilde{\dot{\boldsymbol{\nu}}}-\Big[r_e\mathbf{S}^T\mathbf{R}_{\psi_e}^T(\mathbf{R}_{\tilde{\psi}}-\mathbf{I})\boldsymbol{\nu}_d\right.\\
&\quad\left.-\tilde{r}\mathbf{S}^T\mathbf{R}_{\psi_e}^T\mathbf{R}_{\tilde{\psi}}\boldsymbol{\nu}_d+\mathbf{R}_{\psi_e}^T(\mathbf{R}_{\tilde{\psi}}-\mathbf{I})\dot{\boldsymbol{\nu}}_d\Big]\right)\\
&= \mathbf{A}_f\mathbf{a}_f+\mathbf{B}_f\boldsymbol{\Pi}\dot{\boldsymbol{\nu}}_e \quad \text{(B.9)}\\
&\quad-\mathbf{B}_f\boldsymbol{\Pi}\left(\tilde{\dot{\boldsymbol{\nu}}}+\Big[r_e\mathbf{S}^T\mathbf{R}_{\psi_e}^T(\mathbf{R}_{\tilde{\psi}}-\mathbf{I})\boldsymbol{\nu}_d-\tilde{r}\mathbf{S}^T\mathbf{R}_{\psi_e}^T\mathbf{R}_{\tilde{\psi}}\boldsymbol{\nu}_d+\mathbf{R}_{\psi_e}^T(\mathbf{R}_{\tilde{\psi}}-\mathbf{I})\dot{\boldsymbol{\nu}}_d\Big]\right)
\end{aligned}
$$

Summing it all up, the applied output feedback controller can be expressed as:

$$
\begin{aligned}
\dot{\boldsymbol{\xi}} &= \boldsymbol{\eta}_e-\tilde{\boldsymbol{\eta}}\\
\dot{\mathbf{a}}_f &= \mathbf{A}_f\mathbf{a}_f+\mathbf{B}_f\boldsymbol{\Pi}\dot{\nu}_e\\
&\quad-\mathbf{B}_f\boldsymbol{\Pi}\left(\tilde{\dot{\boldsymbol{\nu}}}+r_e\mathbf{S}^T\mathbf{R}_{\psi_e}^T(\mathbf{R}_{\tilde{\psi}}-\mathbf{I})\boldsymbol{\nu}_d-\tilde{r}\mathbf{S}^T\mathbf{R}_{\psi_e}^T\mathbf{R}_{\tilde{\psi}}\boldsymbol{\nu}_d+\mathbf{R}_{\psi_e}^T(\mathbf{R}_{\tilde{\psi}}-\mathbf{I})\dot{\boldsymbol{\nu}}_d\right)\\
\hat{\boldsymbol{\tau}} &= \boldsymbol{\tau}-\mathbf{K}_i\mathbf{R}_{\tilde{\psi}}^T(\mathbf{R}_{\tilde{\psi}}-\mathbf{I})\boldsymbol{\xi}-\mathbf{K}_p\mathbf{R}_{\tilde{\psi}}^T(\mathbf{R}_{\tilde{\psi}}-\mathbf{I})\boldsymbol{\eta}_e+\mathbf{K}_p\mathbf{R}_{\tilde{\psi}}^T\mathbf{R}_{\tilde{\psi}}\tilde{\boldsymbol{\eta}}+\mathbf{K}_d\tilde{\boldsymbol{\nu}}\\
&\quad+\left(\mathbf{D}_L+\mathbf{K}_d\right)\mathbf{R}_{\psi_e}^T(\mathbf{R}_{\tilde{\psi}}-\mathbf{I})\boldsymbol{\nu}_d\\
&\quad+\mathbf{M}\left(r_e\mathbf{S}^T\mathbf{R}_{\psi_e}^T(\mathbf{R}_{\tilde{\psi}}-\mathbf{I})\boldsymbol{\nu}_d-\tilde{r}\mathbf{S}^T\mathbf{R}_{\psi_e}^T\mathbf{R}_{\tilde{\psi}}\boldsymbol{\nu}_d+\mathbf{R}_{\psi_e}^T(\mathbf{R}_{\tilde{\psi}}-\mathbf{I})\dot{\boldsymbol{\nu}}_d\right) \quad \text{(B.10)}
\end{aligned}
$$

The errors made by introducing observer estimates in our dynamic feedback controller can thus be seen as a perturbation connecting the vessel dynamics controlled by state-feedback with the observer errors. More specifically,

$$
\dot{\mathbf{x}}_e=\mathbf{T}^T(\psi)\mathbf{A}_c\mathbf{T}(\psi)\mathbf{x}_e+\mathbf{E}\mathbf{w}+\mathbf{g}(\mathbf{x}_e,\mathbf{x}_o,\boldsymbol{\eta}_d,\boldsymbol{\nu}_d,\dot{\boldsymbol{\nu}}_d) \quad \text{(B.11)}
$$

where $\mathbf{T}(\psi)$ is defined in (5.48) and $\mathbf{A}_c$ is given by (5.50). The perturbation reads

$$
\mathbf{g}(\mathbf{x}_e,\tilde{\mathbf{x}}_o,\boldsymbol{\eta}_d,\boldsymbol{\nu}_d,\dot{\boldsymbol{\nu}}_d)=\begin{bmatrix}\mathbf{g}_1^T & \mathbf{0} & \mathbf{g}_3^T & \mathbf{g}_4^T\end{bmatrix}^T \quad \text{(B.12)}
$$

where again the individual terms are

$$\begin{aligned}
\mathbf{g}_1 &= -\tilde{\boldsymbol{\eta}} && \text{(B.13)}\\
\mathbf{g}_3 &= -\mathbf{M}^{-1}\left[\mathbf{K}_i\mathbf{R}_{\tilde{\psi}}^T(\mathbf{R}_{\tilde{\psi}}-\mathbf{I})\boldsymbol{\xi}+\mathbf{K}_p\mathbf{R}_{\tilde{\psi}}^T(\mathbf{R}_{\tilde{\psi}}-\mathbf{I})\boldsymbol{\eta}_e-\mathbf{K}_p\mathbf{R}_{\tilde{\psi}}^T\mathbf{R}_{\tilde{\psi}}\tilde{\boldsymbol{\eta}}-\mathbf{K}_d\tilde{\boldsymbol{\nu}}\right]\\
&\quad +\mathbf{M}^{-1}\left(\mathbf{D}_L+\mathbf{K}_d\right)\mathbf{R}_{\psi_e}^T(\mathbf{R}_{\tilde{\psi}}-\mathbf{I})\boldsymbol{\nu}_d\\
&\quad +r_e\mathbf{S}^T\mathbf{R}_{\psi_e}^T(\mathbf{R}_{\tilde{\psi}}-\mathbf{I})\boldsymbol{\nu}_d-\tilde{r}\mathbf{S}^T\mathbf{R}_{\psi_e}^T\mathbf{R}_{\tilde{\psi}}\boldsymbol{\nu}_d+\mathbf{R}_{\psi_e}^T(\mathbf{R}_{\tilde{\psi}}-\mathbf{I})\dot{\nu}_d && \text{(B.14)}\\
\mathbf{g}_4 &= -\mathbf{B}_f\boldsymbol{\Pi}\left(\tilde{\boldsymbol{\nu}}+r_e\mathbf{S}^T\mathbf{R}_{\psi_e}^T(\mathbf{R}_{\tilde{\psi}}-\mathbf{I})\boldsymbol{\nu}_d-\tilde{r}\mathbf{S}^T\mathbf{R}_{\psi_e}^T\mathbf{R}_{\tilde{\psi}}\boldsymbol{\nu}_d\right)\\
&\quad -\mathbf{B}_f\boldsymbol{\Pi}\mathbf{R}_{\psi_e}^T(\mathbf{R}_{\tilde{\psi}}-\mathbf{I})\dot{\boldsymbol{\nu}}_d && \text{(B.15)}
\end{aligned}$$

Let $\mathbf{w}=\mathbf{0}$, and use the transformation $\mathbf{z}=\mathbf{T}(\psi)\mathbf{x}_e$. Then the output-feedback system can be regarded as the cascade

$$\begin{aligned}
\Sigma_1: \quad \dot{\mathbf{z}} &= \left(\mathbf{A}_c+\dot{\mathbf{T}}\mathbf{T}^T\right)\mathbf{z}+\mathbf{g}_z(t,\mathbf{z},\tilde{\mathbf{x}}_o)\\
\Sigma_2: \quad \dot{\tilde{\mathbf{x}}}_o &= \mathbf{f}_2(t,\tilde{\mathbf{x}}_o)
\end{aligned} \qquad \text{(B.16)}$$

where the Σ_2-system represents the observer error-dynamics. Theorem 5.1 asserts the existence of a quadratic LFC for $\dot{\mathbf{z}}=(\mathbf{A}_c+\dot{\mathbf{T}}\mathbf{T}^T)\mathbf{z}$ ensuring exponential stability of the nominal system when $|r(t)|\leq r_{\max}$. It is easy to see that this particular $V=\mathbf{z}^T\mathbf{P}\mathbf{z}$ provides us with $\alpha_1(s)=\lambda_{\min}(\mathbf{P})s^2$, $\alpha_2(s)=\lambda_{\max}(\mathbf{P})s^2$, $\alpha_3(s)=\lambda_{\min}(\mathbf{Q})s^2$ and $\alpha_4(s)=2\lambda_{\max}(\mathbf{P})s$ for some $\mathbf{Q}=\mathbf{Q}^T>0$ such that $\mathbf{P}\mathbf{A}_c+\mathbf{A}_c^T\mathbf{P}\leq-\mathbf{Q}$.

Part 2:

From Theorem 5.1 we already know that Σ_1 is exponentially stable for bounded $r_{\max}$ whenever $\mathbf{g}=\mathbf{0}$ and $\mathbf{w}=\mathbf{0}$ by employing a quadratic LFC. Hence, if it can be shown that the perturbation $\mathbf{g}$ is bounded linearly in the state vector $|\mathbf{x}_e|$ Theorem A.2 proves exponential stability of $\mathbf{x}_e=\mathbf{0}$.

Since the trajectory is assumed to be sufficiently smooth, there are bounds

$$\begin{aligned}
|\boldsymbol{\nu}_d| &\leq c_{\nu_d} \quad \forall t\geq t_0 && \text{(B.17)}\\
|\dot{\boldsymbol{\nu}}_d| &\leq c_{\dot{\nu}_d} \quad \forall t\geq t_0 && \text{(B.18)}
\end{aligned}$$

The observer perturbation term $\mathbf{g}$ is now shown to be linearly bounded in $\mathbf{x}_e$ and $\mathbf{x}_o$ such that Theorem A.2 can be employed. Using $m_m=\lambda_{\min}(\mathbf{M})$, the perturbation is bounded by

$$\begin{aligned}
|\mathbf{g}| &\leq |\tilde{\boldsymbol{\eta}}|+m_m^{-1}\left(2\left\|\mathbf{K}_i\right\||\tilde{\psi}|\,|\boldsymbol{\xi}|+2\left\|\mathbf{K}_p\right\||\tilde{\psi}|\,|\boldsymbol{\eta}_e|+\left\|\mathbf{K}_p\right\||\tilde{\boldsymbol{\eta}}|+\left\|\mathbf{K}_d\right\||\tilde{\boldsymbol{\nu}}|\right)\\
&\quad +2m_m^{-1}\left\|\mathbf{D}_L+\mathbf{K}_d\right\||\tilde{\psi}|\,|\boldsymbol{\nu}_d|+2\,|r_e|\,|\tilde{\psi}|\,|\boldsymbol{\nu}_d|+|\tilde{r}|\,|\boldsymbol{\nu}_d|+2|\tilde{\psi}|\,|\dot{\boldsymbol{\nu}}_d|\\
&\quad +\left\|\mathbf{B}_f\boldsymbol{\Pi}\right\|\left(\left|\tilde{\boldsymbol{\nu}}\right|+2\,|r_e|\,|\tilde{\psi}|\,|\boldsymbol{\nu}_d|+|\tilde{r}|\,|\boldsymbol{\nu}_d|+2|\tilde{\psi}|\,|\dot{\boldsymbol{\nu}}_d|\right)\\
&\leq \left(2m_m^{-1}\left(\left\|\mathbf{K}_i\right\|+\left\|\mathbf{K}_p\right\|\right)|\tilde{\psi}|+2|\tilde{\psi}|\,|\boldsymbol{\nu}_d|+2\left\|\mathbf{B}_f\boldsymbol{\Pi}\right\||\tilde{\psi}|\,|\boldsymbol{\nu}_d|\right)|\mathbf{x}_e|\\
&\quad +\left(1+m_m^{-1}\left(\left\|\mathbf{K}_p\right\|+\left\|\mathbf{K}_d\right\|+2\left\|\mathbf{D}_L+\mathbf{K}_d\right\|c_{\nu_d}\right)\right)|\tilde{\mathbf{x}}_o|\\
&\quad +\left(c_\nu+2c_{\dot{\nu}_d}+\left\|\mathbf{B}_f\boldsymbol{\Pi}\right\|\left(1+c_{\nu_d}+2c_{\dot{\nu}_d}\right)\right)|\tilde{\mathbf{x}}_o|\\
&\leq \theta_1(|\tilde{\mathbf{x}}_o|)+\theta_2(|\tilde{\mathbf{x}}_o|)\,|\mathbf{x}_e| && \text{(B.19)}
\end{aligned}$$

where $\theta_i : \mathbb{R}_{\geq 0} \to \mathbb{R}_{\geq 0}$, $i = 1, 2$, are linear functions

$$\begin{aligned} \theta_1(s) &= \left\{1 + m_m^{-1}\left(\|\mathbf{K}_p\| + \|\mathbf{K}_d\| + 2\,\|\mathbf{D}_L + \mathbf{K}_d\|\, c_{\nu_d}\right)\right. \\ &\quad \left. + \|\mathbf{B}_f\mathbf{\Pi}\|\left(1 + c_{\nu_d} + 2c_{\dot{\nu}_d}\right) + c_\nu + 2c_{\dot{\nu}_d}\right\} s \qquad \text{(B.20)} \\ \theta_2(s) &= 2\left(m_m^{-1}\left(\|\mathbf{K}_i\| + \|\mathbf{K}_p\|\right) + c_{\nu_d} + \|\mathbf{B}_f\mathbf{\Pi}\|\, c_{\nu_d}\right) s \qquad \text{(B.21)} \end{aligned}$$

satisfying the continuity requirement. This completes the proof.

B.2 Proof of Theorem 5.5

First, backstepping will be applied in two consecutive steps. This provides a coordinate transformation into the $\mathbf{z}$-error variables, a control law parameterized in $\mathbf{z}$, and a diagonal, quadratic Lyapunov function also in $\mathbf{z}$. Finally, the control law will be rewritten in terms of $\boldsymbol{\xi}$, $\mathbf{e}$, and $\boldsymbol{\nu}_e$.

B.2.1 Backstepping

Step 1: Define the first error variable as

$$\mathbf{z}_1 = \begin{bmatrix} \boldsymbol{\xi} \\ \mathbf{e} \end{bmatrix} \qquad \text{(B.22)}$$

We can write the time derivative of $\mathbf{z}_1$ as follows

$$\dot{\mathbf{z}}_1 = \begin{bmatrix} -\mathbf{\Lambda} & \mathbf{C}_{11}^T\mathbf{R}(\psi_d) \\ \mathbf{0} & -\dot{\psi}_d\mathbf{S} \end{bmatrix}\mathbf{z}_1 + \begin{bmatrix} \mathbf{0} & \mathbf{0} \\ \mathbf{0} & \mathbf{R}(\psi_e) \end{bmatrix}\begin{bmatrix} \mathbf{0} \\ \mathbf{I} \end{bmatrix}\boldsymbol{\nu} - \begin{bmatrix} \mathbf{0} \\ \mathbf{I} \end{bmatrix}\boldsymbol{\nu}_d \qquad \text{(B.23)}$$

or more compactly

$$\dot{\mathbf{z}}_1 = \mathbf{A}_1(\psi_d, \dot{\psi}_d)\mathbf{z}_1 + \mathbf{R}_0(\psi_e)\mathbf{\Pi}^T\boldsymbol{\nu}_e \qquad \text{(B.24)}$$

with $\mathbf{R}_0(\psi_e) = \mathrm{Diag}(\mathbf{0}, \mathbf{R}(\psi_e))$ and

$$\mathbf{A}_1(\dot{\psi}_d) = \begin{bmatrix} -\mathbf{\Lambda} & \mathbf{C}_{11}^T\mathbf{R}(\psi_d) \\ \mathbf{0} & -\dot{\psi}_d\mathbf{S} \end{bmatrix} \quad , \quad \mathbf{\Pi} = \begin{bmatrix} \mathbf{0} & \mathbf{I} \end{bmatrix} \qquad \text{(B.25)}$$

Using $\boldsymbol{\nu}_e$ as the virtual control, the desired control that avoids unnecessary cancellation of skew-symmetric terms is

$$\begin{aligned} \boldsymbol{\alpha}_1 &= -\mathbf{R}^T(\psi_e)\mathbf{\Delta}_2^{-1}\mathbf{R}^T(\psi_d)\mathbf{C}_{11}\mathbf{\Delta}_1\xi - \mathbf{C}_{12}\mathbf{R}^T(\psi_e)\mathbf{e} \qquad \text{(B.26)} \\ &= -\mathbf{C}_1(\psi, \psi_d)\mathbf{z}_1 \qquad \text{(B.27)} \end{aligned}$$

where

$$\mathbf{C}_1(\psi, \psi_d) = \begin{bmatrix} \mathbf{R}^T(\psi_e)\mathbf{\Delta}_2^{-1}\mathbf{R}^T(\psi_d)\mathbf{C}_{11}\mathbf{\Delta}_1 & \mathbf{C}_{12}\mathbf{R}^T(\psi_e) \end{bmatrix} \qquad \text{(B.28)}$$

such that the error-variable $\mathbf{z}_2 = \boldsymbol{\nu}_e - \boldsymbol{\alpha}_1$ becomes

$$\mathbf{z}_2 = \boldsymbol{\nu}_e + \mathbf{C}_1(\psi, \psi_d)\mathbf{z}_1 \qquad \text{(B.29)}$$

The $\mathbf{z}_1$-dynamics can be written as

$$\dot{\mathbf{z}}_1 = \Big(\mathbf{S}_1(\dot{\psi}_d) + \mathbf{A}_1(\psi, \psi_d)\Big)\, \mathbf{z}_1 + \mathbf{R}_0(\psi_e)\mathbf{\Pi}^T \mathbf{z}_2 \tag{B.30}$$

where

$$\mathbf{S}_1(\psi_d, \dot{\psi}_d) = \begin{bmatrix} \mathbf{0} & \mathbf{C}_{11}^T \mathbf{R}(\psi_d) \\ -\mathbf{\Delta}_2^{-1}\mathbf{R}^T(\psi_d)\mathbf{C}_{11}\mathbf{\Delta}_1 & -\dot{\psi}_d \mathbf{S} \end{bmatrix} \tag{B.31}$$

$$\mathbf{A}_1(\psi, \psi_d) = \begin{bmatrix} -\mathbf{\Lambda} & \mathbf{0} \\ \mathbf{0} & -\mathbf{R}(\psi_e)\mathbf{C}_{12}\mathbf{R}^T(\psi_e) \end{bmatrix} \tag{B.32}$$

Observe that the dimension of $\mathbf{z}_2$ is lower than the dimension of $\mathbf{z}_1$ due to the augmented integrator $\boldsymbol{\xi}$.

A1 Assume $\mathbf{\Delta}_2 = \mathbf{\Delta}_2^T > 0$ commutes with $\mathbf{R}(\alpha)$. Then,

$$\mathbf{\Delta}_2 \mathbf{R}(\psi_e)\mathbf{\Delta}_2^{-1}\mathbf{R}^T(\psi_e) = \mathbf{I} \tag{B.33}$$

$$\mathbf{S}^T\mathbf{\Delta}_2 + \mathbf{\Delta}_2\mathbf{S} = \mathbf{0} \tag{B.34}$$

Employ the Lyapunov function $V_1 = \frac{1}{2}\boldsymbol{\xi}^T\mathbf{\Delta}_1\xi + \frac{1}{2}\mathbf{e}^T\mathbf{\Delta}_2\mathbf{e} = \frac{1}{2}\mathbf{z}_1^T\mathbf{P}_1\mathbf{z}_1$ where $\mathbf{P}_1 = \mathrm{Diag}(\mathbf{\Delta}_1, \mathbf{\Delta}_2)$. Its time derivative $\dot{V}_1$ is

$$\begin{aligned} \dot{V}_1 &= \dot{\mathbf{z}}_1^T\mathbf{P}_1\mathbf{z}_1 + \mathbf{z}_1\mathbf{P}_1\dot{\mathbf{z}}_1 \\ &= \mathbf{z}_1^T\left(\mathbf{P}_1\mathbf{A}_1 + \mathbf{A}_1^T\mathbf{P}_1\right)\mathbf{z}_1 + 2\mathbf{z}_1^T\mathbf{P}_1\mathbf{R}_0(\psi_e)\mathbf{\Pi}^T\mathbf{z}_2 \end{aligned} \tag{B.35}$$

because by assumption $\mathbf{\Delta}_2$ commutes with $\mathbf{R}$ such that $\mathbf{P}_1\mathbf{S}_1 + \mathbf{S}_1^T\mathbf{P}_1 = \mathbf{0}$. Written out,

$$\mathbf{P}_1\mathbf{S}_1 + \mathbf{S}_1^T\mathbf{P}_1 = \begin{bmatrix} \mathbf{0} & \mathbf{0} \\ \mathbf{0} & -\dot{\psi}_d\left(\mathbf{\Delta}_2\mathbf{S} + \mathbf{S}^T\mathbf{\Delta}_2\right) \end{bmatrix} = \mathbf{0} \tag{B.36}$$

Consequently,

$$\dot{V}_1 = -\mathbf{z}_1^T\mathbf{R}_1(\psi_e)\mathbf{Q}_1\mathbf{R}_1^T(\psi_e)\mathbf{z}_1 + \mathbf{z}_2^T\mathbf{\Pi}\mathbf{R}_0^T(\psi_e)\mathbf{P}_1\mathbf{z}_1 + \mathbf{z}_1^T\mathbf{P}_1\mathbf{R}_0(\psi_e)\mathbf{\Pi}^T\mathbf{z}_2 \tag{B.37}$$

where

$$\mathbf{Q}_1 = \begin{bmatrix} -\mathbf{\Delta}_1\mathbf{\Lambda} - \mathbf{\Lambda}^T\mathbf{\Delta}_1 & \mathbf{0} \\ \mathbf{0} & \mathbf{\Delta}_2\mathbf{C}_{12} + \mathbf{C}_{12}^T\mathbf{\Delta}_2 \end{bmatrix} \tag{B.38}$$

can be rendered positive definite by proper selections of $\mathbf{\Delta}_1$ and $\mathbf{\Delta}_2$ whenever $-\mathbf{\Lambda}$ is Hurwitz and $\mathbf{C}_{12}$ is positive. The conditions supplied by Theorem 5.5 ensure that $\mathbf{Q}_1$ is positive definite.

The commutation assumption on $\mathbf{\Delta}_2$ implies that $\mathbf{C}_1$ can be written as

$$\mathbf{C}_1(\psi, \psi_d) = \begin{bmatrix} \mathbf{\Delta}_2^{-1}\mathbf{R}^T(\psi)\mathbf{C}_{11}\mathbf{\Delta}_1 & \mathbf{C}_{12}\mathbf{R}^T(\psi_e) \end{bmatrix} \tag{B.39}$$

Step 2: The objective here is as follows: Do not cancel well-behaving terms such as Coriolis and dissipative terms (damping) while deriving an exponentially

stabilizing controller $\boldsymbol{\tau}$. This motivates using some kind of energy-based Lyapunov function

$$V_2 = V_1 + \frac{1}{2}\mathbf{z}_2^T\mathbf{M}\mathbf{z}_2 \tag{B.40}$$

and consequently, the sought $\mathbf{z}_2$-dynamics should read

$$\begin{aligned}\dot{\mathbf{z}}_2 &= -\mathbf{M}^{-1}\boldsymbol{\Pi}\mathbf{R}_0^T(\psi_e)\mathbf{P}_1\mathbf{z}_1 - \mathbf{M}^{-1}\left(\mathbf{C}(\boldsymbol{\nu}) + \mathbf{D}(\boldsymbol{\nu}) + \mathbf{C}_2\right)\mathbf{z}_2 \\ &= -\mathbf{M}^{-1}\boldsymbol{\Delta}_2\mathbf{R}^T(\psi_e)\mathbf{e} - \mathbf{M}^{-1}\left(\mathbf{C}(\boldsymbol{\nu}) + \mathbf{D}(\boldsymbol{\nu}) + \mathbf{C}_2\right)\mathbf{z}_2 \end{aligned} \tag{B.41}$$

because the derivative of V_2 along the trajectories of $(\mathbf{z}_1, \mathbf{z}_2)$ becomes

$$\begin{aligned}\dot{V}_2 &= \dot{V}_1 + \mathbf{z}_2^T\mathbf{M}\dot{\mathbf{z}}_2 + \dot{\mathbf{z}}_2^T\mathbf{M}\mathbf{z}_2 \\ &= -\mathbf{z}_1^T\mathbf{R}_1(\psi_e)\mathbf{Q}_1\mathbf{R}_1^T(\psi_e)\mathbf{z}_1 + \mathbf{z}_2^T\boldsymbol{\Pi}\mathbf{R}_0^T(\psi_e)\mathbf{P}_1\mathbf{z}_1 + \mathbf{z}_1^T\mathbf{P}_1\mathbf{R}_0(\psi_e)\boldsymbol{\Pi}^T\mathbf{z}_2 \\ &\quad -\mathbf{z}_2^T\left(\mathbf{M}^{-1}\boldsymbol{\Pi}\mathbf{R}_0^T(\psi_e)\mathbf{P}_1\mathbf{z}_1 + \mathbf{M}^{-1}\left(\mathbf{C}(\boldsymbol{\nu}) + \mathbf{D}(\boldsymbol{\nu}) + \mathbf{C}_2\right)\mathbf{z}_2\right) \\ &\quad -\mathbf{z}_2^T\left(\mathbf{C}^T(\boldsymbol{\nu}) + \mathbf{D}^T(\boldsymbol{\nu}) + \mathbf{C}_2^T\right)\mathbf{z}_2 - \mathbf{z}_1^T\left(\mathbf{P}_1\mathbf{R}_0(\psi_e)\boldsymbol{\Pi}^T\right)\mathbf{z}_2 \\ &= -\mathbf{z}_1^T\mathbf{R}_1(\psi_e)\mathbf{Q}_1\mathbf{R}_1^T(\psi_e)\mathbf{z}_1 - \mathbf{z}_2^T\left(\mathbf{D}(\boldsymbol{\nu}) + \mathbf{D}^T(\boldsymbol{\nu}) + \mathbf{C}_2 + \mathbf{C}_2^T\right)\mathbf{z}_2 \quad \text{(B.42)} \\ &< 0 \quad \forall \mathbf{z}_1, \mathbf{z}_2 \neq \mathbf{0} \quad \text{(B.43)}\end{aligned}$$

The actual $\mathbf{z}_2$-dynamics is

$$\begin{aligned}\dot{\mathbf{z}}_2 &= \underbrace{\dot{\boldsymbol{\nu}} - \frac{d}{dt}\left(\mathbf{R}^T(\psi_e)\boldsymbol{\nu}_d\right)}_{\dot{\boldsymbol{\nu}}_e} + \dot{\mathbf{C}}_1(\psi, \psi_d)\mathbf{z}_1 + \mathbf{C}_1(\psi, \psi_d)\dot{\mathbf{z}}_1 \\ &= \mathbf{M}^{-1}\left(\boldsymbol{\tau} - \left(\mathbf{C}(\boldsymbol{\nu}) + \mathbf{D}(\boldsymbol{\nu})\right)\boldsymbol{\nu}\right) + \frac{d}{dt}\left(\mathbf{C}_1(\psi, \psi_d)\mathbf{z}_1 - \mathbf{R}^T(\psi_e)\boldsymbol{\nu}_d\right) \end{aligned} \tag{B.44}$$

which means that in order to obtain the desired $\mathbf{z}_2$-dynamics, we should apply the following thrust $\boldsymbol{\tau}$

$$\begin{aligned}\boldsymbol{\tau} &= \left(\mathbf{C}(\boldsymbol{\nu}) + \mathbf{D}(\boldsymbol{\nu})\right)\boldsymbol{\alpha}_1 - \boldsymbol{\Delta}_2\mathbf{R}^T(\psi_e)\mathbf{e} - \mathbf{C}_2\mathbf{z}_2 \\ &\quad -\mathbf{M}\frac{d}{dt}\left(\mathbf{C}_1(\psi, \psi_d)\mathbf{z}_1\right) + \boldsymbol{\tau}_{\text{rff}} \quad \text{(B.45)} \\ \boldsymbol{\tau}_{\text{rff}} &= \left(\mathbf{C}(\boldsymbol{\nu}) + \mathbf{D}(\boldsymbol{\nu})\right)\mathbf{R}^T(\psi_e)\boldsymbol{\nu}_d + \mathbf{M}\frac{d}{dt}\left(\mathbf{R}^T(\psi_e)\boldsymbol{\nu}_d\right) \quad \text{(B.46)}\end{aligned}$$

because by the definition of $\mathbf{z}_2$

$$\boldsymbol{\alpha}_1 + \mathbf{R}^T(\psi_e)\boldsymbol{\nu}_d - \boldsymbol{\nu} = \boldsymbol{\alpha}_1 - \boldsymbol{\nu}_e = -\mathbf{z}_2 \tag{B.47}$$

and this means that cancellation of the nonlinear $\mathbf{C}(\boldsymbol{\nu}) + \mathbf{D}(\boldsymbol{\nu})$ has been avoided by using $\mathbf{z}_1$ and $\boldsymbol{\tau}_{\text{rff}}$.

Summary Closed Loop

The resulting closed loop can now rewritten as $\mathbf{z} = \left[\mathbf{z}_1^T, \mathbf{z}_2^T\right]^T$

$$\dot{\mathbf{z}} = \mathbf{A}_c(\boldsymbol{\nu}, \psi, \psi_d)\mathbf{z} \tag{B.48}$$

where the closed loop matrix $\mathbf{A}_c(\mathbf{z})$ can be decomposed into a negative block diagonal matrix $\mathbf{A}_z(\boldsymbol{\nu}, \psi, \psi_d)$ and the "skew-symmetric" $\mathbf{S}_z(\boldsymbol{\nu}, \psi, \psi_d)$ as defined below

$$\mathbf{A}_c(\boldsymbol{\nu}, \psi, \psi_d, \dot{\psi}_d) = \mathbf{A}_z(\boldsymbol{\nu}, \psi, \psi_d) + \mathbf{S}_z(\boldsymbol{\nu}, \psi, \psi_d, \dot{\psi}_d) \tag{B.49}$$

$$\mathbf{A}_z(\cdot) = \begin{bmatrix} -\boldsymbol{\Lambda} & \mathbf{0} & \mathbf{0} \\ \mathbf{0} & -\mathbf{R}_{\psi_e}\mathbf{C}_{12}\mathbf{R}_{\psi_e}^T & \mathbf{0} \\ \mathbf{0} & \mathbf{0} & -\mathbf{M}^{-1}\left(\mathbf{D}(\boldsymbol{\nu}) + \mathbf{C}_2\right) \end{bmatrix} \tag{B.50}$$

$$\mathbf{S}_z(\cdot) = \begin{bmatrix} \mathbf{0} & \mathbf{C}_{11}^T\mathbf{R}_{\psi_d} & \mathbf{0} \\ -\boldsymbol{\Delta}_2^{-1}\mathbf{R}_{\psi_d}^T\mathbf{C}_{11}\boldsymbol{\Delta}_1 & -\dot{\psi}_d\mathbf{S} & \mathbf{R}_{\psi_e} \\ \mathbf{0} & -\mathbf{M}^{-1}\boldsymbol{\Delta}_2\mathbf{R}_{\psi_e}^T & -\mathbf{M}^{-1}\mathbf{C}(\boldsymbol{\nu}) \end{bmatrix} \tag{B.51}$$

Indeed, $\mathbf{S}_z(\boldsymbol{\nu}, \psi, \psi_d)$ itself is not skew-symmetric, but when employing the above constructed Lyapunov function $\mathbf{V}_2 = \mathbf{z}^T\mathbf{P}\mathbf{z}$ with $\mathbf{P} = \mathrm{Diag}(\boldsymbol{\Delta}_1, \boldsymbol{\Delta}_2, \mathbf{M})$ it is easy to verify that $\mathbf{P}\mathbf{S}_z + \mathbf{S}_z^T\mathbf{P} = \mathbf{0}$ and $\dot{V}_2 < 0$ for all $\mathbf{z} \neq \mathbf{0}$.

B.2.2 Rewriting (B.45)

We now study each individual term in (B.45). In the forthcoming it will be used that $\mathbf{C}_{11}\boldsymbol{\Delta}_1$ and $\mathbf{C}_{11}\boldsymbol{\Delta}_1\boldsymbol{\Lambda}$ "commute" with $\mathbf{R}$, more specifically

$$\mathbf{R}(\psi)\mathbf{C}_{11}\boldsymbol{\Delta}_1 = \mathbf{C}_{11}\boldsymbol{\Delta}_1\mathbf{R}_{\mathbf{C}_{11}}(\psi) \tag{B.52}$$

$$\mathbf{R}(\psi)\mathbf{C}_{11}\boldsymbol{\Delta}_1\boldsymbol{\Lambda} = \mathbf{C}_{11}\boldsymbol{\Delta}_1\boldsymbol{\Lambda}\mathbf{R}_{\mathbf{C}_{11}}(\psi) \tag{B.53}$$

where

$$\mathbf{R}_{\mathbf{C}_{11}}(\psi) = \mathbf{C}_{11}^T\mathbf{R}(\psi)\mathbf{C}_{11} \tag{B.54}$$

Denote $\mathbf{N}(\boldsymbol{\nu}) = \mathbf{C}(\boldsymbol{\nu}) + \mathbf{D}(\boldsymbol{\nu})$. Hence,

$$\begin{aligned} \mathbf{N}(\boldsymbol{\nu})\boldsymbol{\alpha}_1 &= -\mathbf{N}(\boldsymbol{\nu})\mathbf{C}_1(\psi, \psi_d)\mathbf{z}_1 \\ &= -\mathbf{N}(\boldsymbol{\nu})\left(\boldsymbol{\Delta}_2^{-1}\mathbf{R}^T(\psi)\mathbf{C}_{11}\boldsymbol{\Delta}_1\boldsymbol{\xi} + \mathbf{C}_{12}\mathbf{R}^T(\psi_e)\mathbf{e}\right) \\ &= -\mathbf{N}(\boldsymbol{\nu})\left(\boldsymbol{\Delta}_2^{-1}\mathbf{C}_{11}\boldsymbol{\Delta}_1\mathbf{R}_{\mathbf{C}_{11}}^T(\psi)\boldsymbol{\xi} + \mathbf{C}_{12}\mathbf{R}^T(\psi_e)\mathbf{e}\right) \end{aligned} \tag{B.55}$$

$$\mathbf{C}_2\mathbf{z}_2 = \mathbf{C}_2\left(\boldsymbol{\nu}_e + \boldsymbol{\Delta}_2^{-1}\mathbf{C}_{11}\boldsymbol{\Delta}_1\mathbf{R}_{\mathbf{C}_{11}}^T(\psi)\boldsymbol{\xi} + \mathbf{C}_{12}\mathbf{R}^T(\psi_e)\mathbf{e}\right) \tag{B.56}$$

$$\begin{aligned} \dot{\mathbf{C}}_1\mathbf{z}_1 &= \begin{bmatrix} \dot{\psi}\boldsymbol{\Delta}_2^{-1}\mathbf{S}^T\mathbf{R}^T(\psi)\mathbf{C}_{11}\boldsymbol{\Delta}_1 & \mathbf{C}_{12}\dot{\psi}_e\mathbf{S}^T\mathbf{R}^T(\psi_e) \end{bmatrix}\mathbf{z}_1 \\ &= \dot{\psi}\boldsymbol{\Delta}_2^{-1}\mathbf{S}^T\mathbf{C}_{11}\boldsymbol{\Delta}_1\mathbf{R}_{\mathbf{C}_{11}}^T(\psi)\boldsymbol{\xi} + \mathbf{C}_{12}\dot{\psi}_e\mathbf{S}^T\mathbf{R}^T(\psi_e)\mathbf{e} \end{aligned} \tag{B.57}$$

$$\begin{aligned} \mathbf{C}_1\dot{\mathbf{z}}_1 &= \big(-\boldsymbol{\Delta}_2^{-1}\mathbf{R}^T(\psi)\mathbf{C}_{11}\boldsymbol{\Delta}_1\boldsymbol{\Lambda} - \mathbf{C}_{12}\mathbf{R}^T(\psi_e)\boldsymbol{\Delta}_2^{-1}\mathbf{R}^T(\psi_d)\mathbf{C}_{11}\boldsymbol{\Delta}_1\,\boldsymbol{\xi} \\ &\quad + \mathbf{C}_{12}\boldsymbol{\Delta}_2^{-1}\mathbf{R}^T(\psi)\mathbf{C}_{11}\boldsymbol{\Delta}_1\big)\boldsymbol{\xi} \\ &\quad + \left(\boldsymbol{\Delta}_2^{-1}\mathbf{R}^T(\psi)\mathbf{C}_{11}\boldsymbol{\Delta}_1\mathbf{C}_{11}^T\mathbf{R}(\psi_d) + \mathbf{C}_{12}\mathbf{C}_{12}\mathbf{R}^T(\psi_e)\,\mathbf{e}\right. \\ &\quad \left. -\mathbf{C}_{12}\left(\dot{\psi}_d\mathbf{R}^T(\psi_e)\mathbf{S} + \mathbf{C}_{12}\mathbf{R}^T(\psi_e)\right)\right)\mathbf{e} \\ &\quad + \mathbf{C}_{12}\boldsymbol{\nu}_e \\ &= -\boldsymbol{\Delta}_2^{-1}\mathbf{C}_{11}\boldsymbol{\Delta}_1\boldsymbol{\Lambda}\mathbf{R}_{\mathbf{C}_{11}}(\psi)\boldsymbol{\xi} + \mathbf{C}_{12}\boldsymbol{\nu}_e \\ &\quad + \left(\boldsymbol{\Delta}_2^{-1}\mathbf{R}^T(\psi)\mathbf{C}_{11}\boldsymbol{\Delta}_1\mathbf{C}_{11}^T\mathbf{R}(\psi) - \dot{\psi}_d\mathbf{C}_{12}\mathbf{S}\right)\mathbf{R}^T(\psi_e)\mathbf{e} \end{aligned} \tag{B.58}$$

Collecting terms we get

$$\begin{aligned}\boldsymbol{\tau} &= -\big(\mathbf{N}(\boldsymbol{\nu})\boldsymbol{\Delta}_2^{-1}\mathbf{C}_{11}\boldsymbol{\Delta}_1 + \mathbf{C}_2\boldsymbol{\Delta}_2^{-1}\mathbf{C}_{11}\boldsymbol{\Delta}_1 - \mathbf{M}\boldsymbol{\Delta}_2^{-1}\mathbf{C}_{11}\boldsymbol{\Delta}_1\boldsymbol{\Lambda} \\ &\quad +\dot{\psi}\mathbf{M}\boldsymbol{\Delta}_2^{-1}\mathbf{S}^T\mathbf{C}_{11}\boldsymbol{\Delta}_1\big)\,\mathbf{R}_{\mathbf{C}_{11}}(\psi)\boldsymbol{\xi} \\ &\quad -\big(\mathbf{N}(\boldsymbol{\nu})\mathbf{C}_{12} + \mathbf{C}_2\mathbf{C}_{12} + \boldsymbol{\Delta}_2 + \mathbf{M}\boldsymbol{\Delta}_2^{-1}\mathbf{R}^T(\psi)\mathbf{C}_{11}\boldsymbol{\Delta}_1\mathbf{C}_{11}^T\mathbf{R}(\psi) \\ &\quad +\dot{\psi}\mathbf{M}\mathbf{C}_{12}\mathbf{S}^T\big)\,\mathbf{R}^T(\psi_e)\mathbf{e} \\ &\quad -\left(\mathbf{C}_2 + \mathbf{M}\mathbf{C}_{12}\right)\boldsymbol{\nu}_e + \boldsymbol{\tau}_{\text{rff}} \end{aligned} \tag{B.59}$$

Thus, the control $\boldsymbol{\tau}$ may be rewritten as a PID-controller with nonlinear (velocity dependent) integral and proportional gains.

$$\boldsymbol{\tau} = -\mathbf{K}_i(\boldsymbol{\nu})\mathbf{R}^T(\psi)\mathbf{C}_{11}\boldsymbol{\xi} - \mathbf{K}_p(\boldsymbol{\nu})\mathbf{R}^T(\psi_e)\mathbf{e} - \mathbf{K}_d\boldsymbol{\nu}_e + \boldsymbol{\tau}_{\text{rff}} \tag{B.60}$$

Here,

$$\begin{aligned}\mathbf{K}_i(\boldsymbol{\nu}) &= \left(\mathbf{N}(\boldsymbol{\nu}) + \mathbf{C}_2 + r\mathbf{M}\mathbf{S}^T\right)\boldsymbol{\Delta}_2^{-1}\mathbf{C}_{11}\boldsymbol{\Delta}_1\mathbf{C}_{11}^T \\ &\quad -\mathbf{M}\boldsymbol{\Delta}_2^{-1}\mathbf{C}_{11}\boldsymbol{\Delta}_1\boldsymbol{\Lambda}\mathbf{C}_{11}^T \qquad \text{(B.61)} \\ \mathbf{K}_p(\boldsymbol{\nu}) &= \boldsymbol{\Delta}_2 + \left(\mathbf{N}(\boldsymbol{\nu}) + \mathbf{C}_2\right)\mathbf{C}_{12} + r\mathbf{M}\mathbf{C}_{12}\mathbf{S}^T \\ &\quad +\mathbf{M}\boldsymbol{\Delta}_2^{-1}\mathbf{R}^T(\psi)\mathbf{C}_{11}\boldsymbol{\Delta}_1\mathbf{C}_{11}^T\mathbf{R}(\psi) \qquad \text{(B.62)} \\ \mathbf{K}_d &= \mathbf{C}_2 + \mathbf{M}\mathbf{C}_{12} \qquad \text{(B.63)}\end{aligned}$$

and these are the gains stated in the theorem.

B.3 Proof of Theorem 5.6

This proof is very similar to the one given in Appendix B.1, and it too consists of two parts: First it will be shown that output feedback is equal to state feedback plus some perturbation term. The second part confirms that this perturbation is bounded linearly in the actual states as long as $\tilde{\psi} = 0$.

Part 1:

The control actually applied is

$$\begin{aligned}\dot{\boldsymbol{\xi}} &= -\boldsymbol{\Lambda}\boldsymbol{\xi} + \mathbf{C}_{11}^T\mathbf{R}(\psi_d)\mathbf{e} - \mathbf{C}_{11}^T\tilde{\boldsymbol{\eta}} \\ \hat{\boldsymbol{\tau}} &= -\left(\mathbf{G}_i + \mathbf{N}(\hat{\boldsymbol{\nu}})\mathbf{X}_{i1} + \hat{r}\mathbf{X}_{i1}\right)\mathbf{R}^T(\hat{\psi})\boldsymbol{\xi} \\ &\quad -\left(\mathbf{G}_p + \mathbf{N}(\hat{\boldsymbol{\nu}})\mathbf{C}_{12} + \hat{r}\mathbf{X}_p\right)\mathbf{R}^T(\hat{\psi}_e)\hat{\mathbf{e}} - \mathbf{K}_d\hat{\boldsymbol{\nu}}_e + \hat{\boldsymbol{\tau}}_{\text{rff}}\end{aligned} \tag{B.64}$$

where

$$-\mathbf{G}_i\mathbf{R}^T(\hat{\psi})\boldsymbol{\xi} = -\mathbf{G}_i\mathbf{R}^T(\psi)\boldsymbol{\xi} + \mathbf{G}_i\mathbf{R}^T(\psi)\left(\mathbf{I} - \mathbf{R}(\tilde{\psi})\right)\boldsymbol{\xi} \tag{B.65}$$

$$\begin{aligned}-\mathbf{G}_p\mathbf{R}^T(\hat{\psi}_e)\hat{\mathbf{e}} &= -\mathbf{G}_p\mathbf{R}^T(\psi_e)\mathbf{e} + \mathbf{G}_p\mathbf{R}^T(\psi_e)\left(\mathbf{I} - \mathbf{R}(\tilde{\psi})\right)\mathbf{e} \qquad \text{(B.66)} \\ &\quad +\mathbf{G}_p\mathbf{R}^T(\psi)\mathbf{R}(\tilde{\psi})\tilde{\boldsymbol{\eta}} \qquad \text{(B.67)}\end{aligned}$$

Let us first study the nonlinear terms in $\hat{\boldsymbol{\tau}}$. Then, for the integral contribution in $\hat{\boldsymbol{\tau}}$ we have

$$\begin{aligned}
\mathbf{N}(\hat{\boldsymbol{\nu}})\mathbf{X}_{i1}\mathbf{R}^T(\hat{\psi})\boldsymbol{\xi} &= (\mathbf{N}(\boldsymbol{\nu}) + \mathbf{N}_{err}(\boldsymbol{\nu}, \tilde{\boldsymbol{\nu}}))\, \mathbf{X}_{i1}\mathbf{R}^T(\psi) \left(\mathbf{I} + \left(\mathbf{R}(\tilde{\psi}) - \mathbf{I}\right)\right) \boldsymbol{\xi} \\
&= \mathbf{N}(\boldsymbol{\nu})\mathbf{X}_{i1}\mathbf{R}^T(\psi)\boldsymbol{\xi} \\
&\quad + \mathbf{N}_{err}(\boldsymbol{\nu}, \tilde{\boldsymbol{\nu}})\mathbf{X}_{i1}\mathbf{R}^T(\psi)\mathbf{R}(\tilde{\psi})\boldsymbol{\xi} \\
&\quad + \mathbf{N}(\boldsymbol{\nu})\mathbf{X}_{i1}\mathbf{R}^T(\psi) \left(\mathbf{R}(\tilde{\psi}) - \mathbf{I}\right) \boldsymbol{\xi}
\end{aligned} \tag{B.68}$$

and

$$\begin{aligned}
\hat{r}\mathbf{X}_{i1}\mathbf{R}^T(\hat{\psi})\boldsymbol{\xi} &= (r - \tilde{r})\, \mathbf{X}_{i2}\mathbf{R}^T(\psi) \left(\mathbf{I} + \left(\mathbf{R}(\tilde{\psi}) - \mathbf{I}\right)\right) \boldsymbol{\xi} \\
&= r\mathbf{X}_{i2}\mathbf{R}^T(\psi)\boldsymbol{\xi} \\
&\quad - \tilde{r}\mathbf{X}_{i2}\mathbf{R}^T(\psi)\mathbf{R}(\tilde{\psi})\boldsymbol{\xi} \\
&\quad + r\mathbf{X}_{i2}\mathbf{R}^T(\psi) \left(\mathbf{R}(\tilde{\psi}) - \mathbf{I}\right) \boldsymbol{\xi}
\end{aligned} \tag{B.69}$$

For the P-term we get

$$\begin{aligned}
\mathbf{N}(\hat{\boldsymbol{\nu}})\mathbf{C}_{12}\mathbf{R}^T(\hat{\psi}_e)\hat{\mathbf{e}} &= (\mathbf{N}(\boldsymbol{\nu}) + \mathbf{N}_{err}(\boldsymbol{\nu}, \tilde{\boldsymbol{\nu}}))\, \mathbf{C}_{12}\mathbf{R}^T(\psi_e) \left(\mathbf{I} + \left(\mathbf{R}(\tilde{\psi}) - \mathbf{I}\right)\right) \mathbf{e} \\
&\quad - (\mathbf{N}(\boldsymbol{\nu}) + \mathbf{N}_{err}(\boldsymbol{\nu}, \tilde{\boldsymbol{\nu}}))\, \mathbf{C}_{12}\mathbf{R}^{\mathbf{T}}(\hat{\psi})\tilde{\boldsymbol{\eta}} \\
&= \mathbf{N}(\boldsymbol{\nu})\mathbf{C}_{12}\mathbf{R}^T(\psi_e)\mathbf{e} \\
&\quad + \mathbf{N}_{err}(\boldsymbol{\nu}, \tilde{\boldsymbol{\nu}})\mathbf{C}_{12}\mathbf{R}^T(\psi_e)\mathbf{R}(\tilde{\psi})\mathbf{e} \\
&\quad - \mathbf{N}(\boldsymbol{\nu})\mathbf{C}_{12}\mathbf{R}^{\mathbf{T}}(\hat{\psi})\tilde{\boldsymbol{\eta}} - \mathbf{N}_{err}(\boldsymbol{\nu}, \tilde{\boldsymbol{\nu}})\mathbf{C}_{12}\mathbf{R}^{\mathbf{T}}(\hat{\psi})\tilde{\boldsymbol{\eta}} \\
&\quad + \mathbf{N}(\boldsymbol{\nu})\mathbf{C}_{12}\mathbf{R}^T(\psi_e) \left(\mathbf{R}(\tilde{\psi}) - \mathbf{I}\right) \mathbf{e}
\end{aligned} \tag{B.70}$$

and

$$\begin{aligned}
\hat{r}\mathbf{X}_p\mathbf{R}^T(\hat{\psi}_e)\hat{\mathbf{e}} &= r\mathbf{X}_p\mathbf{R}^T(\psi_e)\mathbf{e} \\
&\quad - \tilde{r}\mathbf{X}_p\mathbf{R}^T(\psi_e)\mathbf{R}(\tilde{\psi})\mathbf{e} \\
&\quad - r\mathbf{X}_p\mathbf{R}^T(\hat{\psi})\tilde{\boldsymbol{\eta}} + \tilde{r}\mathbf{X}_p\mathbf{R}^T(\hat{\psi})\tilde{\boldsymbol{\eta}} \\
&\quad + r\mathbf{X}_p\mathbf{R}^T(\psi_e) \left(\mathbf{R}(\tilde{\psi}) - \mathbf{I}\right) \mathbf{e}
\end{aligned} \tag{B.71}$$

Observe that the first term in and every of (B.68)-(B.71) is identical to state-feedback such that the remaining ones are the perturbations introduced using observer estimates. Each of the last terms in all of these perturbations are not linearly bounded in the system variables. They may be small for bounded $\tilde{\psi}$, though, and they vanish completely when $\tilde{\psi} = 0$.

The reference feed-forward $\hat{\boldsymbol{\tau}}_{\text{rff}}$ contributes with

$$\begin{aligned}
\hat{\boldsymbol{\tau}}_{\text{rff}} &= \mathbf{N}(\hat{\boldsymbol{\nu}})\mathbf{R}_{\hat{\psi}_e}^T\boldsymbol{\nu}_d + \mathbf{M}\left((\hat{r}-r_d)\,\mathbf{S}^T\mathbf{R}_{\hat{\psi}_e}^T\boldsymbol{\nu}_d + \mathbf{R}_{\hat{\psi}_e}^T\dot{\boldsymbol{\nu}}_d\right)\\
&= \mathbf{N}(\boldsymbol{\nu})\mathbf{R}_{\psi_e}^T\boldsymbol{\nu}_d + \mathbf{M}\left(r_e\mathbf{S}^T\mathbf{R}_{\psi_e}^T\boldsymbol{\nu}_d + \mathbf{R}_{\psi_e}^T\dot{\boldsymbol{\nu}}_d\right)\\
&\quad +\mathbf{N}(\boldsymbol{\nu})\mathbf{R}_{\psi_e}^T\left(\mathbf{R}_{\tilde{\psi}}-\mathbf{I}\right)\boldsymbol{\nu}_d + \mathbf{N}_{err}(\boldsymbol{\nu},\tilde{\boldsymbol{\nu}})\mathbf{R}_{\psi_e}^T\mathbf{R}_{\tilde{\psi}}\boldsymbol{\nu}_d\\
&\quad +\mathbf{M}\left(r_e\mathbf{S}^T\mathbf{R}_{\psi_e}^T(\mathbf{R}_{\tilde{\psi}}-\mathbf{I})\boldsymbol{\nu}_d - \tilde{r}\mathbf{S}^T\mathbf{R}_{\psi_e}^T\mathbf{R}_{\tilde{\psi}}\boldsymbol{\nu}_d + \mathbf{R}_{\psi_e}^T(\mathbf{R}_{\tilde{\psi}}-\mathbf{I})\dot{\boldsymbol{\nu}}_d\right) \qquad \text{(B.72)}
\end{aligned}$$

and thus poses no threat to the stability since $\boldsymbol{\nu}_d$ is presumed bounded.

Consequently,

$$\begin{aligned}
\hat{\boldsymbol{\tau}} &= -\left(\mathbf{G}_i + \mathbf{N}(\boldsymbol{\nu})\mathbf{X}_{i1} + r\mathbf{X}_{i2}\right)\mathbf{R}_{\psi}^T\boldsymbol{\xi} - \left(\mathbf{N}_{err}(\boldsymbol{\nu},\tilde{\boldsymbol{\nu}})\mathbf{X}_{i1} - \tilde{r}\mathbf{X}_{i2}\right)\mathbf{R}_{\psi}^T\mathbf{R}_{\tilde{\psi}}\boldsymbol{\xi}\\
&\quad +\left(\mathbf{G}_i + \mathbf{N}(\boldsymbol{\nu})\mathbf{X}_{i1} + r\mathbf{X}_{i2}\right)\mathbf{R}_{\psi}^T\left(\mathbf{I}-\mathbf{R}_{\tilde{\psi}}\right)\boldsymbol{\xi}\\
&\quad -\left(\mathbf{G}_p + \mathbf{N}(\boldsymbol{\nu})\mathbf{C}_{12} + r\mathbf{X}_p\right)\mathbf{R}_{\psi_e}^T\mathbf{e} - \left(\mathbf{N}_{err}(\boldsymbol{\nu},\tilde{\boldsymbol{\nu}})\mathbf{C}_{12} - \tilde{r}\mathbf{X}_p\right)\mathbf{R}_{\psi_e}^T\mathbf{R}_{\tilde{\psi}}\mathbf{e}\\
&\quad +\left(\mathbf{G}_p + \mathbf{N}(\boldsymbol{\nu}) + \mathbf{N}_{err}(\boldsymbol{\nu},\tilde{\boldsymbol{\nu}}) + (r-\tilde{r})\,\mathbf{X}_p\right)\mathbf{R}_{\psi}^T\mathbf{R}_{\tilde{\psi}}\tilde{\boldsymbol{\eta}}\\
&\quad +\left(\mathbf{G}_p + \mathbf{N}(\boldsymbol{\nu})\mathbf{C}_{12} + r\mathbf{X}_p\right)\mathbf{R}^T(\psi_e)\left(\mathbf{I}-\mathbf{R}_{\tilde{\psi}}\right)\mathbf{e}\\
&\quad -\mathbf{K}_d\hat{\boldsymbol{\nu}}_e + \mathbf{K}_d\left(\tilde{\boldsymbol{\nu}} + \mathbf{R}^T(\psi_e)\left(\mathbf{R}_{\tilde{\psi}}-\mathbf{I}\right)\boldsymbol{\nu}_d\right)\\
&\quad +\mathbf{N}(\boldsymbol{\nu})\mathbf{R}^T(\psi_e)\boldsymbol{\nu}_d + \mathbf{M}\left(r_e\mathbf{S}^T\mathbf{R}_{\psi_e}^T\boldsymbol{\nu}_d + \mathbf{R}_{\psi_e}^T\dot{\boldsymbol{\nu}}_d\right) + \mathbf{N}(\boldsymbol{\nu})\mathbf{R}_{\psi_e}^T\left(\mathbf{R}_{\tilde{\psi}}-\mathbf{I}\right)\boldsymbol{\nu}_d\\
&\quad +\mathbf{N}_{err}(\boldsymbol{\nu},\tilde{\boldsymbol{\nu}})\mathbf{R}_{\psi_e}^T\mathbf{R}_{\tilde{\psi}}\boldsymbol{\nu}_d\\
&\quad +\mathbf{M}\left(r_e\mathbf{S}^T\mathbf{R}_{\psi_e}^T(\mathbf{R}_{\tilde{\psi}}-\mathbf{I})\boldsymbol{\nu}_d - \tilde{r}\mathbf{S}^T\mathbf{R}_{\psi_e}^T\mathbf{R}_{\tilde{\psi}}\boldsymbol{\nu}_d + \mathbf{R}_{\psi_e}^T(\mathbf{R}_{\tilde{\psi}}-\mathbf{I})\dot{\boldsymbol{\nu}}_d\right) \qquad \text{(B.73)}
\end{aligned}$$

Recognizing the state feedback control terms and substituting those with $\boldsymbol{\tau}$ yields

$$\begin{aligned}
\hat{\boldsymbol{\tau}} &= \boldsymbol{\tau} - \left(\mathbf{N}_{err}(\boldsymbol{\nu},\tilde{\boldsymbol{\nu}})\mathbf{X}_{i1} - \tilde{r}\mathbf{X}_{i2}\right)\mathbf{R}_{\psi}^T\mathbf{R}_{\tilde{\psi}}\boldsymbol{\xi}\\
&\quad -\left(\mathbf{N}_{err}(\boldsymbol{\nu},\tilde{\boldsymbol{\nu}})\mathbf{C}_{12} - \tilde{r}\mathbf{X}_p\right)\mathbf{R}_{\psi_e}^T\mathbf{R}_{\tilde{\psi}}\mathbf{e}\\
&\quad +\left(\mathbf{G}_p + \mathbf{N}(\boldsymbol{\nu}) + \mathbf{N}_{err}(\boldsymbol{\nu},\tilde{\boldsymbol{\nu}}) + (r-\tilde{r})\,\mathbf{X}_p\right)\mathbf{R}_{\psi}^T\mathbf{R}_{\tilde{\psi}}\tilde{\boldsymbol{\eta}}\\
&\quad +\mathbf{K}_d\tilde{\boldsymbol{\nu}}\\
&\quad +\left(\mathbf{N}(\boldsymbol{\nu}) + \mathbf{K}_d\right)\mathbf{R}_{\psi_e}^T\left(\mathbf{R}_{\tilde{\psi}}-\mathbf{I}\right)\boldsymbol{\nu}_d + \mathbf{N}_{err}(\boldsymbol{\nu},\tilde{\boldsymbol{\nu}})\mathbf{R}_{\psi_e}^T\mathbf{R}_{\tilde{\psi}}\boldsymbol{\nu}_d\\
&\quad +\mathbf{M}\left(r_e\mathbf{S}^T\mathbf{R}_{\psi_e}^T(\mathbf{R}_{\tilde{\psi}}-\mathbf{I})\boldsymbol{\nu}_d - \tilde{r}\mathbf{S}^T\mathbf{R}_{\psi_e}^T\mathbf{R}_{\tilde{\psi}}\boldsymbol{\nu}_d + \mathbf{R}_{\psi_e}^T(\mathbf{R}_{\tilde{\psi}}-\mathbf{I})\dot{\boldsymbol{\nu}}_d\right)\\
&\quad +\left(\mathbf{G}_i + \mathbf{N}(\boldsymbol{\nu})\mathbf{X}_{i1} + r\mathbf{X}_{i2}\right)\mathbf{R}_{\psi}^T\left(\mathbf{I}-\mathbf{R}_{\tilde{\psi}}\right)\boldsymbol{\xi}\\
&\quad +\left(\mathbf{G}_p + \mathbf{N}(\boldsymbol{\nu})\mathbf{C}_{12} + r\mathbf{X}_p\right)\mathbf{R}_{\psi_e}^T\left(\mathbf{I}-\mathbf{R}_{\tilde{\psi}}\right)\mathbf{e} \qquad \text{(B.74)}
\end{aligned}$$

Part 2:

The resulting closed loop can now rewritten as the nominal state feedback system perturbed with the observer errors

$$\dot{\mathbf{z}} = \mathbf{A}_c(\boldsymbol{\nu},\psi,\psi_d)\mathbf{z} + \mathbf{g}_z(t,\mathbf{z},\tilde{\mathbf{x}}_o,\boldsymbol{\nu}_d,\dot{\boldsymbol{\nu}}_d) \qquad \text{(B.75)}$$

where $\mathbf{A}_c(\boldsymbol{\nu}, \psi, \psi_d)$ is given by (B.49) and

$$\mathbf{g}_z(\mathbf{z}, \mathbf{x}_o, \boldsymbol{\eta}_d, \boldsymbol{\nu}_d, \dot{\boldsymbol{\nu}}_d) = \begin{bmatrix} \mathbf{g}_1 \\ \mathbf{0} \\ \mathbf{g}_3 + \mathbf{n}_3 \end{bmatrix} \tag{B.76}$$

where the terms of $\mathbf{g}_z$ bounded in the state variables, that is $\mathbf{g}_1$ and $\mathbf{g}_3$, are

$$\begin{aligned}
\mathbf{g}_1 &= -\tilde{\boldsymbol{\eta}} \qquad (B.77)\\
\mathbf{g}_3 &= -\mathbf{M}^{-1}\left(\mathbf{N}_{err}(\boldsymbol{\nu}, \tilde{\boldsymbol{\nu}})\mathbf{X}_{i1} - \tilde{r}\mathbf{X}_{i2}\right)\mathbf{R}_{\tilde{\psi}}^T\mathbf{R}_{\tilde{\psi}}\boldsymbol{\xi} \\
&\quad -\mathbf{M}^{-1}\left(\mathbf{N}_{err}(\boldsymbol{\nu}, \tilde{\boldsymbol{\nu}})\mathbf{C}_{12} - \tilde{r}\mathbf{X}_p\right)\mathbf{R}_{\psi_e}^T\mathbf{R}_{\tilde{\psi}}\mathbf{e} \\
&\quad +\mathbf{M}^{-1}\left(\mathbf{G}_p + \mathbf{N}(\boldsymbol{\nu}) + \mathbf{N}_{err}(\boldsymbol{\nu}, \tilde{\boldsymbol{\nu}}) + (r - \tilde{r})\,\mathbf{X}_p\right)\mathbf{R}_{\tilde{\psi}}^T\mathbf{R}_{\tilde{\psi}}\tilde{\boldsymbol{\eta}} \\
&\quad +\mathbf{M}^{-1}\mathbf{K}_d\tilde{\boldsymbol{\nu}} \\
&\quad +\mathbf{M}^{-1}\left(\mathbf{N}(\boldsymbol{\nu}) + \mathbf{K}_d\right)\mathbf{R}_{\psi_e}^T(\mathbf{R}_{\tilde{\psi}} - \mathbf{I})\boldsymbol{\nu}_d + \mathbf{M}^{-1}\mathbf{N}_{err}(\boldsymbol{\nu}, \tilde{\boldsymbol{\nu}})\mathbf{R}_{\psi_e}^T\mathbf{R}_{\tilde{\psi}}\boldsymbol{\nu}_d \\
&\quad +\left(r_e\mathbf{S}^T\mathbf{R}_{\psi_e}^T(\mathbf{R}_{\tilde{\psi}} - \mathbf{I})\boldsymbol{\nu}_d - \tilde{r}\mathbf{S}^T\mathbf{R}_{\psi_e}^T\mathbf{R}_{\tilde{\psi}}\boldsymbol{\nu}_d + \mathbf{R}_{\psi_e}^T(\mathbf{R}_{\tilde{\psi}} - \mathbf{I})\dot{\boldsymbol{\nu}}_d\right) \\
&\quad +\mathbf{M}^{-1}\mathbf{G}_i\mathbf{R}_{\psi}^T\left(\mathbf{I} - \mathbf{R}_{\tilde{\psi}}\right)\boldsymbol{\xi} + \mathbf{G}_p\mathbf{R}_{\psi_e}^T\left(\mathbf{I} - \mathbf{R}_{\tilde{\psi}}\right)\mathbf{e}
\end{aligned}$$

However, $\mathbf{n}_3$ as given by

$$\begin{aligned}
\mathbf{n}_3 &= \mathbf{M}^{-1}\left(\mathbf{N}(\boldsymbol{\nu})\mathbf{X}_{i1} + r\mathbf{X}_{i2}\right)\mathbf{R}_{\psi}^T\left(\mathbf{I} - \mathbf{R}_{\tilde{\psi}}\right)\boldsymbol{\xi} \\
&\quad + \left(\mathbf{N}(\boldsymbol{\nu})\mathbf{C}_{12} + r\mathbf{X}_p\right)\mathbf{R}_{\psi_e}^T\left(\mathbf{I} - \mathbf{R}_{\tilde{\psi}}\right)\mathbf{e} \qquad (B.78)
\end{aligned}$$

is not linear in the states and this ruins our hope of using Theorem A.2.

Admittedly, by imposing bounds on the velocity $\boldsymbol{\nu}$ and the estimated heading error $\tilde{\psi}$ it would still be possible to establish asymptotic stability by completing the squares. This, however, contradicts the objective of obtaining UGAS under observer feedback. Instead we assume that $\tilde{\psi} = 0$ (ψ is perfectly measured). Thus, $\mathbf{n}_3 = \mathbf{0}$ since $\mathbf{I} - \mathbf{R}(0) = \mathbf{0}$. It now suffices to show that $\mathbf{g}_1$ and $\mathbf{g}_3$ is linearly bounded in the states. For completeness, terms dependent on $\tilde{\psi}$ in $\mathbf{g}_3$ will not be cancelled.

$$\begin{aligned}
|\mathbf{g}_z| \leq\ & |\tilde{\boldsymbol{\eta}}| + m_m^{-1}\left(\left((d_{err} + c_M)\,\|\mathbf{X}_{i1}\| + \|\mathbf{X}_{i2}\|\right)|\tilde{\boldsymbol{\nu}}| + 2|\tilde{\psi}|\,\|\mathbf{G}_i\|\right)|\boldsymbol{\xi}| \\
&+m_m^{-1}\left(\left((d_{err} + c_M)\,\|\mathbf{C}_{12}\| + \|\mathbf{X}_p\|\right)|\tilde{\boldsymbol{\nu}}| + 2\,\|\mathbf{G}_p\|\,|\tilde{\psi}|\right)|\mathbf{e}| \\
&+m_m^{-1}\left(\|\mathbf{G}_p + \mathbf{D}_L\| + (d_{err} + c_M + \|\mathbf{X}_p\|)\,|\tilde{\boldsymbol{\nu}}| + (d_M + c_M + \|\mathbf{X}_p\|)\,|\boldsymbol{\nu}|\right)|\tilde{\boldsymbol{\eta}}| \\
&+m_m^{-1}\,\|\mathbf{K}_d\|\,|\tilde{\boldsymbol{\nu}}| \\
&+m_m^{-1}\left(2\left((d_M + c_M)\,|\boldsymbol{\nu}| + \|\mathbf{D}_L + \mathbf{K}_d\|\right)|\tilde{\psi}|c_{\nu_d} + (d_{err} + c_M)\,c_{\nu_d}\,|\tilde{\boldsymbol{\nu}}|\right) \\
&+2c_{\nu_d}\left(|\boldsymbol{\nu}| + c_{\nu_d}\right)|\tilde{\psi}| + c_{\nu_d}\,|\tilde{\boldsymbol{\nu}}| + 2c_{\dot{\nu}_d}|\tilde{\psi}| \qquad (B.79)
\end{aligned}$$

From the definition of $\mathbf{z}_2$ we get that

$$|\boldsymbol{\nu}| \leq |\mathbf{z}_2| + \|\mathbf{C}_1(\psi, \psi_d)\|\,|\mathbf{z}_1| + c_{\nu_d} \tag{B.80}$$

such that

$$
\begin{aligned}
|\mathbf{g}_z| \leq & |\tilde{\boldsymbol{\eta}}| + m_m^{-1} \left(\left((d_{err} + c_M) \left\| \mathbf{X}_{i1} \right\| + \left\| \mathbf{X}_{i2} \right\| \right) |\tilde{\boldsymbol{\nu}}| + 2|\tilde{\psi}| \left\| \mathbf{G}_i \right\| \right) |\boldsymbol{\xi}| \\
& + m_m^{-1} \left(\left((d_{err} + c_M) \left\| \mathbf{C}_{12} \right\| + \left\| \mathbf{X}_p \right\| \right) |\tilde{\boldsymbol{\nu}}| + 2 \left\| \mathbf{G}_p \right\| |\tilde{\psi}| \right) |\mathbf{e}| \\
& + m_m^{-1} \left(\left\| \mathbf{G}_p + \mathbf{D}_L \right\| + (d_{err} + c_M + \left\| \mathbf{X}_p \right\|) |\tilde{\boldsymbol{\nu}}| \right) |\tilde{\boldsymbol{\eta}}| \\
& + m_m^{-1} \left(d_M + c_M + \left\| \mathbf{X}_p \right\| \right) \left(|\mathbf{z}_2| + \left\| \mathbf{C}_1(\psi, \psi_d) \right\| |\mathbf{z}_1| + c_{\nu_d} \right) |\tilde{\boldsymbol{\eta}}| \\
& + m_m^{-1} \left(\left\| \mathbf{K}_d \right\| + (d_{err} + c_M) \, c_{\nu_d} \right) |\tilde{\boldsymbol{\nu}}| \\
& + m_m^{-1} \left(2 \left((d_M + c_M) \left(|\mathbf{z}_2| + \left\| \mathbf{C}_1(\psi, \psi_d) \right\| |\mathbf{z}_1| + c_{\nu_d} \right) + \left\| \mathbf{D}_L + \mathbf{K}_d \right\| \right) |\tilde{\psi}| c_{\nu_d} \right) \\
& + 2 c_{\nu_d} \left(|\mathbf{z}_2| + \left\| \mathbf{C}_1(\psi, \psi_d) \right\| |\mathbf{z}_1| + c_{\nu_d} + c_{\nu_d} \right) |\tilde{\psi}| + c_{\nu_d} |\tilde{\boldsymbol{\nu}}| + 2 c_{\dot{\nu}_d} |\tilde{\psi}| \qquad \text{(B.81)}
\end{aligned}
$$

Collecting the terms we get

$$
|\mathbf{g}_z| \leq \theta_1(|\tilde{\mathbf{x}}_o|) + \theta_2(|\tilde{\mathbf{x}}_o|) \, |\mathbf{z}|
$$

where

$$
\begin{aligned}
\theta_1(s) \;=\; & s + m_m^{-1} \left(\left\| \mathbf{G}_p + \mathbf{D}_L \right\| + (d_M + c_M) \left(1 + 2 c_{\nu_d} \right) c_{\nu_d} + \left\| \mathbf{K}_d \right\| \right) s \\
& + m_m^{-1} \left(\left(1 + d_{err} + c_M + \left\| \mathbf{D}_L + \mathbf{K}_d \right\| + 4 c_{\nu_d} \right) c_{\nu_d} + 2 c_{\dot{\nu}_d} \right) s \\
& + m_m^{-1} \left(d_{err} + c_M + \left\| \mathbf{X}_p \right\| \right) s^2 \qquad \text{(B.82)} \\
\theta_2(s) \;=\; & m_m^{-1} \left((d_{err} + c_M) \left(\left\| \mathbf{X}_{i1} \right\| + \left\| \mathbf{C}_{12} \right\| \right) + \left\| \mathbf{X}_{i2} \right\| \right) s \\
& + m_m^{-1} \left(2 \left\| \mathbf{G}_i \right\| + 2 \left\| \mathbf{G}_p \right\| + \left\| \mathbf{X}_p \right\| \right) s \qquad \text{(B.83)} \\
& + m_m^{-1} \left(\left\| \mathbf{X}_p \right\| + \left(1 + 2 c_{\nu_d} \right) (d_M + c_M) \left(1 + \left\| \mathbf{C}_1(\psi, \psi_d) \right\| \right) \right) s \\
& + 2 c_{\nu_d} \left(1 + \left\| \mathbf{C}_1(\psi, \psi_d) \right\| \right) s \qquad \text{(B.84)}
\end{aligned}
$$

Since $\theta_i : \mathbb{R}_{\geq 0} \to \mathbb{R}_{\geq 0}$ for $i = 1, 2$ are continuous and $\theta_i(0) = 0$, the conditions of Theorem A.2 are satisfied. This completes the proof.

Appendix C

Restoring Forces

In this appendix a new formulation of gravitational and hydrostatic restoring forces for ocean vehicles is derived.

C.1 Definitions

The Earth-fixed coordinate frame is denoted n while the vessel-fixed is called b. The vector $\mathbf{r}^n_{nb}$ is the position vector similar to $\boldsymbol{\eta}_1$ (Fossen 2002) and the vector $\boldsymbol{\theta}_{nb}$ contains the Euler angles describing the orientation of frame b relative to frame n, known as $\boldsymbol{\eta}_2$.

$$\begin{array}{ll} \mathbf{r}^n_{nb} = \begin{bmatrix} x^n_{nb} & y^n_{nb} & z^n_{nb} \end{bmatrix}^T & \boldsymbol{\theta}_{nb} = \begin{bmatrix} \phi & \theta & \psi \end{bmatrix}^T \\ \mathbf{r}^p_{pb} = \mathbf{0} & \boldsymbol{\theta}_{pb} = \begin{bmatrix} \phi & \theta & 0 \end{bmatrix}^T \end{array} \tag{C.1}$$

The xy-plane of the b-frame is assumed to coincide with the static water plane A_{wp}, thus at equilibrium the xy-planes of both the p- and b-frames coincide with A_{wp}. Displaced volume in equilibrium will be denoted V_0.

The center of flotation $\mathbf{r}^b_{bf}$ is the geometrical center of the static water plane surface A_{wp}

$$\mathbf{r}^b_{bf} = \frac{1}{A_{wp}} \begin{bmatrix} S^b_x \\ S^b_y \\ 0 \end{bmatrix} \tag{C.2}$$

$$S^b_x = \int_{A_{wp}} x^b_{ba} dS \tag{C.3}$$

$$S^b_y = \int_{A_{wp}} y^b_{ba} dS \tag{C.4}$$

such that $x^b_{bf} = S^b_x / A_{wp}$ and $y^b_{bf} = S^b_y / A_{wp}$ denote the respective longships and atwarthships position relative to the origin of the b-frame. In the integrals $\mathbf{r}^b_{ba} =$

$[x^b_{ba}, y^b_{ba}, 0]^T$ is the distance from the b-frame's origin to some arbitrary point on A_{wp}.

The position of the center of gravity (CG) in vessel-fixed coordinates is called $\mathbf{r}^b_{bG}$. For rigid bodies, $\mathbf{r}^b_{bG}$ is a constant vector. The center of buoyancy (CB) $\mathbf{r}^b_{bB}$ defined as the geometrical center of the instantaneous submerged volume V is likely to change for surface vessels. For submerged vehicles, on the other hand, $\mathbf{r}^b_{bB}$ will always be. Nevertheless, we choose to define $\mathbf{r}^b_{bB}$ as the geometrical center of the constant displaced volume V_0.

Remember also that the rotation from the b-frame to the vessel parallel p-frame is given by

$$\mathbf{R}^p_b = \mathbf{R}\left(\boldsymbol{\theta}_{pb}\right) = \begin{bmatrix} \cos\phi & \sin\theta\sin\phi & \sin\theta\cos\phi \\ 0 & \cos\phi & -\sin\phi \\ -\sin\theta & \cos\theta\sin\phi & \cos\theta\cos\phi \end{bmatrix} \tag{C.5}$$

C.1.1 The Basic Assumption

For the moment we state only the most important assumption that will allow us to deduce the general form of the buoyancy terms.

A1 At the static water line, the walls of the hull are approximately vertical.

This assumption will be used calculating the instantaneous submerged volume of the vessel.

C.2 Gravity Forces and Moments

The gravity forces acts in the vessel's center of gravity $\mathbf{r}^b_{bG}$. In vessel-parallell and in the Earth-fixed frames the gravity force is

$$\mathbf{f}^p_G = \mathbf{f}^n_G = \begin{bmatrix} 0 & 0 & mg \end{bmatrix}^T \tag{C.6}$$

Letting $\boldsymbol{\zeta}$ be the unit vector in the z-direction, that is

$$\boldsymbol{\zeta} = \vec{\mathbf{k}} = \begin{bmatrix} 0 & 0 & 1 \end{bmatrix}^T \tag{C.7}$$

a compact form of $\mathbf{f}^p_G$ reads

$$\mathbf{f}^p_G = mg\boldsymbol{\zeta} \tag{C.8}$$

Decomposed in the vessel-fixed frame b, the gravity forces and moments are

$$\begin{bmatrix} \mathbf{f}^b_G \\ \mathbf{m}^b_{bG} \end{bmatrix} = \begin{bmatrix} \mathbf{R}^b_p \mathbf{f}^p_G \\ \mathbf{r}^b_{bG} \times \mathbf{R}^b_p \mathbf{f}^p_G \end{bmatrix} = \mathbf{T}(\mathbf{r}^b_{bG})\mathbf{R}^b_p \mathbf{f}^p_G \tag{C.9}$$

where $\mathbf{T}(\cdot)$ is a constant matrix given by

$$\mathbf{T}(\mathbf{r}^b_{bG}) = -\begin{bmatrix} \mathbf{I} \\ \mathbf{S}(\mathbf{r}^b_{bG}) \end{bmatrix} \tag{C.10}$$

and $\mathbf{S}(\cdot)$ is defined in (2.6).

On component form, the vessel fixed gravity forces and moments are

$$\begin{bmatrix} \mathbf{f}_G^b \\ \mathbf{m}_{bG}^b \end{bmatrix} = mg \begin{bmatrix} -\sin\theta \\ \sin\phi\cos\theta \\ \cos\phi\cos\theta \\ y_{bG}^b \cos\phi\cos\theta - z_{bG}^b \sin\phi\cos\theta \\ -z_{bG}^b \sin\theta - x_{bG}^b \cos\phi\cos\theta \\ x_{bG}^b \sin\phi\cos\theta + y_{bG}^b \sin\theta \end{bmatrix} \tag{C.11}$$

C.3 Buoyancy Forces

The buoyancy forces are found by integrating the hydrostatic pressure on the instantaneous wetted surface S_B.

$$\mathbf{f}_B^p = -\rho g \int_{S_B} \mathbf{n}_a^p z_{na}^p dS \tag{C.12}$$

Here, $\mathbf{n}_a$ is a surface normal on S_B pointing outwards and z_{pa}^p is the vertical distance from the free surface to that point.

Note that

$$\int_{S_B} \mathbf{n}_a^p z_{pa}^p dS = \int_{\overline{S_B}} \mathbf{n}_a^p z_{pa}^p dS \tag{C.13}$$

because there is no contribution to the integral at $z^p = 0$, see Figure 2.1. Thus, we may utilize Gauss' theorem on the volume V enclosed by $\overline{S_B}$. We get

$$\mathbf{f}_B^p = -\rho g \int_V \nabla z_{na}^p dV = -\rho g \boldsymbol{\zeta} \int_V dV \tag{C.14}$$

which we recognize as Archimedes' principle. However, the volume V is unknown, so we utilize the common technique of separating the volume integral into two parts.

From Figure C.1 we recognize that the volume V is the union $V = V_0 \cup V_1$ where V_0 is the static displacement. Thus,

$$\mathbf{f}_B^p = -\rho g \boldsymbol{\zeta} \left(V_0 + \int_{V_1} dV \right) \tag{C.15}$$

By applying Assumption A1, we may approximate the integral $\int_{V_1} dV$ as the volume between A_{wp} and the free surface $z^p = 0$.

$$\int_{V_1} dV \approx \int_{A_{wp}} z_{wa}^p dS \tag{C.16}$$

where z_{wa}^p is the distance between the plane $z^p = 0$ and some point a on A_{wp} such that $(\mathbf{r}_{ba}^b)^T \mathbf{r}_{wa}^b = 0$.

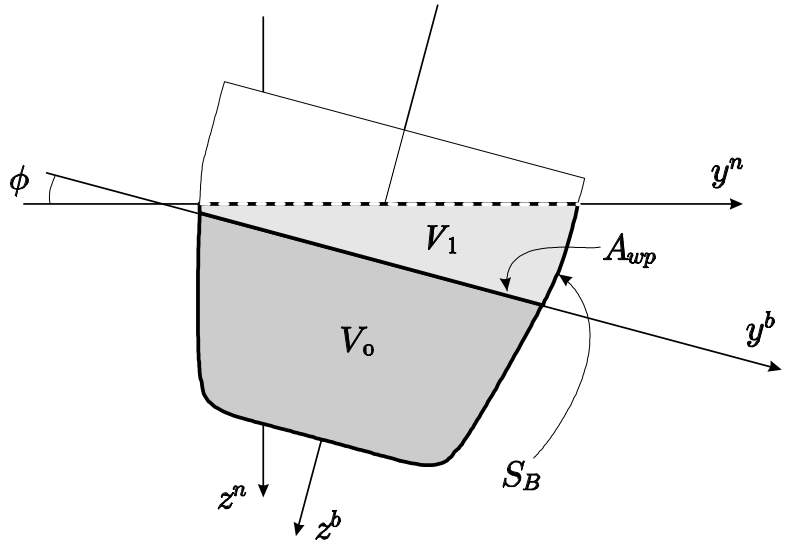

Figure C.1: A two-dimensional sketch showing the defintions of volumes and surfaces.

By examining Figure C.2, we see that

$$z_{qa}^p = \boldsymbol{\zeta}^T \mathbf{R}_b^p \begin{bmatrix} 0 \\ 0 \\ z_{wa}^b \end{bmatrix} = \boldsymbol{\zeta}^T \mathbf{R}_b^p \boldsymbol{\zeta} z_{wa}^b \tag{C.17}$$

and

$$z_{qa}^p = z_{nb}^p + \boldsymbol{\zeta}^T \mathbf{R}_b^p \mathbf{r}_{ba}^b \tag{C.18}$$

When solving for z_{wa}^b we get

$$z_{wa}^b = \frac{\boldsymbol{\zeta}^T}{\boldsymbol{\zeta}^T \mathbf{R}_b^p \boldsymbol{\zeta}} \left(\mathbf{r}_{nb}^p + \mathbf{R}_b^p \mathbf{r}_{ba}^b \right) \tag{C.19}$$

By inserting (C.19) into (C.16) we get the volume of the wedge V_1:

$$\begin{aligned} V_1 &= \int_{V_1} dV \approx \int_{A_{wp}} z_{wa}^b dS \\ &= \frac{\boldsymbol{\zeta}^T}{\boldsymbol{\zeta}^T \mathbf{R}_b^p \boldsymbol{\zeta}} \int_{A_{wp}} \left(\mathbf{r}_{nb}^p + \mathbf{R}_b^p \mathbf{r}_{ba}^b \right) dS \\ &= A_{wp} \frac{\boldsymbol{\zeta}^T}{\boldsymbol{\zeta}^T \mathbf{R}_B^L \boldsymbol{\zeta}} \left(\mathbf{r}_{nb}^p + \mathbf{R}_b^p \mathbf{r}_{bf}^b \right) \end{aligned} \tag{C.20}$$

On component form, the integral can be written as ($\cos\theta \neq 0$,$\cos\phi \neq 0$)

$$\int_{A_{wp}} z_{wa}^b dS = \frac{1}{\cos\theta \cos\phi} \left(z_{nb}^p A_{wp} - S_x^b \sin\theta + S_y^b \cos\theta \sin\phi + A_{wp} z_{bf}^b \cos\phi \cos\theta \right) \tag{C.21}$$

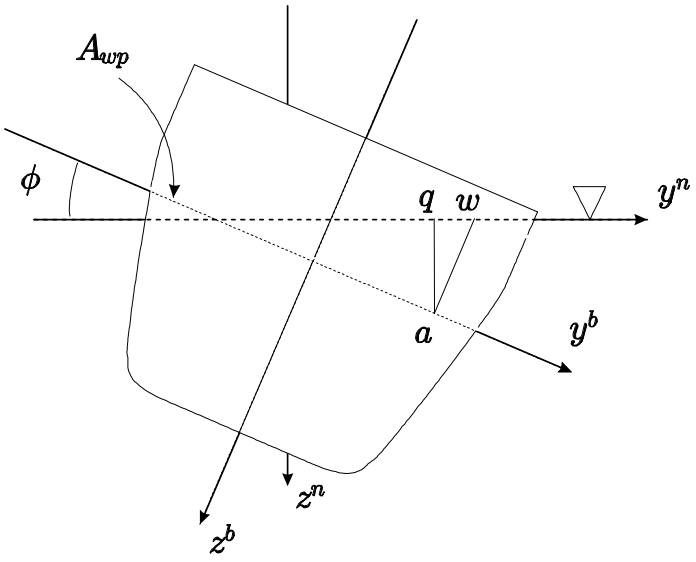

Figure C.2: Sketch illustrating how to approximate the volume integral in V_1 by a surface integral on A_{wp}.

And the total buoyancy force is therefore

$$\mathbf{f}_B^p = -\rho g \boldsymbol{\zeta} \left(V_0 + A_{wp} \frac{\boldsymbol{\zeta}^T}{\boldsymbol{\zeta}^T \mathbf{R}_b^p \boldsymbol{\zeta}} \left(\mathbf{r}_{pb}^p + \mathbf{R}_b^p \mathbf{r}_{bf}^b \right) \right) \tag{C.22}$$

and in a vessel fixed frame we get

$$\mathbf{f}_B^b = \mathbf{R}_p^b \mathbf{f}_b^p = -\rho g \mathbf{R}_p^b \boldsymbol{\zeta} \left(V_0 + A_{wp} \frac{\boldsymbol{\zeta}^T}{\boldsymbol{\zeta}^T \mathbf{R}_b^p \boldsymbol{\zeta}} \left(\mathbf{r}_{nb}^p + \mathbf{R}_b^p \mathbf{r}_{bf}^b \right) \right) \tag{C.23}$$

where A_{wp} is the static waterplane area and $\mathbf{r}_{bf}^b$ is the vessel-fixed distance between the center of the b-frame and the center of flotation f.

Remark 4 *If the origin of vessel fixed frame b is placed in the center of flotation, obviously* $\mathbf{r}_{bf}^b = \mathbf{0}$ *and*

$$\mathbf{f}_B^b = -\rho g \begin{bmatrix} -\sin\theta \\ \sin\phi\cos\theta \\ \cos\phi\cos\theta \end{bmatrix} \left(V_0 + \frac{A_{wp}}{\cos\theta\cos\phi} z_{nb}^p \right) \tag{C.24}$$

However, if the b-frame is located somewhere else, S_x^b *and* S_y^b *are non-zero and their contributions should be accounted for.*

C.4 Buoyancy Moments

In the vessel parallel frame, the buoyancy moments are

$$\begin{aligned}
\mathbf{m}_{pB}^{p} &= -\rho g \int_{S_B} \left(\mathbf{r}_{ps}^{p} \times \mathbf{n}_{s}^{p}\right) z_{ns}^{p} dS \\
&= \rho g \int_{V} \nabla \times z_{na}^{p} \mathbf{r}_{pa}^{p} dV \\
&= \rho g \int_{V} \mathbf{S}\left(\boldsymbol{\zeta}\right) \mathbf{r}_{pa}^{p} dV \\
&= \rho g \mathbf{S}\left(\boldsymbol{\zeta}\right) \mathbf{R}_{b}^{p} \int_{V} \mathbf{r}_{ba}^{b} dV
\end{aligned} \tag{C.25}$$

And in vessel-fixed coordinates, we get

$$\begin{aligned}
\mathbf{m}_{bB}^{b} &= \mathbf{R}_{p}^{b} \mathbf{m}_{pB}^{p} \\
&= \rho g \mathbf{R}_{p}^{b} \mathbf{S}\left(\boldsymbol{\zeta}\right) \mathbf{R}_{b}^{p} \int_{V} \mathbf{r}_{ba}^{b} dV \\
&= \rho g V \mathbf{R}_{p}^{b} \mathbf{S}\left(\boldsymbol{\zeta}\right) \mathbf{R}_{b}^{p} \mathbf{r}_{bB}^{b} \\
&= -\rho g V \mathbf{S}(\mathbf{r}_{bB}^{b}) \mathbf{R}_{p}^{b} \boldsymbol{\zeta} \\
&= \mathbf{r}_{bB}^{b} \times \mathbf{R}_{p}^{b} \begin{bmatrix} 0 \\ 0 \\ -\rho g V \end{bmatrix} = \mathbf{r}_{bB}^{b} \times \mathbf{f}_{B}^{b}
\end{aligned} \tag{C.26}$$

where $\mathbf{S}$ is defined in (2.6) and V is the immediate displaced volume with $\mathbf{r}_{bB}^{b}$ as its geometric center. However, $\mathbf{r}_{bB}^{b}$ is unknown because of the changing volume V, so instead we split the volume integral into two parts just as we did for buoyancy forces:

$$\begin{aligned}
\int_{V} \mathbf{r}_{ba}^{b} dV &= \int_{V_0} \mathbf{r}_{ba}^{b} dV + \int_{V_1} \mathbf{r}_{ba}^{b} dV \\
&= V_0 \mathbf{r}_{bB}^{b} + \int_{V_1} \mathbf{r}_{ba}^{b} dV
\end{aligned} \tag{C.27}$$

where

$$\begin{aligned}
\int_{V_1} \mathbf{r}_{ba}^b dV &\approx \int_{A_{wp}} z_{wa}^b \mathbf{r}_{bs}^b dS \\
&= \int_{A_{wp}} \mathbf{r}_{bs}^b \frac{\boldsymbol{\zeta}^T}{\boldsymbol{\zeta}^T \mathbf{R}_b^p \boldsymbol{\zeta}} \left(\mathbf{r}_{nb}^p + \mathbf{R}_b^p \mathbf{r}_{bs}^b \right) dS \\
&= \frac{1}{\boldsymbol{\zeta}^T \mathbf{R}_b^p \boldsymbol{\zeta}} \int_{A_{wp}} \mathbf{r}_{bs}^b \left(z_{nb}^p + \boldsymbol{\zeta}^T \mathbf{R}_b^p \mathbf{r}_{bs}^b \right) dS \\
&= \frac{1}{\boldsymbol{\zeta}^T \mathbf{R}_b^p \boldsymbol{\zeta}} \left(z_{nb}^p \int_{A_{wp}} \mathbf{r}_{bs}^b dS + \int_{A_{wp}} \mathbf{r}_{bs}^b \boldsymbol{\zeta}^T \mathbf{R}_b^p \mathbf{r}_{bs}^b dS \right) \\
&= \frac{1}{\boldsymbol{\zeta}^T \mathbf{R}_b^p \boldsymbol{\zeta}} \left(z_{nb}^p A_{wp} \mathbf{r}_{bf}^b + \int_{A_{wp}} \mathbf{r}_{bs}^b \boldsymbol{\zeta}^T \mathbf{R}_b^p \mathbf{r}_{bs}^b dS \right) \qquad \text{(C.28)}
\end{aligned}$$

By examining the last integrand, we simplify it as follows

$$\mathbf{r}_{bs}^b \boldsymbol{\zeta}^T \mathbf{R}_b^p \mathbf{r}_{bs}^b = \mathbf{r}_{bs}^b \left(\mathbf{r}_{bs}^b \right)^T \mathbf{R}_p^b \boldsymbol{\zeta} = \begin{bmatrix} -\left(x_{bs}^b \right)^2 \sin\theta + x_{bs}^b y_{bs}^b \sin\phi \cos\theta \\ -x_{Bs}^b y_{Bs}^b \sin\theta + \left(y_{Bs}^b \right)^2 \sin\phi \cos\theta \\ 0 \end{bmatrix} \qquad \text{(C.29)}$$

Now,

$$\begin{aligned}
\int_{A_{wp}} z_{wa}^b \mathbf{r}_{bs}^b dS &= \frac{1}{\boldsymbol{\zeta}^T \mathbf{R}_b^p \boldsymbol{\zeta}} \left(z_{nb}^p A_{wp} \mathbf{r}_{bf}^b + \int_{A_{wp}} \mathbf{r}_{bs}^b \left(\mathbf{r}_{bs}^b \right)^T \mathbf{R}_p^b \boldsymbol{\zeta} dS \right) \\
&= \frac{1}{\boldsymbol{\zeta}^T \mathbf{R}_b^p \boldsymbol{\zeta}} \left(z_{nb}^p A_{wp} \mathbf{r}_{bf}^b + \left(\int_{A_{wp}} \mathbf{r}_{bs}^b \left(\mathbf{r}_{bs}^b \right)^T dS \right) \mathbf{R}_p^b \boldsymbol{\zeta} \right) \\
&= \frac{1}{\boldsymbol{\zeta}^T \mathbf{R}_B^L \boldsymbol{\zeta}} \left(A_{wp} z_{nb}^p \mathbf{r}_{bf}^b + \mathbf{H}^b \mathbf{R}_p^b \boldsymbol{\zeta} \right) \qquad \text{(C.30)}
\end{aligned}$$

where the matrix $\mathbf{H}^b = \left(\mathbf{H}^b \right)^T$ contains the moments of inertia of the static water plane surface A_{wp}. $\mathbf{H}^b$ is defined in (C.31)-(C.34)

$$\mathbf{H}^b = \int_{A_{wp}} \mathbf{r}_{bs}^b \left(\mathbf{r}_{bs}^b \right)^T dS = \begin{bmatrix} S_{xx}^b & S_{xy}^b & 0 \\ S_{xy}^b & S_{yy}^b & 0 \\ 0 & 0 & 0 \end{bmatrix} \qquad \text{(C.31)}$$

$$S_{xx}^b = \int_{A_{wp}} \left(x_{bs}^b \right)^2 dS \qquad \text{(C.32)}$$

$$S_{xy}^b = \int_{A_{wp}} x_{bs}^b y_{bs}^b dS \qquad \text{(C.33)}$$

$$S_{yy}^b = \int_{A_{wp}} \left(y_{bs}^b \right)^2 dS \qquad \text{(C.34)}$$

The moments due to buoyancy are in the p-frame given by

$$\begin{aligned}\mathbf{m}_{pB}^{p} &= \rho g V_0 \mathbf{S}(\boldsymbol{\zeta})\mathbf{R}_b^p \mathbf{r}_{bB}^b + \rho g \mathbf{S}(\boldsymbol{\zeta})\mathbf{R}_b^p \frac{1}{\boldsymbol{\zeta}^T \mathbf{R}_b^p \boldsymbol{\zeta}} \left(A_{wp} z_{nb}^p \mathbf{r}_{bf}^b + \mathbf{H}^b \mathbf{R}_p^b \boldsymbol{\zeta}\right) \\ &= \rho g \mathbf{S}(\boldsymbol{\zeta})\mathbf{R}_b^p \left\{ V_0 \mathbf{r}_{bB}^b + \frac{1}{\boldsymbol{\zeta}^T \mathbf{R}_b^p \boldsymbol{\zeta}} \left(A_{wp} z_{nb}^p \mathbf{r}_{bf}^b + \mathbf{H}^b \mathbf{R}_p^b \boldsymbol{\zeta}\right) \right\} \end{aligned} \tag{C.35}$$

and trivially in the b frame we get,

$$\begin{aligned}\mathbf{m}_{bB}^{b} &= \rho g \mathbf{R}_p^b \mathbf{S}(\boldsymbol{\zeta}) \mathbf{R}_b^p \left\{ V_0 \mathbf{r}_{bB}^b + \frac{1}{\boldsymbol{\zeta}^T \mathbf{R}_b^p \boldsymbol{\zeta}} \left(A_{wp} z_{nb}^p \mathbf{r}_{bf}^b + \mathbf{H}^b \mathbf{R}_p^b \boldsymbol{\zeta}\right) \right\} \\ &= \rho g \mathbf{S}(\mathbf{R}_p^b \boldsymbol{\zeta}) \left\{ V_0 \mathbf{r}_{bB}^b + \frac{1}{\boldsymbol{\zeta}^T \mathbf{R}_b^p \boldsymbol{\zeta}} \left(A_{wp} z_{nb}^p \mathbf{r}_{bf}^b + \mathbf{H}^b \mathbf{R}_p^b \boldsymbol{\zeta}\right) \right\} \\ &= -\rho g V_0 \mathbf{S}(\mathbf{r}_{bB}^b) \mathbf{R}_p^b \boldsymbol{\zeta} + \frac{\rho g}{\boldsymbol{\zeta}^T \mathbf{R}_b^p \boldsymbol{\zeta}} \left(\mathbf{S}(\mathbf{R}_p^b \boldsymbol{\zeta}) \mathbf{H}^b - A_{wp} z_{nb}^p \mathbf{S}(\mathbf{r}_{bf}^b) \right) \mathbf{R}_p^b \boldsymbol{\zeta} \end{aligned} \tag{C.36}$$

C.5 Summary

The results are summarized as

$$\mathbf{f}_G^b = mg \mathbf{R}_p^b \boldsymbol{\zeta} \tag{C.37}$$

$$\mathbf{m}_{bG}^b = mg \mathbf{S}(\mathbf{r}_{bG}^b) \mathbf{R}_p^b \boldsymbol{\zeta} \tag{C.38}$$

$$\mathbf{f}_B^b = -\rho g \left(V_0 \mathbf{R}_p^b \boldsymbol{\zeta} + A_{wp} \frac{\mathbf{R}_p^b \boldsymbol{\zeta} \boldsymbol{\zeta}^T}{\boldsymbol{\zeta}^T \mathbf{R}_b^p \boldsymbol{\zeta}} \left(\mathbf{r}_{nb}^p + \mathbf{R}_b^p \mathbf{r}_{bf}^b \right) \right) \tag{C.39}$$

$$\mathbf{m}_{bB}^b = -\rho g V_0 \mathbf{S}(\mathbf{r}_{bB}^b) \mathbf{R}_p^b \boldsymbol{\zeta} + \frac{\rho g}{\boldsymbol{\zeta}^T \mathbf{R}_b^p \boldsymbol{\zeta}} \left(\mathbf{S}(\mathbf{R}_p^b \boldsymbol{\zeta}) \mathbf{H}^b - A_{wp} z_{nb}^n \mathbf{S}(\mathbf{r}_{bf}^b) \right) \mathbf{R}_p^b \boldsymbol{\zeta} \tag{C.40}$$

The sum of gravity and buoyancy forces and moments is the complete restoring force description

$$\boxed{\begin{aligned} \mathbf{f}^b &= -\rho g A_{wp} \tfrac{\mathbf{R}_p^b \boldsymbol{\zeta} \boldsymbol{\zeta}^T}{\boldsymbol{\zeta}^T \mathbf{R}_b^p \boldsymbol{\zeta}} \left(\mathbf{r}_{nb}^p + \mathbf{R}_b^p \mathbf{r}_{bf}^b \right) \\ \mathbf{m}^b &= mg \mathbf{S}(\mathbf{r}_{bG}^b - \mathbf{r}_{bB}^b) \mathbf{R}_p^b \boldsymbol{\zeta} \\ &\quad + \tfrac{\rho g}{\boldsymbol{\zeta}^T \mathbf{R}_b^p \boldsymbol{\zeta}} \left(\mathbf{S}(\mathbf{R}_p^b \boldsymbol{\zeta}) \mathbf{H}^b - A_{wp} \mathbf{S}(\mathbf{r}_{bf}^b) \boldsymbol{\zeta}^T \mathbf{r}_{nb}^n \right) \mathbf{R}_p^b \boldsymbol{\zeta} \end{aligned}} \tag{C.41}$$

C.5.1 Underwater Vehicles

For a completely submerged body the waterplane integrals are all zero and V_0 is the volume of the entire craft, so we get

$$\mathbf{f}_B^b = -\rho g V_0 \mathbf{R}_p^b \boldsymbol{\zeta} \tag{C.42}$$

$$\mathbf{m}_{bB}^b = -\rho g V_0 \mathbf{S}(\mathbf{r}_{bB}^b) \mathbf{R}_p^b \boldsymbol{\zeta} \tag{C.43}$$

where $\mathbf{r}_{bB}^b$ is the vessel-fixed center of buoyancy and V_0 is the displacement. Gravity forces and moments are the same as in the general case, see (C.37)-(C.38).

A closer look on $\mathbf{m}_{bB}^b$ reveals that

$$\mathbf{m}_{bB}^b = \mathbf{r}_{bB}^b \times \mathbf{R}_p^b \mathbf{f}_B^p = \mathbf{r}_{bB}^b \times \mathbf{f}_B^b \tag{C.44}$$

which is simply the cross product of the center of buoyancy with the buoyancy force.

Equivalently,

$$\begin{bmatrix} \mathbf{f}_B^b \\ \mathbf{m}_{bB}^b \end{bmatrix} = -\rho g V_0 \mathbf{T}(\mathbf{r}_{bB}^b) \mathbf{R}_p^b \boldsymbol{\zeta} \tag{C.45}$$

These expressions are equivalent to the ones in Fossen (2002) and Sagatun (1992).

C.6 Surface Vessels

In this section we provide two approximations of (C.41) for surface vessels that show they are both special cases of the general nonlinear formulation. Furthermore, the concept of *metacentric height* is identified.

We consider vessels that are neutrally buoyant, which means that the pitch and roll angles are zero at equilibrium. Moreover, $V_0 = m/\rho$ and $\rho g V_0 = mg = W$.

For vessels symmetric about the xz-plane

$$\mathbf{r}_{bf}^b = \begin{bmatrix} S_x^b & 0 & 0 \end{bmatrix}^T \tag{C.46}$$

$$\mathbf{r}_{bG}^b = \begin{bmatrix} x_{bG}^b & 0 & z_{bG}^b \end{bmatrix}^T \tag{C.47}$$

$$\mathbf{r}_{bB}^b = \begin{bmatrix} x_{bB}^b & 0 & z_{bB}^b \end{bmatrix}^T \tag{C.48}$$

Furthermore (Newman 1977), $S_{xy}^b = 0$ such that the water plane inertia matrix $\mathbf{H}^b$ is reduced to

$$\mathbf{H}^b = \mathrm{diag}(S_{xx}^b, S_{yy}^b, 0) \tag{C.49}$$

C.6.1 Linearization

The linearization is performed on a neutrally buoyant xz-symmetric vessel in order to obtain the linear term $\mathbf{G}\boldsymbol{\eta}$ in the vessel-fixed dynamics. Consequently, the x- and y-distances between CG and CB have to be zero

$$x_{GB}^b = x_{bB}^b - x_{bG}^b = 0 \tag{C.50}$$

$$y_{GB}^b = y_{bB}^b - y_{bG}^b = 0 \tag{C.51}$$

A3 Angular displacements can be considered small, $\boldsymbol{\theta}_{pb} \approx \mathbf{0}$.

This means that $\sin\alpha = \alpha$, and $\cos\alpha = 1$ are appropriate approximations and we can substitute $\mathbf{R}_b^p$ and $\mathbf{R}_p^b$ with their respective Taylor expansions

$$\begin{aligned} \mathbf{R}_b^p &\approx \mathbf{I} + \mathbf{S}(\boldsymbol{\theta}_{pb}) && \text{(C.52)} \\ \mathbf{R}_p^b &\approx \mathbf{I} - \mathbf{S}(\boldsymbol{\theta}_{pb}) && \text{(C.53)} \end{aligned}$$

Hence, the restoring forces become

$$\begin{aligned} \mathbf{f}^b &= -\rho g A_{wp} \frac{\mathbf{R}_p^b \boldsymbol{\zeta}\boldsymbol{\zeta}^T}{\boldsymbol{\zeta}^T \mathbf{R}_b^p \boldsymbol{\zeta}} \left(\mathbf{r}_{nb}^p + \mathbf{R}_b^p \mathbf{r}_{bf}^b\right) \\ &\approx -\rho g A_{wp} \left(\mathbf{I} - \mathbf{S}(\boldsymbol{\theta}_{pb})\right) \boldsymbol{\zeta}\boldsymbol{\zeta}^T \left(\mathbf{r}_{nb}^p + \left(\mathbf{I} + \mathbf{S}(\boldsymbol{\theta}_{pb})\right) \mathbf{r}_{bf}^b\right) \\ &= -\rho g A_{wp} \left(\boldsymbol{\zeta}\boldsymbol{\zeta}^T \left(\mathbf{r}_{nb}^p + \left(\mathbf{I} + \mathbf{S}(\boldsymbol{\theta}_{pb})\right) \mathbf{r}_{bf}^b\right) - \mathbf{S}(\boldsymbol{\theta}_{pb}) \boldsymbol{\zeta}\boldsymbol{\zeta}^T \left(\mathbf{r}_{nb}^p + \mathbf{r}_{bf}^b\right)\right) \\ &\approx -\rho g A_{wp} \left(\boldsymbol{\zeta}\boldsymbol{\zeta}^T \left(\mathbf{r}_{nb}^p + \mathbf{r}_{bf}^b - \mathbf{S}(\mathbf{r}_{bf}^b)\boldsymbol{\theta}_{pb}\right) + \mathbf{S}(\boldsymbol{\zeta}\boldsymbol{\zeta}^T \mathbf{r}_{bf}^b)\boldsymbol{\theta}_{pb}\right) \\ &= -\rho g A_{wp} \boldsymbol{\zeta}\boldsymbol{\zeta}^T \left(\mathbf{r}_{nb}^p + \mathbf{r}_{bf}^b\right) - \rho g A_{wp} \left(\boldsymbol{\zeta}\boldsymbol{\zeta}^T \mathbf{S}(\mathbf{r}_{bf}^b) - \mathbf{S}(\boldsymbol{\zeta}\boldsymbol{\zeta}^T \mathbf{r}_{bf}^b)\right) \boldsymbol{\theta}_{pb} \quad \text{(C.54)} \end{aligned}$$

Substituting that $\mathbf{r}_{bf}^b = \left[S_x^b, 0, 0\right]^T$ we get

$$\begin{aligned} \mathbf{f}^b &\approx -\rho g A_{wp} \boldsymbol{\zeta}\boldsymbol{\zeta}^T \mathbf{r}_{nb}^n + \rho g A_{wp} \left(\mathbf{S}(\boldsymbol{\zeta}\boldsymbol{\zeta}^T \mathbf{r}_{bf}^b) - \boldsymbol{\zeta}\boldsymbol{\zeta}^T \mathbf{S}(\mathbf{r}_{bf}^b)\right) \boldsymbol{\theta}_{pb} \\ &= -\mathbf{G}_{11} \mathbf{r}_{nb}^n - \mathbf{G}_{12} \boldsymbol{\theta}_{pb} \quad \text{(C.55)} \end{aligned}$$

where

$$\begin{aligned} \mathbf{G}_{11} &= \rho g A_{wp} \mathrm{diag}(0, 0, 1) && \text{(C.56)} \\ \mathbf{G}_{12} &= \rho g \begin{bmatrix} 0 & 0 & 0 \\ 0 & 0 & 0 \\ 0 & S_x^b & 0 \end{bmatrix} && \text{(C.57)} \end{aligned}$$

Now, for the restoring moments we employ

$$\begin{aligned} \mathbf{R}_p^b \boldsymbol{\zeta} &\approx \boldsymbol{\zeta} - \mathbf{S}(\boldsymbol{\theta}_{pb})\boldsymbol{\zeta} = \boldsymbol{\zeta} + \mathbf{S}(\boldsymbol{\zeta})\boldsymbol{\theta}_{pb} \\ \boldsymbol{\zeta}^T \mathbf{R}_b^p \boldsymbol{\zeta} &\approx 1 \end{aligned} \quad \text{(C.58)}$$

Hence, by using $\mathbf{H}^b\boldsymbol{\zeta} = \mathbf{0}$ we are disregarding all terms nonlinear in the state-variables.

$$\begin{aligned}
\mathbf{m}^b &= mg\mathbf{S}\left(\mathbf{r}^b_{bG} - \mathbf{r}^b_{bB}\right)\mathbf{R}^b_p\boldsymbol{\zeta} + \frac{\rho g}{\boldsymbol{\zeta}^T\mathbf{R}^p_b\boldsymbol{\zeta}}\left(\mathbf{S}(\mathbf{R}^b_p\boldsymbol{\zeta})\mathbf{H}^b - A_{wp}z^n_{nb}\mathbf{S}(\mathbf{r}^b_{bf})\right)\mathbf{R}^b_p\boldsymbol{\zeta} \\
&\approx mg\mathbf{S}\left(\mathbf{r}^b_{bG} - \mathbf{r}^b_{bB}\right)(\boldsymbol{\zeta} + \mathbf{S}(\boldsymbol{\zeta})\boldsymbol{\theta}_{pb}) \\
&\quad + \rho g\left(\mathbf{S}(\mathbf{R}^b_p\boldsymbol{\zeta})\mathbf{H}^b - A_{wp}z^n_{nb}\mathbf{S}(\mathbf{r}^b_{bf})\right)(\boldsymbol{\zeta} + \mathbf{S}(\boldsymbol{\zeta})\boldsymbol{\theta}_{pb}) \\
&\approx mg\mathbf{S}(\mathbf{r}^b_{bG} - \mathbf{r}^b_{bB})\boldsymbol{\zeta} + mg\mathbf{S}(\mathbf{r}^b_{bG} - \mathbf{r}^b_{bB})\mathbf{S}(\boldsymbol{\zeta})\boldsymbol{\theta}_{pb} \\
&\quad + \rho g\left(\mathbf{S}(\mathbf{R}^b_p\boldsymbol{\zeta})\mathbf{H}^b\mathbf{S}(\boldsymbol{\zeta})\boldsymbol{\theta}_{pb} - A_{wp}z^n_{nb}\mathbf{S}(\mathbf{r}^b_{bf})\boldsymbol{\zeta}\right) \\
&\approx mg\mathbf{S}(\mathbf{r}^b_{bG} - \mathbf{r}^b_{bB})\boldsymbol{\zeta} + mg\mathbf{S}(\mathbf{r}^b_{bG} - \mathbf{r}^b_{bB})\mathbf{S}(\boldsymbol{\zeta})\boldsymbol{\theta}_{pb} \\
&\quad + \rho g\left(\mathbf{S}(\boldsymbol{\zeta} + \mathbf{S}(\boldsymbol{\zeta})\boldsymbol{\theta}_{pb})\mathbf{H}^b\mathbf{S}(\boldsymbol{\zeta})\boldsymbol{\theta}_{pb} - A_{wp}\mathbf{S}(\mathbf{r}^b_{bf})\boldsymbol{\zeta}\boldsymbol{\zeta}^T\mathbf{r}^n_{nb}\right) \\
&\approx mg\mathbf{S}(\mathbf{r}^b_{bG} - \mathbf{r}^b_{bB})\boldsymbol{\zeta} - \rho g A_{wp}\mathbf{S}(\mathbf{r}^b_{bf})\boldsymbol{\zeta}\boldsymbol{\zeta}^T\mathbf{r}^n_{nb} + mg\mathbf{S}(\mathbf{r}^b_{bG} - \mathbf{r}^b_{bB})\mathbf{S}(\boldsymbol{\zeta})\boldsymbol{\theta}_{pb} \\
&\quad + \rho g\mathbf{S}(\boldsymbol{\zeta})\mathbf{H}^b\mathbf{S}(\boldsymbol{\zeta})\boldsymbol{\theta}_{pb} \\
&= \mathbf{m}^b_0 - \mathbf{G}_{21}\mathbf{r}^n_{nb} - \mathbf{G}_{22}\boldsymbol{\theta}_{pb} \qquad \text{(C.59)}
\end{aligned}$$

where

$$\begin{aligned}
\mathbf{m}^b_0 &= mg\mathbf{S}(\mathbf{r}^b_{bG} - \mathbf{r}^b_{bB})\boldsymbol{\zeta} &\text{(C.60)}\\
\mathbf{G}_{21} &= -\rho g A_{wp}\mathbf{S}(\mathbf{r}^b_{bf})\boldsymbol{\zeta}\boldsymbol{\zeta}^T &\text{(C.61)}\\
\mathbf{G}_{22} &= -mg\mathbf{S}(\mathbf{r}^b_{bG} - \mathbf{r}^b_{bB})\mathbf{S}(\boldsymbol{\zeta}) - \rho g\mathbf{S}(\boldsymbol{\zeta})\mathbf{H}^b\mathbf{S}(\boldsymbol{\zeta}) &\text{(C.62)}
\end{aligned}$$

On component form we get

$$\mathbf{G}_{21} = \rho g\begin{bmatrix} 0 & 0 & 0 \\ 0 & 0 & S^b_x \\ 0 & 0 & 0 \end{bmatrix} \qquad \text{(C.63)}$$

$$\begin{aligned}
\mathbf{G}_{22} &= -mg\mathbf{S}(\mathbf{r}^b_{bG} - \mathbf{r}^b_{bB})\mathbf{S}(\boldsymbol{\zeta}) - \rho g\mathbf{S}(\boldsymbol{\zeta})\mathbf{H}^b\mathbf{S}(\boldsymbol{\zeta}) \\
&= -mg\begin{bmatrix} -z^b_{bG} + z^b_{bB} & 0 & 0 \\ 0 & -z^b_{bG} + z^b_{bB} & 0 \\ x^b_{bG} - x^b_{bB} & 0 & 0 \end{bmatrix} + \rho g\begin{bmatrix} S^b_{yy} & 0 & 0 \\ 0 & S^b_{xx} & 0 \\ 0 & 0 & 0 \end{bmatrix} \\
&= \rho g\mathrm{diag}(V_0 z^b_{BG} + S^b_{yy}, V_0 z^b_{BG} + S^b_{xx}, 0) \qquad \text{(C.64)}
\end{aligned}$$

where we recognize the transverse and longitudinal metacenters

$$\begin{aligned}
GM_T \triangleq z^b_{GB} + \frac{1}{V_0}S^b_{yy} &= \left(z^b_{bG} - z^b_{bB}\right) + \frac{1}{V_0}S^b_{yy} &\text{(C.65)}\\
GM_L \triangleq z^b_{GB} + \frac{1}{V_0}S^b_{xx} &= \left(z^b_{bG} - z^b_{bB}\right) + \frac{1}{V_0}S^b_{xx} &\text{(C.66)}
\end{aligned}$$

such that

$$\mathbf{G}_{22} = \rho g V_0\mathrm{diag}(GM_T, GM_L, 0) \qquad \text{(C.67)}$$

Keep in mind that the z-axis is positive down such that $z^b_{GB} > 0$ if CG is below CB.

For the bias term

$$\mathbf{m}^b_0 = mg\mathbf{S}(\mathbf{r}^b_{bG} - \mathbf{r}^b_{bB})\boldsymbol{\zeta} \tag{C.68}$$

$$= mg \begin{bmatrix} 0 & -z^b_{bG} + z^b_{bB} & 0 \\ z^b_{bG} - z^b_{bB} & 0 & -x^b_{bG} + x^b_{bB} \\ 0 & x^b_{bG} - x^b_{bB} & 0 \end{bmatrix} \begin{bmatrix} 0 \\ 0 \\ 1 \end{bmatrix} = \mathbf{0} \tag{C.69}$$

Appendix D

Thruster-Rudder Modeling

D.1 Introduction

For centuries rudders have been used to control the heading of ships in transit and even today when rotatable propeller devices, so called PODs, are becoming more and more common, a rudder will in many situations still be the natural choice for steering a marine craft.

In contrast to a POD, or any other active device, a rudder looses its entire effect as the velocity decreases. This means that rudders can not directly be used in low speed operations such as dynamic positioning. The rudder will not be able to produce any force neither laterally (lift) nor longitudinally (drag) unless it is located in the induced jet from an active device, for instance a propeller. This means that a pair consisting of a longships propeller and a rudder is unable to produce a sideforce without simultaneously having a longships component: At zero speed, the lateral force will be a function of the longitudinal force produced by the propeller.

Rudders are usually placed in the propeller slipstream. This has several advantages (Brix 1993):

1. A profiled rudder increases propeller efficiency.
2. In steady ahead motion, rudder forces will be typically two times higher compared to a rudder outside the slipstream.
3. For a stationary or slowly moving vessel, substantial rudder forces may be generated by propeller action.

We aim to use the latter advantage in low speed operations such as positioning and docking. The objective is to devise a fundamental mapping H for a propeller-rudder device that relates nominal propeller thrust T, rudder angle δ and forward

speed u on one side and the produced surge and sway forces (F_x and F_y respectively) on the other

$$(F_x, F_y) = H(T, \delta, u) \tag{D.1}$$

The mapping H must be "suitable for control design", which means that we focus on

1. *Structural accuracy.* The mapping must be able to predict with acceptable accuracy all dominating effects.

2. *Structural simplicity.* A ship controller will apply a specified force that has to be distributed to the propulsion system. This means that we need the "inverse" of H

   $$(T, \delta) = H^{-1}(F_x, F_y, u) \tag{D.2}$$

   Therefore, we seek an H that is simple to invert or at least we seek a mapping for which a reasonably simple approximation of the inverse exists.

Finding the inverse mapping H^{-1} is vital for the *thrust allocation problem*, which is the mapping between commanded force $\boldsymbol{\tau}_c$ from the controller to thruster/rudder set-points (typically pitch/RPM set-points and desired angles), see Chapter 7. The majority of low-speed applications do not use rudders actively. This has two explanations. First, vessels able to perform dynamic positioning are *overactuated*, and using rudders in a positioning operation is thus superfluous. Consequently, dealing with nonlinear and complex mappings H was unnecessary. Second, the priority for most low-speed designs has been safety and controllability rather than minimizing fuel consumption.

It is not apparent that advanced propeller-rudder models have an analytic solution to the inverse (D.2) because of the complexity of the $H(T, \delta, u)$. Even though numerical solvers could be applied relatively simple, analytical approximations should do the job well enough because the mapping is, to some extent, uncertain. A numerical, and thereby computationally more complicated, solution is not always the best approach. We show that with a minimum of knowledge a smooth inverse mapping can be derived.

Using the rudders actively in a positioning operation is purely beneficial; reducing costs and gas emissions without compromising safety. Moreover, we obtain an extra degree of freedom to generate forces that otherwise had to be produced by a propeller. Also, active rudder usage can reduce the required number of tunnel thrusters, which implies that ships meant for transit will be able to perform for instance DP and automatic docking more easily. This entire refinement of control systems technology relies on a propeller-rudder model "suitable for control design".

D.1.1 Previous Work

Due to the complex fluid flow patterns, propeller behavior is a science that depends heavily on empirical results. However, some general results on propeller

action can be described with rather simple physical laws like Rankine's principle for conservation of momentum (consult Carlton (1994) for a historical review). Rankine modelled the propeller as an "impulse disc". By using Bernoulli's theorem (White 1999) he was able to relate delivered propeller thrust forces to axial fluid flow through a uniform propeller disc. Later R. E. Froude included fluid rotation, and the synthesis is often called Rankine-Froude momentum theory. Rankine's momentum theory is fundamental material covered by most textbooks on naval architecture (Gillmer and Johnson 1982) and fluid dynamics (White 1999). Despite its many shortcomings, the momentum theory can be used to describe a variety of the observed phenomena, for instance force and axial flow velocity during transient thrusting (Yoerger *et al.* 1990, Healey *et al.* 1995, Whitcomb and Yoerger 1999, Bachmayer *et al.* 2000, Fossen and Blanke 2000, Blanke *et al.* 2000). This is perhaps a bit surprising since the momentum theory is a valid for static flows only.

The concept of an actuator disc has been extended to study the flow field around propellers, see Breslin and Andersen (1994) and references therein. Greenberg and Powers (Greenberg and Powers 1970, Greenberg 1972) computed streamlines generated by actuator discs at low speed, so-called heavily loaded discs. They found that the streamtube pattern was insensitive to applied propeller thrust when the distribution of circulation was uniform across the disk. Considering also a non-uniform radial distribution of thrust, which reduce the frictional losses (Munk 1922), they were able to show that higher thrusting levels resulted in a sharper contraction of the slipstream.

Rudder modeling and design is closely related to the study of airfoils. In spite being a three-dimensional problem, more convenient methods using two-dimensional flow are sufficient for studying the phenomenon. The simplest three-dimensional wing theory is that based on the concept of the *lifting line* (Prandtl 1923) where the wing is replaced by a straight line along the span. The wing is constructed as the spanwise integral of 2D wing sections. By separating the effects of the symmetric (along the chord) *thickness distribution* from the effect caused by the *mean camber line*, see e.g. Newman (1977) for a linearized proof, NACA systematized the performance for a variety of 2D foil shapes (Abbot and von Doenhoff 1959). A direct consequence is that the lift force generated by profiles without a camber, such as rudders, can be analyzed by thin plates and therefore static rudder forces may be fairly described by very simple models. Parameters can also be predicted approximately, although exact parameters are still found through experiments and curve-fitting. For instance, Brix (1993) suggests using trigonometric functions for rudder lift and drag coefficients $C_L(\alpha)$ and $C_D(\alpha)$.

Compared to the vast amount of publications and textbooks on propellers and airfoils, the field of *propeller and rudder interaction* is limited. One recent series of wind tunnel experiments were conducted by Molland and co-workers in the early 1990s (Molland and Turnock 1993, Molland and Turnock 1996). Unfortunately, due to the fact that it was a lifting line approach, the results were parameterized using the advance number, that is the ratio between advance speed and propeller shaft velocity, and are consequently hard to apply at zero speed. As pointed out by Kracht commenting on Molland and Turnock (1993), this could have been

circumvented using a different reference speed. However, there is not a universal presentation format which accurately reflects the physics over the entire range of operation and especially the bollard condition. In a follow-up paper (Molland and Turnock 1994) the authors focused more on zero advance ratio.

The integration of advanced propeller rudder models, that is the mapping (D.1), into ship simulators have been treated by several authors. In particular, Shouji *et al.* (1990) used a model in six quadrants of operation and in Molland *et al.* (1996) the authors suggest a two-regime algorithm for low and standard speed. Still, we were unable to find any sophisticated "inverse mappings" (D.2). This suggests that this problem has not yet been properly addressed.

D.1.2 Outline

The next section is dedicated to standard hydrodynamic concepts such as momentum theory and standard foil-theory to deduce a static mapping structure H of a propeller-rudder pair that incorporates what is believed to be the most dominating effects. In Section D.3 we discuss practical issues and suggest a pragmatic model structure for thrust and rudder forces. Section D.3 discusses an inverse mapping as well as an algorithm for allocation of desired forces the propeller rudder couple should deliver. The conjecture introduced in Section D.3 enables us to explain the experienced nonlinear increase in rudder lift and drag observed in bollard-pull test of a model-ship reported in Section D.5. Concluding remarks are given in Section D.6.

D.2 Modeling

First, we summarize Rankine's theory on axial flow. Then, a few remarks about fluid rotation is made.

D.2.1 Axial Flow

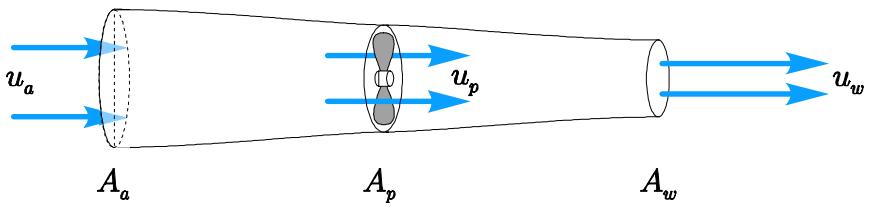

Figure D.1: Bernoulli tube with definitions of axial fluid velocity far upstream u_a, through the propeller u_p and far downstream u_w.

Using Bernoulli's equation on the linear flow upstream and downstream of the

propeller disc (Figure D.1), we have that

$$p_a + \frac{1}{2}\rho u_a^2 = p_u + \frac{1}{2}\rho u_p^2 \tag{D.3}$$

$$p_a + \frac{1}{2}\rho u_w^2 = p_d + \frac{1}{2}\rho u_p^2 \tag{D.4}$$

where p_a, p_u and p_d are the ambient pressure and the pressures upstream and downstream of the propeller disc. Delivered thrust T is the pressure difference multiplied with propeller disc area A_p

$$T = A_p\left(p_d - p_u\right) = \frac{1}{2}\rho A_p\left(u_w^2 - u_a^2\right) \tag{D.5}$$

By assumption the power absorbed by the propeller and the delivered thrust are equal to the increase in kinetic energy of the slipstream per time unit and the increase of axial momentum, respectively

$$P_D = \frac{1}{2}\dot{m}\left(u_w^2 - u_a^2\right) \tag{D.6}$$

$$T = \dot{m}\left(u_w - u_a\right) \tag{D.7}$$

where $\dot{m}$ is the mass flow per time unit through the propeller disc, that is $\dot{m} = \rho A_p u_p$. We also know that the work per unit time by the propeller equals $P_D = Tu_p$ such that the velocities through the disc and far downstream are

$$u_p = \frac{1}{2}\left(u_w + u_a\right) \tag{D.8}$$

$$u_w = 2u_p - u_a \tag{D.9}$$

which shows that the axial flow velocity through the disc is the mean of the velocities far upstream and downstream in the wake.

Hence,

$$T = 2\rho A_p u_p\left(u_p - u_a\right) \tag{D.10}$$

If the ship is surging at a certain forward velocity u, the ambient water velocity u_a can be expressed using the wake fraction number w

$$u_a = \left(1 - w\right)u \tag{D.11}$$

From (D.10) we get that the mean velocity of the axial flow through the propeller disc is

$$u_p^2 - u_a u_p - \frac{T}{2\rho A_p} = 0 \tag{D.12}$$

$$u_p = \frac{1}{2}\left(u_a + \sqrt{u_a^2 + \frac{2T_{\max}}{\rho A_p}T_{rel}}\right) \tag{D.13}$$

We use normalized thrust $T = T_{\max}T_{rel}$. If $u_a = 0$ we are left with

$$u_p|_{u_a=0} = \frac{1}{2}\sqrt{\frac{2T_{\max}}{\rho A_p}T_{rel}} \tag{D.14}$$

D.2.2 Slipstream Radius and Mean Velocity

The area of the propeller wake or the slipstream, will decrease downstream by the principle of mass conservation. The mass-flow through two arbitrary cross-sections i and j are related by

$$\rho A_i u_i = \rho A_j u_j \tag{D.15}$$

where u_i and u_j are the mean velocities through the respective sections. Evidently, the radius of the wake far downstream becomes

$$r_w = \sqrt{\frac{A_w}{\pi}} = \sqrt{\frac{A_p \frac{u_p}{u_w}}{\pi}} = r_p \sqrt{\frac{u_p}{2u_p - u_a}} \tag{D.16}$$

Because the rudder is located quite close to the propeller, see Figure D.2, it is not very likely that the wake has contracted completely, that is $r_p \geq r_r \geq r_w$. An approximation of the radius at an arbitrary point located x meters behind the propeller disc is given as (Brix 1993)

$$r(x) = r_p \frac{0.14\left(\frac{r_w}{r_p}\right)^3 + \frac{r_w}{r_p}\left(\frac{x}{r_p}\right)^{1.5}}{0.14\left(\frac{r_w}{r_p}\right)^3 + \left(\frac{x}{r_p}\right)^{1.5}} \tag{D.17}$$

Inserting (D.9) and (D.16) we get

$$r(x, u_p, u_a) = r_p \sqrt{\frac{u_p}{2u_p - u_a}} \frac{0.14\left(\frac{u_p}{2u_p - u_a}\right) + \left(\frac{x}{r_p}\right)^{\frac{3}{2}}}{0.14\left(\frac{u_p}{2u_p - u_a}\right)^{\frac{3}{2}} + \left(\frac{x}{r_p}\right)^{\frac{3}{2}}} \tag{D.18}$$

At zero advance speed ($u_a = 0$) the wake geometry becomes independent of thrust T (equivalently u_p)

$$r(x)|_{u_a=0} = \frac{r_p}{\sqrt{2}} \frac{0.14\frac{1}{2} + \left(\frac{x}{r_p}\right)^{1.5}}{0.14\left(\frac{1}{2}\right)^{1.5} + \left(\frac{x}{r_p}\right)^{1.5}} \tag{D.19}$$

From the conservation of mass (D.15) the rudder flow velocity u_r is proportional to u_p and proportional to the square-root of the thrust T.

$$u_r \overset{u_a=0}{\propto} u_p \quad , \quad u_r^2 \overset{u_a=0}{\propto} T \tag{D.20}$$

Remark 5 *In practice, the radius will be somewhat larger due to turbulent mixing with the surrounding fluid. A correction of the ideal radius can be approximated by (Brix 1993)*

$$\hat{r}(x) = r(x) + 0.15 \frac{u_x - u_a}{u_x + u_a} x \tag{D.21}$$

where u_x is the mean velocity through the disc given by $r(x)$

$$u_x(x) = u_p \left(\frac{r_p}{r(x)} \right)^2 \tag{D.22}$$

By conservation of mass (D.15), the corrected velocity $\hat{u}(x) \leq u_x(x)$ is

$$\hat{u}_x(x) = u_p \left(\frac{r_p}{\hat{r}(x)} \right)^2 \tag{D.23}$$

It must be remarked that $\hat{r}(x)$ and $\hat{u}(x)$ are local approximations only valid for "small" distances x. For example, if $u_a = 0$, we see that $\hat{r}(x)$ would grow linearly in x.

What is important from a low-speed point of view, $u_a = 0$ and $|u_p| > 0$, is that, corrected for mixing or not, the formulas predict that the shape of the wake tube is independent of thrust T.

D.2.3 Rudder Forces

The forces generated by a rudder in a fluid flow can be calculated using traditional foil theory. In this section we focus primarily on rudder forces generated by the propeller, that is when the propeller generates the passing flow. First, we will use axial momentum theory to develop an expression for lift and drag forces on the foil and then we will make a few comments on tangential flow effects.

Lift and Drag Forces

A foil submerged in a moving fluid will experience lift and drag forces. Kutta-Joukowski's theorem states that the lift is perpendicular to the incoming flow and that drag is tangential to it. For 2D problems, cross-sections with span dz in a uniform flow, the lift force dL and drag dD are proportional to the square of the inflow velocity u

$$dL = \frac{1}{2}\rho c C'_L(\alpha) u^2 dz \tag{D.24}$$

$$dD = \frac{1}{2}\rho c C'_D(\alpha) u^2 dz \tag{D.25}$$

$C_L(\alpha)$ and $C_D(\alpha)$ are the lift and drag coefficients respectively parameterized as function of the angle of attack α. The product of the chord length c and dx becomes the locally projected area of the rudder that is being exposed to the flow. The total lift L and drag D is obtained by integration along the span (z-axis)

$$L = \int_{-\frac{b}{2}}^{\frac{b}{2}} dL = \frac{1}{2}\rho \int_{-\frac{b}{2}}^{\frac{b}{2}} c(z) C'_L(\alpha, z) u^2(z) dz \tag{D.26}$$

$$D = \int_{-\frac{b}{2}}^{\frac{b}{2}} dD = \frac{1}{2}\rho \int_{-\frac{b}{2}}^{\frac{b}{2}} c(z) C'_D(\alpha, z) u^2(z) dz \tag{D.27}$$

where b is the width of the foil, or equivalently the rudder height. We have also assumed that streamtube radius r_r is constant past the chord.

For a rudder situated in the propeller race, as in Figure D.2, two-dimensional theory will provide a plausible approximation because the rudder is wider than the wake tube. If the span is smaller than the slipstream radius r_r, vortices will be generated at the tips.

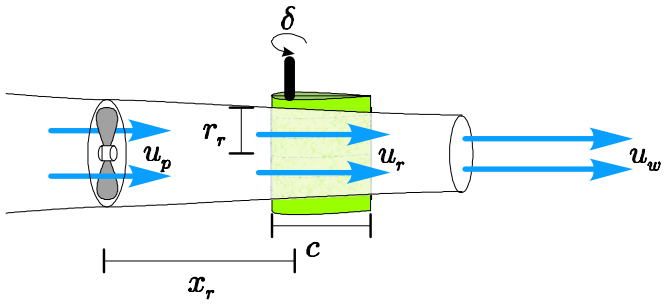

Figure D.2: Rudder located a distance x_r downstream in the wake of a propeller.

D.2.4 The Influence of Tangential Velocity

A rotating propeller will induce not only an axial velocity component as described in the previous section, but it will also force the passing fluid to rotate. The Rankine-Froude momentum approach derive that, as for axial flow, the angular fluid velocity through a propeller disc equals the mean of the far upstream and downstream velocities. Let ω_a, ω_p and ω_w denote angular velocities far upstream, at the propeller disc and far downstream respectively. Then, it can be shown that

$$\omega_p = \frac{1}{2}(\omega_a + \omega_w) \tag{D.28}$$

The angular velocity component does not contribute to the thrusting force; the angular momentum is a loss factor. The increased fluid velocity in the propeller race yields a lower pressure behind the disc and hence the pressure increase across the disc forcing the vessel forward decreases. From a propeller blade section point of view, the rotational velocity components reduce the local angle of attack, and hence propeller blade lift forces are reduced also. On the other hand, it is well documented that devices such as rudders placed in a propeller wake, or even upstream to the propeller, will reduce ω_p compared to the rotation the propeller would have caused if the rudder was removed. This means that, neglecting the rudder drag forces, the pressure behind the propeller disc will rise due to lower fluid velocity. Again, this will increase the propeller efficiency rate (Brix 1993).

We shall not pursue this tangential velocity component further except pointing out that induced lift force will be asymmetrically distributed along the rudder span.

This is due to the rotation's influence on the rudder's *effective angle of attack*. However, for rudder angles encountered in low speed vessel maneuvering, and if the rudder is located in the center of the wake tube, the net sum is zero. Consequently, the effect of rotation can be incorporated in the lift and drag coefficients $C_L(\alpha)$ and $C_D(\alpha)$.

D.3 Pragmatic Model

Due to the small dimensions and thrust forces involved the experiments will experience scale effects because the flow regime will be laminar rather than turbulent. This is supported by rough estimates of the Reynholds numbers R_n involved. Again, this should motivate a more detailed description for propeller thrust and rudder lift and drag. On the other, doing so constructively would for a number of reasons be impossible with our equipment:

- The geometry was too complex (propeller and rudder are mounted on a hull).
- The pressure sensor and laboratory equipment in general were unsuited for such studies.
- We had only a single propller and rudder available. The results could not be generalized.

These limitations imposed taking a more pragmatic path towards identifying the propeller rudder characteristics, and that is the topic of this subsection.

D.3.1 Ideal Model at Zero Advance Speed

When it is assumed that the velocoity profile inside the wake tube is independent of applied thrust, the propeller induced lift and drag become

$$L = \frac{1}{2}\rho A C_L(\delta) u_r^2 \tag{D.29}$$

$$D = \frac{1}{2}\rho A C_D(\delta) u_r^2 \tag{D.30}$$

where $A = cr_r$ is the area of the rudder exposed to the wake and $C_L(\delta)$ and $C_D(\delta)$ are the resulting lift and drag coefficients incorporating the effect of the velocity profile.

We suggest using a model quadratic in shaft speed for the propellers' nominal thrust

$$T_i = \begin{cases} k_{iTp}\omega_i^2 & \omega \geq 0 \\ k_{iTn}|\omega_i|\omega_i & \omega \leq 0 \end{cases} \tag{D.31}$$

where k_{iTp} and k_{iTn} are to be determined empirically.

D.3.2 Velocity Correction Factors

To handle variations in lift and drag caused by increasing R_n we introduce velocity corrections $\Delta L(T)$ and $\Delta D(T)$ for lift and drag respectively such that

$$L(T,\delta,u) = \frac{1}{2}\rho A C_L(\delta) u_r^2 \Delta L(T) \tag{D.32}$$

$$D(T,\delta,u) = \frac{1}{2}\rho A C_D(\delta) u_r^2 \Delta D(T) \tag{D.33}$$

Theoretically they should be functions of R_n or u_r, meaning that ΔL and ΔD should be used around zero speed. Observe also that these corrections, $\Delta D(T)$ in particular, will incorporate the scale effects effecting the propeller as well. This is the price paid for the simple quadratic thrust characteristics. Later we shall discuss the shapes of $C_L(\delta)$, $C_D(\delta)$, $\Delta L(T)$ and $\Delta D(T)$.

D.4 Inverse Mapping

We have substantiated a structure for the mapping (D.1)

$$\begin{bmatrix} F_x \\ F_y \end{bmatrix} = H(T,\delta,u) = \begin{bmatrix} T - D(T,\delta,u) \\ L(T,\delta,u) \end{bmatrix} \tag{D.34}$$

Using the assumption that $u_r^2 \propto T$ (at $u_a = 0$ we have that $u_r^2 = kT$ for some $k \in \mathbb{R}$) we end up with

$$H = \begin{bmatrix} T\left(1 - k_x C_D(\alpha)\Delta D(T)\right) \\ T k_y C_L(\alpha)\Delta L(T) \end{bmatrix} \tag{D.35}$$

for some constants k_x,$k_y \in \mathbb{R}$. If the velocity profile corrections $\Delta L(T) = \Delta D(T) = 1$, that is independent of the thrusting T, the mapping H is affine in T and it is possible to find an exact solution to the inverse mapping H^{-1} provided that the inverse functions of of drag and lift coefficients $C_D(\alpha)$ and $C_L(\alpha)$ can be determined analytically. If on the other hand either $\Delta L(T) \neq 1$ or $\Delta D(T) \neq 1$, finding H^{-1} becomes a non-trivial task. In order to regain suitability for control design we therefore suggest an approximation $\hat{H}^{-1}$ of the actual inverse H^{-1} such that for all T and δ that $\hat{H}^{-1} \approx H^{-1}$.

D.4.1 Re-parameterized Profile Corrections

One way to deal with this problem is to approximate $\Delta L(T)$ and $\Delta D(T)$ in terms of the *commanded* generalized force components F_x and F_y instead of nominal thrust T. By doing so, we have made the mapping H linear in T. In other words, we seek the approximations $\widehat{\Delta L}(F_x,F_y)$ and $\widehat{\Delta D}(F_x,F_y)$ so that for all admissible T and δ

$$\widehat{\Delta L}(F_x,F_y) \approx \Delta L(T) \tag{D.36}$$

$$\widehat{\Delta D}(F_x,F_y) \approx \Delta D(T) \tag{D.37}$$

The idea is now to propose a plausible structure for $\widehat{\Delta L}$ and $\widehat{\Delta D}$ by assuming that the actual $\Delta L(T)$ and $\Delta D(T)$ are known.

Small rudder angles $0 < |\delta| < \varepsilon$

Consider small rudder angles δ such that $0 < |\delta| < \varepsilon$. For some small $\varepsilon > 0$ the longships force is close to nominal thrust, that is

$$F_x \approx T \tag{D.38}$$

And hence

$$\Delta L(T) \approx \Delta L(F_x) \tag{D.39}$$

This means that for small rudder angles, that is when $F_y \approx 0$ we should use

$$\widehat{\Delta L}(F_x, F_y) \overset{F_y \approx 0}{=} \Delta L(F_x) \tag{D.40}$$

Constant δ **and** $\Delta D(T)$ **small**

Now let the rudder angle $\delta > 0$ be constant. Then, the lift F_y will depend on the applied thrust T

$$\frac{\partial F_y}{\partial T} = c_1 \left(\Delta L(T) + T \frac{\partial \left(\Delta L(T) \right)}{\partial T} \right) \tag{D.41}$$

where $c_1 = k_y C_L(\alpha)$.

Suppose $\Delta L = 1 + k_1 \sqrt{T} + k_2 T$. Then

$$\frac{\partial F_y}{\partial T} = c_1 \left(1 + \frac{3}{2} k_1 \sqrt{T} + 2 k_2 T \right) \tag{D.42}$$

is possessing in terms of T-dependence the same structure as ΔL. The constant parameters differ though. It can be shown that as long ΔL is a polynomial in T, $\frac{\partial F_y}{\partial T}$ is a function in T with the same structure as $\Delta L(T)$. Consequently, the approximation $\widehat{\Delta L}(F_x, F_y)$ should increase with F_y in a linear fashion.

D.4.2 Approximation Summary

Considering the structure we proposed for small δ's we now get

$$\widehat{\Delta L}(F_x, F_y) = \Delta L(F_x) + c_{F_y} |F_y| \tag{D.43}$$

$$\widehat{\Delta D}(F_x, F_y) = \Delta D(F_x) + c_{F_x} |F_y| \tag{D.44}$$

where we have assumed that ΔD has the same structure as ΔL. The coefficients c_{F_y} and c_{F_x} can be found using curve-fitting techniques once the ΔD and ΔL are found. This analysis indicates that even very simple expressions fit the task, although other forms of $\widehat{\Delta L}$ and $\widehat{\Delta D}$ may of course be used as well.

D.4.3 Algorithm

We assume that the lift and drag coefficients can be sufficiently approximated with the second order polynomials

$$C_L(\delta) = c_{L1}\delta + c_{L2}|\delta|\delta \quad \text{(D.45)}$$
$$C_D(\delta) = c_{D1}|\delta| + c_{D2}\delta^2 \quad \text{(D.46)}$$

The absolute functions indicate that the C_L is symmetric around the origin and C_D around the y-axis.

Using $\widehat{\Delta L}$ and $\widehat{\Delta D}$ it is now trivial to find $\hat{H}^{-1}$. All that needs to be done is to solve for T and δ in

$$\begin{bmatrix} F_{xd} \\ F_{yd} \end{bmatrix} = \begin{bmatrix} T\left(1 - k_x C_D(\delta)\widehat{\Delta D}(F_{xd}, F_{yd})\right) \\ T k_y C_L(\delta)\widehat{\Delta L}(F_{xd}, F_{yd}) \end{bmatrix} \quad \text{(D.47)}$$

where F_{xd} and F_{yd} are the desired generalized forces. The proposed algorithm is:

1. Use the known equivalent angle β

$$\tan\beta = \frac{F_y}{F_x} = \frac{F_{yd}}{F_{xd}} \quad \text{(D.48)}$$

   to eliminate nominal thrust T and solve for rudder angle δ. This yields a quadratic expression in δ. Pick the solution that has the same sign as F_{yd}.

2. Once the correct δ has been found it is straightforward to find the matching T from F_{xd}

$$T = \frac{F_{xd}}{\left(1 - k_x C_D(\delta)\widehat{\Delta D}(F_{xd}, F_{yd})\right)} \quad \text{(D.49)}$$

D.5 Model Experiments

Bollard pull tests were conducted on CS2. In the bow there is a small RPM-controlled tunnel-thruster producing a sway force, and at the stern there are two RPM-controlled main propellers with rudders.

The model ship was kept in a fixed position by two struts as illustrated in Figure D.3. Longships and lateral effective propeller thrust forces were measured by a freely rotatable pressure sensor with an amplifier scaling the measured voltage to a range suited for using the onboard 12-bit analog to digital converter.

For positive shaft speed ω_i, the main propeller-rudder pairs are able to generate forces in sway, for $1 \leq i \leq 2$ we get

$$F_{xi} = T_i - D_i \quad \text{(D.50)}$$
$$F_{yi} = L_i \quad \text{(D.51)}$$

while the bow thruster can thrust in sway only

$$F_{x3} = 0 \quad , \quad F_{y3} = T_3 \quad \text{(D.52)}$$

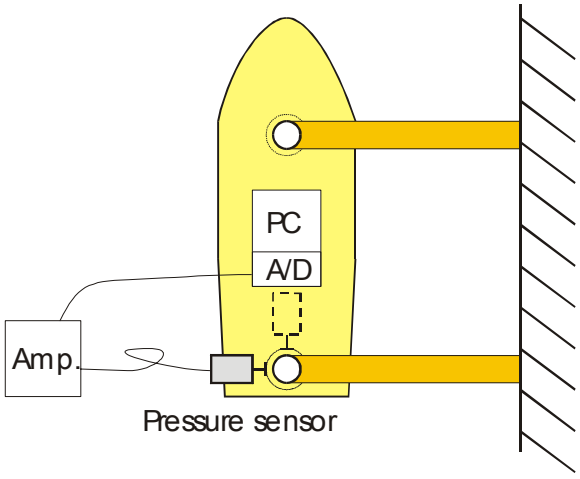

Figure D.3: Bollard pull experiment setup.

D.5.1 Nominal Thrust

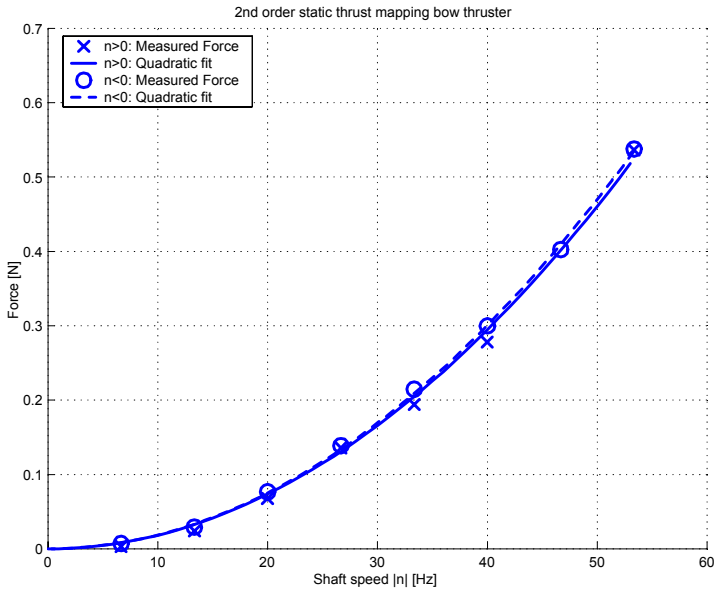

Figure D.5: Bow-thruster nominal force T_3 for positive n (solid) and negative n (dashed) at $u_a = 0$.

As it was easier to measure the sum of the surge forces produced rather than for one thruster at a time, it was assumed that the two main-propeller couples have

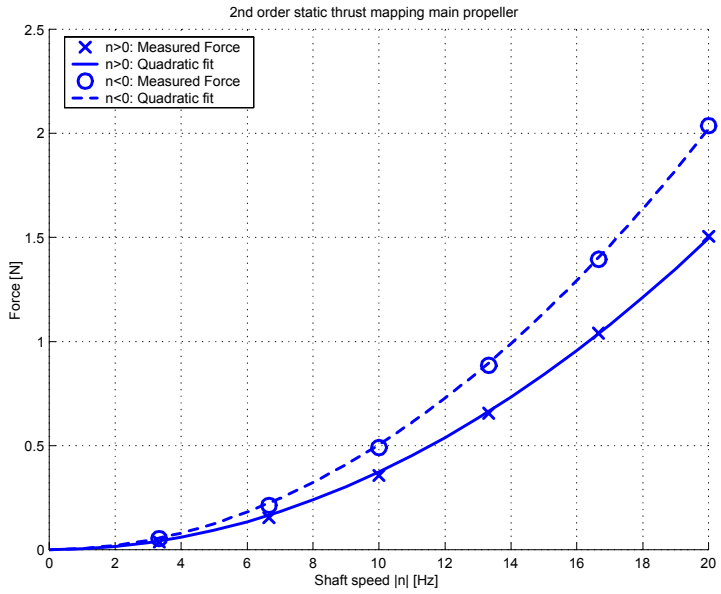

Figure D.4: Nominal static thrust T_i for the main propellers at $u_a = 0$.

identical parameters.

Identification of nominal thrust was based on the already described structure (D.31) for all three devices. For the main propellers, the bollard pull tests were conducted at zero rudder deflection $\delta_i = 0$. As a consequence, the constant rudder drag, mainly due to viscous friction, is incorporated in the nominal thrust parameters. Moreover, the propulsive force regained by the rudder is also taken care of by k_{iTp} and k_{iTn}.

Figure D.4 shows the quadratic response for the main propellers. We observed, surprisingly, that the main propellers performed better in the reverse. One explanation could be that in the reverse the rudder works as a large fin stabilizing the fluid rotation induced by the propeller, effectively increasing the propeller blade angle of attack.

The bow thruster response on the other hand, as shown in Figure D.5, was as expected symmetric in the sense that $k_{3Tp} \approx k_{3Tn}$.

The nominal thrust coefficients were identified using a least-squares fit (Table E.2).

A frequently used parametrization for static thrusters is to express the produced force in terms of the K_T constant

$$T = \rho d^4 K_T |\omega| \omega \tag{D.53}$$

where K_T is taken as a function of the advance number J. So called four quadrant thrust characteristics are (empirical) static descriptions of the generated force for all combinations of positive and negative values of J and ω. As we do not have any

Parameter	**Value** $[Ns^2]$
k_{1Tp}, k_{2Tp}	$3.74 \cdot 10^{-3}$
k_{1Tn}, k_{2Tn}	$5.05 \cdot 10^{-3}$
k_{3Tp}	$1.84 \cdot 10^{-4}$
k_{3Tn}	$1.88 \cdot 10^{-4}$

Table D.1: Nominal thrust coefficient at zero advance speed

incoming velocity u_a, the advance number being zero at all times, it suffices to find K_{Tp} and K_{Tn} for positive and negative ω respectively. The non-dimensionalized thrust coefficient K_T is defined as follows

$$K_T = \frac{T}{\rho d^4 |\omega| \omega} \tag{D.54}$$

Re-parameterizing the results coefficients for the main propellers in Table E.2 yields

$$K_T = \begin{cases} 0.288 & \omega \geq 0 \\ 0.390 & \omega < 0 \end{cases} \tag{D.55}$$

Comparison with the B-series

The main propellers have a shape resembling that of the "Wageningen B-series" (van Lammeren *et al.* 1969). The propellers are four-bladed with a diameter of $d = 60$ millimeters. It seemed that the P/D-ratio was rather small and that the blade-area ratio was approximately 70 percent. Consequently, the data for a "B 4-70" could serve as an indication of whether the nominal thrust coefficients are reasonable.

Again it must be stressed that our results are *not* open water tests. Since the propellers were mounted on a hull, wake effects and thrust losses as well as propeller-rudder interaction did influence the produced thrust force. With these effects in mind it should be plausible to assume that in open water we would have had something around $K_T = 0.25$ for positive ω. This value corresponds to a "B 4-70" with P/D ratio around 0.6 (van Lammeren *et al.* 1969, page 274), close to the manufacturer's specification 0.5. Hence, the identified nominal thrust characteristics seem to be reasonable.

D.5.2 Rudder Forces

The rudders used were so called "Becker" rudders. A Becker rudder is equipped with an extra flap on the trailing edge. The flap angle increases proportionally to the rudder deflection, effectively cambering it. The result is a steeper increase in rudder lift C_L but also increased drag C_D, and as a consequence the effective angle β increases accordingly

$$\beta = \arctan \frac{F_y}{F_x} = \arctan \frac{L}{T - D} \tag{D.56}$$

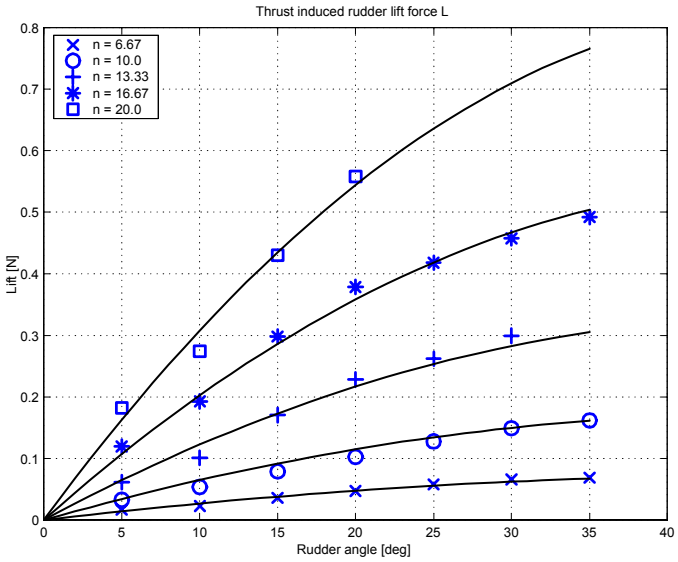

Figure D.6: Rudder lift force at zero advance speed $u_a = 0$ parameterised by shaft speed n.

Rudder Lift

For a range of shaft speeds, the port rudder (actuator 1) was turned inwards producing a lift force in the negative y-direction (port). Several lift-approximations were tried out:

$$L_{1a} = T_1 k_{1L\alpha_1} \delta_1 \tag{D.57}$$

$$L_{1b} = T_1 \left(1 + k_{1L\omega} \omega_1\right) k_{1L\delta_1} \delta_1 \tag{D.58}$$

$$L_{1c} = T_1 \left(1 + k_{1L\omega_1} \omega_1 + k_{1L\omega_2} |\omega_1| \omega\right) k_{1L\delta_1} \delta_1 \tag{D.59}$$

$$L_{1d} = T_1 \left(1 + k_{1L\omega} \omega_1\right) \left(k_{1L\delta_1} \delta_1 + k_{1L\delta_2} |\delta_1| \delta_1\right) \tag{D.60}$$

$$L_{1e} = T_1 \left(1 + k_{1L\omega_1} \omega_1 + k_{1L\omega_2} |\omega_1| \omega\right) \left(k_{1L\delta_1} \delta_1 + k_{1L\delta_2} |\delta_1| \delta_1\right) \tag{D.61}$$

In Figure D.6 the approximation L_{1d} is plotted along with the measured forces and the normalized lift coefficient

$$C_L = \frac{L}{\frac{1}{2} \rho A_d d^2 K_T |\omega| \omega} \tag{D.62}$$

Figure D.7 demonstrates that the lift forces increases faster than the square of ω, an effect handled by the velocity correction factors.

The individual parameters were found by minimizing the squared error between the measured response $y(k)$ and the approximated curve

$$\sigma_i = \min \sum_{k=1}^{N} \left(y(t_k) - L_{1i}(\omega_1(t_k), \alpha_1(t_k))\right)^2 \tag{D.63}$$

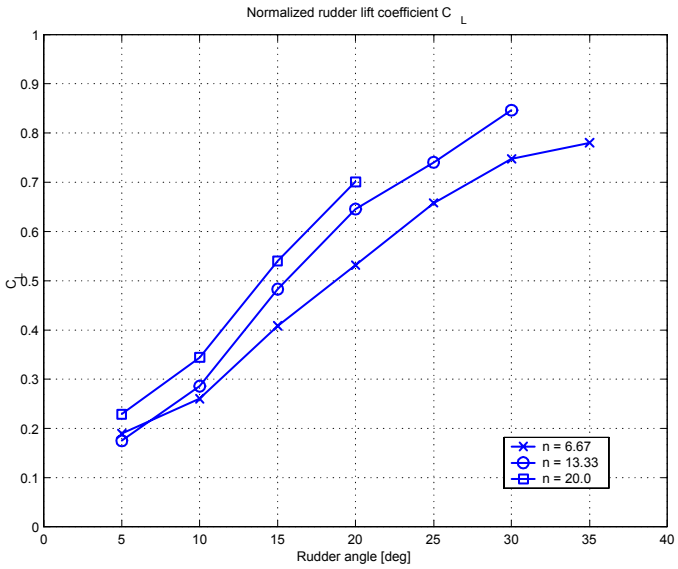

Figure D.7: Normalized rudder lift coefficient C_L.

The approximation was done numerically using a line-search method. Table D.2 contains the results and with a low variance σ_i implying a better approximation.

Approx.	$k_{1L\delta_1}$	$k_{1L\delta_2}$	$k_{1L\omega_1}$	$k_{1L\omega_2}$	σ_i
L_{1a}	0.920				6.05
L_{1b}	0.462		$6.09 \cdot 10^{-2}$		3.77
L_{1c}	1.09		$-5.42 \cdot 10^{-2}$	$2.66 \cdot 10^{-2}$	3.35
L_{1d}	0.927	-0.557	$2.10 \cdot 10^{-2}$		0.67
L_{1e}	0.666	-0.406	$8.22 \cdot 10^{-2}$	$-1.67 \cdot 10^{-3}$	0.66

Table D.2: Rudder Lift Coefficients

Since σ_b is significantly lower than σ_a, employing a velocity distribution compensation is required for an accurate force prediction. Using a higher order velocity compensation $k_{1L\omega_2} \neq 0$, as in L_{1c}, does reduce the variance further, but the 10% reduction is negligible compared to the improvement from L_{1a} to L_{1b} (Table D.2). We could therefore conclude that the lift increases proportionally to $T\left(1 + c\sqrt{T}\right)$ or equivalently

$$\frac{\partial L_1}{\partial T} \approx c_1 T + c_2 T^{\frac{3}{2}} = c_3\omega^2 + c_4\omega^3 \tag{D.64}$$

Approximation L_{1d} suffices because it incorporates quadratic rudder angle dependency which is more influential than quadratic ΔL-terms (Figure D.6). It seemed that the nonlinear thrust dependency was more pronounced for our vessel than what could have been expected from the results in Molland and Turnock (1994).

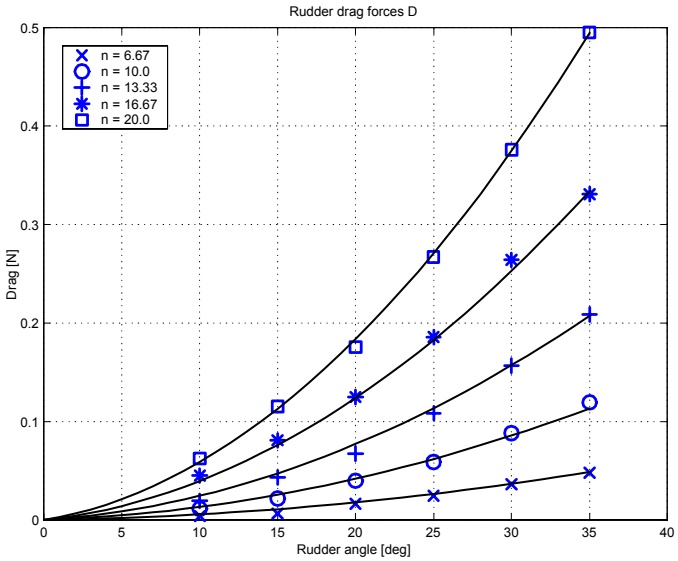

Figure D.8: Rudder drag force D.

Rudder Drag

The drag component from the rudder is expected to have the same structure as the lift. For thin plates, the drag is known to be proportional to the squared angle of attack. The suggested approximations thus include linear and squared rudder angle terms.

$$D_{1a} = T_1 \left(k_{1D\delta_1}|\delta_1| + k_{1D\delta_1}\delta_1^2\right) \tag{D.65}$$

$$D_{1b} = T_1 \left(1 + k_{1D\omega}\omega_1\right)\left(k_{1D\delta_1}|\delta_1| + k_{1D\delta_1}\delta_1^2\right) \tag{D.66}$$

$$D_{1c} = T_1 \left(1 + k_{1D\omega_1}\omega_1 + k_{1D\omega_2}|\omega_1|\omega\right)\left(k_{1D\delta_1}|\delta_1| + k_{1D\delta_1}\delta_1^2\right) \tag{D.67}$$

The measured rudder drag D and the normalized rudder drag coefficient

$$C_D = \frac{D}{\frac{1}{2}\rho A_d d^2 K_T|\omega|\omega} \tag{D.68}$$

are reproduced in Figure D.8 and D.9 respectively. Figure D.8 shows that the drag force increases with the rudder angle in a nonlinear fashion, and from Figure D.9 we see that C_D, just like C_L as shown above, increases proportionally with ω. This behavior and the estimated parameters are summarized in Table D.3. Without thrust corrections, that is $k_{1D\omega_j} = 0$ the variance of the estimate is about 70% greater than for approximation b and c. As for rudder lift force, it seems that a linear thrust correction, approximation D_{1b} is sufficient because the variance σ_c is not significantly lower than σ_b.

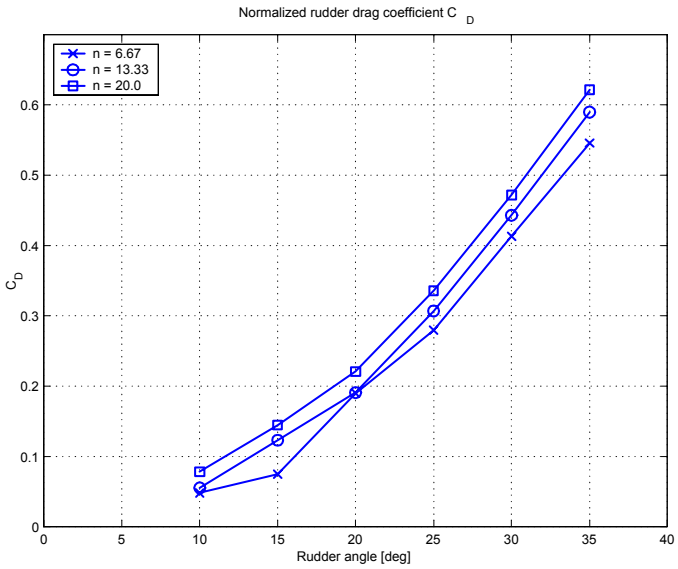

Figure D.9: Normalized rudder drag coefficient C_D.

Approx.	$k_{1D\delta_1}$	$k_{1D\delta_2}$	$k_{1D\omega_1}$	$k_{1D\omega_2}$	σ_i
D_{1a}	0.093	0.727			0.18
D_{1b}	0.079	0.615	$9.64 \cdot 10^{-3}$		0.11
D_{1c}	0.079	0.615	$2.19 \cdot 10^{-2}$	$-3.63 \cdot 10^{-4}$	0.10

Table D.3: Rudder Drag Coefficients

D.5.3 Velocity Correction Factors

The parameters of the velocity distribution corrections are found in Tables D.2-D.9. In particular, for correction terms linear in the shaft speed

$$\Delta L = 1 + k_{1L\omega_1}\omega = 1 + \frac{k_{1L\omega_1}}{\sqrt{k_{1Tp}}}\sqrt{T} = 1 + 0.343\sqrt{T} \tag{D.69}$$

$$\Delta D = 1 + k_{1D\omega_1}\omega = 1 + \frac{k_{1D\omega_1}}{\sqrt{k_{1Tp}}}\sqrt{T} = 1 + 0.158\sqrt{T} \tag{D.70}$$

The suggested crude approximations were on the form

$$\widehat{\Delta L}(F_{xd}, F_{yd}) = \Delta L(F_{xd}) + c_{\hat{L}y}|F_{yd}| = 1 + \frac{k_{1L\omega_1}}{\sqrt{k_{1Tp}}}\sqrt{F_{xd}} + c_{\hat{L}y}|F_{yd}| \tag{D.71}$$

$$\widehat{\Delta D}(F_{xd}, F_{yd}) = \Delta D(F_{xd}) + c_{\hat{D}y}|F_{yd}| = 1 + \frac{k_{1D\omega_1}}{\sqrt{k_{1Tp}}}\sqrt{F_{xd}} + c_{\hat{D}y}|F_{yd}| \tag{D.72}$$

that is proportional to $\sqrt{F_x}$ and $|F_y|$. A least-square fit of parameters was performed for this structure and for two other ones that seemed appropriate. Since

the $\widehat{\Delta L}$ and $\widehat{\Delta D}$ were assumed to have the same structure only the suggested functions of $\widehat{\Delta L}$ are given

$$\widehat{\Delta L}_a(F_{xd}, F_{yd}) = 1 + c_{\hat{L}x}\sqrt{F_{xd}} + c_{\hat{L}y}|F_{yd}| \tag{D.73}$$

$$\widehat{\Delta L}_b(F_{xd}, F_{yd}) = 1 + c_{\hat{L}x}\sqrt{F_{xd}} + c_{\hat{L}y}\sqrt{|F_{yd}|} \tag{D.74}$$

$$\widehat{\Delta L}_c(F_{xd}, F_{yd}) = 1 + c_{\hat{L}x}\sqrt{F_{xd}} + \frac{c_{\hat{L}y}|F_{yd}|}{1 + c_{\hat{L}x2}F_{xd}} \tag{D.75}$$

Approx.	$c_{\hat{L}x}$	$c_{\hat{L}y}$	$c_{\hat{L}x2}$	σ_i
$\widehat{\Delta L}_a$	0.3396	0.0883		1.0
$\widehat{\Delta L}_b$	0.3189	0.0871		0.74
$\widehat{\Delta L}_c$	0.3341	0.4168	3.512	0.23

Table D.4: Inverse Mapping, Lift Velocity Corrections

Approx.	$c_{\hat{L}x}$	$c_{\hat{L}y}$	$c_{\hat{L}x2}$	σ_i
$\widehat{\Delta D}_a$	0.1559	0.0405		1.0
$\widehat{\Delta D}_b$	0.1464	0.0400		0.73
$\widehat{\Delta D}_c$	0.1529	0.1923	3.366	0.23

Table D.5: Inverse Mapping, Drag Velocity Corrections

It can be seen from the variance parameter that approximation c is the best candidate. More detailed proposals generate a better fit in terms of variance σ_i, yet these simplified approximations show good agreement with the actual response.

Even though approximation a is significantly poorer than approximation c, it does actually fit the identified correction model quite well (see the contour plot in Figure D.10). The contours of the actual model are dashed while the approximations $\widehat{\Delta L}_a$ and $\widehat{\Delta L}_c$ are drawn as a solid line. The difference between approximation a and c is that the slope of the contours as a function of F_y depends on the magnitude of F_x.

The same pattern could be seen for drag $\widehat{\Delta D}$, those plots are, however, not reproduced here.

D.6 Concluding Remarks

Based on classic momentum theory considerations, a simple polynomial mapping for longships and lateral forces produced by a propeller-rudder pair at zero advance speed has been proposed. The effects present at low Reynholds number were incorporated by conjecturing the existence of so-called velocity corrections. These corrections enabled us to express the non-linear behavior of the static rudder

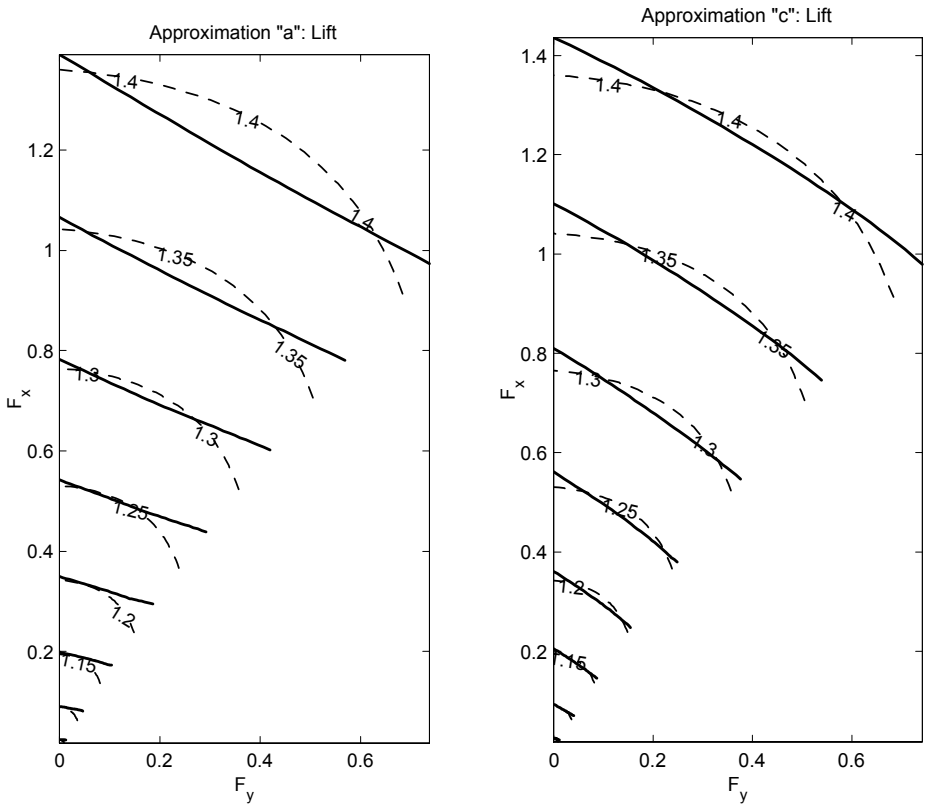

(a) $\widehat{\Delta L}_a(F_{xd}, F_{yd})$ (b) $\widehat{\Delta L}_c(F_{xd}, F_{yd})$

Figure D.10: Approximated Lift corrections $\widehat{\Delta L}$ (solid)and actual $\Delta L(T)$ (dashed)

sideforce with great accuracy. Bollard pull tests with a model ship verified that the presented structure predicted the recorded data well.

For full scale vessels it is believed that velocity corrections loose importance in the sense that $\Delta L \approx 1$ and $\Delta D \approx 1$ due to increased Reynholds numbers. If so, finding appropriate inverse mappings is trivial.

Appendix E

Description of Cybership II

E.1 Introduction

In order to conduct more technically advanced and computationally demanding ship maneuvering operations, a new model ship was built from scratch at the Department of Engineering Cybernetics. Being the successor of "Cybership", its official name became "Cybership II" (CS2). The initial phase started early 2000 and the boat was considered finished late 2001 when the last sensor was satisfactorily integrated.

Figure E.1: Cybership II exposed to waves.

A desired feature of CS2 was portability: It should be possible with a minimum of effort to physically move the laboratory set-up from one facility to another. As the ship was built and tested at the Department of Engineering Cybernetics, the "Guidance, Navigation and Control Laboratory" (GNC-Lab) served as the test basin. Later on, in December 2001 CS2 was moved to the "Marine Cybernetics Laboratory" (MCL-Lab) at Tyholt. Moreover, portability in terms of hardware configuration was also stressed. This called for using standard off-the-shelf hardware and software components.

In the next section we give a brief description of CS2 itself, the new camera system, and the developed control system.

E.2 Cybership II

CS2 is a scaled replica of an offshore supply vessel. The overall length is $L_{OA} = 1.255$ meters, and it is equipped with three propulsive devices: In the bow there is a small two-bladed RPM-controlled tunnel-thruster producing a sway force, and at the stern there are two RPM-controlled main propellers with rudders.

CS2 has an inboard micro PC powered by a 244 MHz Pentium clone running QNX and it is connected to the local LAN through a BreezeCOM 2 Mbit wireless Ethernet link. The control software was developed and tested a priori under Matlab Simulink and Real Time Workshop on the host PC. Opal RT-Lab handles the compilation of the code as well as any other communication with the target system such as transmission of various signals during the experiments.

Figure E.2 is an illustration of the implemented system.

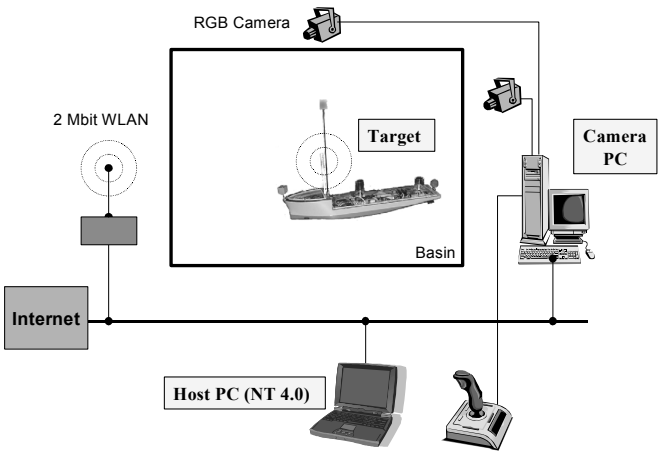

Figure E.2: Overview of the GNC Laboratory.

During start-up, CS2 automatically logs on to the camera PC in order to receive

position and attitude data. The six DOF positions and orientations (attitude) are measured with two standard RGB cameras with the aid of two MagTrak ISA-cards. This system first locates the three colored markers on CS2 using Tsai's algorithm (Tsai 1987). An alternative version of the QUEST algorithm (Shuster and Oh 1981) based on singular value decomposition instead of eigenvalues calculates the ship's attitude in unit quaternions and converts it to Euler angles, that is the roll, pitch and heading angles. Once the orientation is found, determining the position of the ship is a straightforward operation.

The Litton LN-200 IMU is what really distinguishes CS2 from other model ships. To the best of our knowledge, this is the first model ship that actively utilizes measured linear accelerations for control purposes. It is important to realize that accelerometer output can not be used directly in planar control because as the ship rolls and pitches, the measured surge and sway accelerations will be contaminated with gravity components. In order to cancel gravity and calculate horizontal accelerations, it is required to have accurate estimates of roll and pitch angles available. The filter that estimates roll and pitch by integration of gyro and accelerometer measurements, a so called vertical reference unit (VRU), is described in Section 3.3.2. Successful use of measured acceleration relies on having a well performing VRU.

E.2.1 Software Description

Operator Station and Modes

An operator station (OS) consisting of a graphical user interface (GUI) and a three-axis joystick used for manual control was developed under LabView 6.0i (Figure E.3). The user was allowed to monitor and operate the vessel in three different modes:

DP Fully automatic positioning control, i.e. station keeping. The observer, controller and thrust allocation modules were enabled and running.

Manual In manual mode the joystick was used to control each one of the three DOFs independently. The controller was disabled but the observer and the thrust allocation module were active.

Init In init mode neither the observer, controller nor the thrust allocation module were active. The thrusters and rudders could however be controlled by setpoints given on the OS.

An additional feature of the OS was access to controller gains enabling the operator to adjust the controller tuning and strategy (e.g. nonlinear control, acceleration) online. Furthermore, estimation of accelerometer and gyro biases could be activated (Figure E.4). Typically, these biases were estimated during init mode and frozen during the conducted experiments.

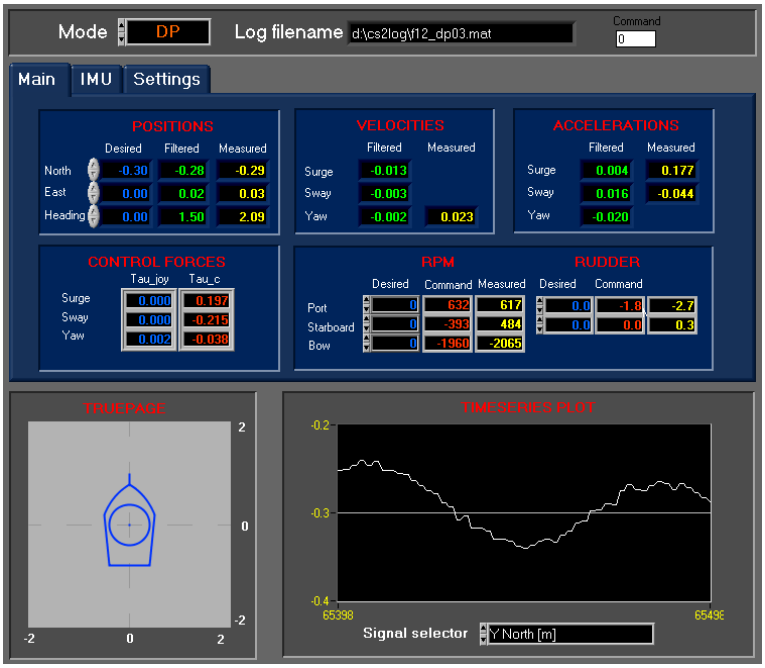

Figure E.3: Main page of the operation station.

Camera System

The camera system is responsible for measuring the actual position and orientation of the vessel. In order to be comparable with DGPS, which is the most commonly used position reference system in the North Sea, the accuracy had to be around 1 cm. The sampling rate, the rate at which new measurements are available, should be around 10 Hz. This rate is more realistic than the 50 Hz rate used by Cybership (Strand 1999, Berge 1999).

Portability of the camera system imposed two requirements. First of all, the weight and size of the camera system had to be low. Secondly, it must be easy to calibrate, because a camera system needs calibration every time the equipment is moved.

The resulting system (Figure E.5) uses two standard video cameras with standard RGB-signal output. Each camera is connected to a MagTrak prototype color recognition card developed at the University of Girona, Spain. The MagTrak cards are capable of detecting the pixel coordinates of up to three distinct colors present in each grabbed frame. By employing Tsai's algorithm (Tsai 1987), the marker's pixel coordinates from each of the two cameras are then converted to three-dimensional positions relative to the origin of the "Earth-fixed" frame, the n-frame.

When the positions of the three markers $\mathbf{p}_j^b$ are known, it is straight-forward to apply the QUEST-algorithm (Shuster and Oh 1981) to solve for the optimal

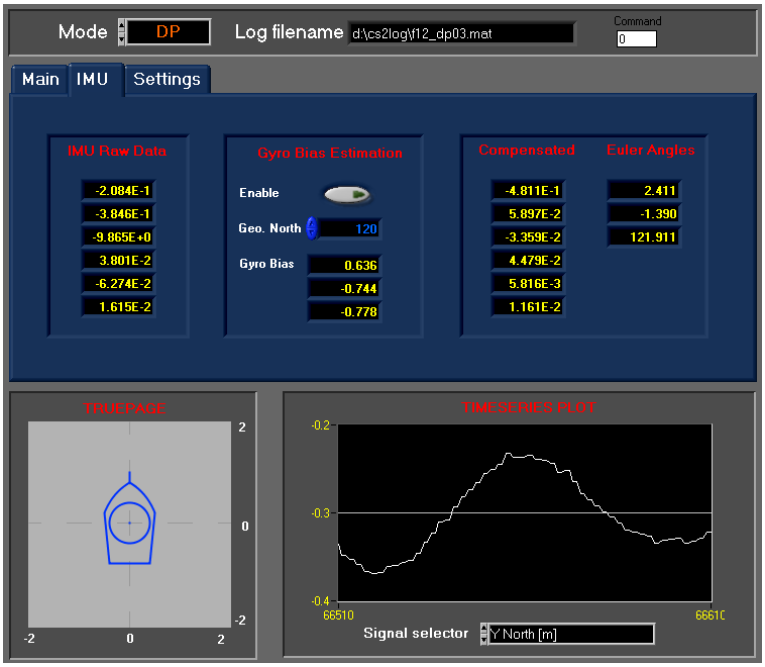

Figure E.4: IMU page.

orientation of the vessel. QUEST determines the orientation in unit quaternions $\mathbf{q}$ between a set of vectors in two different coordinate frames. In terms of the Euler angles QUEST finds the optimal orientation $\boldsymbol{\theta}_{nb}$ such that given m measurements, the following performance index is minimized

$$\min_{\boldsymbol{\theta}_{nb}} \sum_{k=1}^{m} \left\| \mathbf{z}_k^n - \mathbf{R}(\boldsymbol{\theta}_{nb}) \mathbf{z}_k^b \right\|_2^2 \tag{E.1}$$

The actual marker positions on Cybership II are

$$\mathbf{p}_1^b = \begin{bmatrix} 0.545 \\ 0.000 \\ -0.155 \end{bmatrix}, \quad \mathbf{p}_2^b = \begin{bmatrix} 0.210 \\ 0.000 \\ -0.770 \end{bmatrix}, \quad \mathbf{p}_3^b = \begin{bmatrix} -0.690 \\ 0.000 \\ -0.060 \end{bmatrix} \tag{E.2}$$

and as input to QUEST, the following data was used in order to remove the $\mathbf{r}^n$ dependency

$$\begin{aligned} \mathbf{z}_1^n &= \mathbf{y}_1^n - \mathbf{y}_3^n & \mathbf{z}_1^b &= \mathbf{p}_1^b - \mathbf{p}_3^b \\ \mathbf{z}_2^n &= \mathbf{y}_2^n - \mathbf{y}_3^n & \mathbf{z}_1^b &= \mathbf{p}_2^b - \mathbf{p}_3^b \\ \mathbf{z}_2^n &= \mathbf{y}_1^n - \mathbf{y}_2^n & \mathbf{z}_1^b &= \mathbf{p}_1^b - \mathbf{p}_2^b \end{aligned} \tag{E.3}$$

Once the attitude $\boldsymbol{\theta}_{nb}^n$ is found, the optimal position $\mathbf{r}^n$ of the vessel can be found from

$$\mathbf{r}^n = \frac{1}{3} \sum_{k=1}^{3} \left(\mathbf{y}_k^n - \mathbf{R}(\boldsymbol{\theta}_{nb}) \mathbf{p}_k^b \right) \tag{E.4}$$

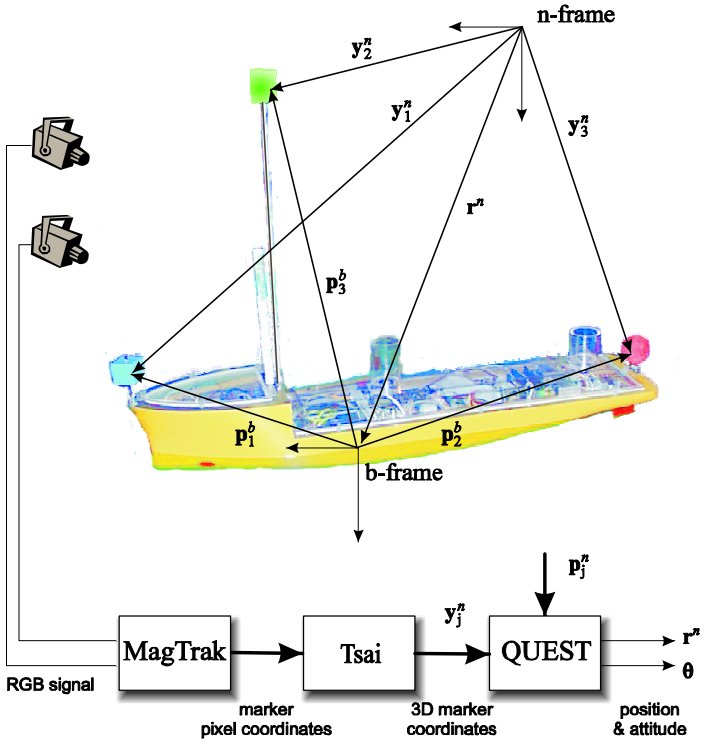

Figure E.5: Camera system details

which is the minimum variance estimate of $\mathbf{r}^n$ for the given $\mathbf{R}_b^n$ and $\mathbf{y}_k^n$'s.

E.2.2 Vessel Model Description

Low Speed Vessel Model

The following low speed model was considered

$$\begin{aligned} \dot{\boldsymbol{\eta}} &= \mathbf{R}(\psi)\boldsymbol{\nu} \\ \mathbf{M}\dot{\boldsymbol{\nu}} &= -\mathbf{D}_L\boldsymbol{\nu} + \boldsymbol{\tau} \end{aligned}$$

and the actual parameters used in the mass and linear damping matrices

$$\mathbf{M} = \begin{bmatrix} m - X_{\dot{u}} & 0 & 0 \\ 0 & m - Y_{\dot{v}} & m x_{bG}^b - Y_{\dot{r}} \\ 0 & m x_{bG}^b - N_{\dot{v}} & I_z - N_{\dot{r}} \end{bmatrix}$$

$$\mathbf{D}_L = \begin{bmatrix} -X_u & 0 & 0 \\ 0 & -Y_v & -Y_r \\ 0 & -N_v & -N_r \end{bmatrix}$$

are listed in Table E.1

Parameter	Value	Unit
L_{OA}	1.255	m
m	23.8	kg
I_z	1.76	kg m^2
x_{bG}^b	0.0	m
$X_{\dot{u}}$	-2.0	kg
$Y_{\dot{v}}$	-10.0	kg
$Y_{\dot{r}} = N_{\dot{v}}$	0.0	kg m
$N_{\dot{r}}$	-1.0	kg m^2
X_u	-2.0	kg/s
Y_v	-7.0	kg/s
$Y_r = N_v$	-0.1	kg m/s
N_r	-0.5	kg m^2/s

Table E.1: Vessel Parameters

Thruster and Rudder Models

For fixed pitch propellers the generated thrust force is more or less proportional to the square of the propeller shaft speeds ω_i. The low speed propeller/rudder model for CS2 can conveniently be separated into two parts: The first one is the nominal thrust (rudder angles $\delta_i = 0$, $i = 1, 2$)

$$T_i = \begin{cases} k_{iT_p}\omega_i^2 & \omega_i \geq 0 \\ k_{iT_n}|\omega_i|\omega_i & \omega_i \leq 0 \end{cases} \qquad i \in [1, 3] \tag{E.5}$$

and the second part gives additional rudder lift and drag forces, $i = 1, 2$,

$$L_i = \begin{cases} T_i(1 + k_{iL\omega}\omega_i)(k_{iL\delta_1} + k_{iL\delta_2}|\delta_i|)\delta_i & \omega_i \geq 0 \\ 0 & \omega_i < 0 \end{cases} \tag{E.6}$$

$$D_i = \begin{cases} T_i(1 + k_{iD\omega}\omega_i)(k_{iD\delta_1}|\delta_i| + k_{iD\delta_2}\delta_i^2) & \omega_i \geq 0 \\ 0 & \omega_i < 0 \end{cases} \tag{E.7}$$

For the main propellers, $i = 1, 2$, the resulting surge and sway forces are

$$u_i = \begin{bmatrix} T_i - D_i \\ L_i \end{bmatrix} \tag{E.8}$$

The thruster and rudder parameters are given in Table E.2 and E.3, and the positions of the individual thrusters relative to the b-frame are

$$\mathbf{r}_{bt_1}^b = \begin{bmatrix} -0.54 & -0.075 \end{bmatrix}^T \tag{E.9}$$

$$\mathbf{r}_{bt_2}^b = \begin{bmatrix} -0.54 & 0.075 \end{bmatrix}^T \tag{E.10}$$

$$\mathbf{r}_{bt_3}^b = \begin{bmatrix} 1.14 & 0.0 \end{bmatrix}^T \tag{E.11}$$

Figure E.6 shows the resulting feasible thrust domains.

Table E.2: Nominal thrust parameters

Parameter	**Value** [Ns^2]
k_{1Tp} , k_{2Tp}	$3.74 \cdot 10^{-3}$
k_{1Tn} , k_{2Tn}	$5.05 \cdot 10^{-3}$
k_{3Tp}	$1.84 \cdot 10^{-4}$
k_{3Tn}	$1.88 \cdot 10^{-4}$

Table E.3: Rudder lift and drag parameters

Parameter	**Value**	**Unit**
k_{1Ln} , k_{2Ln}	$2.10 \cdot 10^{-2}$	s
$k_{1L\delta_1}$, $k_{2L\delta_1}$	0.927	rad^{-1}
$k_{1L\delta_2}$, $k_{2L\delta_2}$	-0.557	rad^{-2}
k_{1Dn} , k_{2Dn}	$9.64 \cdot 10^{-3}$	s
$k_{1D\delta_1}$, $k_{2D\delta_1}$	0.079	rad^{-1}
$k_{1D\delta_2}$, $k_{2D\delta_2}$	0.615	rad^{-2}

E.3 Inertial Sensor Feedback

The IMU was interfaced with CS2 over a 1 Mbit/s RS-485 synchronous serial link. The six raw measurements, three accelerations and three gyro rates, were received at a rate of 400 Hz. Especially the acceleration signals were contaminated with extremely rapid oscillations of a large magnitude, and those fluctuations had to be removed. None of the incoming measurements could be lost, because any further processing of the data would introduce errors in the filtered signal. Hence, a dedicated low-level driver buffering up these measurements was developed to handle the high data rate and the inherent signal variations.

The input received by the low-level driver had to be processed by some kind of low-pass filter, and it was decided to implement a low-pass FIR-filter. The advantage of such filters is that they have no memory and the output is simply a weighed sum of the last N inputs. In order to avoid phase lag, the filter algorithm was applied twice; forwards on the incoming data and backwards on the temporary processed filtered results. The sequence is illustrated in Figure E.7. Given an array of filter coefficients B_j where $0 \leq j \leq N$, the following operations formed the basis of the filter.

$$\text{Forwards} \quad : \quad x_k = \sum_{j=1}^{N} B_j u_{k-N+j} \tag{E.12}$$

$$\text{Backwards} \quad : \quad y_k = \sum_{j=1}^{N} B_j x_{k-j+1} \tag{E.13}$$

A 40th order low-pass filter ($N = 40$) with cut-off a frequency $f_c = 2$ Hz seemed appropriate for this purpose.

The price paid by re-applying the filter backwards is a signal delay of 10 ms. This,

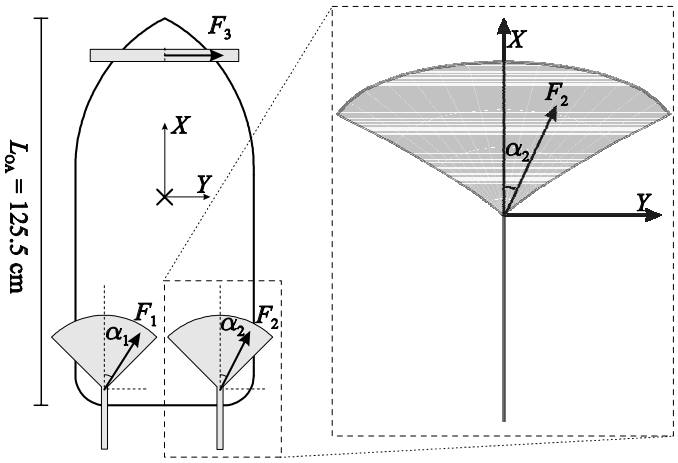

Figure E.6: Outline of Cybership II: Feasible thrust domains.

however, was not considered a problem, because the delay leads to the inertial measurements being better synchronized with the measured position and heading.

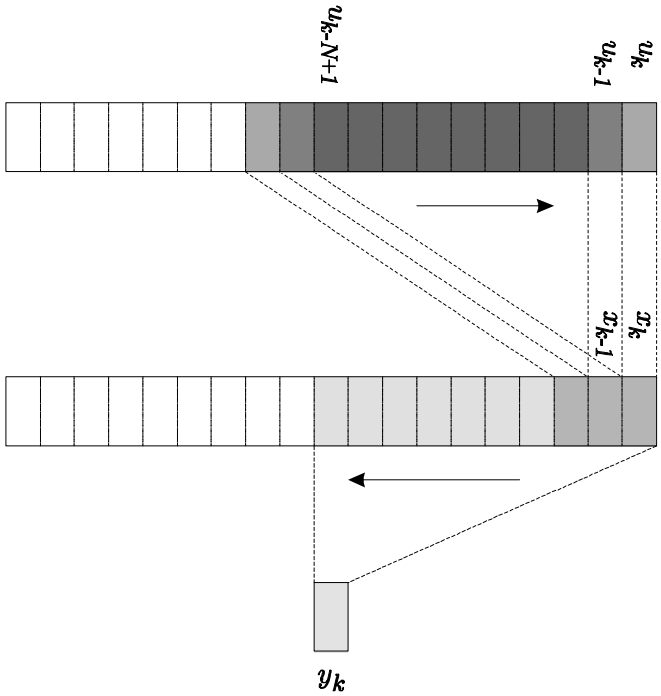

Figure E.7: Filtering of the IMU-measurements u_k. Forwards into x_k, and backwards into y_k.

Erratum for "Acceleration Feedback in Dynamic Positioning"

Karl-Petter Lindegaard

November 5, 2003

Page	Location	Reads	Should read
34	(3.27)	$\mathbf{f}^b_{\text{imu}} = \mathbf{a}^b - \mathbf{R}^b_p \mathbf{g}^p$	$\mathbf{f}^b_{\text{imu}} = \mathbf{a}^b_{nb} - \mathbf{R}^b_p \mathbf{g}^p$
34	(3.29)	$\hat{\mathbf{a}}^b = ...$	$\hat{\mathbf{a}}^b_{nb} = ...$
34	under (3.29)	$\tilde{\mathbf{a}}^b = \mathbf{a}^b - \hat{\mathbf{a}}^b$	$\tilde{\mathbf{a}}^b_{nb} = \mathbf{a}^b_{nb} - \hat{\mathbf{a}}^b_{nb}$
34	(3.31)	$\tilde{\mathbf{a}}^b \approx ...$	$\tilde{\mathbf{a}}^b_{nb} \approx ...$
35	last equation	$\hat{\mathbf{a}}^b = ...$	$\hat{\mathbf{a}}^b_{nb} = ...$
37	(3.40)	$\mathbf{z}_{WF} = ...$	$\mathbf{z}^b_{WF} = ...$
52	(4.74)	$\mathbf{C}_y(\psi_y) = ...$	$\mathbf{C}_y(\psi_y) = \begin{bmatrix} \mathbf{C}_{pw} & \mathbf{I} & \mathbf{0} & \mathbf{0} & \mathbf{0} & \mathbf{0} \\ \mathbf{0} & \mathbf{0} & \mathbf{0} & \mathbf{C}_{vw} & \mathbf{0} & \boldsymbol{\Upsilon}_2 \\ \mathbf{0} & -\boldsymbol{\Upsilon}_3\mathbf{M}^{-1}\mathbf{G}\mathbf{R}^T(\psi_y) & \boldsymbol{\Upsilon}_3\mathbf{M}^{-1}\mathbf{R}^T(\psi_y) & \mathbf{0} & \mathbf{C}_{aw} & -\boldsymbol{\Upsilon}_3\mathbf{M}^{-1}\mathbf{D} \end{bmatrix}$
54	Figure 4.1	$\mathbf{K}_{31}$	$\mathbf{K}_{21}$
54	(4.86)	$\mathbf{A}_{21} = ...$	$\mathbf{A}_{21} = \begin{bmatrix} \mathbf{0} & \mathbf{0} & \mathbf{0} \\ \mathbf{0} & \mathbf{K}_{53}\boldsymbol{\Upsilon}_3\mathbf{M}^{-1}\mathbf{G} & -\mathbf{K}_{53}\boldsymbol{\Upsilon}_3\mathbf{M}^{-1} \\ -\mathbf{K}_{61}\mathbf{C}_{pw} & -\mathbf{M}^{-1}\mathbf{G} - \mathbf{K}_{61} & \mathbf{M}^{-1} \end{bmatrix}$
54	(4.87)	$\mathbf{A}_{22} = ...$	$\mathbf{A}_{22} = \begin{bmatrix} \mathbf{A}_{vw} - \mathbf{K}_{42}\mathbf{C}_{vw} & \mathbf{0} & -\mathbf{K}_{42}\boldsymbol{\Upsilon}_2 \\ \mathbf{0} & \mathbf{A}_{aw} - \mathbf{K}_{53}\mathbf{C}_{aw} & \mathbf{K}_{53}\boldsymbol{\Upsilon}_3\mathbf{M}^{-1}\mathbf{D} \\ -\mathbf{K}_{62}\mathbf{C}_{vw} & \mathbf{0} & -\mathbf{M}^{-1}\mathbf{D} - \mathbf{K}_{62}\boldsymbol{\Upsilon}_2 \end{bmatrix}$
54	(4.88)	$\mathbf{C}_3 = ...$	$\mathbf{C}_3 = \begin{bmatrix} \mathbf{0} & -\boldsymbol{\Upsilon}_3\mathbf{M}^{-1}\mathbf{G} & \boldsymbol{\Upsilon}_3\mathbf{M}^{-1} & \mathbf{0} & \mathbf{C}_{aw} & -\boldsymbol{\Upsilon}_3\mathbf{M}^{-1}\mathbf{D} \end{bmatrix}$
57	above (4.102)	... in $\mathbf{K}_{11}$ and $\mathbf{K}_{31}$...	... in $\mathbf{K}_{11}$ and $\mathbf{K}_{21}$...
57	(4.106)	$k_{31,i} = \omega_{c,i}$	$k_{21,i} = \omega_{c,i}$
57	(4.108)	$\mathbf{c}_i = ...$	$\mathbf{c}_i = \begin{bmatrix} 2\beta_{p,i}\left(\delta_{p,i} - 1\right) \\ \beta^2_{p,i}\left(\delta^2_{p,i} - 1\right) + 2\beta_{p,i}\left(\delta_{p,i} - 1\right)\omega_{c,i} \\ 2\alpha_{p,i}\beta_{p,i}\left(\delta_{p,i} - 1\right) + \beta^2_{p,i}\left(\delta^2_{p,i} - 1\right)\omega_{c,i} \\ 2\beta_{p,i}\left(\delta_{p,i} - 1\right)\omega_{c,i} \end{bmatrix}$
129	(A.14)	$\Sigma_1 : \dot{\mathbf{x}}_2 = ...$	$\Sigma_2 : \dot{\mathbf{x}}_2 = ...$
186	Figure E.5	$\mathbf{p}^n_j$	$\mathbf{p}^b_j$